Université Lille 1 Sciences et Technologies

THÉSE

Présentée pour obtenir le grade de :

Docteur de l'Université de Lille 1

Spécialité :

Sciences de la Matière du Rayonnement et de l'Environnement

Soutenue publiquement le 17 décembre 2013 par

Anton Lopatin

Enhanced remote sensing of atmospheric aerosol by joint inversion of active and passive remote sensing observations

Jury :

Rapporteurs :	Valery SHCHERBAKOV
	Iwona STACHLEWSKA
Examinateur :	Ulla WANDINGER
Directeurs :	Oleg DUBOVIK
	Philippe GOLOUB
	Anatoly CHAIKOVSKY

Laboratoire d'Optique Atmosphérique
U.F.R de Physique Fondamentale
Université Lille 1 Sciences et Technologies
59655 Villeneuve d'Ascq, France

Laboratory of Optics of Scattering Media
B.I. Stepanov Institute of Physics, National Academy of Sciences of Belarus
220072 Minsk, Belarus

Abstract

This thesis presents the GARRLiC algorithm (Generalized Aerosol Retrieval from Radiometer and Lidar Combined data) that simultaneously inverts co-incident lidar and sun-photometer observations and derives a united set of aerosol parameters that describe both columnar and vertical aerosol properties.

GARRLiC searches for the best fit of the multi-source measurements together with a priori constraints on aerosol characteristics through the continuous space of all possible solutions under statistically formulated criteria. It retrieves height independent size distribution, complex refractive index and fraction of spherical particles together with vertically resolved aerosol concentration, all differentiated between fine and coarse aerosol modes.

The potential and limitations of the method are demonstrated by sensitivity tests. The tests showed that the complete set of aerosol parameters for each aerosol component can be robustly derived with acceptable accuracy in all considered situations. Limited sensitivity to the properties of the fine mode and dependence of retrieval accuracy on the aerosol optical thickness for both modes were found. It was shown that sensitivity to fine mode refractive index could be improved by accounting for polarization data provided by passive instruments. The effects of the presence of lidar data and random noise on aerosol retrievals were studied.

The algorithm was also applied to the real lidar and radiometer observations obtained over Minsk (Belarus) and Lille (France) AERONET sites.

Suggested approach could be easily modified to retrieve aerosol properties from all possible combinations of existing passive and active remote sensing instruments.

Keywords: atmospheric aerosol; remote sensing; inverse problem; multi-instrument observations; LIDAR; sun-photometer.

Résumé

Ce travail présente l'algorithme GARRLiC (Generalized Aerosol Retrieval from Radiometer and Lidar Combined data). Le but de cet algorithme est d'inverser simultanément les mesures co-localisées d'un LiDAR et d'un photomètre solaire. Cet algorithme original permet de déduire un ensemble très complet de paramètres descriptifs de l'aérosol atmosphérique, paramètres à la fois intégrés sur la colonne atmosphérique et résolus verticalement.

GARRLiC est basée sur la recherche du meilleur ajustement de données multi-sources avec contraintes a priori. Il est basée sur la recherche de la meilleure solution selon un ensemble de critères statistiques. Les paramètres déduits sont de 2 types. Certains sont des quantités intégrées sur la colonne atmosphériques tandis que d'autres sont fonction de l'altitude comme la concentration en particules pour les deux modes dimensionnels fin et grossier.

Une étude de sensibilité a montré que l'ensemble des paramètres peut être restitué avec une bonne précision dans toutes les situations considérées. L'étude indique une précision moins bonne pour le mode fin et qu'en général la précision est moindre à faible épaisseur optique. Elle a également montré que la précision sur l'indice de réfraction pouvait être accrue si l'on prenait en compte la mesure de polarisation issue du photomètre solaire. L'impact de la prise en compte de mesure LiDAR et de bruit sur les mesures a été étudié.

GARRLiC a été appliqué à des mesures réelles obtenues à Minsk (Biélorussie) et Lille (France).

L'approche employée ici peut être facilement modifiée pour retrouver les propriétés de l'aérosol à partir de multiples combinaisons d'instruments de télédétection passif et actif.

Mots clés : aérosol atmosphérique; télédétection; problème inverse; les observations multi-instruments; LIDAR; photomètre solaire.

La thèse a été effectuée en co-tutelle au sein Laboratoire d'Optique Atmosphérique et Laboratory of Scattering Media

Laboratoire d'Optique Atmosphérique
UFR de Physique
Bâtiment P5
Université des Sciences et Technologies de Lille
59655 Villeneuve d'Ascq Cédex (FRANCE)

Laboratory of Scattering Media
National Academy of Sciences of Belarus
Institute of physics
68 Nezavisimosti avenue
220072 Minsk (BELARUS)

Acknowledgements

I would like to thank my scientific advisers Anatoli Chaikovsky, Oleg Dubovik and Philippe Goloub for wise guidance and thorough support.

I'm grateful to the staff of Laboratory of Scattering Media if Institute of Physics of National Academy of Sciences of Belarus for their support during my first steps in science and for the knowledge I've obtained. Special thanks to Alexander Slesar, Dmitry Savitskiy, Michail Korol, Sergey Denisov, Fiodar Osipenka and Leonid Bondarchik for the wonderful remote sensing instrumentation they have created.

I'm thankful for the consular department of France in Belarus and personally to Margarita Kuhareva for their support in the application for the grant of French government. Thanks to the CROUS (Centre Régional des Oeuvres Universitaires et Scolaires) of Lille and personally to Mme. Daniele Fabis for the financial and administrative support during my visits to France. I'm grateful to the director of the Laboratoire D'Optique Atmosphérique, M. Frédéric Parol without whose talent of persuasion this grant application wouldn't make it till the end.

Thanks to my colleagues Andrei Holdak, Tatiana Lapyonok, Pavel Litvinov and Fabrice Ducos for their help in the comprehension and adaptation of the programming codes and to Isabelle Jankowiak and Aleksandr Lapyonok for the moral support while being in a foreign country. To my friends and fellow students Yana Korol, Anton Fedorenka, Marine Desmons, Odran Sourdeval, Andrei Bovchalyuk, Augustin Mortier, Benjamin Torres and Thomas Fauchez for all the fun and for making it worthwhile. Special thanks to Marie-Lyse Liévin for all the help with french bureaucratic runaround.

I sincerely appreciate the efforts of the reviewers Valery Shcherbakov and Iwona Stachlewska together with Ulla Wandinger who served on my thesis jury.

Of course, I would not have been able to take the first steps of this without the continual love and support of my parents, Yury and Natalia, and my grandmothers Ann

and Dina.

I'm also thankful to AERONET for establishing and maintaining the sites used in this work. I'm grateful to the French CNRS (Centre National de la Recherche Scientifique) for the support of publication of my work. The research leading to these results has received funding from the European Union Seventh Framework Program (FP7/2007-2013) under the grant agreement №262254.

Author is also very thankful for the LaTeX developers community whose unselfish efforts made this thesis publication nice and easy.

To my parents.

Contents

Abstract iii

Acknowledgements vi

List of Tables xi

List of Figures xiii

1 Introduction **1**

1.1 Context 1

1.2 Motivation 6

1.3 Objectives 8

1.4 Thesis layout 9

2 Remote sensing of atmospheric aerosols **11**

2.1 Aerosol properties 11

2.1.1 Physical properties of atmospheric aerosols 12

2.1.2 Optical properties of atmospheric aerosols 17

2.2 Aerosol remote sensing 21

2.2.1 Remote sensing of the atmospheric aerosols by AERONET 29

2.2.2 Remote sensing of the atmospheric aerosols by active instruments 37

2.2.3 Remote sensing of the atmospheric aerosols by combination of active and passive instruments 45

3 GARRLiC algorithm description **51**

3.1 Forward model 53

3.1.1 Aerosol single scattering properties 58

3.1.2 Vector radiative transfer 65

3.1.3 Lidar equation 69

3.1.4 Vertical profiling of atmosphere optical properties 72

3.2 Numerical inversion 78

3.2.1 Observation fitting 81

3.2.2 A priori smoothness constraints 91

4 GARRLiC Algorithm functionality and sensitivity tests **100**

4.1 Description of aerosol and noise models used for sensitivity study . . 101

4.2 Sensitivity test results 105

4.3 Improvements introduced by joint inversion of lidar and AERONET 115

4.4 Improvements introduced by inclusion of almucantar measurement of linear polarization degree 120

5 GARRLiC applications to real lidar/sun-photometer observations **133**

6 Conclusion **158**

Bibliography **163**

A Article published in AMT **187**

List of Tables

2.1 Aerosol optical properties retrieved worldwide 22
2.2 Major satellite measurements available for the tropospheric aerosol characterization. 25
2.3 Major intensive field experiments relevant to aerosol research around the globe conducted in the past two decades 26
2.5 Major ground-based remote sensing networks for the tropospheric aerosol characterization and radiative forcing research 28
2.6 Observation angles for sky radiance measurements in the almucantar and principal plane geometries 34
2.7 Technical characteristics of the LIDARs installed at the Laboratory of Scattering Media 39

3.1 Observations used in the GARRLiC algorithm 54
3.2 Aerosol parameters retrieved by the GARRLiC algorithm 56
3.3 Values of parameters of the standard atmosphere 73
3.4 Values of coefficients used for molecular extinction and backscatter coefficients calculations 73
3.5 Description of the vector of unknowns of the GARRLiC algorithm . . 81
3.6 Values of the Lagrange multipliers used in the GARRLiC retrievals . 98

4.1 Parameters of log-normal size distributions used for size distribution modelling for application in GARRLiC sensitivity tests 103
4.2 Relative errors of the retrieval of the spherical particles fraction . . . 120

5.1 Estimations of noise parameters of the used lidar system 134

List of Figures

1.1 Micro-photographs of aerosol particle samples 2
1.2 Schematic diagram of various radiative mechanisms associated with aerosol and cloud interaction effects 3
1.3 Global average radiative forcing (RF) in 2005 4

2.1 SEM images of aerosol particles found in he atmosphere 12
2.2 Number, surface, and volume distributions for a typical aerosol model 14
2.3 A parallel light beam passing through a layer consisting of aerosol particles 18
2.4 The A-train constellation of spacecraft 23
2.5 Global map of the AERONET network 30
2.6 Principal plane and almucantar measurement geometries 32
2.7 Mono-static scheme of the lidar measurement 38
2.8 Map of the EARLINET lidar network 45

3.1 Principal scheme of the GARRLiC algorithm 52
3.2 General scheme of the Forward model of the GARRLiC algorithm . . 57
3.3 Comparison of desert dust phase function and degree of linear polarization simulated with spheroids and spherical aerosol model 61
3.4 Schematic representation of the contributions of the atmosphere radiance as measured by different instruments 66

3.5 General scheme of the measurements model using two-component vertically distributed aerosol model 75
3.6 Comparison of the data flow in LiRIC and GARRLiC algorithms . . 77
3.7 General scheme of numerical inversion 99

4.1 Retrievals of size distributions of "Dust" aerosol model under different noise conditions 106
4.2 Retrievals of size distributions of "Smoke" aerosol model under different noise conditions 107
4.3 Retrievals of size distributions of "Urban" aerosol model under different noise conditions 107
4.4 Retrievals of complex refractive index of "Dust" aerosol model for different AOTs under noise free and noisy conditions 109
4.5 Retrievals of complex refractive index of "Smoke" aerosol model for different AOTs under noise free and noisy conditions 110
4.6 Retrievals of complex refractive index of "Urban" aerosol model for different AOTs under noise free and noisy conditions 111
4.7 Retrievals of single-scattering albedo of "Dust" aerosol model under different noise conditions 112
4.8 Retrievals of single-scattering albedo of "Smoke" aerosol model under different noise conditions 112
4.9 Retrievals of single-scattering albedo of "Urban" aerosol model under different noise conditions 113
4.10 Retrievals of vertical distribution of "Dust" aerosol model under different noise conditions 114
4.11 Retrievals of vertical distribution of "Smoke" aerosol model under different noise conditions 115

4.12 Retrievals of vertical distribution of "Urban" aerosol model under different noise conditions 116
4.13 Dependencies of lidar ratios of fine and coarse modes on complex refractive index and shape 117
4.14 Retrieval errors of lidar ratios with and without accounting for lidar data 117
4.15 Retrieval of the aerosol size distribution with and without accounting of lidar data 119
4.16 Retrievals of size distribution for "Dust" aerosol model using intensity only almucantars and combined intensity and linear polarization almucantars in combination with lidar data 123
4.17 Retrievals of size distribution for "Smoke" aerosol model using intensity only almucantars and combined intensity and linear polarization almucantars in combination with lidar data 123
4.18 Retrievals of size distribution for "Urban" aerosol model using intensity only almucantars and combined intensity and linear polarization almucantars in combination with lidar data 124
4.19 Retrieval of the complex refractive index for "Dust" aerosol model using intensity only almucantars and combined intensity and linear polarization almucantars in combination with lidar data 124
4.20 Retrieval of the complex refractive index for "Smoke" aerosol model using intensity only almucantars and combined intensity and linear polarization almucantars in combination with lidar data 125
4.21 Retrieval of the complex refractive index for "Urban" aerosol model using intensity only almucantars and combined intensity and linear polarization almucantars in combination with lidar data 125

4.22 Retrieval of the vertical distribution for "Dust" aerosol model using intensity only almucantars and combined intensity and linear polarization almucantars in combination with lidar data 126
4.23 Retrieval of the vertical distribution for "Smoke" aerosol model using intensity only almucantars and combined intensity and linear polarization almucantars in combination with lidar data 127
4.24 Retrieval of the vertical distribution for "Urban" aerosol model using intensity only almucantars and combined intensity and linear polarization almucantars in combination with lidar data 128
4.25 Retrieval of the single-scattering albedo for "Dust" aerosol model using intensity only almucantars and combined intensity and linear polarization almucantars in combination with lidar data 129
4.26 Retrieval of the single-scattering albedo for "Smoke" aerosol model using intensity only almucantars and combined intensity and linear polarization almucantars in combination with lidar data 129
4.27 Retrieval of the single-scattering albedo for "Urban" aerosol model using intensity only almucantars and combined intensity and linear polarization almucantars in combination with lidar data 130
4.28 Retrieval of the lidar ratio for "Dust" aerosol model using intensity only almucantars and combined intensity and linear polarization almucantars in combination with lidar data 130
4.29 Retrieval of the lidar ratio for "Smoke" aerosol model using intensity only almucantars and combined intensity and linear polarization almucantars in combination with lidar data 131
4.30 Retrieval of the lidar ratio for "Urban" aerosol model using intensity only almucantars and combined intensity and linear polarization almucantars in combination with lidar data 131

5.1 Air mass back trajectories for the Minsk measurement site on 13.08.2010 134
5.2 Air mass back trajectories for the Minsk measurement site on 02.06.2008 135
5.3 Air mass back trajectories for the Lille measurement site on 14.05.2010 136
5.4 Retrieved aerosol size distribution during measurements at Minsk AERONET site on 02.06.2008 137
5.5 Retrieved aerosol size distribution during measurements at Minsk AERONET site on 13.08.2010 137
5.6 Retrieved aerosol size distribution during measurements at Lille AERONET site on 14.05.2010 138
5.7 Retrieved aerosol complex refractive index during measurements at Minsk AERONET site on 02.06.2008 138
5.8 Retrieved aerosol complex refractive index during measurements at Minsk AERONET site on 13.08.2010 139
5.9 Retrieved aerosol complex refractive index during measurements at Lille AERONET site on 14.05.2010 139
5.10 Retrieved aerosol vertical distribution during measurements at Minsk AERONET site on 02.06.2008 140
5.11 Retrieved aerosol vertical distribution during measurements at Minsk AERONET site on 13.08.2010 141
5.12 Retrieved aerosol vertical distribution during measurements at Lille AERONET site on 14.05.2010 141
5.13 Retrieved aerosol lidar ratios during measurements at Minsk AERONET site on 02.06.2008 142
5.14 Retrieved aerosol lidar ratios during measurements at Minsk AERONET site on 13.08.2010 143
5.15 Retrieved aerosol lidar ratios during measurements at Lille AERONET site on 14.05.2010 143

5.16 Retrieved aerosol single scattering albedo during measurements at Minsk AERONET site on 02.06.2008 145
5.17 Retrieved aerosol single scattering albedo during measurements at Minsk AERONET site on 13.08.2010 145
5.18 Retrieved aerosol single scattering albedo during measurements at Lille AERONET site on 14.05.2010 146
5.19 Retrieved vertical profile of aerosol single-scattering albedo during measurements at Minsk AERONET site on 02.06.2008 147
5.20 Retrieved vertical profile of aerosol single-scattering albedo during measurements at Minsk AERONET site on 13.08.2010 148
5.21 Retrieved vertical profiles of aerosol single scattering albedo during measurements at Lille AERONET site on 14.05.2010 149
5.22 Retrieved vertical profile of aerosol lidar ratio during measurements at Minsk AERONET site on 02.06.2008 149
5.23 Retrieved vertical profile of aerosol lidar ratio during measurements at Minsk AERONET site on 13.08.2010 150
5.24 Retrieved vertical profile of aerosol lidar ratio during measurements at Lille AERONET site on 14.05.2010 150
5.25 Retrieved vertical profiles of aerosol extinction during measurements at Minsk AERONET site on 02.06.2008 151
5.26 Retrieved vertical profiles of aerosol extinction during measurements at Minsk AERONET site on 13.08.2010 151
5.27 Retrieved vertical profiles of aerosol extinction during measurements at Lille AERONET site on 14.05.2010 152
5.28 Comparison of vertical profiles retrieved by GARRLiC and LiRIC inversions for the measurements performed at Minsk AERONET site on 02.06.2008 154

5.29 Comparison of vertical profiles retrieved by GARRLiC and LiRIC inversions for the measurements performed at Minsk AERONET site on 13.08.2010 154
5.30 Comparison of vertical profiles retrieved by GARRLiC and LiRIC inversions for the measurements performed at Minsk AERONET site on 14.05.2010 155
5.31 Achieved lidar measurements fits for the observations performed at Minsk AERONET site on 02.06.2008 155
5.32 Achieved lidar measurements fits for the observations performed at Minsk AERONET site on 13.08.2010 156
5.33 Achieved lidar measurements fits for the observations performed at Lille AERONET site on 14.05.2010 156

Chapter 1

Introduction

> The beginning is the most
> important part of the work.
>
> Plato

1.1 Context

Aerosol is defined as a suspension of solid particles or liquid droplets in a gas. Such particles suspended in the Earth atmosphere originating from natural (maritime winds, dust storms, volcanic eruptions, forest fires etc.) and anthropogenic (fossil fuel combustion, agricultural and industrial activities etc.) sources are referred as atmospheric aerosols. Figure 1.1 gives an incite on variability of the shape of aerosol particles, showing images from scanning electron microscope of *a*) particles from the Sahara desert, *b*) – particles from biomass burning fires in the Amazon (low temperature emissions after the fire), *c*) – a large cluster aggregate of high temperature emissions) and *d*) an example of air pollution particles from China.

Atmospheric aerosols are known to be important part of the complex physical-chemical processes that impact Earth's climate. Such impacts take their effects both on global and regional scales (D'Almeida et al., 1991; Charlson et al., 1992;

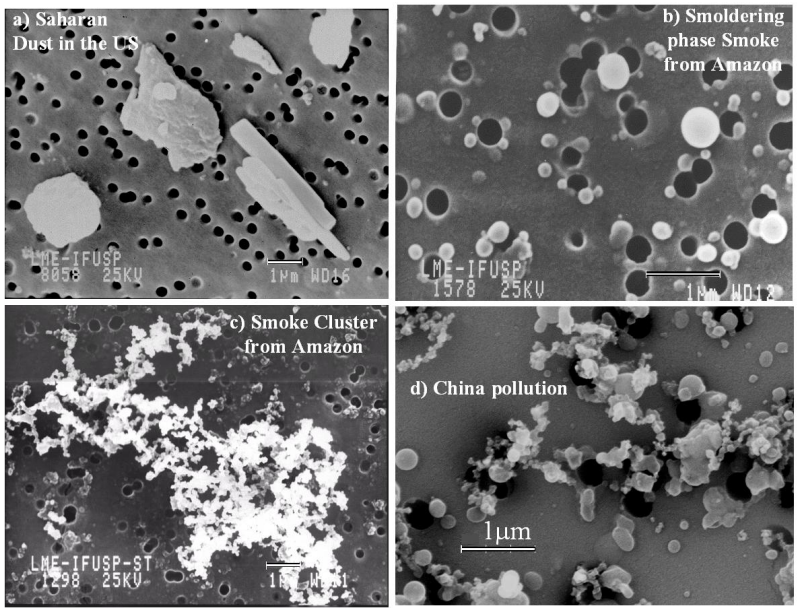

Figure 1.1: Micro-photographs of aerosol particle samples, taken from `http://alg.umbc.edu/usaq/archives/001044.html`.

Hobbs, 1993; Pilinis et al., 1995; on Climate Control , IPCC; Ramanathan et al., 2001; Forster et al., 2007; Hansen et al., 2011).

The effects of aerosol on the climate could be subdivided into three distinct groups including direct, indirect and semi-direct effects, shown in detail in Figure 1.2.

Direct aerosol effect is any direct interaction of atmospheric aerosol and radiation, such as scattering and absorption. The magnitude of the radiation forcing of the direct effects could be both positive and negative and depends on aerosol single-scattering albedo and on the albedo of underlying surface (Haywood and Shine, 1995; Haywood and Boucher, 2000).

The Indirect aerosol effect changes Earth's radiative budget due to the modification of clouds by atmospheric aerosols. The indirect effect could be subdivided in two different groups: Twomey (Twomey, 1974, 1977b) and Albreicht (Albrecht, 1989) effects. In Twomey effect aerosol affects cloud formation providing additional nuclei for droplet or ice crystals growth (Boucher, 1999; Lohmann et al., 2003; Lohmann and Feichter, 2005; Lohmann and Hoose, 2009). Second effect changes

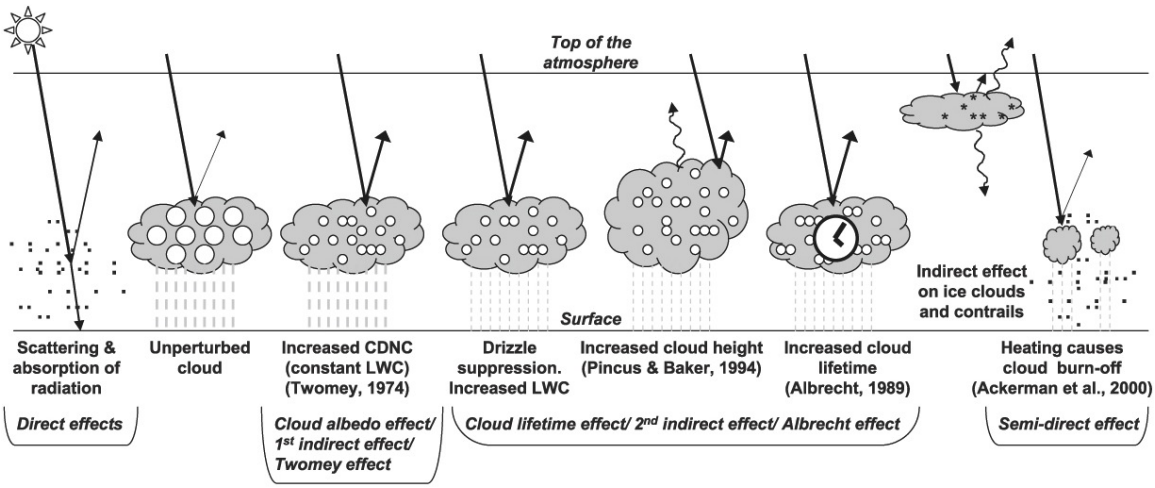

Figure 1.2: Schematic diagram showing the various radiative mechanisms associated with cloud effects that have been identified as significant in relation to aerosols; modified from Haywood and Boucher (2000).

clouds lifetime (Albrecht, 1989) and other cloud properties like liquid water content (LWC) and cloud top height (Pincus and Baker, 1994). All indirect effects are highly depending on aerosol quantity and cloud type (Feingold et al., 2003) and their estimation usually relies on additional model assumptions (Ackerman et al., 2000; Menon et al., 2002), as all the necessary information couldn't be provided by observations.

Semi-direct effect consists of modification the atmospheric temperature profile by absorbing aerosols, therefore affecting the presence of clouds. The impact of absorbing aerosols depends on their altitude (Koch and Del Genio, 2010) and the local meteorological conditions.

Anthropogenic particulate air pollution results in increased concentrations of fine particles in the air which is usually associated with lung function declines, increases in respiratory symptoms (Dockery et al., 1989; Pope et al., 1991; Pope and Dockery, 1992; Pope et al., 2002), lung cancer and cardiopulmonary mortality (Dockery et al., 1993; Pope et al., 1995; Schwartz et al., 1996; Pope et al., 2002).

Despite of the achieved progress in aerosol observation, the limited accuracy in

the knowledge of aerosol properties remains one of the main uncertainties in climate assessments. Reports on global climate change (on Climate Control , IPCC; Forster et al., 2007; Hansen et al., 2011) still indicate the level of scientific understanding of both direct and indirect aerosol effects on climate as "medium-low" and "low" correspondingly. Specifically, the columnar aerosol properties such as optical thickness, single-scattering albedo are important for direct aerosol forcing estimations both on global and regional scale (Pilinis et al., 1995; Costa et al., 2004). Such estimations could be improved by increasing both the accuracy of the basic aerosol optical properties estimations and detalization of spatial coverage of the aerosol observations.

On the other hand vertical structure of the aerosol is an important piece of informa-

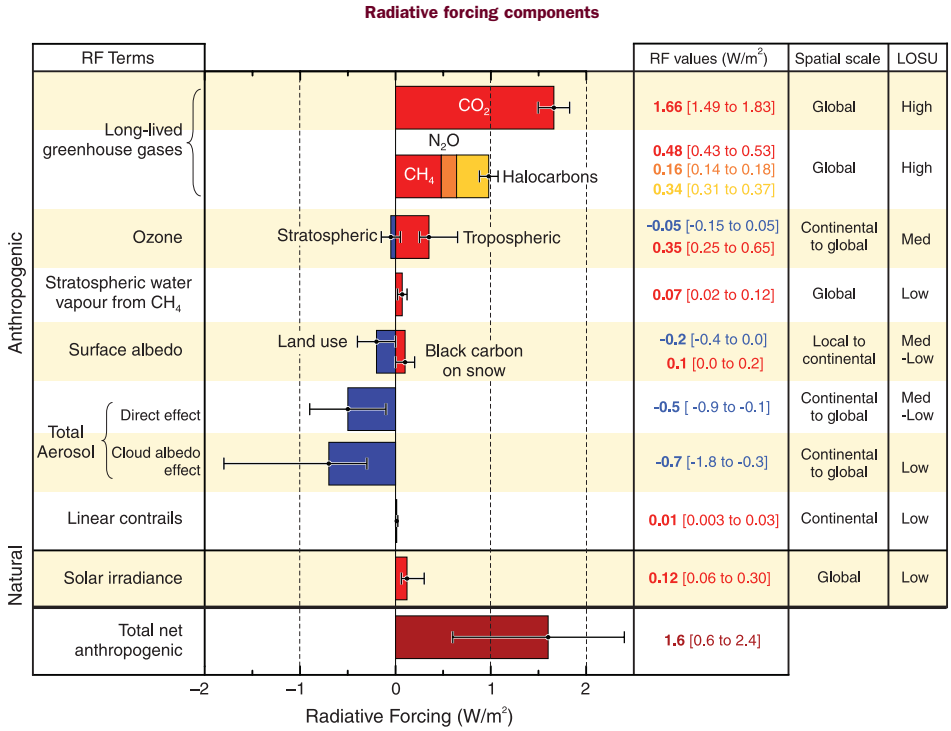

Figure 1.3: Global average radiative forcing (RF) in 2005 (best estimates and 5 to 95% uncertainty ranges) with respect to all important agents and mechanisms, together with the typical geographical extent (spatial scale) of the forcing and the assessed level of scientific understanding (LOSU); according to IPCC2007 (Forster et al., 2007).

tion needed for accounting of the indirect and semi-direct effects (McCormick et al., 1993; Bréon, 2006) mentioned above. In these regards, the aerosol columnar properties together with vertical profiles of aerosol are clearly complimentary pieces of information, both important for climatic studies.

The importance of obtaining simultaneous information about both columnar and vertical aerosol properties is rather evident for scientific community, and in order to estimate mentioned impacts large variety of methods for monitoring atmospheric aerosols were developed. Among others remote sensing methods, that in a contrast with the in-situ studies do not need a physical contact with the aerosol to acquire information about its properties, proved to be fruitful and convenient. Two main types of remote sensing could be distinguished:

- passive remote sensing
- active remote sensing

In general passive sensors detect natural radiation that is scattered or reflected by the aerosol or surrounding areas. Reflected or scattered sunlight is the most common source of radiation measured by passive sensors. Development of passive remote sensors begun from film photography resulting in charge-coupled devices and radiometers. On the other hand, active observation starts with energy emittance in order to scan aerosol and areas whereupon a sensor then detects and measures the radiation that is reflected or backscattered from the target. RADAR (RAdio Detection And Ranging) and LIDAR (LIght Detection And Ranging) are examples of active remote sensing techniques where the time delay between emission and return is measured, allowing to establish the location and, in some cases, velocity of the layer of aerosol particles.

Each of the approaches has its own particularities and provides different data on aerosol optical and microphysical properties based on a set of assumptions. Passive

observations, for example, have limited sensitivity to the variability of vertical distribution of different aerosol layers, while they provide some indication of possible aerosol mixtures. On the other hand, spectral lidar measurements are sensitive to variations of aerosols particle sizes and shape and can trace rather clear qualitative picture of aerosol vertical mixture.

1.2 Motivation

The expected improvements in the aerosol monitoring are associated with enhancement of the observation completeness by means of employing variety of complimentary observational techniques and with improvement in the accuracy of derived aerosol information. Therefore, lately more and more aerosol monitoring sites are equipped with several instruments (Takamura et al., 1994; Waquet et al., 2005; Müller et al., 2004; Ansmann et al., 2010) and a number of extensive multi-instrumental aerosol campaigns have been organized (Ramanathan et al., 2001; Müller et al., 2003; McKendry et al., 2007; Papayannis et al., 2005; Holben et al., 2011). At present, there is a variety of orbital platforms equipped with passive and active instruments (Bréon et al., 2002; Stephens et al., 2002) and a substantial number of sites within ground-based networks that conduct co-incident lidar and photometric measurements provide a vast database of joint passive/active aerosol observations.

The availability of a variety of observations results not only in positive accumulation of complementary data, but it also serves for improving the accuracy of obtained data and deriving qualitatively new aerosol characteristics. Indeed, processing of both passive and active remote measurements relies on a set of several assumptions. The uncertainties in this assumption may have noticeable effect on the retrieval result, especially in a case of polarimetric observations. Retrievals from active

sounding, on the other hand, deal with relatively limited information from the altitude profiles of the spectral backscattering and usually rely on some assumptions about aerosol columnar properties. However, inconsistencies in these estimations directly propagate into derived results and may strongly affect the lidar retrievals (Sasano et al., 1985; Kovalev, 1995). The most reliable and, therefore, preferable approach is to define these properties by developing enhanced lidar capabilities or by means of transfer of missing information from another instruments (Ferrare et al., 1998b; Gobbi et al., 2003). All these approaches using non-elastic observations result in significant enhancement of the information contents in backscattering observations what allows derivation of profiles of aerosol properties without a-priori constraints on aerosol type or loading (Müller et al., 1999, 2005; Veselovskii et al., 2004).

In addition to such straightforward methods, several more sophisticated approaches of combining two types of measurements were proposed recently for exploring additional sensitivities in both lidar and photometric observations (Chaikovsky et al., 2002a; Cuesta et al., 2008). Such methods are usually aimed not only at improving accuracy of the retrieved aerosol characteristics, but rather retrieving qualitatively new aerosol information.

Utilization of lidar data in a combination with co-incident radiometric data allows some quantitative description of vertical distribution of aerosol layers, for example, when background aerosol is mixed with layers of transported aerosols as those from desert dust or biomass burning aerosols (Chaikovsky et al., 2004). Ground-based radiometric data have practically no sensitivity to the variability of vertical distribution of different vertical layers, while they provide some indication of possible aerosol mixtures. On the other hand, spectral lidar measurements sensitive to variations of aerosols sizes and polarimetric lidar measurements sensitive to aerosol particle shape can trace rather clear qualitative picture of aerosol vertical mixing.

1.3 Objectives

The main objectives of this PhD work is to explore the possibilities of the advanced aerosol remote sensing by means of combination of passive and active instruments and contribute to the aerosol remote sensing efforts. As it seen from above, at present the most advanced methods that involve active and passive remote sensing in aerosol characterization (Chaikovsky et al., 2002a; Cuesta et al., 2008) are aimed at enhanced processing of lidar data and do not include any feedback of aerosol columnar properties. But at the same time, lidar measurements provide some additional sensitivity to columnar properties of aerosol compared to radiometric data that could be used.

The primary objective is to develop a new retrieval method that pursues a deep synergy of lidar and sun-photometer data in the retrievals. The approach proposed in this work is aimed to take advantage from all sensitivities in lidar and radiometric data to both vertical and columnar aerosol properties. In order to achieve that, the retrieval should be designed as simultaneous fitting of both lidar and sun-photometer data by a single set of aerosol parameters describing both vertical and columnar properties of aerosol. In such approach lidar data can affect retrieval of columnar as well as vertical properties of aerosol.

To achieve this objective, a unified aerosol model suitable for description of both columnar and vertical variability of aerosol optical properties should be developed. At the same time this model should utilize the positive heritage of the aerosol modelling achieved in the previous studies (Dubovik and King, 2000; Dubovik et al., 2006), be simple (in terms of quantity of parameters used to describe the model and ease of their interpretation) and yet applicable for use with large variety of available remote sensing instruments.

Such approach should minimize the amount of a-priori estimations used in aerosol retrievals, and it is expected to provide more accurate information about both vertical and columnar properties of aerosol.

The last but not least objective of this work is to test the realization of the proposed method in a variety of realistic application scenarios, including both synthetic and real data.

1.4 Thesis layout

This PhD-thesis is structured into five logical parts, each describing a milestone in proposed method development.

First chapter provides an insight on the overall situation in the field of study followed by the objectives and structural outline of this work.

Second chapter is dedicated to the atmospheric aerosols and their properties, as well as to the remote sensing techniques both passive and active, including their sensitivity analysis and discussion of approaches and perspectives of different measurements combinations in the aerosol retrievals.

Third chapter contains detailed description of the proposed method, focusing on the assumptions implied in aerosol forward modelling, and adjustments introduced in the retrieval routines in comparison with the standard AERONET inversion.

Fourth chapter deals with the sensitivity study, dedicated to illustrate both the possibilities and limitations of the proposed method. In this chapter we provide an insight of the aerosol properties of the "Dust" (coarse mode predominant, absorbing, non spherical), "Smoke" (fine mode predominant, non-absorbing) and "Urban" (fine, absorbing) aerosol models selected from AERONET climatology for the sensitivity study. It also contains the description of the testing approach as well as the discussion of the retrieved results, including algorithm performance under different aerosol loads and measurements combinations. This chapter also studies how the presence of random noise in the measurements affects the retrievals.

Fifth chapter contains illustrations and discussion of the algorithm performance in a

variety of typical real observational situations, as well as comparison of the retrieval results with the alternative methods.

The last part of the PhD-thesis contains the conclusions and outlook of the whole work. The article published on the base of results of this work (Lopatin et al., 2013) is presented in Appendix A.

Chapter 2

Remote sensing of atmospheric aerosols

> Copy from one, it's plagiarism; copy from two, it's research.
>
> Wilson Minzer

2.1 Aerosol properties

Aerosol particles in the atmosphere could be principally characterized by the two sets of properties: physical and optical. The first set describes size, shape and composition of the particles and widely used in in-situ aerosol observations, while the second set is more used in remote sensing applications and describes the aerosol particles from the point of their interaction with light. On the other hand from the point of remote sensing it is more suitable to characterize optical properties of the atmospheric aerosols. Both this descriptions are connected through the efforts of modelling of optical properties of aerosol particles.

2.1.1 Physical properties of atmospheric aerosols

The properties of the aerosols in the atmosphere depend directly on the source and formation mechanism of the particles. By the source aerosols could be rather anthropogenic or natural, whilst primary or secondary aerosols are distinguished by the formation. Aerosol particles could be characterized by thee basic parameters, describing their micro physical properties such as shape, size and composition.

The *shape* of aerosol particles is very variable and may be irregular, whereas droplet aerosols are mostly spherical. Scanning electron microscopy (SEM) studies have shown that solid aerosol particles could have different shapes, e.g., cubic (salts), lattice (dust), agglomerates of spheres (soot) and spherical (see Figure 2.1). Particle shape can affect its surface area, aerodynamic behaviour and optical properties.

Particle size is one of the most important parameters for characterizing the aerosol

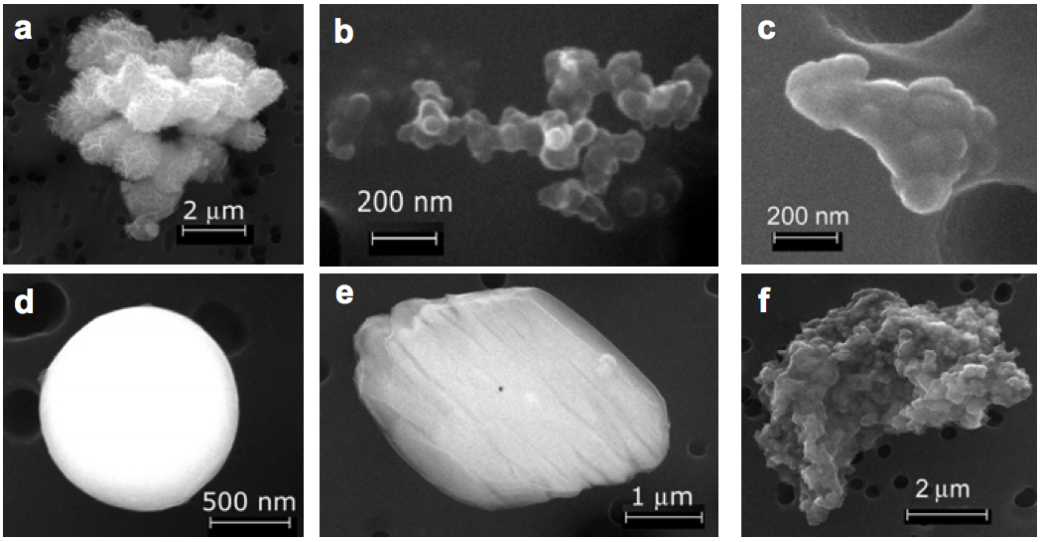

Figure 2.1: Secondary electron images of different types of aerosol particles found in he atmosphere obtained from a Scanning Electron Microscope a) iron-silicon, b) soot c) organic d) iron e) calcium f) silicon-aluminium; adapted from Targino (2005).

behaviour. Description of the size of aerosol particles could be difficult because of the complex shapes which some particles have. To address this problem an equivalent diameter is often used, which is defined as the diameter of a sphere that has the

same value of a particular physical property as that of the irregular particle (Hinds, 1999). A number of different types of equivalent diameters are currently in use, e.g. equivalent volume diameter, equivalent optical diameter and equivalent aerodynamic diameter (Hinds, 1999). The diameters of atmospheric aerosols span over four orders of magnitude, from a few nano-meters to around 100 μm. Atmospheric aerosols are normally classified into separate modes according to their size, formation process and atmospheric age.

Based on the number, surface, and volume distributions of aerosol particles (see Figure 2.2), four distinct groups of atmospheric particles can be defined. The smallest particles with diameters not exceeding 0.01 μm (not shown in Figure 2.2) are known as *ultrafine* particles. They are thought to be generated by gas-to-particle conversion processes. Because of their very small size and mass, they are difficult to study with the available measurement techniques. These particles have been observed in bursts of very large numbers in the presence of either biogenic or anthropogenic emissions under favourable local conditions in many different environments, including forests (Kulmala et al., 2004) and coastal zones (O'Dowd et al., 2002), and have been referred to as the nucleation mode. These particles are only observed as a distinct mode at their source and have a very short lifetime, some times on the order of minutes, due to their rapid coagulation or random impaction onto surfaces.

The Aitken mode particles, extending from 0.01 to 0.1 μm in diameter, are formed from ambient-temperature gas-to-particle conversion as well as condensation of hot vapours during combustion processes. These particles act as nuclei for the condensation of low-vapour pressure gaseous species, causing them to grow into the bigger mode. The lifetime of these particles is short, as they are lost principally by coagulation with larger particles. The Aitken and accumulation mode particles are collectively referred to as *fine* particles.

Particles with diameters between 0.1-1.0 μm are considered as the *accumulation*

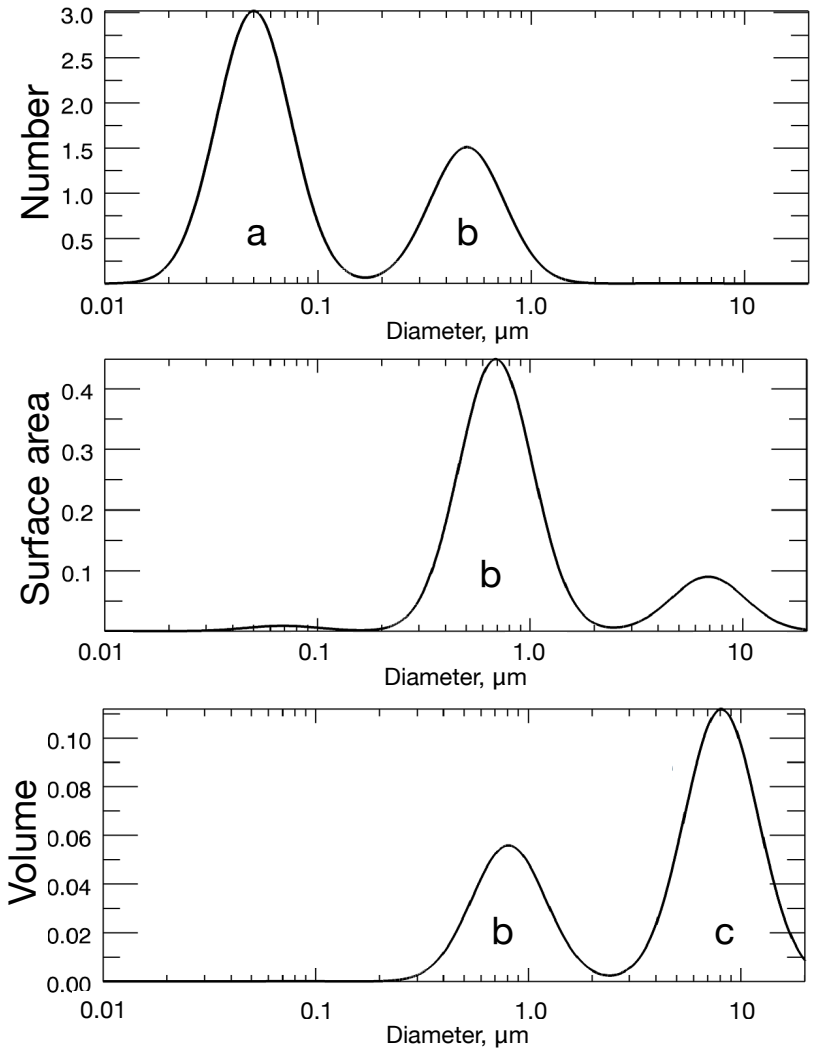

Figure 2.2: Number, surface, and volume distributions for the same log-normal aerosol distribution of a typical aerosol model, a) Aitken mode, b) Accumulation mode and c) Coarse mode. Each distribution is normalised so that the total area is 1; modified from Seinfeld and Pandis (1998).

mode, representing a region of particle growth mainly due to the condensation of vapours onto existing particles and coagulation of the Aitken mode particles, causing them to grow into this size range. They can also be introduced directly into the atmosphere, mainly through the incomplete combustion of wood, oil, coal, gasoline and other fuels. Because of the nature of their sources, particles in the accumulation size range generally contain substantial amounts of organic material as well as soluble inorganics such as ammonium, nitrate and sulphate. The accumulation mode is named so because particle removal mechanisms are least efficient in this regime, causing particles to accumulate in the atmosphere until they are ultimately lost through different forms of precipitation (so called wet deposition).

The final type of particles are identified as the *coarse mode* and have diameters larger than 1.0 μm. These particles are mainly produced by mechanical processes and introduced directly into the atmosphere from both natural and anthropogenic sources. The most significant source is the bursting of bubbles in the ocean, which creates coarse particles of sea salt. The wind also picks up dust, soil and biological particles and suspends them in the air. Anthropogenic coarse particles are introduced into the atmosphere through the industrial and agricultural processes, and the abrasion of machinery and on the surface of roads. Because of their relatively large size, coarse particles settle out of the atmosphere in a reasonably short time by sedimentation, except on windy days, where fallout is balanced by re-entrainment.

Both the nucleation and Aitken mode particles account for the majority of atmospheric particles by number, but due to their small sizes, they rarely account for more than a few percent of the total mass. Hence the toxicological effects are determined primarily by the number of particles, rather than their mass, these small particles could ultimately prove to be of high importance. The accumulation mode particles generally account for a significant fraction of the total aerosol mass and have the greatest surface area. This makes these particles to be very important to

gas phase deposition and atmospheric heterogeneous chemistry. Most of the aerosol mass is found in the coarse mode, where large particles contribute significantly to the optical properties of atmospheric aerosols. All these modes, in general, originate separately, are transformed separately, are removed from the atmosphere by different mechanisms, have different lifetimes, have different chemical composition and have different optical properties. Therefore, the distinction of particles between nucleation, Aitken, accumulation and coarse modes is a fundamental one in any discussion of the physics, chemistry, or measurement of aerosols.

Knowledge of the *chemical composition* of atmospheric aerosol particles is necessary for identifying their sources and accounting for their effect on various atmospheric processes. According to IPCC 2001 (IPCC, 2001), aerosols are mostly composed of variable amounts of water, crustal elements, carbonaceous material, sulphate, ammonium, nitrate, sodium, chloride and traces of metals.

Crustal materials originate from soil dust and windblown minerals and are contained mostly in the coarse particle fraction. Their composition varies greatly according to local geology and surface conditions.

The carbonaceous fraction of the aerosols is presented by elemental and organic carbon. Elemental carbon (black carbon, graphitic carbon or soot) is emitted directly into the atmosphere, predominantly from combustion processes. Particles containing organic carbon can be not only directly emitted into the atmosphere (e.g., from biomass burning and combustion), they can also be introduced by secondary organic aerosol formation, which occurs when volatile organic compounds undergo atmospheric oxidation reactions and form the products that have volatilities low enough to form aerosol via nucleation or gas-to-particle partitioning (Hoffmann et al., 1997; Kamens and Jaoui, 2001).

The sulphate component is derived predominantly from the atmospheric oxidation of anthropogenic and natural sulphur-containing compounds, such as sulphur diox-

ide and dimethyl sulphide respectively. Sulphate in aerosol particles is present as sulphuric acid, ammonium sulphate, and intermediate compounds, depending on the availability of gaseous ammonia to neutralize the sulphuric acid formed from SO_2 (Adams et al., 1999). Nitrate is formed mainly from the oxidation of atmospheric nitrogen dioxide (NO_2).

The main source of chlorides is sea spray, even at distant locations from the coast. Sea salt particles cover a wide size range ($0.05 < d < 10\ \mu m$), and have a correspondingly wide range of atmospheric lifetimes. This aerosol is dominant contributor to both light scattering and cloud nuclei. It is very efficient cloud condensation nuclei, making them an important part of aerosol indirect effects (Gong et al., 1998). Chlorides also enter atmospheric particles as a result of ammonia neutralisation of vapour of hydrochloric acid, which is emitted from such anthropogenic sources as power stations and incinerators.

2.1.2 Optical properties of atmospheric aerosols

In the most general way light scattering on aerosol particles could be described as a plane electro-magnetic wave scattered in the direction of the unit vector **z**:

$$\begin{aligned} E_{\parallel} &= A_{\parallel} e^{i\left(\varpi t - kz - \phi_{\parallel}\right)}, \\ E_{\perp} &= A_{\perp} e^{i(\varpi t - kz - \phi_{\perp})}, \end{aligned} \tag{2.1}$$

where $A_{...}$ denotes the component electro-magnetic amplitude, $\phi_{...}$ is the phase, t indicates the time, k is the wave number ($k = \frac{2\pi}{\lambda}$, where λ is wavelength), ϖ is the angular frequency and $i = \sqrt{-1}$. If the plane of scattering is defined to include both the vectors pointing in the incident and scattering directions, $E_{\parallel}$ is the electric field parallel and $E_{\perp}$ is the electric field perpendicular to this plane. Electromagnetic radiation is often described as a four element vector. One of the possible formulations

is the Stokes vector $\mathbf{I}$ (van de Hulst, 1957):

$$\mathbf{I} = \begin{pmatrix} I \\ Q \\ U \\ V \end{pmatrix}, \quad \begin{aligned} I &= \left\langle E_\parallel E_\parallel^* + E_\perp E_\perp^* \right\rangle, \\ Q &= \left\langle E_\parallel E_\parallel^* - E_\perp E_\perp^* \right\rangle, \\ U &= \left\langle E_\parallel E_\perp^* + E_\perp E_\parallel^* \right\rangle, \\ V &= -i \left\langle E_\parallel E_\perp^* - E_\perp E_\parallel^* \right\rangle, \end{aligned} \tag{2.2}$$

where $\langle \ldots \rangle$ indicates time averaging, and * denotes the complex conjugation. The Stokes vector element I is the intensity, which is equal to the rate of energy flow across a unit area perpendicular to $\mathbf{z}$ (Wm^{-2}). The magnitude and direction of linearly polarized intensity could be expressed with the vector elements Q and U, while the V component describes the circular polarization. Such polarization formulation is commonly used due to a convenient representation for numerical modelling of multiple scattering problems, and because it provides a straightforward expression of easily obtained observations. A parallel light beam passing through a layer of aerosol par-

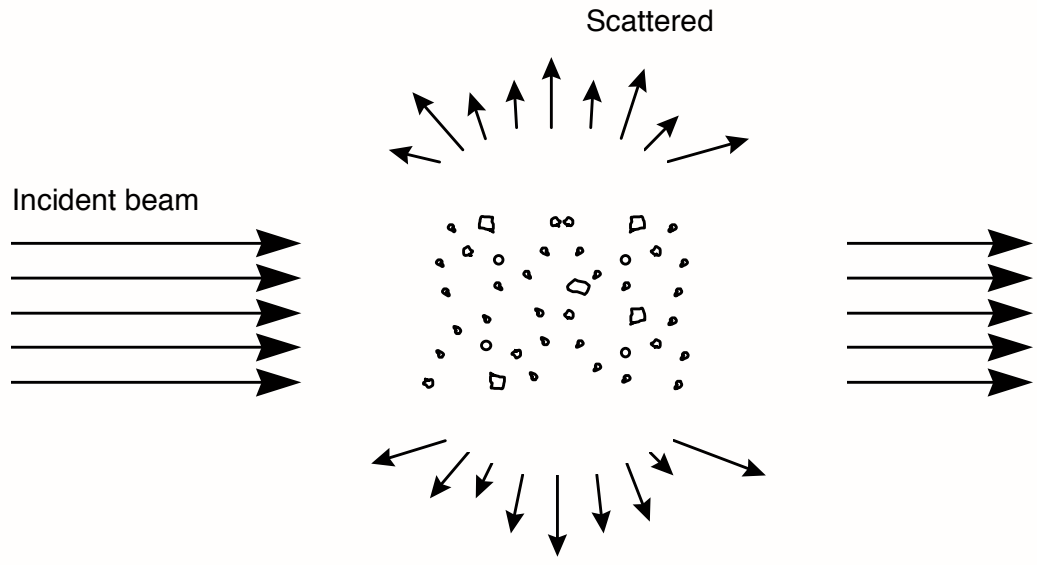

Figure 2.3: A parallel light beam passing through a layer consisting of aerosol particles. The incident beam is attenuated by scattering and absorption. The scattered light is re-distributed over all directions.

ticles is attenuated by absorption and scattering (see Figure 2.3). The one of major optical properties of the aerosol that is involved in the extinction of light is *refractive index*. Its complex value is determined as:

$$m = n + i\kappa, \tag{2.3}$$

where $n = \mathrm{Re}(m)$ is the real part and $\kappa = \mathrm{Im}(m)$ is the imaginary part of the complex refractive index. The real part n defines the speed of propagation of the electromagnetic wave in the medium and defines the deflection of light by the particle. The imaginary part κ is connected to the absorption properties of aerosols. The complex refractive index could be incorporated in 2.1 by relating the wave number to the refractive index through $k = \frac{2\pi m}{\lambda_0}$, where λ_0 is the wavelength in vacuum. This will transform 2.1 into:

$$\begin{aligned} E_{\parallel} &= e^{\frac{-2\pi\kappa z}{\lambda_0}} A_{\parallel} e^{i\left(\varpi t - \frac{-2\pi n z}{\lambda_0} - \phi_{\parallel}\right)}, \\ E_{\perp} &= e^{\frac{-2\pi\kappa z}{\lambda_0}} A_{\perp} e^{i\left(\varpi t - \frac{-2\pi n z}{\lambda_0} - \phi_{\perp}\right)}. \end{aligned} \tag{2.4}$$

Thus, considering equation 2.2, Eq. 2.4 forms into a variation of the Bouger-Lambert-Beer law, with *absorption coefficient* $\sigma_a = \frac{4\pi\kappa}{\lambda_0}$. Generally the attenuation from the initial intensity is described by the *extinction coefficient* $\sigma_e(\lambda)$ that is defined as the fraction of intensity lost from a collimated beam per unit of layer thickness at the given wavelength λ (units of m^{-1} or km^{-1}. This coefficient can be considered as the sum of the the *absorption coefficient* $\sigma_a(\lambda)$ and *scattering coefficient* $\sigma_s(\lambda)$:

$$\sigma_e(\lambda) = \sigma_a(\lambda) + \sigma_s(\lambda). \tag{2.5}$$

The relative contribution of absorption to the extinction by aerosol particles is usually expressed by aerosol *single-scattering albedo* ω_0, which is defined as the ratio between

particle scattering and particle extinction coefficient:

$$\omega_0(\lambda) = \frac{\sigma_s}{\sigma_e}. \tag{2.6}$$

Another important optical property of atmospheric aerosols is the *total column aerosol optical depth* (AOD), which is defined as integration of the aerosol extinction coefficient of the layers $\sigma_e(\lambda, h)$ over a vertical path of a light beam from the ground to the top of the atmosphere (TOA):

$$\tau(\lambda) = \int_0^{h_{TOA}} \sigma_e(\lambda, h)\, dh. \tag{2.7}$$

The angular distribution of the scattered electromagnetic wave in the far field, where the distance between the scattering particle and the observation location is much larger than wavelength, is characterized by the *phase matrix* $\mathbf{P}(\Theta)$. The phase matrix specifies the directionality of scattering, and transformation matrix from the incident Stokes vector $\mathbf{I}_i$ to the scattered vector $\mathbf{I}_s$:

$$\mathbf{I}_s \propto \mathbf{P}(\Theta)\, \mathbf{I}_i, \tag{2.8}$$

where Θ is the scattering angle. The element $P_{11}(\Theta)$ of the phase matrix is called the scattering phase function and for non-polarized light satisfies the following normalization condition:

$$\frac{1}{2}\int_0^{\pi} \sin(\Theta)\, P_{11}(\Theta)\, d\Theta = 1. \tag{2.9}$$

Generally, $\mathbf{P}(\Theta)$ is a 4x4 element matrix. In certain conditions, it can be reduced to six individual elements, rather than the full sixteen, thus transforming Equation 2.8

into:

$$\begin{pmatrix} I_s \\ Q_s \\ U_s \\ V_s \end{pmatrix} \propto \begin{pmatrix} P_{11}(\Theta) & P_{12}(\Theta) & 0 & 0 \\ P_{12}(\Theta) & P_{22}(\Theta) & 0 & 0 \\ 0 & 0 & P_{33}(\Theta) & P_{34}(\Theta) \\ 0 & 0 & -P_{34}(\Theta) & P_{44}(\Theta) \end{pmatrix} \begin{pmatrix} I_i \\ Q_i \\ U_i \\ V_i \end{pmatrix}, \tag{2.10}$$

Such reduction could be made under one of the following conditions:

- a group of randomly oriented particles, each with a plane of symmetry (such as spheres or spheroids),
- a group of randomly oriented particles with an equal number of mirror particles,
- a group of particles that are much smaller than the wavelength of radiation so the theory of Rayleigh scattering can be used to determine the scattering matrix.

The typical observed values for the optical properties of key types of atmospheric atmospheric aerosols are summarized in the Table 2.1 (Dubovik et al., 2002a).

2.2 Aerosol remote sensing

All methods of atmospheric aerosol remote sensing could be divided into two groups: (i) active and (ii) passive, both proved to be fruitful and convenient in atmospheric aerosol characterization. Passive observations most commonly detect and measure natural sun radiation that is transmitted and scattered by the aerosol in the atmosphere or reflected from the underlying surface. Passive remote sensors for aerosol observation include radiometers, photometers and polarimeters.

Active observations, on the other hand, emit energy in order to scan atmosphere whereupon a sensor then detects and measures the radiation that is backscattered by

Table 2.1: Summary of Aerosol optical properties retrieved worldwide from AERONET network of ground-based radiometers; adapted from (Dubovik et al., 2002a). All spectral parameters are given for wavelengths $\lambda = 0.44$, 0.67, 0/87 and 1.02 μm correspondingly if not indicated.

Site	τ_{min}	$\langle\tau\rangle$	τ_{max}	n	$\kappa(\lambda)$	$\omega_0(\lambda)$
Urban - Industrial and mixed						
GSFC, Greenbelt, MD	0.1	0.24(0.44)	1.0	$1.41 - 0.03\tau$ ± 0.01	0.003 ± 0.003	0.98/0.97/0.96/0.95 $\pm$ 0.02
Mexico city	0.1	0.43(0.44)	1.8	1.47 ± 0.03	0.014 ± 0.07	0.90/0.88/0.85/0.83 $\pm$ 0.02
Biomass burning						
African savanna, Zambia	0.1	0.38(0.44)	1.5	1.51 ± 0.01	0.021 ± 0.004	0.88/0.84/0.80/0.78 $\pm$ 0.015
Desert dust and oceanic						
Solar-Village, Saudi Arabia	0.1	0.17(1.02)	1.5	1.56 ± 0.03	0.0029/0.0013 /0.001/0.001 $\pm$ 0.001	0.92/0.96/0.97/0.97 $\pm$ 0.02
Lanai, HI	0.01	0.04(1.02)	0.2	1.36 ± 0.01	0.0015 ± 0.001	0.98/0.97/0.97/0.97 $\pm$ 0.03

the aerosol. LiDAR systems are widely used examples of active remote sensing, where the time delay between emission and return of laser pulse is measured, providing information about the aerosol altitude and location.

A number of developed and launched space instruments Bréon et al. (2002); Winker et al. (2007) provide global monitoring of aerosol properties King et al. (1999); Kokhanovsky et al. (2007). Satellite remote sensing is the only means of characterizing the large spatial and temporal heterogeneities of aerosol distributions. Monitoring aerosols from space has been performed for over two decades and is planned for the coming decade with enhanced capabilities King et al. (1999); Forster et al. (2007); Mishchenko et al. (2007). Table 2.2 summarizes major satellite measurements currently available for the tropospheric aerosol characterization and radiative forcing research.

Over the past decade, satellite aerosol retrievals have become increasingly sophisticated. Now, satellites measure the angular dependence of radiance and polarization

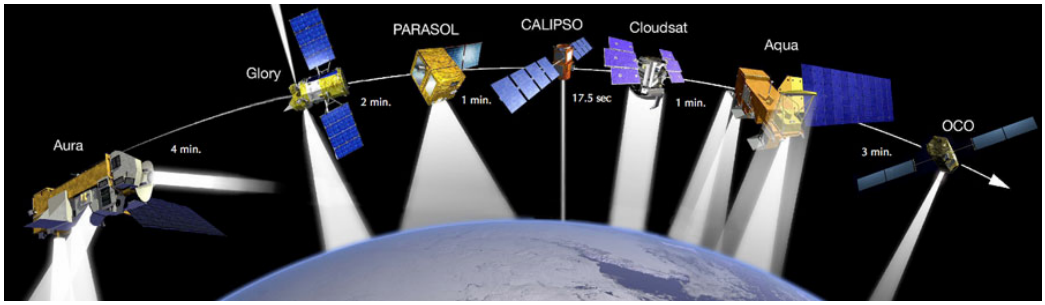

Figure 2.4: The constellation of spacecraft that overfly the Equator at about 1:30 PM, the so-called A-Train consists of four satellites, with another two failed (Glory and OCO), and one no longer in the constellation (PARASOL); adapted from `http://www-calipso.larc.nasa.gov/about/atrain.php`.

at multiple wavelengths from ultra violet (UV) through the infrared (IR) at fine spatial resolution. From these observations, retrieved aerosol products include not only optical depth at one wavelength, but also spectral optical depth and some information about particle size over both ocean and land, as well as more direct measurements of polarization and phase function. In addition, cloud screening is much more robust than before and on-board calibration is now widely available. Examples of such new and enhanced sensors include among others the MODerate resolution Imaging Spectro-radiometer (MODIS), the Multi-angle Imaging Spectro-Radiometer (MISR) and Polarization and Directionality of the Earth's Reflectance (POLDER). Complementary to these passive sensors, active remote sensing from space is also now possible and ongoing (see Table 2.2). Both the Geo-science Laser Altimeter System (GLAS) and the Cloud and Aerosol Lidar with Orthogonal Polarization (CALIOP Winker et al., 2010) are collecting essential information about aerosol vertical distributions. Furthermore, the constellation of six afternoon-overpass spacecrafts (as illustrated in Figure 2.4), the so-called A-Train (Stephens et al., 2002) makes it possible for the first time to conduct near simultaneous (within 15-minutes) measurements of aerosols, clouds, and radiative fluxes in multiple dimensions with sensors in complementary capabilities (Pelon et al., 2011).

Over the past two decades, numerous focused field campaigns have examined the physical, chemical, and optical properties and radiative forcing of aerosols in a variety of aerosol regimes around the world, as listed in Table 2.3. These campaigns, which have been designed with aerosol characterization as the main goal or as one of the major themes in more interdisciplinary studies, were conducted mainly over or downwind of known continental aerosol source regions, but in some instances in low-aerosol regimes. During each of these comprehensive campaigns, aerosols were studied in great detail, using combinations of in-situ and remote sensing observations of physical and chemical properties from various platforms (e.g., aircraft, ships, satellites, and ground-based stations). In spite of their relatively short duration, these field studies have acquired comprehensive data sets of regional aerosol properties that have been used to understand the properties and evolution of aerosols within the atmosphere and to improve the climatology of aerosol micro-physical properties used in Chemistry and Transport Models and satellite retrieval algorithms.

Observations by ground-based instruments generally provide more detailed and accurate information about aerosol properties Nakajima et al. (1996); Dubovik and King (2000) but cover only local area nearby the observation site. In order to obtain such data at extended geographical scales, the ground-based observations are often collected within observational networks employing identical instrumentation and standardized data processing procedures. At present, there are a number of global and regional networks conducting both passive and active ground-based observations. For example, global AERONET (Holben, 1998) and South-Eastern SKYNET (Nakajima et al., 2007) networks of sun photometers, as well as, a variety of lidar networks including regional EARLINET (Bösenberg, 2000), ADNET (Murayama and et al., 2000), MPL-Net (Welton and et al., 2002), ALiNe (Antuña et al., 2006), Cis-Linet (Chaikovsky et al., 2006a) and a recent global lidar network GALION (Bösenberg and Hoff, 2007; Wandinger et al., 2004) have been

Table 2.2: Summary of major satellite measurements currently available for the tropospheric aerosol characterization and radiative forcing research; adapted from Chin (2009).

Category	Properties	Sensor/ Platform	Parameters	Spatial coverage	Temporal coverage
Column-integrated	Loading	AVHRR/NOAA-series	Optical depth	~ daily coverage of global ocean	1981-present
		TOMS/Nimbus, ADEOS1, EP		~ daily coverage of global land and ocean	1979 -2001
		POLDER-1, -2, PARASOL			1997-present
		MODIS/Terra, Aqua			2000-present (Terra) 2002-present (Aqua)
		MISR/Terra		~ weekly coverage of global land and ocean, including bright desert and nadir sun-glint	2000-present
		OMI/Aura		~ daily coverage of global land and ocean	2005-present
	Size shape	AVHRR/NOAA-series	Ångström exponent	global ocean	1981-present
		POLDER-1, -2, PARASOL	fine-mode fraction, Ångström exponent, non-spherical fraction	global land+ocean	1997-present
		MODIS/Terra, Aqua	fine-mode fraction	global land+ocean (better quality over ocean)	2000-present (Terra) 2002-present (Aqua)
			Ångström exponent		
			effective radius	global ocean	
			asymmetry factor		
		MISR/Terra	Ångström exponent, small, medium, large fractions, non-spherical fraction	global land+ocean	2000-present
	Absorption	TOMS/Nimbus, ADEOS1, EP	absorbing aerosol index, single-scattering albedo, absorbing optical depth	global land+ocean	1979 -2001
		OMI/Aura			2005-present
		MISR/Terra	single-scattering albedo (2-4 bins)		2000-present
Vertically resolved	Loading, size, and shape	GLAS/ICESat	extinction/backscatter	global land+ocean, 16-day repeating cycle, single-nadir measurement	2003-present (~3months/ year)
		CALIOP/CALIPSO	extinction/backscatter, color ratio, depolarization ratio		2006-present

Table 2.3: List of major intensive field experiments that are relevant to aerosol research in a variety of aerosol regimes around the globe conducted in the past two decades; updated from Chin (2009).

Aerosol regimes	Name	Location	Time period	Major references
Anthropogenic aerosol and boreal forest from North America and West Europe	TARFOX	North Atlantic	July 1996	Russell et al. (1999)
	NEAQS	North Atlantic	July-August 2002	Quinn and Bates (2003)
	SCAR-A	North America	1993	Remer et al. (1997)
	CLAMS	East Coast of U.S.	July-August 2001	Smith et al. (2005)
	INTEX-NA, ICARTT	North America	Summer 2004	Fehsenfeld et al. (2006)
	DOE AIOP	northern Oklahoma	May 2003	Ferrare et al. (2006)
	MILAGRO	Mexico city, Mexico	March 2006	Molina et al. (2008)
	TexAQS/ GoMACCS	Texas and Gulf of Mexico	August-September 2006	Jiang et al. (2008); Lu et al. (2008)
	ARCTAS	North - central Alaska to Greenland (Arctic haze)	March-April 2008	`http://www.espo.nasa.gov/arctas/`
	ARCTAS	Northern Canada (smoke)	June-July 2008	
	ACE-2	North Atlantic	June-July 1997	Raes et al. (2000)
	MINOS	Mediterranean region	July-August 2001	Lelieveld et al. (2002)
	LACE98	Lindberg, Germany	July-August 1998	Ansmann et al. (2002)
	DRAGON	Washington, DC metropolitan	August 2011	Holben et al. (2011)
	Aerosols99	Atlantic	January-February 1999	Bates et al. (2001)
Brown Haze in South Asia	INDOEX	Indian subcontinent and Indian Ocean	January-April 1998 and 1999	Ramanathan et al. (2001)
	ABC	South and East Asia	ongoing	Ramanathan and Crutzen (2003)
Anthropogenic aerosol and desert dust mixture from East Asia	EAST-AIRE	China	March-April 2005	Li et al. (2007)
	INTEX-B	north-eastern Pacific	Singh et al. (2009)	
	ACE-Asia	East Asia and Northwest Pacific	April 2001	Huebert et al. (2003); Seinfeld et al. (2004)
	TRACE-P		March-April 2001	Jacob et al. (2003)
	PEM-West A & B	Western Pacific off East Asia	September-October 1991 February-March 1994	Hoell et al. (1996, 1997)

Table 2.3 continued

Aerosol regimes	Name	Location	Time period	Major references
Biomass burning smoke in the tropics	BASE-A	Brazil	1989	Kaufman et al. (1992)
	SCAR-B	Brazil	August-September 1995	Kaufman et al., 1998 Kaufman et al. (1998)
	LBA-SMOCC	Amazon basin	September-November 2002	Andreae et al. (2004)
	SAFARI2000	South Africa and South Atlantic	August - September 2000	King et al. (2003)
	SAFARI92		September-October 1992	Lindesay et al. (1996)
	TRACE-A	South Atlantic	September-October 1992	Fishman et al. (1996)
	DABEX	West Africa	January-February 2006	Haywood et al. (2008)
Mineral dusts from North Africa and Arabian Peninsula	SAMUM	Southern Morocco	May-June 2006	Heintzenberg (2009)
	SAMUM-2	Cape verde	January - February 2008	Ansmann et al. (2011)
	SHADE	West coast of North Africa	September 2000	Tanré et al. (2003)
	PRIDE	Puerto Rico	June-July 2000	Reid et al. (2003)
	UAE2	Arabian Peninsula	August-September 2004	Reid et al. (2008)
Remote Oceanic Aerosol	ACE-1	Southern Oceans	December 1995	Bates et al. (1998); Quinn et al. (1998)

established during two last decades. Obtaining accurate aerosol extinction profile observations is pivotal to improving aerosol radiative forcing and atmospheric response calculations.Aerosol data collected by these networks provide highly valuable information for monitoring of aerosol that is widely used for validating satellite observations and constraining aerosol properties in climate simulation efforts (Kinne et al., 2003, 2006; Textor et al., 2006; Koch et al., 2009).

Table 2.5: Summary of major ground-based remote sensing networks for the tropospheric aerosol characterization and radiative forcing research. All the reported quantities are column-integrated or column-effective, except as indicated.

Network	Derived parameters		Coverage
	Optical	Physical	
NASA AERONET `http://aeronet.gsfc.nasa.gov`	Optical depth, Single- scattering albedo, Ångström exponents, asymmetry factor, phase function	Volume size distribution, refractive indices, non-spherical fraction	$\sim$ 200 sites over global land and islands (since 1993)
DOE ARM `http://www.arm.gov`			6 sites and 1 mobile facility in N. America, Europe, and Asia (since 1989)
SKYNET `http://atmos.cr.chiba-u.ac.jp`			$\sim$ 20 sites in Asia and Europe (since 1998)
NOAA SURFRAD `http://www.srrb.noaa.gov/surfrad/`	Optical depth	N/A	7 sites in the U.S. (since 1995)
AERONET- MAN `http://aeronet.gsfc.nasa.gov/maritime_aerosol_network.html`			global ocean (periodically since 2004)
NASA MPLNET `http://mplnet.gsfc.nasa.gov`	vertical profiles of backscatter /extinction coefficient	N/A	$\sim$ 30 sites in major continents, (since 2000)
ALINE `http://lalinet.no-ip.org`			8 stations in S. America (since 2001)
AD-NET `http://www-lidar.nies.go.jp/AD-Net/`			20 stations in East Asia (since 2001)
EARLINE`http://http://www.earlinet.org`			27 stations in Europe] (since 2000)

2.2.1 Remote sensing of the atmospheric aerosols by AERONET

Among all passive instruments taken into account the most remarkable results belong to the AErosol RObotic NETwork (AERONET). AERONET (Holben, 1998) is a federation of regional and national networks deployed in the 90s by collaboration of the National Aeronautics and Space Administration (NASA) with PHOTONS (Laboratoire d'Optique Atmosphérique-LOA, University of Lille) in the form of automatic stations for monitoring atmospheric aerosols. The aims of the AERONET project were to facilitate the characterization of the aerosol properties and validation of satellite measurements providing reliable monitoring of global aerosol optical and microphysical properties.

An automatic sun and sky photometer Cimel Électronique 318 is equipped with 8 or 9 spectral channels covering the spectral range from 0.340 to 1.640 μm was chosen as standard instrument for the AERONET. Neglecting specifics it could be considered as a generic passive instrument with aerosol sensing capabilities. Although the algorithm presented in this work could be adapted to almost any type of passive instruments that exist, AERONET was chosen due to the vast amount of easily accessible observation data `http://aeronet.gsfc.nasa.gov/` , and the state of the art inversion algorithm with open and easy-to-use code (Dubovik and King, 2000; Dubovik et al., 2011).

All instruments operating within AERONET perform direct sun measurements and sky radiance observations in both the almucantar and principal plane configurations at least within the spectral channels of 0.440, 0.670, 0.870, and 1.020 μm that are used for aerosol characterization. The pre-programmed measurements sequence consists of a series of direct sun and sky radiance measurements at fixed solar elevations during sunrise and sunset (so called "Langley sequence"). Direct sun measurements are performed every 15 minutes and sky radiances are acquired every hour both for

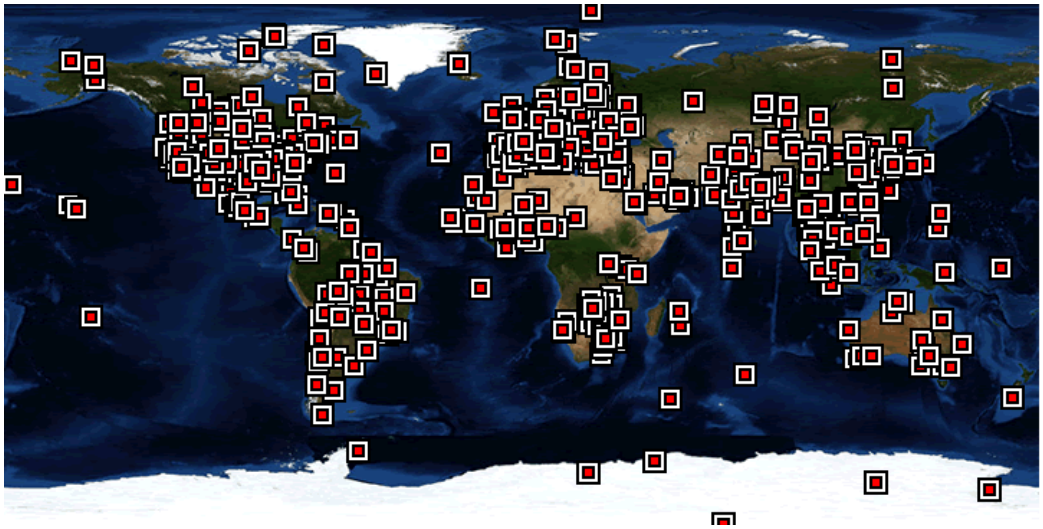

Figure 2.5: Global map of the sites of the AERONET network; according to `http://aeronet.gsfc.nasa.gov`.

almucantar and principal plane configurations when the solar zenith angles are below 60°. Additional triplet observation of direct sun measurements are taken 30 seconds afterwards per each wavelength. These measurements are used for operational cloud screening (Smirnov et al., 2000).

All data collected by the AERONET sun photometers are automatically transferred to NASA's Goddard Space Flight Center (GSFC) where they are processed by the same algorithm. Processing includes conversion of data collected from the different sources in a unique format, saving it in a database and producing instrument status reports that are available from the web page. There are several levels of data quality: Level 1.0 indicates unscreened data, level 1.5 contains cloud-screened, but not quality assured data, as final calibration may not be applied. Level 2 data are reprocessed after calibration post-deployment (assuming linear change rate in the calibration coefficients) and manually inspected to fulfil a set of criteria `http://aeronet.gsfc.nasa.gov/new_web/PDF/AERONETcriteria_final1.pdf` and considered to be quality assured data.

The data are accessible from the AERONET website what ensures the usage of latest

version of the data processing. It should be noted that for scientific research only level 2.0 data are quality assured, this data level is only available after an operation period when the instrument is re-calibrated, therefore theirs availability could take several months.

AERONET measurements description

Measurements performed within the AERONET consist of two sequences of spectral and angular measurements, that could be divided into two groups according to the way aerosol products are retrieved from them: direct sun measurements and sky radiance measurements. The direct sun measurements at each spectral channel $I(\lambda)$ allow the determination of the attenuation of sunlight passing through the atmosphere containing aerosol particles, molecules, and absorbing gases, which is known as the total optical depth of the atmosphere (τ) and is described by the Bouger-Lambert-Beer Law, which expresses monochromatic direct solar flux density I ($Wm^{-2}\mu m^{-1}$) on the Earths surface as follows:

$$I(\lambda) = I_0(\lambda)\, e^{-m_s \tau}, \tag{2.11}$$

where I_0 is the flux at the upper limit of the atmosphere, τ is the total optical thickness and $m_s = 1/\cos\theta_s$ (while $\theta_s < 75°$) is the optical air mass (exact formulation can be found in Kasten and Young, 1989).

Under cloud-free conditions, the total optical depth can be separated into the aerosol scattering and absorption τ_a, the molecular scattering or Rayleigh scattering τ_m and the gaseous absorption τ_g. Therefore, the aerosol optical depth (AOD or τ_a) can be derived from the total optical depth if the molecular optical thickness (τ_m) and the gaseous absorptions (τ_g) are known. Thus, considering that the atmospheric components are not equally distributed in the atmospheric vertical profile, so their

air mass are different, one could obtain:

$$I(\lambda, 0^\circ) = I_0(\lambda, 0^\circ)\, e^{-\tau_a m_a - \tau_m \frac{P}{P_0} m_m - \tau_g m_g}, \tag{2.12}$$

where $P_0 = 101\ kPa$ is the standard atmosphere pressure, and P is local pressure. The channels that are used for the aerosol optical depth retrieval are chosen to be with low or no absorption by atmospheric gases and therefore performed at wavelengths of 0.340, 0.380, 0.440, 0.500, 0.670, 0.870 and 1.020 μm. The number of wavelength available could vary with the instrument type, but all instruments within the network utilize at least four standard spectral channels: 0.440, 0.670, 0.870 and 1.020 μm.

The multi-wavelength and multi-angle sky radiances measurements provide the bulk of information about aerosol optical properties. Application of inversion algorithms to these measurements allows the retrieval of optical and microphysical properties of the aerosol particles, such as size distribution, single scattering albedo, refractive index and phase function (Dubovik and King, 2000).

There are two geometries followed within AERONET to perform the sky radiance measurements: almucantar and principal plane. They are carried out for the same aerosol channels as direct sun measurements. In the almucantar configuration (see

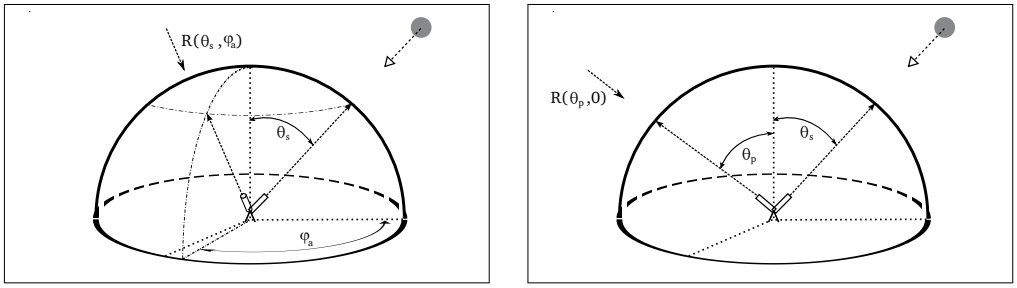

Figure 2.6: Figures describing the two geometries used within AERONET network for the measurements of the sky radiances: on the left, the almucantar is represented while the principal plane appears on the right; adapted from Torres (2012).

figure 2.6 on the left) the sun-photometers keep the zenith angle equal to the solar zenith angle θ_s. The measurement sequence contains a direct sun measurement executed previously to almucantar; afterwards the instrument covers the range from 3° to 180° of azimuth angles. At first the movement is done to the right from the sun and then is repeated to the left. The observation angles are the same for both branches and are listed in Table 2.6 in the row corresponding to the description of almucantar. The sequence is repeated for each of the channels taking about 5 minutes for the entire measurement.

Under assumption of homogeneous atmosphere, the measurements taken in both right and left branches should be symmetrical so the almucantar radiance values are averaged between them when used in the AERONET inversion algorithm. This operation procedure is performed only for almucantar measurements and allows eliminating data contaminated by clouds: the measurements with differences in radiances more than 20 % between right and left branches are disregarded (see `http://aeronet.gsfc.nasa.gov/new_web/Documents/AERONETcriteria_final1_excerpt.pdf`).

In the principal plane geometry (see Fig. 2.6 on the right) the azimuth angle remains equal to the solar azimuth angle and after a direct sun measurement the sky radiance measurements are performed for the different zenith angles depicted in Table 2.6. It should be noted that the current AERONET database does not offer any retrieval data from the principal plane measurements.

The relations between the scattering angle (Θ), the observation angles (θ_v, ϕ_v) and the solar zenith and azimuth angles (θ_s, ϕ_s) are $\cos(\Theta) = \cos^2(\theta_s) + \sin^2(\theta_s)\cos(\phi_v - \phi_s)$ in the case of almucantar geometry and $\cos(\Theta) = \cos(\theta_v \mp \theta_s)$ for the principal plane geometry (Nakajima et al., 1996), where the sign is minus when $\phi_v - \phi_s = 0°$ and plus for the case of $\phi_v - \phi_s = 180°$.

Consequently, the scattering angle observed with the almucantar geometry is limited

Table 2.6: Observation angles for sky radiance measurements in the almucantar and principal plane geometries. In the almucantar, angles are azimuth positions relative to the azimuth solar position (with 2 branches, right and left from the Sun). In the principal plane, angles are zenith angles relative to the zenith solar position (negative means below the Sun). Note the double observation at 6°, indicating the change from Aureole to Sky channels.

Measurement type	**Observation angles**
Almucantar	0, 2.0, 2.5, 3.0, 3.5, 4.0, 4.5, 5.0, 6.0, 6.0, 8.0, 10.0, 12.0, 14.0, 16.0, 18.0, 20.0, 25.0, 30.0, 35.0, 40.0, 45.0, 50.0, 60.0, 70.0, 80.0, 90.0, 100.0, 110.0, 120.0, 130.0, 140.0, 160.0, 180.0
Principal plane	0 -6.0, -5.0, -4.5, -4.0, -3.5, -2.5, -2.0, 2.0, 2.5, 3.0, 3.5, 4.0, 4.5, 5.0, 6.0, 6.0, 8.0, 10.0, 12.0, 14.0, 16.0, 18.0, 20.0, 25.0, 30.0, 35.0, 40.0, 45.0, 50.0, 60.0, 70.0, 80.0, 90.0, 100.0, 110.0, 120.0, 130.0, 140.0

by $0° \leq \Theta \leq 2\theta_s$ reaching its maximum when $\phi_s = 180°$. At the same time the maximum scattering angle in the principal plane measurement is the value of the maximum angle (θ_M) from the set of values of the principal plane (see Table 2.6), which fulfils the condition $\theta_m < 90° - \theta_s$. This condition describes the measurements geometry that is not pointing to the ground. Such restrictions have important consequences in the retrievals resulting in inability to make measurements of backscattered radiation. It should be noted that usually the azimuth origin is taken in the sun position and therefore $\phi_s = 0°$. This assumption also was made in Figure 2.6.
According to the standard AERONET measurement sequence the almucantar and principal plane measurements are acquired each hour.

AERONET measurements calibration

The calibration of the AERONET instruments is carried according to a strict protocol, which assures the data quality within the network. The instruments are calibrated approximately each year before and after deployment in the field by comparison with

master instruments. The master instruments meet high operating standards and are calibrated at high altitude stations (Mauna Loa Observatory in Hawaii (USA) or Izaña in Canary Islands (Spain)). AERONET has distributed calibration facilities including the radiance sphere calibration for the sky channels and the inter-calibration for the direct sun channels. Inter-calibration is performed at the following sites: GSFC, Carpentras and Autilla.

In case of direct sun measurement the calibration coefficient for each spectral channel is the extraterrestrial signal $I_0(\lambda)$. As explained above, field instruments are calibrated by comparison with master instruments previously calibrated at high altitude stations. The calibration uncertainty is about 0.5% for the master and 1 – 2% for field instruments. The calibration accuracy is smaller for the shorter wavelengths due to uncertainty in the calibration transfer (Holben et al., 2006).

The inter-calibration procedure is based on the simultaneous co-located measurements of the master and instruments being calibrated under certain atmospheric conditions. These restrictions are established to minimize the uncertainty of the inter-calibration procedure: clear sky and aerosol optical depth (0.440 μm) stable at noon and below 0.3, the number of co-located measurements is big enough to ensure the stability of the ratios between master and field instrument over a wide range of air masses. When this conditions are fulfilled the field instrument can be calibrated by a ratio of raw signals ($I^{field}(\lambda)$) to the master raw signal $I^{master}(\lambda)$ for each channel:

$$I_0{}^{field}(\lambda) = I_0{}^{master}(\lambda)\,\frac{I^{field}(\lambda)}{I^{master}(\lambda)}. \tag{2.13}$$

The calibration of the master instruments is carried out by the Langley plot method (Shaw, 1983). This method is based on the Bouguer-Lambert-Beer law and derives the extraterrestrial signal of the instrument from a set of direct sun observations

carried out for a range of air masses (typically from 7 to 2):

$$\ln I(\lambda) = \ln I_0(\lambda) - \tau m_s. \tag{2.14}$$

These measurements provide a straight line ($\ln I$ vs. m_s), which defines extraterrestrial signal (I_0). The main requirement for this method is that the total optical thickness of the atmosphere (τ) remains constant during performance of the measurement set. That's why high altitude stations, located at low latitudes, are very suitable for the Langley calibrations, because low content of the aerosol and the water vapour together with short duration of the sunrise and sunset assures the constant total optical thickness during measurements.

AERONET calibrates its masters in the Mauna Loa Observatory, while PHOTONS and RIMA masters are calibrated at Izaña Observatory.

The sky radiance observations are acquired with two different gains. Low gain is used for close to the Sun, due to the higher radiance in the aureole region. For observation angles (azimuth in the almucantar or zenith in the principal plane) bigger than 6°, the instrument uses the high gain channels. At 6° the observations are made with both channels, allowing performing consistency checks. As standard instruments measure aureole and sky radiances with different physical channels (collimator, optics, detector) they have independent calibration coefficients. The low/high gain ratio at 6° is usually used to detect obstructions in one of the collimators or front windows.

The radiance calibration is made with integrating spheres operational at three calibration facilities (GSFC, Lille and Valladolid). These spheres are in turn calibrated every 3 month with a travelling master instrument, which is calibrated at GSFC Calibration Facility to a NIST standard.

During calibration procedure, the photometer acquires radiances in all high and low gain channels being placed in front of the sphere port. The calibration coefficients are

calculated as the ratio between the output radiance at the given wavelength and the raw signal at each channel. The main precaution for this procedure is the stability of the sphere output; therefore the ageing of the lamps must be controlled to avoid miscalibration due to degradation.

2.2.2 Remote sensing of the atmospheric aerosols by active instruments

LIDAR is a technology to obtain information about distant objects using active optical systems based on the reflection and scattering of the light in the transparent or semi transparent media. LIDAR works precisely as RADAR: a pointed beam from the light source is reflected from the targets, returned to the source and registered by a receiver. The response time is directly proportional to the distance to the target. The main difference between RADAR and LIDAR is that radar uses radio waves that effectively reflected from the large metallic targets, while LIDAR uses light that is scattered by any media allowing both to measure the distance to the transparent targets and analyse the intensity of the light scattered by them. Such features lead to the wide use of LIDARs in the atmospheric aerosol studies. The beam that is reflected from the aerosol layer is secondly scattered by the lower layers thus making the retrieval of the aerosol parameters a challenging task.

LIDAR instrumental design

Although lidars have larger instrumental variety compared to the passive instruments (with AERONET in particular) and their measurements inter-comparison is more challenging (e.g. Böckmann et al., 2004) some similarities in LIDAR constructions could be easily observed.

Each LIDAR consists at least of three elements: emitter, receiving optics and signal

registration system. The majority of the LIDARs use lasers as *emitters* due to their ability to form short light pulses with high power. The pause between two consequent pulses should be bigger than maximum response time from the targets that could be situated farther than operating range of the LIDAR. The selection of the wavelength and pulse power depends on the lidar purpose and safety regulations. The most frequently used wavelength for the aerosol LIDARs are 0.355, 0.532 and 1.064 μm which correspond to the second and third harmonics of the Nd:YAG lasers (Wandinger, 2005a). The *receiving optics* in atmospheric LIDARs is usually made as telescopes,

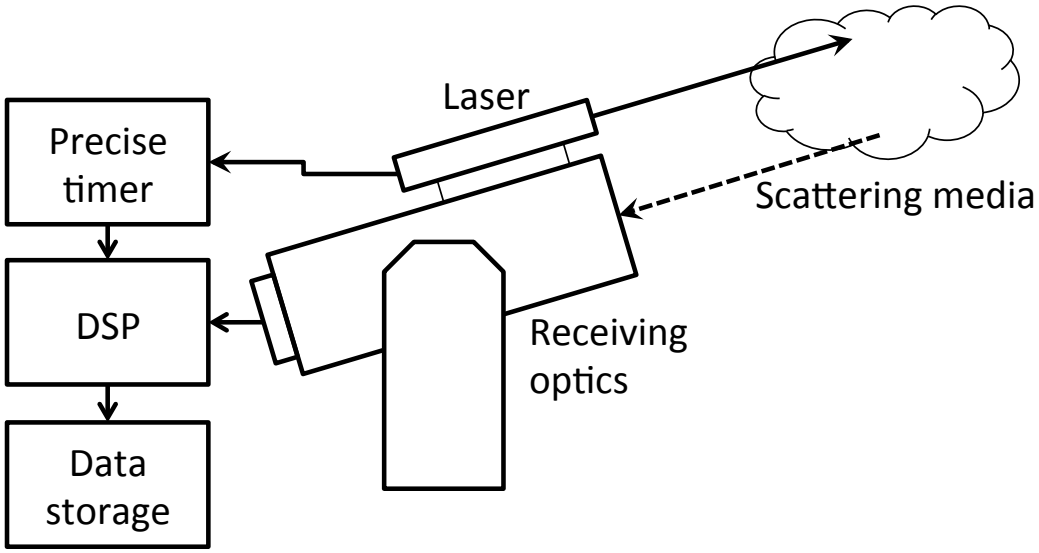

Figure 2.7: Mono-static scheme of the lidar measurement of the aerosol backscatter.

pointed at zenith or coupled with alt-azimuthal mount.

The *signal registration system* usually includes several photo receivers, analog-to-digital converter (ADC) and a digital signal processing system (DSP), usually coupled with a personal computer. Usually photomultiplier tubes (PMTs) or avalanche photo-diodes (APDs) functioning in both analog and photon counting regimes are used as photo-receivers. Usage of semiconductor receivers proved to be fruitful for infra red light detection.

The performance attributes of the atmospheric LIDAR systems that were used in this

study developed in laboratory of scattering media of Institute of Physics of National Academy of Sciences of Belarus (IP NASB) are listed in Table 2.7.

Generally emitter and receiving optics are combined in so called "mono-static

Table 2.7: Technical characteristics of the LIDARs installed at the Laboratory of Scattering Media, Institute of Physics of National Academy of Sciences of Belarus

	Stationary	LMR
	Emitter	
Laser type	YAG:Nd	YAG:Nd
Wavelength, μm	0.355, 0.532 and 1.064	0.355, 0.532 and 1.064
Pulse energy, mJ	50 - 200	30 - 100
Beam divergence, $mRad$	0.5	0.5
Pulse frequency, Hz	10	10
	Receiver	
Telescope	Cassegrain	Cassegrain
Mirror diameter, mm	200	300
Elastic channels wavelengths, μm	0.355, 0.532 and 1.064	0.355, 0.532 and 1.064
Polarization measurements	Depolarization at 0.532 μm	Depolarization at 0.532 μm
Near field cut-off	Distributed base	Distributed base
Raman channels wavelengths, μm	0.387	0.387, 0.407 and 0.687
Registration regime	Analog and photon counting	Analog and photon counting

scheme" as shown in Figure 2.7. In this scheme emitter and receiver are installed in proximity to each other. The idea of this method is to send the short light pulses and register the back-scattered radiation in the sequential time moments during the light propagation through the atmosphere. The propagation and scatter of such light pulses is described by non-stationary radiative transfer equation. Such calculations are very challenging and usually solved in the single-scattering assumption, which is reasonable when the total optical thickness (τ) is lower than 1, and both emitter and receiver have narrow view angles.

In this case scattered radiation received at the moment of time t after the sounding pulse is returned from the atmospheric layer at the distance $h = \frac{ct}{2}$ and received

power of the light flux $P(t,\lambda)$ is described by lidar equation:

$$P(\lambda,h)=\frac{Y(h)\,S}{h^2}E(\lambda)\,\beta(\lambda,h)\exp\left(-2\int_o^h\sigma(\lambda,h')\,dh'\right), \tag{2.15}$$

where $\sigma(\lambda,h) = \sigma_a(\lambda,h)+\sigma_m(\lambda,h)$ is the spectral extinction coefficient and $\beta(\lambda,h)=\beta_a(\lambda,h)+\beta_m(\lambda,h)$ is the backscatter coefficient of the atmospheric layer at altitude h, $\beta_a,\beta_m,\sigma_a,\sigma_m$ are the coefficients of aerosol and molecular backscatter and extinction correspondingly, $E(\lambda)$ is the energy of the sounding pulse, $Y(h)$ is geometrical factor (overlap function) and S is the area of receiving optics.

Considering range (h^2) and overlap ($Y(h)$) correction (for e.g. Wandinger and Ansmann, 2002), Equation 2.15 could be written in the following form:

$$P(\lambda,h)=C(\lambda)\,\beta(\lambda,h)\exp\left(-2\int_0^h\sigma(\lambda,h')\,dh'\right), \tag{2.16}$$

where $C(\lambda)$ is so-called system parameter, which unites the specifics of the lidar receiving system for the given spectral channel. It should be noted that above Equations 2.15, 2.16 are applicable only in the case when time of light interaction with the media is small as well as duration of the sounding pulse, and both these periods are smaller than time between two sequential scatter acts (single-scattering approximation).

As it seen Equation 2.16 depends on two profiles of extinction and backscatter and on a system parameter. It is evident that the straightforward retrieval of the aerosol properties $\beta_a(\lambda,h),\sigma_a(\lambda,h)$ from Eq. 2.16 is impossible, and will require some additional information about both lidar measurements and aerosols which could be supplied in a form of constrains and a priori estimations.

LIDAR measurements calibration

To deal with the aerosol characterization from Equation 2.16, Klett (1981, 1985) suggested additional assumptions. First is so-called LIDAR calibration at a reference altitude. Commonly, aerosol retrievals from LIDARs use the attenuated backscatter normalized by attenuated backscatter at the reference altitude h_{ref}. This reference altitude is chosen under the assumption that amount of the aerosol over this altitude is negligible, i.e. signal at the reference altitude could be written in the following form:

$$P^{*}\left(\lambda, h_{ref}\right) = C\left(\lambda\right)\beta_{m}\left(\lambda, h_{ref}\right)\exp\left(-2\int\limits_{0}^{h_{ref}}\sigma\left(\lambda, h\right)dh'\right). \tag{2.17}$$

As $P\left(h_{ref}, \lambda\right)$ could be estimated from the measurements, such procedure allows excluding unknown system parameter $C\left(\lambda\right)$:

$$C\left(\lambda\right) = \frac{P^{*}\left(\lambda, h_{ref}\right)}{\beta_{m}\left(\lambda, h_{ref}\right)\exp\left(-2\int\limits_{h_{0}}^{h_{ref}}\sigma\left(\lambda, h'\right)dh'\right)}, \tag{2.18}$$

where molecular backscatter $\beta_{m}\left(\lambda\right)$ is usually known from the modelling, thus leading to the following calibrated lidar equation, also known as attenuated backscatter:

$$L^{*}\left(\lambda, h\right) = \frac{P^{*}\left(\lambda, h\right) - B\left(\lambda\right)}{P^{*}\left(\lambda, h_{ref}\right)}\beta_{m}\left(\lambda, h\right)\exp\left(-2\int\limits_{h}^{h_{ref}}\sigma_{m}\left(\lambda, h'\right)dh'\right), \tag{2.19}$$

where $B\left(\lambda\right)$ is background noise estimation, usually taken from altitude averaging and extended time accumulation of the LIDAR signal far above its maximum altitude range h_{max}. The second assumption, used by Klett, deals with the a priori estimation of such optical property of the aerosol as extinction-to-backscattering ratio, lately known as lidar ratio:

$$S_{a}\left(\lambda, h\right) = \frac{\sigma_{a}\left(\lambda, h\right)}{\beta_{a}\left(\lambda, h\right)}. \tag{2.20}$$

Aerosol lidar ratio depends on the aerosol type and could be both provided in the form of constant (Klett, 1981) or vertical profile (Klett, 1985). Commonly lidar ratio is chosen using a-priori climatological data sets. For example, processing of lidar observations from CALIPSO space-borne platform relies on the lidar ratio climatological models derived by cluster analysis from entire database of AERONET retrievals (Omar et al., 2005).

The described *Klett method* was one of the successful attempts to deal with the ill-posed problem of lidar sounding. The other methods support the general idea of the method proposed by Klett: they try to provide additional information for the ill-posed problem of lidar sounding. However, as it was already outlined in the introduction, such information cannot be extracted from lidar measurements without some assumptions on aerosol properties. For example, lidar observation could be enhanced by employing the following lidar techniques:

- implication of lidar measurements under a set of several different zenith angles or so-called slope methods,
- conduction of multi-wavelength of high spectral resolution lidar measurements,
- registration of combined elastic-Raman signals,
- performance of polarimetric LIDAR observations.

Multi-angular measurements (slope methods). Method consists in measuring of several slopes with different zenith angles, allowing discrimination of aerosol extinction profile under assumption of horizontal homogeneity of the atmosphere (Gutkowicz-Krusin, 1993; Pahlow et al., 2004; Sicard et al., 2002). Such assumption couldn't be used at low zenith angles, fast changing observation conditions or in the presence of clouds.

Multi-wavelength measurements. The idea of this method is to measure aerosol backscatter at several sounding wavelengths (usually harmonics of the lasers used). This provides additional information to resolve lidar equation under assumption that parameters of aerosol backscatter and extinction at different wavelengths $(\beta_a(\lambda), \sigma_a(\lambda))$ could be calculated on a base of some microphysical aerosol model. For example, optical characteristics could be calculated through its microphysical parameters, under assumption that aerosol particles are spherical:

$$\sigma_a(\lambda) = \int_{r_{min}}^{r_{max}} \pi r^2 K_\varepsilon(\lambda, r, m) \frac{dV(r)}{r} dr, \tag{2.21}$$

$$\beta_a(\lambda) = \int_{r_{min}}^{r_{max}} \pi r^2 K_\beta(\lambda, r, m) \frac{dV(r)}{r} dr, \tag{2.22}$$

where K_σ and K_β are the cross-sections of aerosol extinction and backscatter correspondingly, $\frac{dV(r)}{r}$ is aerosol volume size distribution, $m = n + i\kappa$ is the complex refractive index of aerosol particles.

Therefore, measurements at several wavelengths allow resolving a system of Equations 2.21, 2.22 with some additional a priori constraints and assumptions taken into account, such as particle shape, size distribution of the aerosol particles and their complex refractive index. It is evident that the more wavelength are taken into account the more aerosol properties could be retrieved from spectral lidar measurements (Shipley et al., 1983; Liu et al., 2002; Hair et al., 2008; Burton et al., 2012; Groß et al., 2013), allowing even estimations of aerosol microphysics (Müller et al., 1999).

Raman LIDAR measurements. Combined elastic-Raman scatter LIDARs additionally use registration of the Raman shifted radiation induced by the elastic lidar sounding in atmospheric gases (Ansmann et al., 1992; Ferrare et al., 1998b,a; Turner et al., 2002; Wandinger, 2005b; Müller et al., 2007). This allows discrimi-

nation of aerosol extinction profile at Raman wavelengths and even estimations of aerosol microphysical properties without a priori constraints on aerosol type or loading (Müller et al., 1999, 2005; Veselovskii et al., 2004; Shcherbakov, 2007) if the vertical profiles of atmospheric gases are known.

However, lidar systems with capabilities to register non-elastic (Raman shifted) signals are rather complex and often require special observational conditions as non-elastic signal is very weak during daytime. And despite of the achieved progress in non-elastic lidar technology (Baars et al., 2009; Althausen et al., 2009) the bulk of monitoring of vertical aerosol variability is conducted by the conventional lidars.

Polarimetric measurements. Polarimetric LIDARs additionally register the radiation cross-polarized to the polarization plane of the sounding beam. This allows qualitative description of aerosol particle anisotropy. For example, Ansmann et al. (2011) used measured depolarization profiles in order to derive vertical distribution of spherical and non-spherical aerosol components with size distributions and complex refractive indices fixed from modelling.

All these methods despite of limited applicability due to the applied assumptions have influenced the approaches for LIDAR system construction, and most of the modern LIDARs (ones participating in EARLINET project, see, e.g., Bösenberg and et al. (2000)) have Raman-scattering channels together with several elastic channels as well as possibility to perform polarimetric and multi-angular measurements. However, all mentioned methods rely on additional a priori information about aerosol microstructure. Such information could be retrieved by multiple ways, including estimations taken from additional measurements performed by passive instruments. Such estimations are considered to be very reliable and a variety of perspective methods using mentioned a-priori information were developed.

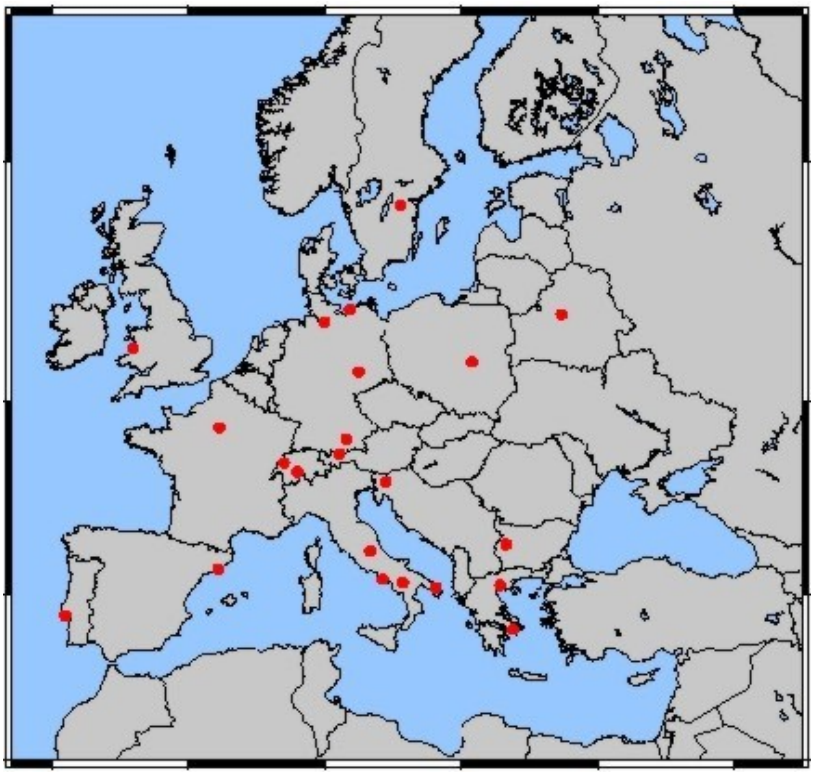

Figure 2.8: Map of observation sites equipped with lidars participating in European AeRosol LIdar NETwork; adapted from `http://www.physics.ntua.gr/~papayannis/publications_site.htm`.

2.2.3 Remote sensing of the atmospheric aerosols by combination of active and passive instruments

As it was already mentioned, aerosol retrievals from lidar observations depend on the auxiliary data about aerosol properties. This has resulted in creation of several approaches of lidar measurements that were pursuing the idea to fulfil the informational gaps in the aerosol description. However, further development of the methods that allow expansion of the informational contents of the lidar sounding is constrained by technological boundaries. In these regards, the most logical approach to improve the retrievals qualitatively was to widen the amount of instruments used in the aerosol retrievals. It is clear that both active and passive measurements provide complementary pieces of information about atmospheric aerosols while both are relying on the

set of assumptions about aerosol properties.

For example, retrievals of aerosol columnar properties from passive measurements use an assumption of the vertical distribution of aerosol, and information about aerosol type is usually used for constraining lidar ratio (Eq. 2.20) that defines dependence between aerosol backscatter and extinction in lidar retrievals.

Described situation led to the development of a variety of multi-instrumental aerosol retrievals that combined data from passive and active observations. Such methods generally could be subdivided into two distinct groups by the way they use the constraints on aerosol properties provided by the passive observations: methods with implicit and explicit constraining.

Implicit methods follow the approach of direct usage of the available coincident passive measurements. The straightforward constraining of the lidar retrievals by means of using values of total aerosol optical thickness is a most common way of utilizing co-incident sun-photometer observations for improving the processing of lidar observations.

General idea of explicit methods is to estimate the aerosol extinction and lidar ratio from the optics or microphysics retrieved from passive measurements, with consequent inversion of lidar equation in order to obtain vertical profiles of aerosol concentration. Such methods exploit positive heritage of multi-wavelength and Klett (Klett, 1981, 1985) approaches. Generally, information about aerosol sizes and composition of aerosol particles obtained from sun-photometers is used for defining number of different aerosol components and their detailed properties (size distributions, complex refractive index and particle shape). Then lidar data are fitted using optical properties of these assumed aerosol components by searching for their vertical mixing that provides the best match of lidar data.

These methods are based on the assumption that aerosol optical properties at arbitrary altitude could be represented as a combination of optical properties of several

aerosol components, which are usually called aerosol modes:

$$\beta_a(\lambda, h) = \sum_{i=1}^{k} \frac{\beta_a^i(\lambda)}{v_i} c_i(h), \tag{2.23}$$

where v_i is the columnar volume concentration of the i-th mode, $\beta_a^i(\lambda)$ is the columnar backscatter coefficient of the mode, $c_i(h)$ is the vertical profile of aerosol mode concentration.

The main difference between the aerosol modes is particle sizes. Different methods could use different number of aerosol modes. Usually the number of the modes is chosen small (2 or 3). For example, studies by Chaikovsky et al. (2002a, 2004, 2006b, 2012) and Cuesta et al. (2008) used the measured spectral dependence of backscatter and extinction to derive vertical distribution of several optically distinct aerosol modes assuming that only concentrations of the each aerosol mode can change vertically.

The number of the modes used in those studies varied from 2 or 3 in works of Chaikovsky et al. (2006b, 2012) and up to 6 in retrievals by Cuesta et al. (2008).

The size distributions and complex refractive indices of each of the aerosol components were fixed using the aerosol retrievals from AERONET sun-photometers. In LiRIC (Lidar-Radiometer Inversion Code) Chaikovsky et al. (2006b, 2012) assumed two mono-modal fine and coarse aerosol components with size distributions obtained by dividing AERONET derived distribution into two using the minimum in the range of sizes from 0.194 to 0.576 μm as a separation point. The complex refractive indices for both modes were assumed to be the same and equal to the one retrieved by AERONET. Cuesta et al. (2008) used a more complex procedure. First, the AERONET size distribution was decomposed into log-normal mono-modal distributions. Then both bi-modal size distributions of each mode and complex refractive indices were defined using available ancillary data.

Additional a priori constraints and estimations are also used in these retrievals, such as smoothness constraints as well as estimations of complex refractive index for each mode, in order to stabilize numerical inversions of the lidar equation.

One of the biggest disadvantages of explicit methods is their dependence on the retrieval results of passive measurements, which in the case of ground-based measurements are insensitive to backscatter, what could lead to high errors in estimation of this parameter very crucial for lidar retrievals. Also such methods rely on some a priori information on refractive index of the aerosol modes. For example, Chaikovsky et al. (2002a, 2012) assumes both fine and coarse mode to have equal complex refractive index, while Cuesta et al. (2008) fixes this parameter from the modelling. Mentioned particularities could lead to high errors in estimation of aerosol optical properties, propagating directly to the retrieved vertical concentration profiles, specifically in the cases with mixture of aerosols with different microstructure.

In addition, radiation field observed by the sun-photometers, in particular its polarimetric properties, has some sensitivity to aerosol vertical distribution. Benefiting from this sensitivity is practically unachievable without using independent information about vertical variability of aerosol, which is impossible in the described approaches to combined passive-active multi-instrumental aerosol retrieval.

Despite of mentioned disadvantages, explicit methods have proven their ability to provide qualitatively new results in the form of vertical profiles of aerosol mode concentrations. Regarding this, this work was aimed at combination of the best sides of the implicit and explicit methods proposing a new approach for treating sun-photometer and lidar data combination.

The general idea of the new method is to use directly all the information content of the passive measurements, like in implicit methods, together with providing a possibility of measurements cross-influence, providing a deep synergy between two types of the measurements, thus allowing the retrieval of qualitatively new results, as in

explicit methods.

It should be noted that this concept was realized by Sinyuk et al. (2008). They had proposed a synergetic retrieval of both columnar and vertical aerosol properties by inverting a combined data from coincident observation by CALIPSO satellite lidar and AERONET sun-photometers. However, due to the limited spectral information available from CALIPSO, the approach uses only one aerosol mode, assuming lidar ratio of the aerosol to be constant in the whole atmosphere column.

The new approach should also rely on a unified aerosol model. That will allow reducing the amount of assumptions about aerosol properties that are usually used for the retrievals, therefore, leading to more accurate results.

This model is one of the first attempts to provide a full microphysical description of the aerosol in the atmosphere that is suitable to characterize both columnar and vertical variability of the aerosols. Usage of the unified model for each aerosol component will provide different complex refractive index for each of the aerosol mode, as well as accounting to the aerosol vertical distribution in passive observations modelling. It is expected that this particularities will allow more accurate reproduction of both lidar and sun-photometer observations.

It is also expected that spectral sensitivity of lidar observations will provide not only the information about aerosol vertical mixture, but due to the synergy with passive observations will allow better discrimination of columnar properties of the aerosol components. For example, lidar capability to register backscatter light is expected to improve the retrieval of such columnar properties of aerosol components as lidar ratios and spherical/non-spherical particles fraction.

In conclusion, the new method will introduce the unified microphysical aerosol model describing both columnar and vertical aerosol properties and capable of full description of the radiative field produced by aerosols. Compared with other advanced methods of passive and active observations processing new method will provide both

qualitative (i.e. vertical profiles and different complex refractive indexes for aerosol modes) and quantitative (more accurate estimations of spherical/non-spherical particles fraction and lidar ratios) improvements.

Compared with the most advanced methods of lidar data processing, the combined retrieval will provide two vertical profiles of fine and coarse mode similar to method by Chaikovsky et al. (2002a) but with higher accuracy, because, the used lidar ratios will be generated during the inversion procedure using also information in lidar measurements instead of relying solely on AERONET retrievals as in LiRIC (Chaikovsky et al., 2002a, 2004, 2006b, 2012) method.

Chapter 3

GARRLiC algorithm description

I do not fear computers.

I fear the lack of them.

Isaac Asimov

This chapter describes in detail the new **G**eneralized **A**erosol **R**etrieval from **R**adiometer and **Li**dar **C**ombined data (**GARRLiC**) that simultaneously inverts coincident lidar and radiometer observations and derives a united set of aerosol parameters.

Retrieval of optical and microphysical properties of atmospheric aerosols from radiation measurements requires two distinct types of development efforts. First, a capability of modelling atmospheric characteristics is demanded. That capability is important for a creation of so-called "forward model", a retrieval algorithm that could quantitatively simulate the the measured atmospheric radiation emitted by the surface or atmospheric objects with given properties. The second necessary component of the retrieval is called an "inversion" procedure and allows recovering unknown input parameters of the forward model from its known output by utilizing an inverse transformation.

Method proposed in this work is based on the latest POLDER retrieval algorithm

(Dubovik et al., 2011), witch general structure is shown in Fig. 3.1. Although the algorithm was developed for inverting PARASOL observations, some aspects of aerosol parametrization and inversion implementation can be modified and adjusted for application to other remote sensing observations, in the present case for AERONET observations.

This flexible algorithm is divided into several independent modules with particular

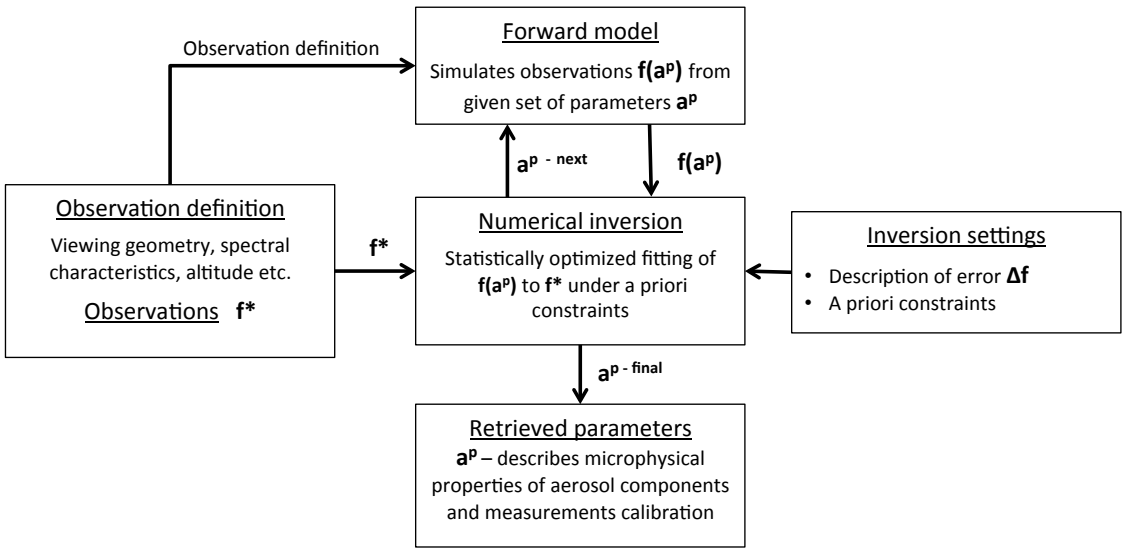

Figure 3.1: Principal scheme of the GARRLiC algorithm.

functions, whose interactions are minimized to straightforward exchange of limited set of parameters. Flexibility of the modular construction of the used algorithm allows utilization of several modules with very small changes. For example, "Numerical inversion" module that has almost no connection to observation physics implements universal operations of statistically optimized inversion and could be used not only in remote sensing applications.

The most changes were introduced into "Forward model" as the most complex module of the algorithm that directly deals with the observation specifics. However, its unified structure was easily tuned to work with ground-based observations and adjusted to account for bi-modal aerosols with retrievable vertical distributions,

leaving several key modules intact. Detailed description of the intact modules could be found in a publication by Dubovik et al. (2011), the following sections will focus on the changes that were introduced and on the results such changes have provided.

3.1 Forward model

The aerosol retrieval algorithm is designed to invert the AERONET almucantar observations combined with elastic lidar observations acquired in window channels shown in Table 3.1, that are: the scattered radiance in 4 window channels: 0.44, 0.675, 0.87 and 1.02 μm, and attenuated backscatter in 3 additional channels: 0.355, 0.532 and 1.064 μm. In each almucantar channel, observations are performed nearly simultaneously in up to 35 viewing directions (Holben, 1998, Table 2.6). In each lidar channel observations are performed in $\simeq 600$ altitude strobes, and it is assumed that the backscattered light from the reference altitude (h_{ref}) is mostly provided by molecular scattering. In order to account for possible presence of the aerosol at the reference altitude, and, therefore, for its impact on calibration procedure (Matsumoto and Takeuchi, 1994; Rocadenbosch et al., 2010), retrievable lidar calibration parameters $A(\lambda)$ were introduced.

Under assumption of plane-parallel multi-layered atmosphere, the following optical properties are needed to model combined AERONET and elastic lidar observations by means of vector radiative transfer and lidar equation: surface reflectance, optical thickness, single scattering albedo and phase matrix for each layer. The optical properties of each atmospheric layer include the contributions of aerosol and molecular scatter and atmospheric gases absorption:

$$\tau = \tau_a + \tau_{mol} + \tau_{gas}. \tag{3.1}$$

Table 3.1: Observations used in the GARRLiC algorithm. Note: the measurements of degree of linear polarization marked with asterisk (*) were used for sensitivity studies only.

AERONET measurements	
$I(\Theta_i, \lambda_j)$	Scattered total radiances
$P(\Theta_j, \lambda_i) = \frac{\sqrt{Q^2(\Theta_j,\lambda_i)+U^2(\Theta_j,\lambda_i)}}{I(\Theta_j,\lambda_i)}$	Degree of linear polarization*
Observation specifications	
Angular $I(\Theta_i, \lambda_j), P(\Theta_j, \lambda_i)$	Measured in up to 30 viewing directions that may cover scattering angle Θ from 0° to 150°
Spectral $I(\Theta_i, \lambda_j), P(\Theta_j, \lambda_i)$	Measured in 4 window channels $\lambda_j = 0.44$, 0.67, 0.87 and 1.02 μm
LIDAR measurements	
$L(h_i, \lambda_j)$	Vertical profile of backscattered radiances
Observation specifications	
Angular $L(h_i, \lambda_j)$	Measured in one viewing direction with scattering angle $\Theta = 180^\circ$
Altude $L(h_i, \lambda_j)$	Measured in up to 1000 h_i with resolution of 15 m within altitude range $h_{min} \leq h_i \leq h_{max}$
Spectral $L(h_i, \lambda_j)$	Measured in 3 window channels $\lambda_j =$ 0.355, 0.532 and 1.064 μm

The properties of molecular scattering are well known and could be calculated with sufficient accuracy. The absorption of atmospheric gases can be accounted for using known models (e.g. SA (1976); ISA (1975); ICA (1993); Tomasi et al. (1998)) or climatologies (for e.g. CIRA model: `http://badc.nerc.ac.uk/view/badc.nerc.ac.uk__ATOM__dataent_CIRA`), as well as using available information from ancillary observations. The reflection matrix of the land surface may also be estimated from additional methods and instruments (Wanner et al., 1997; Deering and Leone, 1986; Roujeau et al., 1997). This distinguishes proposed algorithm from the original one used for PARASOL retrievals (Dubovik et al., 2011), where parameters defying surface reflectance were included into the set of retrieved parameters. Such decision was made following ideas introduced in the inversion procedures of AERONET Dubovik and King (2000).

Thus, the most challenging part in modelling single scattering properties of the atmosphere is the modelling of aerosol contribution. These properties depend on aerosol microphysics: particle size, shape and composition (refractive index).

As far as photometric measurements accumulate optical properties of all of the atmospheric layers, their sensitivity to vertical distribution of these properties remains negligible. Lidar measurements, in contrast, are highly sensitive to these parameters, so simulation of the combined lidar-photometric measurements needed more accurate vertical distribution of aerosol optical properties. This led to expansion of aerosol microphysical model with additional parameters describing aerosol vertical distribution (see Table 3.2) compared to original ones used in AERONET or POLDER retrievals.

All other parameters like particle size and complex refractive indices were considered to be altitude independent. Thus, in order to describe the differences of optical properties between atmospheric layers only one profile of concentration wasn't sufficient. Therefore, aerosol in each layer was considered as a mixture of two components, each having a different set of microphysical properties, including size distribution, complex

Table 3.2: Aerosol parameters retrieved by the GARRLiC algorithm.

Aerosol characteristics	
$\frac{dV(r_i)}{d\ln r}$	$(i = 1, ..., N_r^k; k = 1, 2)$ values of volume size distribution in N_i size bins r_i of k-th aerosol component, $\mu m^3 \mu m^{-2}$
$c_k(h_i)$	$(k = 1, 2)$ vertical distribution of aerosol concentration of k-th aerosol component, normalized to 1
C_{sph}	Fraction of spherical particles of the coarse aerosol component
$n^k(\lambda_i)$	$(i = 1, ..., 7; k = 1, 2)$ the real part of the refractive index for k-th aerosol component at every λ_i of combined lidar-photometric measurement
$\kappa^k(\lambda_i)$	$(i = 1, ..., 7; k = 1, 2)$ the imaginary part of the refractive index for k-th aerosol component at every λ_i of combined lidar-photometric measurement
Lidar calibration parameters	
$A(\lambda_i)$	$(i = 1, ..., 3)$ Lidar calibration coefficient at each λ_i of the lidar measurement

refractive index and vertical profile of aerosol distribution. All these characteristics are driven by the parameters included in the vector of unknowns and trough inversion could be retrieved from the observations.

It should be noted that the forward model for reproducing combined lidar-photometric observations is adapting the atmospheric modelling strategies and computer routines developed within previous POLDER and AERONET activities. At the same time, several important modifications required for simulation of light propagation in the atmosphere during lidar sounding have been implemented in the mentioned algorithms. Specifically, additional module that provides vertical profiles of the optical properties necessary for lidar sounding simulations, as well as module that makes such simulation were introduced. In the modified algorithm AERONET observations are modelled by means of solving vector radiative transfer equation and elastic lidar observations are simulated by lidar equation. Thus, the forward model of scattered radiances measured by complex AERONET and lidar observations contains four main components:

- aerosol single scattering,
- aerosol optical properties vertical profiling,
- lidar equation and
- vector radiative transfer equation.

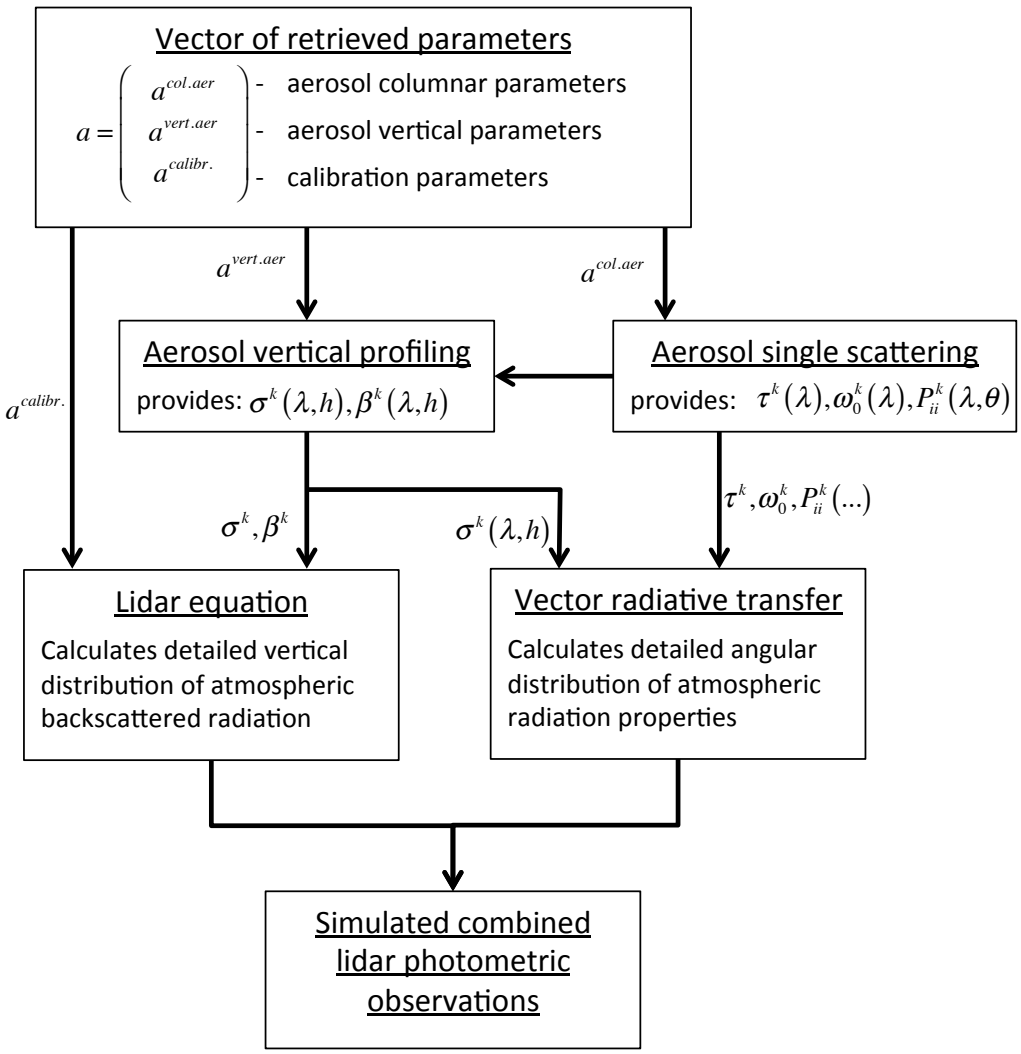

Figure 3.2: General scheme of the Forward model of the GARRLiC algorithm.

Figure 3.2 shows the data flow within the "Forward model" block of the algorithm. The following parts of this section will describe each of these components in detail.

3.1.1 Aerosol single scattering properties

The modelling of aerosol columnar optical properties has been implemented following the ideas employed in AERONET retrieval algorithm by Dubovik and King (2000) and Dubovik et al. (2002b, 2006). This concept was developed to model the particles as a mixture of spherical and non-spherical aerosol components.

The scattering from spherical particles can be predicted given the number concentration of those spheres in a volume, along with their size and complex refractive index by Lorenz-Mie theory that was independently developed at the turn of the XX^{th} century by Ludvig Lorenz and Gustav Mie as a solution to Maxwell's equations in spherical polar coordinates. Derivation of the solution can be found in many sources, such as Bohren and Huffman (1983) and Mishchenko et al. (2002).

Unlike spheres, accurate modelling of light scattering by non-spherical particles is one of the major difficulties in remote sensing of tropospheric aerosols (Dubovik et al., 2006). Specifically, the exact solutions describing the interaction of the electromagnetic field with a single particle exist only for a few selected geometrical shapes (Mishchenko et al., 2000, 2002). For example Mishchenko et al. (1997) used the simplest non-spherical shapes, such as spheroids (ellipsoids of revolution) and showed that a mixture of randomly oriented spheroids with different sizes and axis ratios can reproduce the specific shape of the phase function for desert dust — one of the most common types of non-spherical aerosols. At the same time, there is no physical reason to expect non-spherical aerosol particles to be perfect spheroids, and, indeed, microphotographs of natural aerosols show a great variety of shapes, often different from spheroids (see Figures 1.1 and 2.1). However, all existing numerical methods that could provide computations of scattering properties of the particles of more realistic geometrical shapes, such as the discrete dipole approximation (e.g., Draine and Flatau, 1994) and the finite difference time domain technique (e.g., Yang et al., 2000) require excessive computer resources. This is why the spheroid

approximation remains appealing from an operational perspective. Moreover, the following considerations can be listed as further motivations for the utilization and exploration of spheroid models (Dubovik et al., 2006):

- A spheroid is the simplest non-spherical shape that can generalize the spherical shape (a sphere is a spheroid with an axis ratio $\varepsilon = 1$). Accordingly, conventional spherical models of atmospheric aerosol can be easily generalized in terms of a model of randomly oriented spheroids with only one extra characteristic — the distribution of axis ratios (assuming, as the first-order approximation, that shape is independent of size).

- The scattering of electromagnetic radiation by spheroids can be accurately simulated with the T-matrix method that provides an exact solution for light scattering by randomly oriented spheroids with different sizes, axis ratios, and complex refractive indices (Mishchenko et al., 1996; Mishchenko and Travis, 1998; Mishchenko et al., 2000).

- The observations of scattering by non-spherical aerosol (desert dust in particular) show a considerable degree of averaging of contributions from individual particles with different orientations, shapes, and compositions. Hence one can expect and compositions. Hence one can expect (Mishchenko et al., 1997) that specific shape details of a single particle may be insignificant after such an averaging and that scattering by an ensemble of particles can be approximated by that of a mixture of simplified particles (such as spheroids).

It also should be noted, that the developed spheroid model (Dubovik et al., 2002b, 2006) proved to be useful not only for AERONET but for other aerosol remote sensing applications. First, the utilization of this model has significantly improved the AERONET operational retrieval of aerosol with pronounced coarse mode fraction (Reid et al., 2003; Eck et al., 2005; Dubovik et al., 2006). The same model has been

shown to reproduce adequately the ground-based polarimetric observations of non-spherical desert dust (Li et al., 2009). In addition, it was shown that the spheroid model allows qualitative reproduction of the main characteristic features of lidar observations of non-spherical desert dust, like lidar ratio and high depolarization of signal (Cattrall et al., 2005; Schuster et al., 2012). Furthermore, Veselovskii et al. (2010) and Müller et al. (2012) have used the approach suggested by Dubovik et al. (2006) and incorporated the spheroid model into the algorithm retrieving aerosol properties from lidar observations.

The non-spherical coarse aerosol models derived from climatologies of AERONET retrievals had been successfully incorporated into satellite retrievals (Levy et al., 2007b,a; Govaerts et al., 2010; Wagner et al., 2010; Dubovik et al., 2011) and accurate calculations of atmospheric broadband fluxes and aerosol radiative forcing (Derimian et al., 2008; Garcia et al., 2008).

Figure 3.3 demonstrates the differences in phase function and linear polarization degree calculated from spheroid and spherical models. It should be emphasized that differences between spherical and spheroid models for scattering matrices (left panel of Fig. 3.3) are situated at bigger angles, resulting in a significant deviations of the aerosol backscatter. At the same time many lidar studies of desert dust (for e.g. Welton et al., 2000; Liu et al., 2002; Müller et al., 2003, 2004) indicate that observed lidar ratios ($S_a(\lambda)$) has higher values (i.e. lower backscatter) than suggested by dust modelling based on Mie calculations for spherical particles. Right panel of Fig. 3.3 also demonstrates that it is impossible to get satisfying fit of degree of linear polarization (DoLP) using only spherical model.

Thus, following the considerations listed above GARRLiC uses the "spheroidal" aerosol model to simulate the properties of atmospheric aerosols.

According to this model, aerosol particles of non-spherical component have size-independent distribution of shapes and the modelling of the aerosol scattering matrix

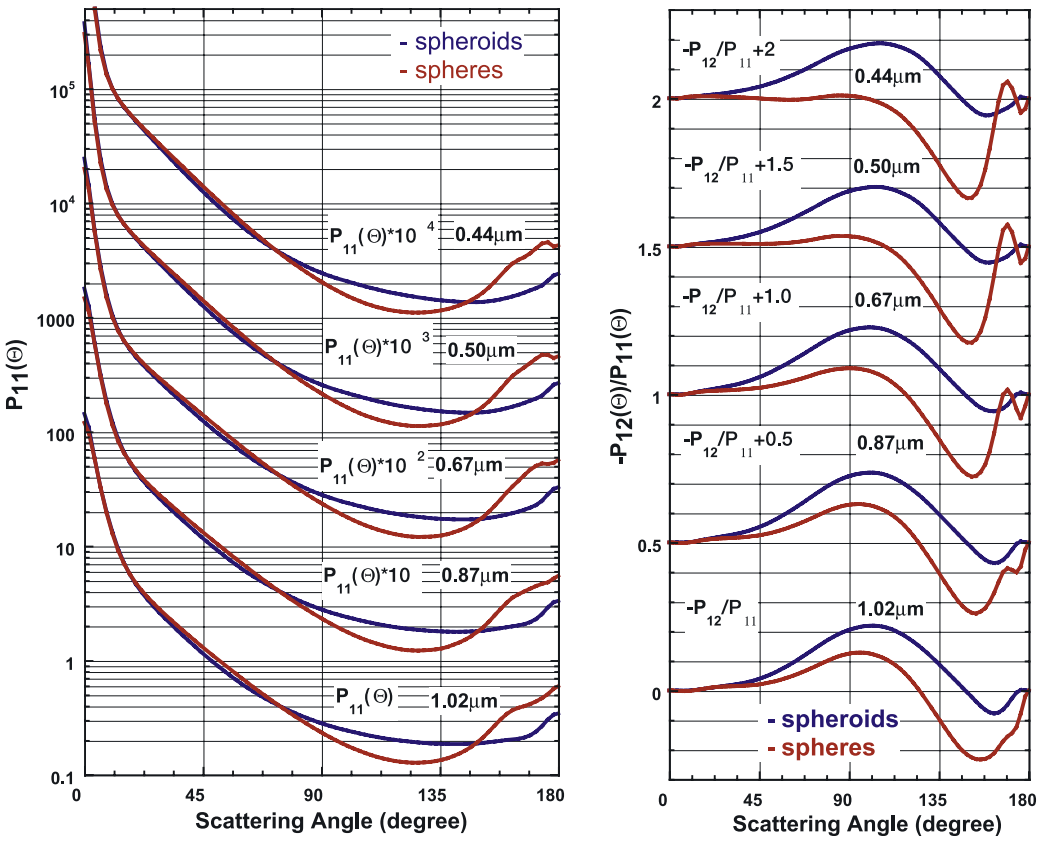

Figure 3.3: Comparison of desert dust phase function and degree of linear polarization simulated with spheroids and spherical aerosol model with the same size distribution and complex refractive index, taken from Dubovik et al. (2006).

$P_{ij}(\lambda,\Theta)$ and total aerosol optical thickness of extinction and scattering $\tau_{ext/scat}(\lambda)$ of non-spherical aerosol can be written as the following:

$$\tau_{scat}(\lambda)\,P_{ij}(\lambda,\Theta)=\sum_{p=1,\ldots,N_r}\sum_{k=1,\ldots,N_\varepsilon}K_{ij}^{\varepsilon}(\lambda,\kappa,n,r_p,\varepsilon_k)\,\frac{dN(\varepsilon_k)}{d\ln\varepsilon}\frac{dV(r_p)}{d\ln r}, \tag{3.2}$$

and

$$\tau_{ext/scat}(\lambda)=\sum_{p=1,\ldots,N_r}\sum_{k=1,\ldots,N_\varepsilon}K_{ext/scat}^{\varepsilon}(\lambda,\kappa,n,r_p,\varepsilon_k)\,\frac{dN(\varepsilon_k)}{d\ln\varepsilon}\frac{dV(r_p)}{d\ln r}, \tag{3.3}$$

where

$$K^{\varepsilon}_{...}(\lambda, k, n, r_p, \varepsilon_k) = \int_{\ln r_p - \Delta \ln r}^{\ln r_p + \Delta \ln r} \int_{\ln \varepsilon_k - \Delta \ln \varepsilon}^{\ln \varepsilon_k + \Delta \ln \varepsilon} \frac{C^{\varepsilon}_{...}(\lambda, \kappa, n, r_p, \varepsilon_k)}{v(r)} A_k(\varepsilon) B_p(r) d\ln\varepsilon d\ln r, \tag{3.4}$$

and $C^{\varepsilon}_{...}(\lambda, k, n, r, \varepsilon)$ denotes the scattering and extinction cross-sections of spherical particles and randomly oriented spheroids, λ - wavelength, n and κ - real and imaginary parts of the complex refractive index (m) , $\varepsilon = a/b$ spheroid axis ratio (a - axis of spheroid rotational symmetry, b - axis perpendicular to the axis of spheroid rotational symmetry), r - radius of volume equivalent sphere, $V(r)$ is the volume of particle, $dV(r_p)/d\ln r$ – the volume particle size distribution, $A_k(\varepsilon)$ and $B_p(r)$ are the functions providing correspondingly the interpolation of shape and size distributions between the selected points ε_k and r_i. In studies by Dubovik et al. (2002b, 2006), the coefficients $A_k(\varepsilon)$ were assumed as rectangular, and $B_p(r)$ as trapezoidal functions Dubovik and King (2000).

In the AERONET retrieval (Dubovik and King, 2000) volume size distribution was represented by $N_r = 22$ bins of equidistant in logarithmic scale, covering the size range from 0.05 to 15 μm. The size range was chosen on the base of the sensitivity analysis, which showed that the aerosol particles of smaller and larger sizes produce negligible contribution to AERONET radiometer observations (Dubovik and King, 2000).

This range of aerosol particle sizes is slightly wider than the one used in earlier studies by Nakajima et al. (1996). Using the approximation given by Eqs. 3.2 – 3.4, Dubovik et al. (2006) developed a numerical tool for fast calculations of scattering properties of spheroid mixture. The quadrature coefficients $K_{...}(\lambda, n, \kappa, r_p)$ for the extinction, as well as for absorption cross-sections and scattering matrices have been calculated and stored into the look-up tables for a wide range of n, κ, ε ($1.3 \leq n \leq 1.7$; $0.0005 \leq \kappa \leq 0.5$; $0.3 \leq \varepsilon \leq 3.0$) and for 41 narrow size bins covering

the size-parameter range from $\simeq 0.012$ to $\simeq 625$.

In addition, the developed software was used to show (Dubovik et al., 2006) that spheroids could closely reproduce single-scattering matrices of mineral dust measured in the laboratory (Volten et al., 2001). It was shown that scattering matrices have rather limited sensitivity to the minor details of axis ratio distribution $dN(\varepsilon_k)/d\ln\varepsilon$. Therefore, it was demonstrated that AERONET retrieval might rely on assumption that shape distribution in the non-spherical fraction of any tropospheric aerosol is the same. Based on this conclusion $dN(\varepsilon_k)/d\ln\varepsilon$ obtained by Dubovik et al. (2006) from fitting Volten et al. (2001) measurements was employed as shape distribution for non-spherical fraction:

$$\frac{dN(\varepsilon_k)}{d\ln\varepsilon} = \begin{cases} 0, 0.7 < \varepsilon < 1.44 \\ const, 1.44 \leq \varepsilon \leq 0.7 \end{cases}. \tag{3.5}$$

Based on this assumption, the integration over ε in Eq. 3.4 can be done once and for all and, modelling of aerosol optical properties $\tau_a(\lambda)$, ω_0^a, $P_{ij}^a(\lambda,\Theta)$ was implemented in the retrieval in a following form:

$$\begin{aligned} &\tau_{scat}(\lambda) P_{ij}(\lambda,\Theta) = \\ &\sum_{p=1,\ldots,N_r} \Big(C_{sph} K_{ij}^{sph}(\lambda,\kappa,n,r_p) + (1-C_{sph}) K_{ij}^{nons}(\lambda,\kappa,n,r_p) \Big), \end{aligned} \tag{3.6}$$

and

$$\begin{aligned} &\tau_{ext/scat}(\lambda) = \tau_{ext/scat}^{sph}(\lambda) + \tau_{ext/scat}^{nons}(\lambda) = \\ &\sum_{p=1,\ldots,N_r} \Big(C_{sph} K_{ext/scat}^{sph}(\lambda,\kappa,n,r_p) + (1-C_{sph}) K_{ext/scat}^{nons}(\lambda,\kappa,n,r_p) \Big), \end{aligned} \tag{3.7}$$

where

$$K_{\ldots}^{sph}(\lambda,n,\kappa,r_p) = \int_{\ln r_p - \Delta\ln r}^{\ln r_p - \Delta\ln r} \frac{C_{\ldots}^{sph}(\lambda,\kappa,n,r)}{v(r)} B_k(r) d\ln r, \tag{3.8}$$

and

$$K_{...}^{nons}(\lambda, n, \kappa, r_p) = \int_{\ln r_p - \Delta \ln r}^{\ln r_p - \Delta \ln r} B_p(r) \int \frac{C_{...}^{sph}(\lambda, \kappa, n, r)}{v(r)} \frac{dN(\varepsilon)}{d \ln \varepsilon} d \ln \varepsilon d \ln r. \qquad (3.9)$$

C_{sph} is the fraction of the spherical particles, and included in the set of retrieved parameters. Note, that described look up tables $K_{...}(\lambda, n, \kappa, r_p)$ allow very fast simulations of scattering by non-spherical aerosol particles.

The GARRLiC algorithm described here uses the same modelling strategy as described above to represent columnar properties of aerosol.

However, due to differences in information content of AERONET and lidar measurements bi-modal description of aerosol was used. This was implemented by introduction of two independent sets of aerosol parameters describing each aerosol component. In order to conserve compatibility of the retrieval with the ones based on AERONET-only observations the values of r_p were chosen the same, covering the same particle size range from 0.05 to 15 μm. Possibility to account for uni-modal or tri-modal distributions was provided by introduction of small (3 radius bins r_p) overlap of fine and coarse modes size distributions. Therefore, size distribution of the fine mode was represented by $N_r = 10$ bins equidistant in logarithmic scale within size range 0.05 – 0.58 μm, and coarse mode by 15 within the range of 0.33 to 15.0 μm. Correspondingly, aerosol size distribution parameters, aerosol particle shape and complex refractive indices are defined for each aerosol component (see Table 3.2) and used to calculate τ_a, ω_0^a and $P_{ij}(\theta)$ for each aerosol mode. Such bi-modal assumption has a good statistical background: in most of the observed cases size distribution of aerosols retrieved from AERONET observations could be described as bi-modal (Holben et al., 2001).

3.1.2 Vector radiative transfer

Photons can reach the instrument sensors either by single or multiple scattering in the atmosphere, reflection on the surface, and by combinations of atmospheric scattering and reflection on the surface (see Fig. 3.4). Single-scattering approximations can only be addressed to lidar measurements and satellite observations from the upper layers of the atmosphere. That is why to model the atmospheric radiation field observed by the sun-photometer some efforts should be involved to account for multiple scattering effects.

Simulation of AERONET almucantar measurements is implemented by the successive order of scattering radiative transfer code (Lenoble et al., 2007) that was used in PARASOL operational retrievals (Deuzé et al., 2001; Herman et al., 2005; Tanré et al., 2011). The code provides full information about the atmospheric radiation field including I and Q, U components of the Stoke's vector under the assumption of the plane parallel atmosphere. The developed version of successive order of scattering radiative transfer code allows calculations of atmospheric radiances for several N_k aerosol components. This allowed direct implementation of the code to the bimodal aerosol model. Each aerosol component is described by defined vertical profile of spectral extinction $\sigma_a^k(\lambda, h)$ and altitude independent phase matrix $P_{ij}^k(\lambda, \theta)$ and single-scattering albedo $\omega_0^k(\lambda)$. In the present set up of the aerosol retrieval code these optical properties are determined on the base of microphysical model of atmospheric aerosol. Correspondingly, only parameters describing aerosol microphysics are directly included in the set of retrieved parameters listed in Table 3.2. Specifically, the vertically invariant driven by: the shape of the size distribution $dV(r_i)/d\ln r$ giving the aerosol particle volume in the total atmospheric column per unit of surface area (in the unites of $\mu m^3/\mu m^2$); the real $n_k(\lambda)$ and imaginary $\kappa_k(\lambda)$ parts of the complex refractive index; and the fraction of the spherical particles C_{sph}. In order to account for vertical variability of aerosol extinction additional normalized functional

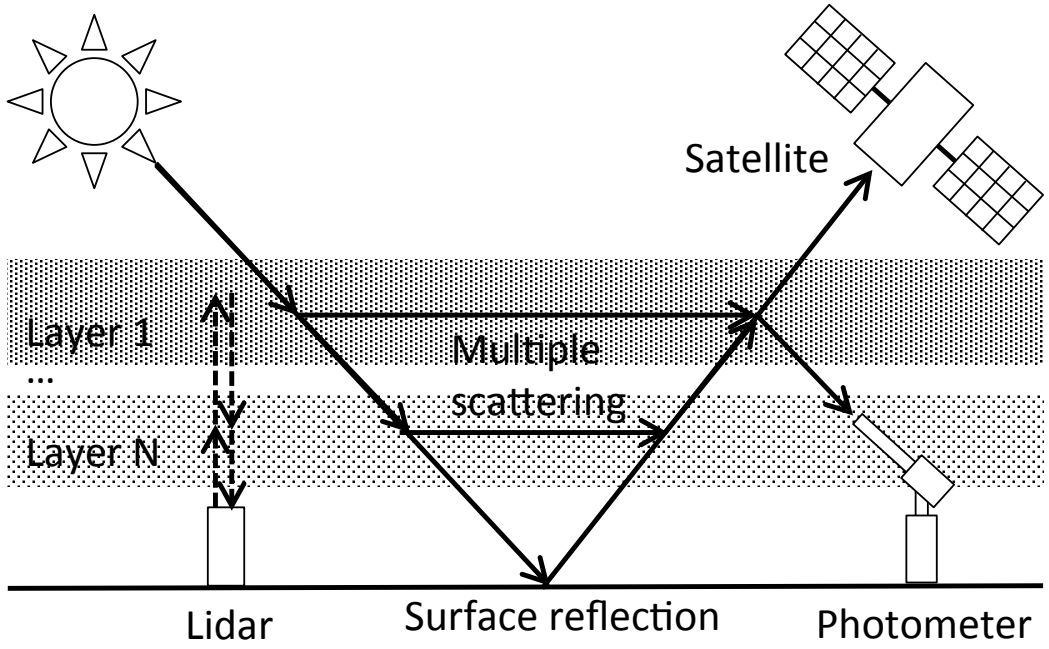

Figure 3.4: Schematic representation of the contributions of the atmosphere radiance as measured by different instruments.

characteristic $c_k(h)$ is used, which defines the vertical distribution of aerosol concentration. The optical thickness of k-th aerosol component in each of i-th atmospheric layer is defined as:

$$\Delta\tau_{i,k}(\lambda) = \tau_k(\lambda) \int_{h_{i+1}}^{h_i} c_k(h)\, dh. \tag{3.10}$$

Correspondingly, optical properties ($\Delta\tau_i(\lambda)$, ω_0^i and $P_{ij}^i(\Theta,\lambda)$) of the i-th atmospheric homogeneous layer are calculated using the following equations:

$$\Delta\tau_i = \Delta\tau_i^{gas} + \Delta\tau_i^{mol} + \sum_{k=1,2} \Delta\tau_i^{aer,k}, \tag{3.11}$$

$$\omega_0^i(\lambda) = \frac{\Delta\tau_i^{mol} + \sum\limits_{k=1,2} \Delta\tau_i^{aer,k}\omega_0(\lambda)}{\Delta\tau_i^{gas} + \Delta\tau_i^{mol} + \sum\limits_{k=1,2} \Delta\tau_i^{aer,k}}, \tag{3.12}$$

$$P_{ij}^i(\Theta,\lambda) = \frac{\Delta\tau_k^{mol} P_{ij}(\Theta,\lambda) + \sum\limits_{k=1,2} \Delta\tau_i^{aer,k}\omega_0^k(\lambda) P_{ij}^{aer,k}(\Theta,\lambda)}{\Delta\tau_i{}^{mol} + \sum\limits_{k=1,2} \Delta\tau_i^{aer,k}\omega_0(\lambda)}. \tag{3.13}$$

In the original PARASOL/POLDER retrieval (Dubovik et al., 2011) $c_k(h)$ was defined a priori as Gaussian function normalized to unity that depended on the retrievable parameter that has a meaning of the medium altitude of the layer of the k-th aerosol component (Dubovik et al., 2011). This assumption was made due to the limited sensitivity of the passive radiometric and polarimetric observations from space to aerosol vertical variability. On the other hand sensitivity studies by Dubovik and King (2000) show practically no sensitivity to aerosol vertical profile and, as a result, the operational AERONET retrievals are conducted under the assumption of vertically homogeneous atmosphere.

However such assumptions can't be used for combined lidar photometric retrievals as lidar sensitivity to the vertical structure of the aerosol is much stronger than in listed instruments. Instead of a priori estimation of vertical distribution of aerosol fractions these parameters were included into the set of microphysical parameters that are retrieved by the described algorithm (see Table 3.2), allowing vertical profiles of aerosol concentrations to have practically arbitrary shapes. In principle, such accurate accounting for aerosol vertical variability in radiative transfer calculations is not necessary for processing of passive observations, however, this may have some positive effects once radiometric data are combined with lidar observations, as it was done in the present study.

Ground-based lidar measurements don't cover all atmosphere altitudes and usually have upper and lower limits h_{min} and h_{max} correspondingly. Therefore, vertical profile of aerosol distribution should be extrapolated in order to represent vertical distribution of aerosol in the whole atmosphere column, what is strongly important for radiative transfer calculations. This extrapolation is made on the assumptions that the aerosol amount on the altitudes higher than upper limit of lidar measurement is negligible, and amount of the aerosol in the atmospheric layer close to the ground is

the same, as on the lower altitude limit of lidar measurement:

$$c_k(h) = \begin{cases} c_k(h_{\min}), h_{BOA} < h < h_{min} \\ \sum_{i=1}^{N_h} c_k(h_i) D(h_i), h_{min} < h < h_{max} \\ c_k(h_{max}) \exp(-\alpha h), h_{max} < h < h_{TOA}, \end{cases} \tag{3.14}$$

where α is chosen according to the following equation:

$$\exp(\alpha h_{TOA}) = o, \tag{3.15}$$

where o denotes estimation of aerosol vertical distribution on the altitude of the top of the atmosphere (h_{TOA}), and chosen as a small value (10^{-6}). In general, the third part of the Equation 3.15 could be chosen as any monotonously decreasing function, that returns a close to zero value on the top of atmosphere (TOA). Middle term in Equation 3.15 represents the vertical distribution profile that is included in the set of aerosol microphysical parameters. As used radiative transfer code operates with the functional representation of $c_k(h)$, trapezoidal interpolation $D(h_i)$ between neighbor values of $c_k(h)$ was used to estimate aerosol concentration profile at any altitude needed. Additional normalization to unity of the $c_k(h)$ was implemented as a part of forward calculations.

Used lidar observations had an altitude range $\simeq$ 0.5 km up to $\simeq$ 10 km, with the altitude resolution Δh of 15 m, which provides information about aerosol backscatter properties in $N_h \simeq 600$ altitude points h_i. This provides information to retrieve aerosol concentration profile at the same altitude points. Although it is possible for the algorithm to operate with such tremendous set of the retrieved parameters, the computational times would be an issue. So, to decrease amount of necessary computations, N_h was set to 60. In order to prevent loss of significant information provided by lidar observations about vertical distribution of aerosol components logarithmical

scale with equidistant $\Delta \ln h$ was used:

$$h_i = h_{min} \exp\left(\frac{\ln\left(h_{max}/h_{min}\right)(i-1)}{N_h - 1}\right), \tag{3.16}$$

where i and N_h are the indexes of the current and upper limit altitudes correspondingly: $h_i = i\Delta h$, $h_{max} = N_h \Delta h$. The lidar observations used in the combined retrieval should be down-sampled to the same altitude resolution, in detail it will be described in the following section. Consequently, the modified version of the radiative transfer module used in the combined lidar photometric retrieval code is set to retrieve two aerosol components. The algorithm derives single values of complex refractive index and fraction of spherical particles for particles of all sizes for each aerosol component. It should be noted that earlier sensitivity studies of AERONET retrievals (Dubovik and King, 2000; Dubovik et al., 2006) indicated major limitations in discriminating between refractive indices and shapes of aerosol particles of fine and coarse modes. But it will be demonstrated that combination with lidar gives possibility of retrieving two aerosol components with different complex refractive indices together with their vertical distributions.

3.1.3 Lidar equation

To model the attenuated backscatter provided by lidar (Eq. 2.19) a lidar equation (Eq. 2.16) could be used. However, $L^*(\lambda, h)$ depends on the estimation of the measured signal at the reference point h_{ref}. Selection of the reference point is generally a manual procedure that could influence the lidar retrievals (Kovalev and Oller, 1994; Matsumoto and Takeuchi, 1994). To lessen the errors caused by non-optimal reference point selection, Chaikovsky et al. (2004) have used additional parameter

$R(\lambda, h_{ref})$, transforming Eq. 2.17 into:

$$L(\lambda, h_{ref}) = C(\lambda) R(\lambda, h_{ref}) \beta_m(\lambda, h_{ref}) \exp\left(-2\left(\tau_a(\lambda, h_{ref}) + \tau_m(\lambda, h_{ref})\right)\right), \tag{3.17}$$

where parameter $R(\lambda, h) = \frac{\beta_a(\lambda,h)+\beta_m(\lambda,h)}{\beta_m(\lambda,h)}$ is known as backscatter ratio and describes the uncertainty of the calibration procedure and allows accounting for the presence of aerosol on the reference altitude (see, e.g., Russell et al., 1979).

With these regards, Equation 2.16 should be reformulated. Also it should follow the same calibration procedure described by Equations 2.18 and 2.19 to adequately represent the acquired lidar measurements $L^*(\lambda, h)$:

$$L(\lambda, h) = A(\lambda)\left(\beta_a(\lambda, h) + \beta_m(\lambda, h)\right) \exp\left(2 \int_h^{h_{ref}} \sigma_a(\lambda, h')\, dh'\right), \tag{3.18}$$

where $A(\lambda) = 1/R(\lambda, h_{ref})$ (see Table 3.2) is the lidar calibration parameter that is included in the set of retrieved parameters, following the same approach as proposed by Chaikovsky et al. (2004). The main difference is the application of the calibration parameter: in LiRIC $R(\lambda, h_{ref})$ is applied to the measurements of attenuated backscatter 2.19, while in GARRLiC it is applied to the lidar equation (Eq. 3.18), that is used for modelling these measurements. It should be outlined that the goal of the introduction of this additional retrievable parameter is the reduction of uncertainties of the lidar calibration procedure, and it remains the same for both algorithms.

As it was mentioned above, lidar measurements are made with constant altitude sampling Δh within altitude range $[h_{min}; h_{max}]$, which provides information about aerosol backscatter properties in $N_h \simeq 600$ altitude points h_i. In order to avoid excessively high number of the retrieved parameters and to decrease the amount of computations needed for the inversion N_h was limited to a smaller number ($\simeq 60$). The quantity of altitude samples is decreased using equidistant logarithmic scale (Eq. 3.16). It

should be mentioned that described method itself could work with any vertical profile sampling.

On the other hand, in most sounding conditions vertical variability of aerosol distribution decreases with altitude. Therefore in the upper layers lidar signal is usually oversampled. A power of the laser pulse during lidar sounding decreases as square of the altitude providing lower signal levels from upper layers, which means that noise increase with the altitude. In described situation down-sampling of lidar signal with logarithmical scale over altitude provides sufficient noise suppression. In order to preserve as much information content of the sounding signal as possible the decimation of the signal were made using averaging over the points lower than re-sampling altitude h_i ($h_{i-1} \leq j\Delta h \leq h_i$):

$$L(\lambda, h_i) = \sum_{j=n_1}^{n_2} \frac{L^*(\lambda, j\Delta h)}{n_1 - n_2} + O(\lambda, n_1, h_i) + O(\lambda, n_2, h_{i-1}), \tag{3.19}$$

where i and j denote new and original sampling indexes correspondingly, n_1 and n_2 are the closest integer numbers to $\frac{h_i}{\Delta h}$ and $\frac{h_{i-1}}{\Delta h}$, $n_1 - n_2$ is the number of altitude samples of original lidar signal situated between h_i and h_{i-1}, and $O(\lambda, n, h) = (L^*(\lambda, (n+1)\Delta h) - L^*(\lambda, n\Delta h))(h_i - n\Delta h)/\Delta h$ is the linear interpolation of the lidar signal within the original altitude sample Δh, that accounts for part of the signal that is left behind in the case when $h_i \neq i\Delta h$.

According to the Kotelnikov-Nyquist theorem (Nyquist, 1928; Kotelnikov, 1933) the lower sampling rate at high altitudes decreases the amplitudes of high frequency oscillations, which usually are attributed to noise. The described decimation method could be considered as expanding sliding window low pass filter, allowing efficient noise suppression without loss of significant information about aerosol vertical structure.

3.1.4 Vertical profiling of atmosphere optical properties

As it was shown in the section above, light back propagation in the atmosphere during lidar sounding could be described by means of Equation 3.18 provided with vertical profiles of backscatter and extinction for aerosol and molecular scattering at the given wavelength λ.

Vertical profiles of molecular backscatter $\beta_m(\lambda, h)$ and extinction $\sigma_m(\lambda, h)$ could be estimated as follows:

$$\sigma_m(\lambda, h) = C_s(\lambda)\frac{P(h)}{T(h)}, \tag{3.20}$$

$$\beta_m(\lambda) = \frac{1}{S_m}\frac{\sigma_m(\lambda, h)}{k(\lambda)}, \tag{3.21}$$

where $S_m = \frac{8}{3}\pi$ is the lidar ratio of Rayleigh scattering, $P(h)$ and $T(h)$ are the vertical profiles of atmospheric pressure (in hPa) and temperature ($^\circ K$) correspondingly. These profiles could be retrieved either from direct measurements, from climatological models (for e.g. COSPAR international reference atmosphere (CIRA) `http://badc.nerc.ac.uk/view/badc.nerc.ac.uk__ATOM__dataent_CIRA` or (Tomasi et al., 1998)) or calculated according to the standard atmosphere model (e.g., ISA, 1975; ICA, 1993; SA, 1976). Standard atmosphere model (SA) allows calculating vertical profiles of temperature and pressure of atmosphere gazes. Temperature profile is defined as follows:

$$T(h) = T^* + b\left(H(h) - H^*\right), \tag{3.22}$$

where H^* denotes lower altitude of the atmosphere layer, $H = \frac{rh}{r+h}$ and r is the Earth radius (6356767 m).

Pressure profile could be calculated on the basis of equations below:

$$p_m(h) = 10^{\lg p(h)}, \tag{3.23}$$

where

$$\lg p\left(h\right)=\left[\begin{array}{l}\lg p^{*}-\frac{g}{bR}\lg\left(\frac{T(h)}{T^{*}}\right),b\neq0\\ \lg p^{*}-\frac{ag}{RT(h)}\left(H\left(h\right)-H^{*}\right),b=0\end{array}\right., \tag{3.24}$$

where $a=0.434294$.

According to the standard atmosphere model, each atmosphere layer is described by its own set of parameters b, H^{*}, T^{*} and p^{*} which could be found in Table 3.3. Coefficients C_s, k in Equation 3.21 are defined for specific wavelengths λ, and are

Table 3.3: Values of parameters of the standard atmosphere; according to (ISA, 1975).

H^{*},m	$b,\frac{^{\circ}K}{m}$	$T^{*},^{\circ}K$	p^{*},Pa
0	-0.0065	288.15	101325
11019	0	216.65	22632.28133
20063	0.001	216.65	5474.992145
32162	0.0028	228.65	868.0055979
47350	0	270.65	110.9070857
51412	-0.0028	270.65	66.94257775
71802	-0.002	214.65	3.956316223
86152	0	186.65	0.363403538

listed in Table 3.4 (Freudenthaler, 2010).

Table 3.4: Values of coefficients used for molecular extinction and backscatter coefficients calculations for different wavelengths; according to Freudenthaler (2010).

Wavelength, μm	$C_s,\frac{^{\circ}K}{hPam}$	k^{T}
0.308	$3.6552{\cdot}10^{-5}$	1.04555
0.351	$2.0959{\cdot}10^{-5}$	1.04338
0.354814	$2.0026{\cdot}10^{-5}$	1.04324
0.355	$1.9981{\cdot}10^{-5}$	1.04323
0.400	$1.2123{\cdot}10^{-5}$	1.04191
0.5106	$4.4272{\cdot}10^{-6}$	1.04026
0.532	$3.7425{\cdot}10^{-6}$	1.04007
0.532221	$3.7361{\cdot}10^{-6}$	1.04007
0.710	$1.1574{\cdot}10^{-6}$	1.03919
0.800	$7.1443{\cdot}10^{-7}$	1.03897
1.064	$2.2647{\cdot}10^{-7}$	1.03863
1.064442	$2.2609{\cdot}10^{-7}$	1.03863

To calculate the molecular optical thickness, calibration procedure that is applied to lidar signal should be taken into account, resulting in the following equation:

$$\tau_m(\lambda, h, h_{ref}) = \begin{cases} \int_h^{h_{ref}} S_m \beta_m(\lambda, h)\, \Delta h \frac{cos\Theta_0}{cos\Theta_i}, h < h_{ref} \\ -\int_h^{h_{ref}} S_m \beta_m(\lambda, h)\, \Delta h \frac{cos\Theta_0}{cos\Theta_i}, h > h_{ref} \\ 0, h = h_{ref}. \end{cases} \tag{3.25}$$

Vertical profile of aerosol extinction coefficient could be retrieved by altitude differentiation of the Eq. 3.10:

$$\sigma_a(\lambda, h) = \tau_a(\lambda)\, c(h), \tag{3.26}$$

To determine the vertical profile of backscatter one can use the dependence between extinction and backscattering also known as lidar ratio (see Eq. 2.20) which could be calculated from the columnar aerosol optical properties:

$$S_a(\lambda) = \frac{4\pi}{\omega_0(\lambda)\, P_{11}(\lambda, 180^\circ)}. \tag{3.27}$$

In the proposed method columnar optical properties that define lidar ratio in Eq. 3.27 are estimated on the base of aerosol microphysical parameters (see Table 3.2) following equations 3.3 – 3.9. Combining Eq. 3.27 with Eq. 3.26 one can get:

$$\beta(\lambda, h) = \frac{1}{4\pi} \left(\tau_a(\lambda)\, c(h)\, \omega_o(\lambda)\, P_{11}(\lambda, 180^\circ)\right). \tag{3.28}$$

Therefore, Equations 3.21 – 3.28 provide all sufficient information needed to model lidar sounding, starting from the set of microphysical aerosol parameters (see Fig. 3.2), consequently allowing the retrieval of the set of aerosol microphysical parameters listed in Table 3.2. General scheme of aerosol vertical profiling is shown in Fig. 3.5. It is clearly seen from the Equations 3.26 – 3.28 that such vertical profiling of aerosol optical properties could be used only in one wavelength lidar sounding. The

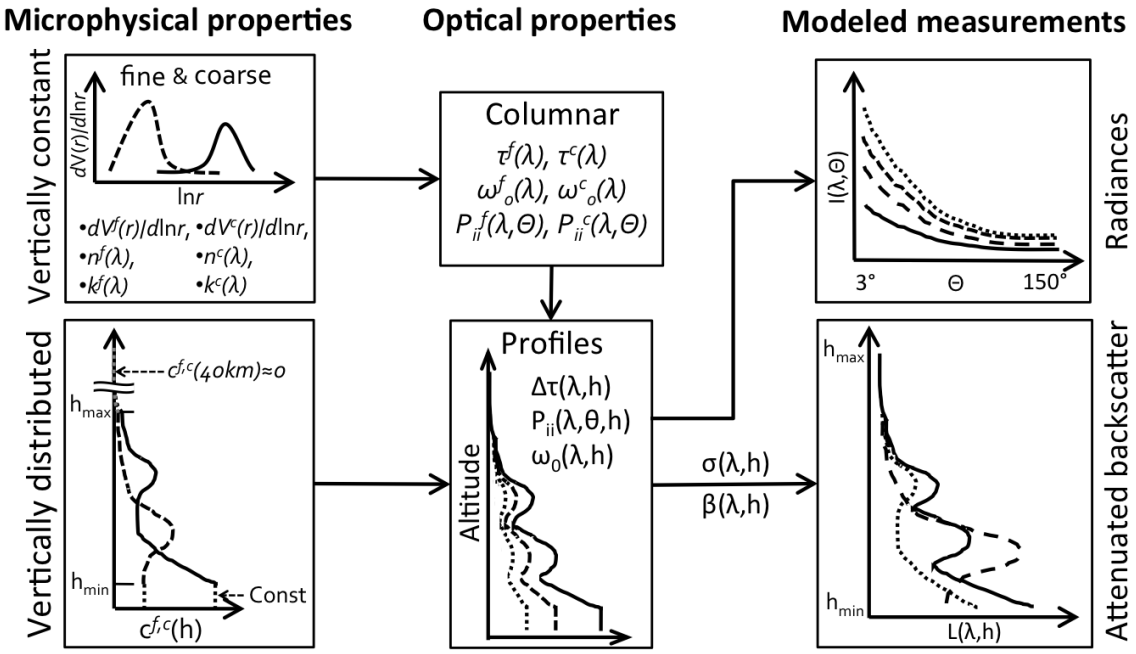

Figure 3.5: General scheme of the measurements model using two-component vertically distributed aerosol model.

vertical profile is defined by altitude independent optical properties and a spectrally independent vertical concentration profile. That means that spectral dependence of the backscatter in the case of multi-wavelength lidar sounding will be the same at each atmosphere layer. Such estimation in fact will adequately describe multi-wavelength lidar sounding only in case of aerosol that has vertically homogeneous optical properties. Therefore such estimation doesn't allow using the information of vertical variability of spectral backscatter that is the most informative part of multi-wavelength lidar observations.

However, as it was shown by Chaikovsky et al. (2002a) and Cuesta et al. (2008) it is possible to describe mentioned variability by splitting aerosol into several N_k components with altitude independent size distributions and different vertical concentration profiles $c_k\,(h)$. Splitting size distribution into a set of modes allowed to characterize different aerosol components with different altitude independent optical properties

(Chaikovsky et al., 2006b; Cuesta et al., 2008):

$$\sigma_a(\lambda) = \sum_{k=1}^{N_k} a_k(\lambda)\, c_k(h), \tag{3.29}$$

and

$$\beta_a(\lambda) = \sum_{k=1}^{N_k} b_k(\lambda)\, c_k(h). \tag{3.30}$$

In the original work Chaikovsky et al. (2002a) used lidar measurements and coincident AERONET microphysical retrievals to estimate coefficients $a_k(\lambda)$ and $b_k(\lambda)$ (see Eqs. 3.29 – 3.30). Combining Equations 3.26 – 3.28 with 3.29 – 3.30 one can get:

$$\sigma_a(\lambda, h) = \sum_{k=1}^{N_k} \tau_a^k(\lambda) c_k(h)\,, \tag{3.31}$$

and

$$\beta_a(\lambda, h) = \frac{1}{4\pi} \sum_{k=1}^{N_k} \tau_a^k(\lambda)\, c_k(h) \omega_o(\lambda)\, P_{11}(\lambda, 180^\circ)\,. \tag{3.32}$$

It should be noted that described algorithm follows the same approaches of estimation of vertical aerosol optical properties on the base of columnar optical properties and aerosol vertical concentration profiles as in LiRIC (Chaikovsky et al., 2002a,b, 2012). The main difference between GARRLiC on the one hand and LiRIC and approach of Cuesta et al. (2008) on the other is how the columnar optical properties of each mode are estimated. In previous approaches aerosol microphysical model was defined by coincident AERONET retrieval. As long as standard AERONET algorithm operates with uni-modal aerosol description, additional assumptions about aerosol refractive index should be made to split aerosol into several modes and use this microphysical properties to estimate optical parameters of each mode.

Listed assumptions could vary from rather simple, assuming refractive index to be the same for fine and coarse mode (Chaikovsky et al., 2002a,b), to more complicated, where particle size dependent refractive indexes for $N_k = 6$ modes are given by the

climatology statistics Cuesta et al. (2008).

On the contrary, GARRLiC uses independent set of the aerosol microphysical parameters for two ($N_k = 2$), fine and coarse, aerosol modes, allowing direct and simultaneous retrieval of the refractive indexes of the aerosol components without any additional assumptions.

The details of LiRIC and GARRLiC comparison concerning the use of measurements and retrieval of results are generalized in Figure 3.6.

Therefore, Equations 3.31 – 3.32 allow vertical profiling of columnar optical prop-

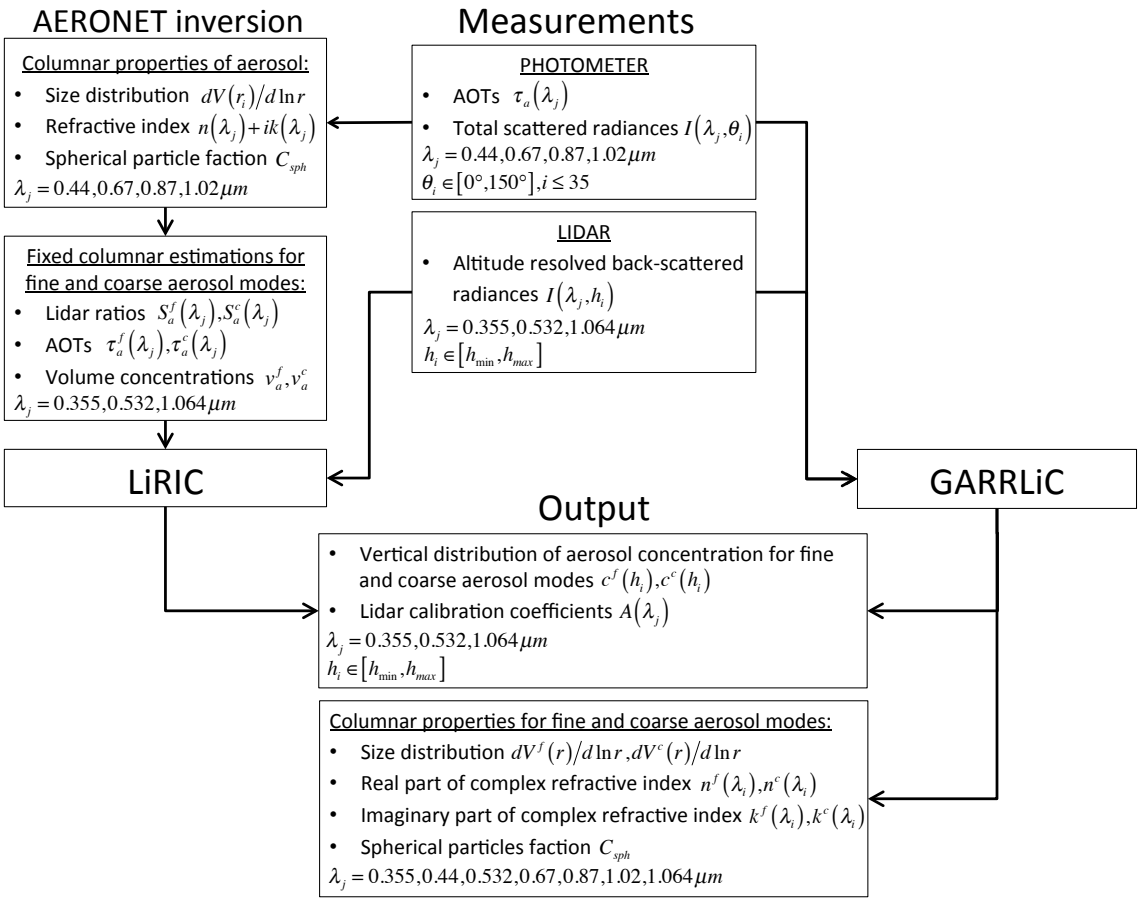

Figure 3.6: Comparison of the data flow in LiRIC and GARRLiC algorithms.

erties of the aerosol, providing sufficient information to simulate back propagation of light in the atmosphere during lidar sounding.

The methodology described in this section allows modelling of optical properties of

aerosol layers from the united set of microphysical parameters of fine and coarse aerosol modes (see Table 3.2). This set contains columnar (size distribution, complex refractive index and spherical particles fraction) and vertically variable (profile of aerosol concentration) parameters for both modes. Aerosol components are modelled as a mixture of randomly oriented spheres and spheroids with retrievable fraction of spherical particles.

Supplied with estimations of gaseous absorption, molecular scatter and assumptions of aerosol distribution in the lower ($h < h_{min}$) and upper ($h > h_{max}$) part of the atmosphere it provides adequate modelling of coincident lidar/sun-photometer measurements. Provided with the real measurements and combined with the numerical inversion methods it will allow retrieving the described set of parameters from the real coincident observations. The details of the numerical inversion module used in the GARRLiC algorithm are given in the following section.

3.2 Numerical inversion

When the atmospheric characteristics are known, including optical and microphysical properties of atmospheric aerosols, as well as their vertical distribution, "Forward model" (described in the Section 3.1) could calculate the radiation field that is observed by both passive and active instruments. Such observations could be used to infer the optical and microphysical properties of aerosol particles in the atmosphere together with their vertical distribution. Often this is accomplished by simple comparison of the measurements with the "forward model" computations for a wide range of aerosol parameters. This method is referred to as *table look-up* procedures and obtains a solution by comparing measurements directly with theoretical calculations. Despite of being stable and fast-and-easy in implementation, the look-up table solution is limited to a set of potentially admissible solutions that are included

in the look-up table.

However, there are methods that are not limited to a predefined set of aerosol classes and instead search for the set of aerosol parameters. These methods optimize the error distribution of the retrieved parameters, providing the best fitting of the measurements through the continuous space of all possible solutions under statistically formulated criteria. These rigorous and more complex methods consist in "inverting" a set of measurements to infer the input properties of the given "forward model" and usually referred to as "numerical inversion".

Nonetheless, in practice, several different combinations of aerosol parameters often produce nearly the same radiative field. Therefore, the general solution is fundamentally non-unique or becomes so in the presence of fundamentally unavoidable measurement noise. Inversion problems with this particularity are known as "ill-posed". An ill-posed inversion could provide a satisfactory result once additional information is added to constrain the solution, while representing the measurement field within the errors established for the measurement. Such information is referred to as "a priori assumptions", and usually applied in the form of constrains of smoothness of aerosol parameters.

In a contrast to the majority of existing aerosol retrieval algorithms, the one used in this work is one of the first attempts to develop an aerosol retrieval using statistically optimized multi-variable fitting of multi-instrumental data.

Detailed descriptions of inversion methods can be found in various textbooks (Tikhonov and Arsenin, 1977; Twomey, 1977a; Tarantola, 1987; Press et al., 1992; Rodgers, 2000; Doicu, 2010). However, the choice of the particular method for the particular application is not discussed in this work.

The approach used here is focused on clarifying the connection between different inversion methods established in atmospheric optics and unifying the key ideas of these methods into a single inversion procedure. It follows the developments by

Dubovik and King (2000) and Dubovik (2004); Dubovik et al. (2008, 2011).

The methodology has several original (compared to standard inverse methods) features optimized for remote sensing applications. It addresses such important aspects of inversion optimization as accounting for errors in the observations, inversion of multi-source data with different levels of accuracy, accounting for a priori and ancillary information, etc. (Dubovik, 2004; Dubovik et al., 2011). The concept uses the principles of statistical estimation and suggests a generalized multi-term Least Square (LSM) type formulation that complementarily unites advantages of a variety of practical inversion approaches, such as Phillips-Tikhonov-Twomey constrained inversion (Phillips, 1962; Tikhonov, 1963; Twomey, 1963), Kalman filter (Kalman, 1960), Newton-Gauss and Levenberg-Marquardt iterations, etc. This approach provides significant transparency and flexibility in development of remote sensing algorithms for deriving such continuous characteristics as vertical profiles, size distributions, spectral dependencies of some parameters, etc. For example, compared to the popular "Optimal Estimation" equations (Rodgers, 2000), the multi-term Least Square type formulation allows harmonious utilization of not only a priori estimate term, but instead, or in addition, using a priori terms limiting derivatives of the solution (Dubovik, 2004; Dubovik et al., 2008). This methodology has resulted from the multi-year efforts on developing inversion algorithms for retrieving comprehensive aerosol properties from AERONET ground-based observations.

The detailed description of the adopted inversion methodology could be found in (Dubovik and King, 2000; Dubovik, 2004; Dubovik et al., 2008, 2011). The following paragraphs will concentrate on the changes made to introduce combined lidar-photometric observations into the retrieval. There are two key aspects in the algorithm organization: the general organization of observation fitting, including the error estimation of different measurements and the a priori data representation.

3.2.1 Observation fitting

The purpose of the proposed method is to retrieve through inversion the vector describing microphysical properties of the atmospheric aerosol:

$$\mathbf{a} = \begin{pmatrix} \mathbf{a}_v \\ \mathbf{a}_n \\ \mathbf{a}_\kappa \\ \mathbf{a}_{sph} \\ \mathbf{a}_h \\ \mathbf{a}_A \end{pmatrix}, \tag{3.33}$$

where $\mathbf{a}_v$, $\mathbf{a}_n$, $\mathbf{a}_\kappa$, $\mathbf{a}_{sph}$, $\mathbf{a}_h$ and $\mathbf{a}_A$ denote the components of the vector of aerosol properties $\mathbf{a}$, corresponding to size distribution $dV(r_i)/d\ln r$, real and imaginary part of refractive index $n(\lambda_i)$, $\kappa(\lambda_i)$, fraction of the spherical particles C_{sph}, vertical profiles of aerosol concentration $c(h_i)$ and lidar calibration coefficient $A(\lambda_i)$.

It should be noted that all of the parameters listed above describing microphysical

Table 3.5: Description of the vector of unknowns ($\mathbf{a}$) retrieved by the GARRLiC algorithm.

Notation	Definition	Variability limits
$\mathbf{a}_v$	$\left\{\mathbf{a}_v^k\right\}_i = \ln\left(\frac{aV(r_i)}{d\ln r}\right), i = 1, ..., N_r^k,\ k = 1, 2$	$0.000005 \leq \frac{dV(r_i)}{d\ln r} \leq 0.03$ $i = 1, N_r^k, (\mu m^3/\mu m^2)$
$\mathbf{a}_n$	$\left\{\mathbf{a}_n^k\right\}_i = \ln\left(n\left(\lambda_i\right)\right), i = 1, ..., N_\lambda, k = 1, 2$	$1.33 \leq n\left(\lambda_i\right) \leq 1.6$
$\mathbf{a}_\kappa$	$\left\{\mathbf{a}_\kappa^k\right\}_i = \ln\left(k\left(\lambda_i\right)\right), i = 1, ..., N_\lambda, k = 1, 2$	$0.0005 \leq k\left(\lambda_i\right) \leq 0.1$
$\mathbf{a}_{sph}$	$\mathbf{a}_{sph} = \ln\left(C_{sph}\right)$	$0.001 \leq C_{sph} \leq 1.0$
$\mathbf{a}_h$	$\left\{\mathbf{a}_h^k\right\}_i = \ln\left(c_k\left(h_i\right)\right), i = 1, ..., N_h, k = 1, 2$	$\int_{h_{BOA}}^{h_{TOA}} c_k(h)dh = 1$
$\mathbf{a}_A$	$\left\{\mathbf{a}_A\right\}_i = \ln\left(A\left(\lambda_i\right)\right), i = 1, ..., N_{\lambda_{lidar}}$	$0.1 \leq A\left(\lambda_i\right) \leq 3.0$

state of the aerosol in the atmosphere, except for the lidar calibration parameters,

consist of two subsets of parameters, each describing independent aerosol component, corresponding to fine and coarse aerosol mode:

$$\mathbf{a}_{...} = \begin{pmatrix} \mathbf{a}^{f}_{...} \\ \mathbf{a}^{c}_{...} \end{pmatrix}. \tag{3.34}$$

Lidar calibration parameter $A(\lambda_i)$ is defined for the number of lidar wavelengths $N_{\lambda_{lidar}}$ included in the combined observation.

As it was mentioned above inversion is considered as multi-term Least Squares Method (LSM) that solves the following system of equations (Dubovik and King, 2000; Dubovik et al., 2011):

$$\begin{cases} \mathbf{f}^{*} = f(\mathbf{a}) + \Delta\mathbf{f} \\ \mathbf{0}^{*} = (\Delta\mathbf{a})^{*} = \mathbf{S}\mathbf{a} + \Delta(\Delta\mathbf{a}) \\ \mathbf{a}^{*} = \mathbf{a} + \Delta\mathbf{a}^{*}, \end{cases} \tag{3.35}$$

where $\mathbf{f}^{*}$ is a vector of the combined measurements, $\Delta\mathbf{f}$ is a vector of measurement uncertainties and $\mathbf{a}$ is a vector of unknowns.

The second term in Eq. 3.35 represents the a priori smoothness assumptions used to constrain the variability of size distribution, vertical concentration and spectral dependencies of the real and imaginary parts of the refractive index. The matrix $\mathbf{S}$ includes the coefficients for calculating m-th differences (numerical equivalent of the derivatives) of $dV(r_i)/d\ln r$, $c(h_i)$, $n(\lambda_i)$ and $\kappa(\lambda_i)$; $\mathbf{0}^{*}$ is the vector of zeros and $\Delta(\Delta\mathbf{a})$ is the vector of the uncertainties characterizing the deviations of the differences from the zeros.

The third part in Eq. 3.35 includes the vector of a priori estimates $\mathbf{a}^{*}$ and $\Delta\mathbf{a}^{*}$ is the vector of the uncertainties in a priori estimates. The errors $\Delta\mathbf{f}$, $\Delta(\Delta\mathbf{a})$, and $\Delta\mathbf{a}^{*}$ are assumed normally distributed.

According to the multi-term LSM concept, the solution for the Equation 3.35 corre-

sponds to the minimum of the following quadratic form:

$$\begin{aligned}&\Psi\left(\mathbf{a}^p\right)=\Psi_f\left(\mathbf{a}^p\right)+\Psi_\Delta\left(\mathbf{a}^p\right)+\Psi_a\left(\mathbf{a}^p\right)=\\&\tfrac{1}{2}\left(\left(\Delta\mathbf{f}^p\right)^T\mathbf{W}_f^{-1}\Delta\mathbf{f}^p+\gamma_\Delta(\mathbf{a}^p)^T\mathbf{\Omega}\mathbf{a}^p+\gamma_a(\mathbf{a}^p-\mathbf{a}^*)^T\mathbf{W}_a^{-1}\left(\mathbf{a}^p-\mathbf{a}^*\right)\right).\end{aligned}\tag{3.36}$$

The minimum could be obtained by iterative procedure:

$$\mathbf{a}^{p+1}=\mathbf{a}^p-t_p\Delta\mathbf{a}^p,\tag{3.37}$$

where $\mathbf{a}^p$ is the p-th the solution of so called normal system:

$$\mathbf{A}_p\Delta\mathbf{a}^p=\nabla\Psi\left(\mathbf{a}^p\right),\tag{3.38}$$

where $\mathbf{A}_p$ is the Fisher Matrix and the right side and represents the gradient $\nabla\Psi\left(\mathbf{a}^p\right)$:

$$\nabla\Psi\left(\mathbf{a}^p\right)=\mathbf{K}_p^T\mathbf{W}_f^{-1}\Delta\mathbf{f}^p+\gamma_\Delta\mathbf{\Omega}\mathbf{a}^p+\gamma_a\mathbf{W}_a^{-1}\left(\mathbf{a}^p-\mathbf{a}^*\right),\tag{3.39}$$

$$\mathbf{A}_p=\mathbf{K}_p^T\mathbf{W}_f^{-1}\mathbf{K_p}+\gamma_\Delta\mathbf{\Omega}+\gamma_a\mathbf{W}_a^{-1},\tag{3.40}$$

where $\Delta\mathbf{f}^p=f\left(\mathbf{a}^p\right)-\mathbf{f}^*$ and $\mathbf{K}_p$ is the Jacobi matrix of the first derivatives $\frac{\partial f(\mathbf{a}^p)}{\partial a_i}$. It should be noted that Fisher Matrix $\mathbf{A}_p$ can be considered as so-called Hessian matrix of second-order partial derivatives of the quadratic form $\Psi\left(\mathbf{a}^p\right)$ (see for e.g. Bevington, 1969; Tarantola, 1987). Correspondingly, Eq. 3.38 can be also written as follows:

$$\left(\nabla\nabla\Psi\left(\mathbf{a}^p\right)\right)\Delta\mathbf{a}^p=\nabla\Psi\left(\mathbf{a}^p\right),\tag{3.41}$$

where $\nabla\nabla^T\Psi\left(\mathbf{a}^p\right)$ is the matrix with the elements $\left\{\nabla\nabla^T\Psi\left(\mathbf{a}^p\right)\right\}_{ji}=\frac{\partial^2\Psi(\mathbf{a})}{\partial a_j\partial a_i}\Big|_{\mathbf{a}=\mathbf{a}^p}$. $\mathbf{W}$ are the weighting matrices, defined by Dubovik and King (2000) as follows:

$$\mathbf{W}_{...}=\frac{\mathbf{C}_{...}}{\varepsilon_{...}},\tag{3.42}$$

where $\varepsilon^2_{...} = \{\mathbf{C}_{...}\}_{11}$ are the first diagonal elements of the corresponding covariance matrices $\mathbf{C}_{...}$ and $\gamma_{...}$ are Lagrange multipliers, defined by Dubovik (2004):

$$\gamma_{...} = \frac{N_f \varepsilon_f^2}{N_{...} \varepsilon^2_{...}}, \tag{3.43}$$

where $N_{...}$ are the sizes of corresponding vectors.

Equation 3.43 is written under an assumption that increasing the number of measurements in the coordinated set of remote sensing observations inevitably will decrease the accuracy of each single measurement in this observation set.

For example, if a sun-photometer takes one single observation, the expected variance of measurement error is $\varepsilon^2_{f,N}$. If the same sensor makes N_f space- and/or time-coordinated observations the variance of the error in each single observation increases by the factor N_f, i.e. $\varepsilon^2_{f,N} \sim N_f \varepsilon^2_{f,1}$. This increase can be explained by the fact that the consistency of the N_f coordinated observations should be assured by controlling relations between the N_f observations. The control of each of those relationships introduces a random error $\varepsilon^2_{f,N}$, correspondingly the error variance of a single measurement in dimensional observation increases in N_f times.

The coefficient t_p in Eq. 3.37 is adjusted to provide the monotonic decrease of $\Psi(\mathbf{a}^p)$, i.e.

$$\Psi\left(\mathbf{a}^{p+1}\right) < \Psi\left(\mathbf{a}^p\right). \tag{3.44}$$

If all assumptions are correct, the minimum value of the above quadratic form can be theoretically estimated as follows:

$$\Psi(\mathbf{a}) \approx \left(N_f + N_\Delta + N_{a^*} - N_a\right) \varepsilon_f^2. \tag{3.45}$$

Note that the minimum value of $\Psi(\mathbf{a}^p)$ relates to ε_f^2 because the weighting matrices were used instead of using directly the covariance matrices. Once the value of mea-

surement error is known ε_f^2, Eq. 3.45 can be used to verify the consistency of the retrieval. Specifically, the inability to achieve the above minimum can indicate the presence of unidentified biases or inadequacy in the assumptions made.

It should be noted that the control of "measurement residual" $\Psi_f(\mathbf{a}^p)$ (the first term of quadratic form in Eq. 3.36) is a very useful tool for diagnostics of the retrieval dynamics. Specifically, the final value of $\Psi_f(\mathbf{a}^p)$ should be close to the level of the expected measurement noise. Indeed, if the algorithm has found the right solution, the value of the total residual $\Psi(\mathbf{a}^p)$ should be rather small and determined mainly by the random errors of observations. The contributions of the a priori residual terms in Eq. 3.36 should not be significant, because generally the weights of a priori terms $\Psi_\Delta(\mathbf{a}^p)$ and $\Psi_a(\mathbf{a}^p)$ are minor compared to the weight of the "measurement residual" term $\Psi_f(\mathbf{a}^p)$. However, at early iterations, when the solution approximation is very far from the solution, $\Psi_f(\mathbf{a}^p)$ is dominated by linearisation errors and has the value much higher than the level of the expected measurement noise. Therefore, since accuracy of a priori data is independent of the iteration, the weight of the a priori term should be increased. Correspondingly, this additional enhancement of the a priori data impact on the solution improves the convergence of non-linear fitting. For example, in developed GARRLiC algorithm, following Dubovik and King (2000) and Dubovik (2004), the strength of a priori constraints is adjusted dynamically as a function of the measurement residual $\Psi_f(\mathbf{a}^p)$:

$$\varepsilon_f^2(\mathbf{a}^p) = \frac{\Psi_f(\mathbf{a}^p)}{N_f - N_a}, \tag{3.46}$$

where $\Psi_f(\mathbf{a}^p)$ reflects the accuracy of the combined lidar/radiometer observation fit at the p-th iteration and provides an indication of how the iterations converge to the solution. For example, at the last iteration, when the solution estimate $\mathbf{a}^{p_{last}}$ is expected to be in a small vicinity of the actual solution, the value of the residual

$\Psi_f(\mathbf{a})$ of the measurement fit can be estimated as:

$$\Psi_f(\mathbf{a}^{p_{last}}) \approx (N_f - N_a)\,\varepsilon_f^2. \tag{3.47}$$

Using $\varepsilon_f^2(\mathbf{a}^p)$ Eq. 3.46 adjusts the values of the Lagrange multipliers γ_Δ and γ_a in Eqs. 3.36 – 3.41 and enhances the contribution of a priori constraints at the earlier iterations. As suggested by Dubovik (2004), this dynamic determination of a priori constraints improves convergence of non-linear iterations analogously to Levenberg-Marquardt formulations. At the same time, in contrast to the original Levenberg-Marquardt method, the idea of enhancing constraints on the solutions at earlier iterations in the formulations by Dubovik (2004) is included harmoniously within the framework of united statistical estimation approach. For example, if no smoothness constraints are used (i.e. the smoothness terms in the right sides of Eqs. 3.35 – 3.41 are eliminated) and no a priori estimates $\mathbf{a}^*$ are available, then one can assume $\mathbf{a}^* = \mathbf{a}^p$ and Eqs. 3.36 – 3.41 become equivalent to the Levenberg-Marquardt formulations (see more details in (Dubovik, 2004)).

The vector of combined measurement could be considered as consistent of five components, representing independent measurements with different level of accuracies:

$$\mathbf{f}^* = \begin{pmatrix} \mathbf{f}_\theta \\ \mathbf{f}_\tau \\ \mathbf{f}_{\beta_1} \\ \mathbf{f}_{\beta_2} \\ \mathbf{f}_{\beta_3} \end{pmatrix}, \tag{3.48}$$

where index θ denotes sun and sky radiances, τ stands for optical thickness, and $\beta_{...}$ is for lidar measurements at different wavelengths.

As measurements of optical thickness and sun and sky radiances (Dubovik et al.,

2000) are made with different accuracy, as well as lidar measurements at different wavelengths, covariance matrices will have an array structure:

$$\mathbf{C}_f = \begin{pmatrix} \mathbf{C}_\theta & 0 & 0 & 0 & 0 \\ 0 & \mathbf{C}_\tau & 0 & 0 & 0 \\ 0 & 0 & \mathbf{C}_{\beta_1} & 0 & 0 \\ 0 & 0 & 0 & \mathbf{C}_{\beta_2} & 0 \\ 0 & 0 & 0 & 0 & \mathbf{C}_{\beta_3} \end{pmatrix}. \tag{3.49}$$

It should be noted that in many practical situations the observations are uncorrelated and provide equally accurate data, i.e. weighting matrices are equal to unity matrices $\mathbf{W}_{\dots} = \mathbf{I}$. Such weight matrix structure directly applicable to the passive measurements both for sky-radiances and aerosol optical thickness performed at different wavelengths. However such estimations that were implied in the AERONET and POLDER retrievals, are not applicable to lidar measurements, as their variances depend both on the altitude and on the wavelength. Thus, the weight matrix of lidar measurement will have a form of diagonal matrix that describes relative altitude dependence of the variance for the given spectral channel. This will transform Equation 3.49 into:

$$C_f = \begin{pmatrix} \varepsilon_\theta^2 \mathbf{I}_\theta & 0 & 0 & 0 & 0 \\ 0 & \varepsilon_\tau^2 \mathbf{I}_\tau & 0 & 0 & 0 \\ 0 & 0 & \varepsilon_{\beta_1} \mathbf{H}_{\beta_1} & 0 & 0 \\ 0 & 0 & 0 & \varepsilon_{\beta_2} \mathbf{H}_{\beta_2} & 0 \\ 0 & 0 & 0 & 0 & \varepsilon_{\beta_2} \mathbf{H}_{\beta_3} \end{pmatrix}, \tag{3.50}$$

where $\mathbf{I}_{\dots}$ denote the unity matrix of corresponding size and $\mathbf{H}_{\beta_{\dots}}$ is the matrix that describes vertical variability of the lidar measurements accuracy.

The variance of the errors in measurements of scattered radiance is expected at the level of 3 % relative to the magnitude of observed radiance I, i.e. $\varepsilon_\theta = \Delta(\ln I) \approx$

$\frac{\Delta I}{I} = 0.03$, the variance of the errors in measurements of the optical thickness (direct radiance) is expected at the absolute level of 0.005, i.e. $\Delta\tau = 0.005$. The same values were used in AERONET retrievals by Dubovik and King (2000).

Estimation of the dispersion of lidar observations

Unlike photometric measurements the accuracy of the lidar observations is not equal for different spectral channels and it also depends on the altitude. Such dependence for the given spectral channel could be described with a normalized matrix of altitude dependence $\mathbf{H}_{\beta_{...}}$:

$$\{\mathbf{H}_{\beta_{...}}\}_{ii} = \varepsilon_{\beta_{...}} \frac{D_{\beta_{...}}(h_i)}{D^{\min}_{\beta_{...}}}. \tag{3.51}$$

Such estimation of $\mathbf{H}_{\beta_{...}}$ was chosen to define the lagrange coefficients for the lidar measurements in the uniform way with the selection of those for photometric measurements (see Eq. 3.50) and, therefore, assigning ε_{λ_j} with a meaning of minimum variation of the lidar measurement at the given wavelength λ_j. In this case provided vertical profile of lidar measurement dispersion will describe relative to ε_{λ_j} altitude dependence of the measurement variation.

The importance of estimation of noise impacts on backscatter retrievals was illustrated by several papers (on Klett method, for example by Rocadenbosch et al., 2010; Comeron et al., 2004). For the given method, an estimation of the dispersion of the lidar signal $D_{\beta_{...}}$ was used. The method to estimate $D_{\beta_{...}}$ was proposed in works by Denisov et al. (2006) and Chaikovsky et al. (2012). According to this principle, measured lidar signal could be defined as:

$$P^* = P + P_{ns} + P_s + \Delta P + P_B, \tag{3.52}$$

where P is the real magnitude of a signal, P^* is the measured signal, P_{ns} is the non-synchronous noise, P_s is the synchronous noise, ΔP is the non-linear deviation and

P_B is the background signal.

The non-synchronous component of the noise describes the noise that doesn't depend on the moment of sending of laser impulse: dark and fluctuation currents of a photo receiver, random noise in receiving channel. All these components are supposed to be non-correlated. Dispersion of non-synchronous component could be defined by:

$$\frac{(\delta P_{ns})^2}{P^2} = \frac{g^2 + q^2 \left(P\left(\lambda_j, h_i\right) + B\left(\lambda_j\right)\right)}{MAP^2\left(\lambda_j, h_i\right)}, \tag{3.53}$$

where g is the total deviation of dark current and noise in receiving channel, q is the index that characterizes fluctuation noise of the photo receiver and could be estimated on dark measurements of photoreceiving module, $M = n_2 - n_1$ is the number of signal counts in the averaging interval over altitude, A is the accumulation of the signal (number of profiles used for time-averaging). During accumulation of the received signal dispersions of non-synchronous signals are summed up, while synchronous noises are summed up by amplitudes and, therefore, could not be suppressed by accumulation.

The synchronous component of the noise describes signals induced in receiving channel by power supplying systems of the laser and internal noises in electrical circuits of registration system. The dispersion of synchronous noise is defined by the characteristics of receiving channel and depends on M:

$$(\delta P_s)^2 = \frac{u^2}{M}, \tag{3.54}$$

where u is the coefficient that characterize the amplitude of synchronous noise.

The dispersion of the background signal is considered to be negligible as averaging and accumulation of the background signal are usually sufficient. Fluctuations in registered signal added by the background signal are accounted in Equation 3.53 dealing with estimations of non-synchronous noise.

The deviation ΔP caused by the receiving module non-linearity could be determined by the receiving channel characteristics:

$$\frac{\Delta^2 P\left(\lambda_j, h_i\right)}{\left(P\left(\lambda_j, h_i\right) - P\left(\lambda_j, h_{ref}\right)\right)^2} = \nu^2 (P\left(\lambda_j, h_i\right) - P\left(\lambda_j, h_{ref}\right))^2, \tag{3.55}$$

where $v = \frac{\gamma}{P_{max}}$ is the non-linearity parameter, γ is the relative error of signal transmission caused by non-linearity of the receiving channel under maximum signal magnitude P_{max} and h_{ref} is the reference altitude.

The parameters g, u, q and v are system dependent, and usually could be estimated from the testing of the lidar registration system.

During the calibration of lidar signal (see Eq. 2.19) information about molecular scattering $\beta_m\left(\lambda_j, h_i\right)$, $\sigma_m\left(\lambda_j, h_i\right)$ is used, therefore, the impact of the dispersion of these optical parameters estimations (Hughes et al., 1985) on a lidar signal should be taken into account. The dispersion of estimation of optical properties of Rayleigh scatter is determined by the used model (for e.g. ISA, 1975; SA, 1976).

Thus, combining all dispersion estimations one can get the corresponding diagonal elements for the $D_{\beta_{...}}$ (Chaikovsky et al., 2006b; Denisov et al., 2006):

$$D_{\beta_j}\left(h_i\right) = \nu^2 + \frac{g^2 + q^2 P^*\left(\lambda_j, h_i\right)}{AM(P^*\left(\lambda_j, h_i\right) - B^*\left(\lambda_j\right))^2} + \frac{u^2}{\left(P^*\left(\lambda_j, h_i\right) - B^*\left(\lambda_j\right)\right)} + 4\alpha_1^2 + 4\alpha_2^2, \tag{3.56}$$

where $P^*\left(\lambda_j, h_i\right)$ is recorded during measurements, $\alpha_1 = \sqrt{\frac{\delta^2(\tau_m(\lambda_j, h_i))}{\tau_m^2(\lambda_j, h_i)}}$ is the relative error of estimation of molecular optical thickness and $\alpha_2 = \sqrt{\frac{\delta^2(\beta_m(\lambda_j, h_i))}{\beta_m^2(\lambda_j, h_i)}}$ is the relative error of estimation of molecular backscattering.

The vertical profile of the lidar signal dispersion $D_{\beta_j}\left(h_i\right)$ is provided by the complex software developed for the lidar registration system used for observations following Eq. 3.56 (Chaikovsky et al., 2006a; Denisov et al., 2006).

Parameters g, q, u, v are estimated from the testing of the lidar registration system, parameters α_1, α_2 are known for the given model of molecular scattering. Correspond-

ingly, the weight matrix $\mathbf{W}_f$ of the combined lidar/radiometer observation could be defined as:

$$\mathbf{W}_f = \begin{pmatrix} \mathbf{I}_\theta & 0 & 0 & 0 & 0 \\ 0 & \gamma_\tau \mathbf{I}_\tau & 0 & 0 & 0 \\ 0 & 0 & \gamma_{\beta_1} \mathbf{H}_{\beta_1} & 0 & 0 \\ 0 & 0 & 0 & \gamma_{\beta_2} \mathbf{H}_{\beta_2} & 0 \\ 0 & 0 & 0 & 0 & \gamma_{\beta_3} \mathbf{H}_{\beta_3} \end{pmatrix}, \tag{3.57}$$

where $\mathbf{I}_{...}$ denote the unity matrices of corresponding dimension, $\mathbf{H}_{\beta_j}$ denote diagonal matrix of the corresponding dimension, and $\gamma_{...}$ is the ratio of the variances of scattered radiances and variances of the corresponding measurement, including aerosol optical thickness (γ_τ) and lidar measurements (γ_{β_j}) in different spectral channels (following Eq. 3.43):

$$\gamma_{...} = \frac{N_{...} \varepsilon_{...}^2}{N_\theta \varepsilon_\theta^2}. \tag{3.58}$$

The minimum variance of the errors in measurements of backscattered radiance are expected at the level of 20% for channels 0.355 μm, 15% and of 10% for 0.532, 1.064 μm relative to the magnitude of observed attenuated backscatter L, i.e. $\varepsilon_{\beta_1} = \Delta (\ln L) \approx \frac{\Delta L}{L} = 0.2$, $\varepsilon_{\beta_2} = 0.15$ and $\varepsilon_{\beta_3} = 0.1$. It should be noted that these values define only minimum variation of the measurements, and the real values of the variations at each altitude are fully depend on the diagonal elements of matrix $\mathbf{H}_{\beta_j}$.

3.2.2 A priori smoothness constraints

The a priori smoothness constraints are applied in the GARRLiC algorithm on several different components of the vector $\mathbf{a}$ differently, same as in previous approaches (Dubovik and King, 2000; Dubovik, 2004; Dubovik et al., 2011). For example, for the vector of unknowns $\mathbf{a}$, given by Eq. 3.33, the matrix $\mathbf{S}$ has the following array

structure:

$$\mathbf{Sa} = \begin{pmatrix} \mathbf{S}_v & 0 & 0 & 0 & 0 & 0 \\ 0 & \mathbf{S}_n & 0 & 0 & 0 & 0 \\ 0 & 0 & \mathbf{S}_\kappa & 0 & 0 & 0 \\ 0 & 0 & 0 & 0 & 0 & 0 \\ 0 & 0 & 0 & 0 & \mathbf{S}_h & 0 \\ 0 & 0 & 0 & 0 & 0 & 0 \end{pmatrix} \begin{pmatrix} \mathbf{a}_v \\ \mathbf{a}_n \\ \mathbf{a}_\kappa \\ \mathbf{a}_{sph} \\ \mathbf{a}_h \\ \mathbf{a}_A \end{pmatrix}. \tag{3.59}$$

The correspondent matrices $\mathbf{S}_{...}$ have different dimension and represent differences of different order (3 for size distribution, 1 for $n(\lambda_i)$ and 2 for $\kappa(\lambda_i)$ and $c(h_i)$). The lines in Eq. 3.59 corresponding to $\mathbf{a}_{sph}$ and $\mathbf{a}_A$ contain only zeros because no smoothness constraints are applied on them.

In the proposed algorithm each microphysical parameter (including size distribution, complex refractive index and vertical concentration distribution) describes two aerosol components (fine and coarse mode, see also Eq. 3.34). It should be noted that despite of technical possibility to retrieve different fractions of spherical particles ($\mathbf{a}_{sph}$) for each aerosol component, fraction of the fine mode was set to be the same as for the coarse mode due to the low effect of the shape of small particles on intensity measurements:

$$a^f_{sph} = a^c_{sph}. \tag{3.60}$$

Consideration of Equations 3.34 and 3.60 transforms Eq. 3.59 into:

$$\mathbf{Sa} = \begin{pmatrix} \mathbf{S}_v^f & 0 & 0 & 0 & 0 & 0 & 0 & 0 & 0 & 0 & 0 \\ 0 & \mathbf{S}_v^c & 0 & 0 & 0 & 0 & 0 & 0 & 0 & 0 & 0 \\ 0 & 0 & \mathbf{S}_n^f & 0 & 0 & 0 & 0 & 0 & 0 & 0 & 0 \\ 0 & 0 & 0 & \mathbf{S}_n^c & 0 & 0 & 0 & 0 & 0 & 0 & 0 \\ 0 & 0 & 0 & 0 & \mathbf{S}_\kappa^f & 0 & 0 & 0 & 0 & 0 & 0 \\ 0 & 0 & 0 & 0 & 0 & \mathbf{S}_\kappa^c & 0 & 0 & 0 & 0 & 0 \\ 0 & 0 & 0 & 0 & 0 & 0 & 0 & 0 & 0 & 0 & 0 \\ 0 & 0 & 0 & 0 & 0 & 0 & 0 & 0 & 0 & 0 & 0 \\ 0 & 0 & 0 & 0 & 0 & 0 & 0 & 0 & \mathbf{S}_h^f & 0 & 0 \\ 0 & 0 & 0 & 0 & 0 & 0 & 0 & 0 & 0 & \mathbf{S}_h^c & 0 \\ 0 & 0 & 0 & 0 & 0 & 0 & 0 & 0 & 0 & 0 & 0 \end{pmatrix} \begin{pmatrix} \mathbf{a}_v^f \\ \mathbf{a}_v^c \\ \mathbf{a}_n^f \\ \mathbf{a}_n^c \\ \mathbf{a}_\kappa^f \\ \mathbf{a}_\kappa^c \\ a_{sph}^f \\ a_{sph}^c \\ \mathbf{a}_h^f \\ \mathbf{a}_h^c \\ \mathbf{a}_A \end{pmatrix}. \tag{3.61}$$

It should be noted that for making formulations more transparent only one coefficient γ_Δ was shown in the second term in Eq. 3.36. However, the actual algorithm uses 8 multipliers $\gamma_{\Delta,i}$. The errors $\Delta\left(\Delta\mathbf{a}\right)$ are assumed independent for different components of the vector $(\Delta a)^*$ and the smoothness matrix in Eq. 3.36 has the following array

structure:

$$\gamma_{\Delta}\boldsymbol{\Omega} = \begin{pmatrix} \gamma_{\Delta,1}\boldsymbol{\Omega}_1 & 0 & 0 & 0 & 0 & 0 & 0 & 0 & 0 & 0 & 0 \\ 0 & \gamma_{\Delta,2}\boldsymbol{\Omega}_2 & 0 & 0 & 0 & 0 & 0 & 0 & 0 & 0 & 0 \\ 0 & 0 & \gamma_{\Delta,3}\boldsymbol{\Omega}_3 & 0 & 0 & 0 & 0 & 0 & 0 & 0 & 0 \\ 0 & 0 & 0 & \gamma_{\Delta,4}\boldsymbol{\Omega}_4 & 0 & 0 & 0 & 0 & 0 & 0 & 0 \\ 0 & 0 & 0 & 0 & \gamma_{\Delta,5}\boldsymbol{\Omega}_5 & 0 & 0 & 0 & 0 & 0 & 0 \\ 0 & 0 & 0 & 0 & 0 & \gamma_{\Delta,6}\boldsymbol{\Omega}_6 & 0 & 0 & 0 & 0 & 0 \\ 0 & 0 & 0 & 0 & 0 & 0 & 0 & 0 & 0 & 0 & 0 \\ 0 & 0 & 0 & 0 & 0 & 0 & 0 & 0 & 0 & 0 & 0 \\ 0 & 0 & 0 & 0 & 0 & 0 & 0 & 0 & \gamma_{\Delta,7}\boldsymbol{\Omega}_7 & 0 & 0 \\ 0 & 0 & 0 & 0 & 0 & 0 & 0 & 0 & 0 & \gamma_{\Delta,8}\boldsymbol{\Omega}_8 & 0 \\ 0 & 0 & 0 & 0 & 0 & 0 & 0 & 0 & 0 & 0 & 0 \end{pmatrix}, \tag{3.62}$$

where $\boldsymbol{\Omega}_i = \mathbf{S}_i^T \mathbf{W}_i^{-1} \mathbf{S}_i$ uses the derivative matrices $\mathbf{S}_i$ $(i = 1, \ldots, 8)$ $\mathbf{S}_v^f$, $\mathbf{S}_v^c$, $\mathbf{S}_n^f$, $\mathbf{S}_n^c$, $\mathbf{S}_\kappa^f$, $\mathbf{S}_\kappa^c$, $\mathbf{S}_h^f$, $\mathbf{S}_h^c$, $\mathbf{S}_{sph}$. If it is assumed that the covariance matrices of errors $\Delta\,(\Delta\mathbf{a})$ have the structure $\mathbf{C}_{\Delta,i} = \varepsilon_{\Delta,i}^2 \mathbf{I}$ for each component of $(\Delta\mathbf{a})^*$, i.e. weighting matrices are $\mathbf{W}_{\Delta,i} = \mathbf{I}$, where $\mathbf{I}$ has the corresponding size. Correspondingly, the quadratic form $\Psi_\Delta\,(\mathbf{a}^p)$ in Equation 3.36 can be written as the following sum:

$$2\Psi_\Delta\,(\mathbf{a}^p) = \gamma_\Delta (\mathbf{a}^p)^T \boldsymbol{\Omega} \mathbf{a}^p = \sum_{i=1,\ldots,8} 2\Psi_{\Delta,i}\,(\mathbf{a}^p) = \sum_{i=1,\ldots,8} \gamma_{\Delta,i} (\mathbf{a}_i^p)^T \boldsymbol{\Omega}_i \mathbf{a}_i^p, \tag{3.63}$$

where $\gamma_{\Delta,i} = \varepsilon_f^2 \big/ \varepsilon_{\Delta,i}^2$.

The utilization of the smoothness constraints for a single retrieved function $y\,(x_i)$ was originated in the papers by Phillips (1962), Tikhonov (1963) and Twomey (1963). Although application of the smoothness constraints is usually considered to be an implicit constraint on derivatives, in these original papers and most of follow-on

studies the solution $\hat{\mathbf{a}}$ was constrained by minimizing m-th differences Δ^m of the components of vector $\hat{\mathbf{a}}$:

$$\begin{aligned} \Delta^1 &= \hat{a}_{i+1} - \hat{a}_i, \quad (m=1) \\ \Delta^2 &= \hat{a}_{i+2} - 2\hat{a}_{i+1} + \hat{a}_i, \quad (m=2) \\ \Delta^3 &= \hat{a}_{i+3} - 3\hat{a}_{i+2} + 3\hat{a}_{i+1} - \hat{a}_i, \quad (m=3). \end{aligned} \tag{3.64}$$

The corresponding "smoothness" matrix $\mathbf{\Omega} = (\mathbf{S}_i)^T (\mathbf{S}_i)$ was defined using matrices of m-th differences $\mathbf{S}_{(m)}$ (i.e. $\Delta^m = \mathbf{S}_{(m)}\hat{\mathbf{a}}$). For example smoothness matrix with m=2 is:

$$\mathbf{S}_2 = \begin{pmatrix} 1 & -2 & 1 & 0 & ... & & & \\ 0 & 1 & -2 & 1 & 0 & ... & & \\ 0 & 0 & 1 & -2 & 1 & 0 & ... & \\ ... & ... & ... & ... & ... & ... & ... & ... \\ ... & ... & ... & & & 0 & 1 & -2 & 1 \end{pmatrix}. \tag{3.65}$$

The present development follows the concept of Dubovik and King (2000) and Dubovik (2004) that considers smoothness constraints explicitly as a priori estimates of the derivatives of the retrieved characteristic $y(x_i)$. The values of m-th derivatives g_m of the function $y(x_i)$ characterize the degree of its non-linearity and, therefore, can be used as a measure of $y(x_i)$ smoothness. For example, smooth functions $y(x_i)$, such as, a constant, straight line, parabola, etc. can be identified by the m-th derivatives as follows:

$$\begin{aligned} g_1(x) = dy(x)/dx = 0 &\Rightarrow y_1(x) = C; \\ g_2(x) = d^2y(x)/dx^2 = 0 &\Rightarrow y_2(x) = Bx + C; \\ g_3(x) = d^3y(x)/dx^3 = 0 &\Rightarrow y_3(x) = Ax^2 + Bx + C. \end{aligned} \tag{3.66}$$

These derivatives g_m can be approximated by differences between values of the function $y(x_i)$ in N_a discrete points x_i as:

$$\begin{array}{c} \frac{dy(x_{i'})}{dx} \approx \frac{\Delta^1 y(x_i)}{\Delta_1(x_i)} = \frac{y(x_i+\Delta_1(x_i))-y(x_i)}{\Delta_1(x_i)}, \\ \frac{d^2y(x_{i''})}{dx^2} \approx \frac{\Delta^2 y(x_i)}{\Delta_2(x_i)} = \frac{\Delta^1 y(x_{i+1})/\Delta_1(x_{i+1})-\Delta^1 y(x_i)/\Delta_1(x_i)}{(\Delta_1(x_i)-\Delta_1(x_{i+1}))/2}, \\ \frac{d^3y(x_{i'''})}{dx^3} \approx \frac{\Delta^3 y(x_i)}{\Delta_3(x_i)} = \frac{\Delta^2 y(x_{i+1})/\Delta_2(x_{i+1})-\Delta^2 y(x_i)/\Delta_2(x_i)}{(\Delta_2(x_i)-\Delta_2(x_{i+1}))/2}, \end{array} \tag{3.67}$$

where

$$\begin{array}{c} \Delta_1(x_i) = x_{i+1} - x_i; \\ \Delta_2(x_i) = (\Delta_1(x_i) + \Delta_1(x_{i+1}))/2; \\ \Delta_3(x_i) = (\Delta_2(x_i) + \Delta_1(x_{i+1}))/2; \\ x_{i'} = x_i + \Delta_1(x_i)/2; \\ x_{i''} = x_i + (\Delta_1(x_i) + \Delta_2(x_i))/2; \\ x_{i'''} = x_i + (\Delta_1(x_i) + \Delta_2(x_i) + \Delta_3(x_i))/2. \end{array} \tag{3.68}$$

The corresponding matrix of m-th derivatives $\mathbf{S}_{g,(m)}$ (i.e. $g_m = \mathbf{S}_{g,(m)}\hat{\mathbf{a}}$) can easily be defined using Eq. 3.64. For example:

$$\mathbf{S}_{g,(m)} = \begin{pmatrix} \frac{2}{\Delta_1(\Delta_1+\Delta_2)} & \frac{-2}{(\Delta_1\Delta_2)} & \frac{2}{\Delta_2(\Delta_1+\Delta_2)} & 0 & ... & ... \\ 0 & \frac{2}{\Delta_2(\Delta_2+\Delta_3)} & \frac{-2}{(\Delta_2\Delta_3)} & \frac{2}{\Delta_3(\Delta_1+\Delta_3)} & 0 & ... \\ 0 & 0 & \frac{2}{\Delta_3(\Delta_3+\Delta_4)} & \frac{-2}{(\Delta_3\Delta_4)} & \frac{2}{\Delta_4(\Delta_3+\Delta_4)} & 0 \\ ... & ... & ... & ... & ... & ... \end{pmatrix} \tag{3.69}$$

where $\Delta_i = \Delta_1(x_i) = x_{i+1} - x_i$. One can see that $\mathbf{S}_{g,(m)}$ has significantly more complex structure than the conventional definition of smoothing matrix by Eq. 3.64. In difference with Eq. 3.64, Eq. 3.67 allows for applying smoothness constraints in more general situations when $\Delta_1(x_i) \neq const$. For example, in present algorithm there is a number of complex refractive index is the function of λ and the algorithm deals with their values defined for each spectral channel λ_i. Obviously the $\lambda_{i+1} - \lambda_i \neq const$ and

using standard definition of differences by Eq. 3.64 for smoothing spectral complex refractive index is not completely correct. Applying the limitations on the derivatives defined by Eq. 3.67 is more rigorous if no significant changes of derivatives of $y(x)$ are expected for different ordinates x_i. Although using Eq. 3.67 leads to a loose of transparency in definitions of matrices $\mathbf{S}_{(m)}$, generating those matrices on algorithmic level is rather straightforward and defining of Lagrange parameters γ_Δ is more logical. Therefore, in present algorithm, the smoothness constraints are applied to limit directly the numerical equivalents of m-th derivatives given by Eq. 3.64, by a priori assumption that m-th derivatives are equal to zeros with some uncertainty ($g^* = 0^* = 0 + \Delta_g$).

It should be noted that limitations of the derivatives of the vertical profiles appears to be a rather useful and very logical approach to avoid unrealistic spiky vertical variations in profiling that is also used in the LiRIC algorithm by Chaikovsky et al. (2002a). Surprisingly, such apparently natural constraining is rarely used in profiling techniques (with few exceptions: Dubovik et al., 1998; Oshchepkov et al., 2002). For example, even the cornerstone methodological studies of atmosphere profiling (e.g. Rodgers, 1976) propose limiting directly the values of profile using a priori estimations. Such approach is generally rather restrictive and can lead to the notable biases in the retrieval in the case when a priori assumed profiles are significantly different from the real ones. For example, in the aerosol microphysical applications where aerosol size distributions are retrieved from the measurements of spectral and angular scattering such approach appears to be unfruitful. Indeed, the shape and magnitudes of aerosol size distribution may strongly vary and direct restriction of its magnitude by a priori values is too restrictive. As a result, although the use of a priori estimates as a constrain in the retrieval of size distribution was proposed and tried by Twomey (1963) much earlier than in atmospheric profiling (e.g. Rodgers, 1976) it was never widely used. Instead, most of established aerosol retrieval algorithms (e.g. King et al.,

1978; Nakajima et al., 1983, 1996; Dubovik et al., 1995; Dubovik and King, 2000, and others) use the limitations of derivatives of aerosol size distribution. Such limitations are obviously more universal and do not have apparent dependence on aerosol type, loading and so on. The same property of derivatives constraining seems to be very advantageous for constraining vertical profile retrievals (as it was done in the present work).

The values of the Lagrange multipliers used in the retrievals are shown in Table 3.6. Different values of Lagrange multiplier for different aerosol components were chosen due to the found difference in algorithm sensitivity to different modes. More detailed it will be discussed in the sensitivity study section. The significantly greater values of multipliers for the complex refractive index were chosen to suppress indetermination of the used model in the presence of two aerosol components with different refractive indexes.

More detailed description of **S** matrices of m-differences and Lagrange multipliers

Table 3.6: Values of the Lagrange multipliers used in the GARRLiC retrievals, corresponding to the elements of vector of unknowns **a**.

Aerosol parameter	Order of finite differences	Values of γ_Δ
$dV^f(r_i)\big/d\ln r \quad \left(i=1,...,N_{r_f}\right)$	2	0.75
$dV^c(r_i)/d\ln r \quad (i=1,...,N_{r_c})$	2	0.1
$n^f(\lambda_i) \quad (i=1,...,7)$	1	500
$n^c(\lambda_i) \quad (i=1,...,7)$	1	500
$\kappa^f(\lambda_i) \quad (i=1,...,7)$	2	20
$\kappa^c(\lambda_i) \quad (i=1,...,7)$	2	20
$c^f(h_i) \quad (i=1,...,N_h)$	2	0.007
$c^f(h_i) \quad (i=1,...,N_h)$	2	0.007

could be found in Dubovik and King (2000); Dubovik et al. (2011).

The general structure of the numerical inversion data flow implemented for the retrieval of aerosol is summarized in Fig. 3.7.

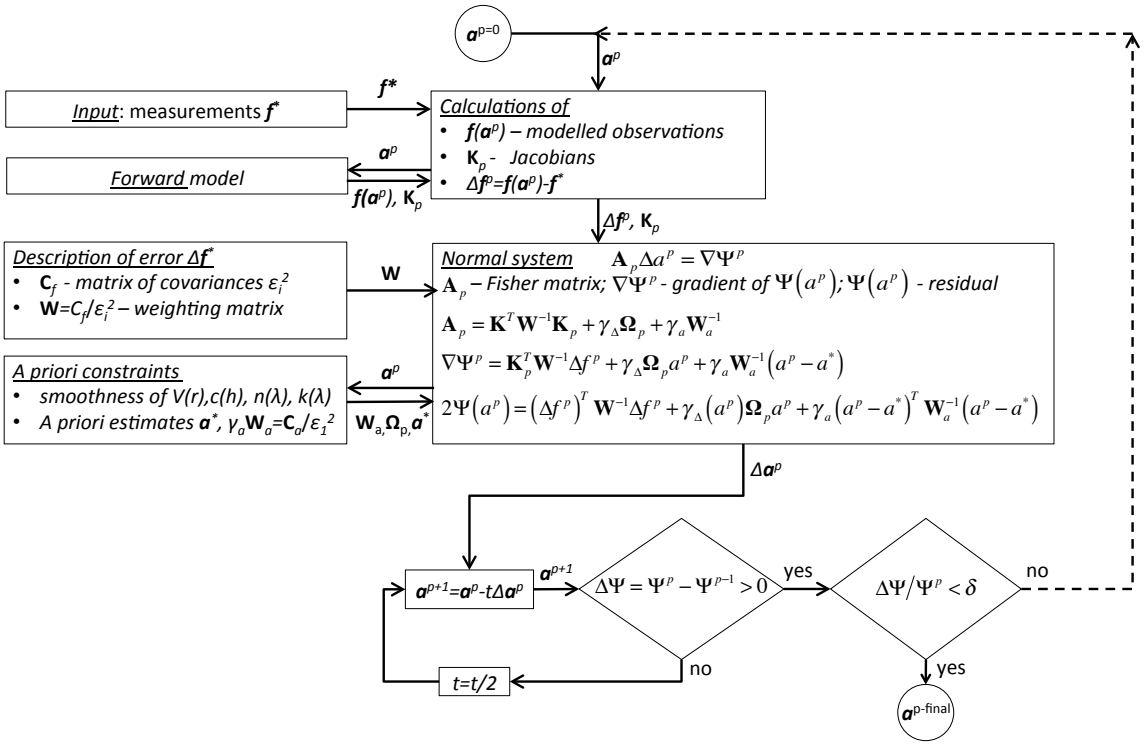

Figure 3.7: General scheme of numerical inversion of the GARRLiC algorithm.

Chapter 4

GARRLiC Algorithm functionality and sensitivity tests

> Data without generalization is just gossip.
>
> Robert Pirsig

Series of sensitivity tests have been performed to verify the performance of the developed algorithm and to provide the illustration of capabilities and limitations of the algorithm to derive a set of aerosol parameters (see Tables 3.2, 3.5) from coincident lidar and sun photometer observations (see Table 3.1).

The sensitivity tests had been designed to conform to realistic conditions of each of the measurement. The analysis was carried out with simulated radiances using several typical and optically distinct aerosol types. Specifically, three aerosols have been considered with the intention of extending the sensitivity to a wide range of different situations that could be encountered in most known aerosol observation sites that have both lidars and sun-photometers. The aerosols considered were: desert dust, non-absorbing urban, and absorbing biomass-burning aerosol.

The tests were carried out for two cases representing situations when desert dust is

mixed with urban pollution or biomass-burning aerosols. Six different scenarios were considered for the each mixture. Among them three scenarios were performed for high aerosol loading with total AOT of $\tau_a(0.532) = 1$ and the other three with very low AOT of $\tau_a(0.532) = 0.05$. These two situations where chosen from the following considerations. At the high aerosol loading we expect that synergetic retrieval would maximally benefit from information from radiometric observations, while at very low AOT, the lidar data should provide maximum benefits. Indeed, the accuracy of AERONET retrievals generally higher at high aerosol loading and significantly falls at very low AOTs (Dubovik et al., 2000). In contrast, the lidar data remain reliable even at low aerosol loadings. For both high and low aerosol loading cases, three different cases of fine/coarse mode partition were modelled: $\tau_f/\tau_c = 4$, $\tau_f/\tau_c = 1$ and $\tau_f/\tau_c = \frac{1}{4}$. Thus, resulting in six mixture scenarios: $\tau_f = 0.8$, $\tau_c = 0.2$, $\tau_f = \tau_c = 0.5$, $\tau_f = 0.2$, $\tau_c = 0.8$ and $\tau_f = 0.04$, $\tau_c = 0.01$, $\tau_f = \tau_c = 0.025$, $\tau_f = 0.01$, $\tau_c = 0.04$ correspondingly.

For each of the six scenarios, two series of the tests were made: (i) tests to estimate the sensitivity to random noise were made without any noise added and with and random noise added to the simulated measurements, and (ii) tests to illustrate the possible improvements introduced by using both radiometric and lidar measurements in comparison with the standard AERONET inversion.

4.1 Description of aerosol and noise models used for sensitivity study

Aerosol optical properties are gathered and discussed in numerous characterization studies. From of all these studies, the article by Dubovik et al. (2002a) was chosen to parametrize the aerosols used in the present study. The Table 2.1 is an extract of the Table 1 of Dubovik et al. (2002a) where values of the optical properties are

given for several key locations. In particular, this work contains information about twelve examples of Urban-industrial, biomass burning, desert dust aerosol and oceanic aerosols. From all these three examples have been selected for the simulations within the thesis: Solar Village site (Saudi Arabia) for desert dust, Goddard Space Flight Center site (Maryland, USA) for clean urban and Mongu site (Zambia) for biomass burning.

Solar Village (24.90°N : 46.40°E, 790 msl) is a solar power plant situated approximately 50 km North-West of Riyadh, inside the Arabian desert; these conditions make that the aerosol registered in this site represent optical properties of the so-called pure desert dust, without signs of urban pollution.

The AERONET calibration center at NASAs Goddard Space Flight Center (GSFC) in Greenbelt, Maryland (38.99°N : 76.84°W, 87 msl) is the one chosen for representing the urban aerosol. The place is located 20 km North-East of Washington inside the Boston-Washington megalopolis which is the second most heavily urbanized area in the United States supporting 50 million people. Nevertheless, GSFC site was selected in the analysis because it has the lowest absorption values of the urban aerosol (see Table 1 in Dubovik et al., 2002a).

Mongu (15.25°S : 23.15°E, 1107.0 msl) is mainly sandy with a seasonal flood plain that is burned to the west annually from July through November. It is the capital of the western region in Zambia and it has an airport where, precisely, the AERONET site is located. This site was chosen due to the larger absorption among other sites observing biomass burning, in order to o enlarge the study range.

The aerosol size distributions are described by Dubovik et al. (2002a) as bi-modal log-normal. For the dust aerosols there is a clear coarse mode predominance and the fine mode volume concentration is larger than the coarse mode for GSFC and Mongu. In this study two uni-modal size distributions were used to generate 25 size bins (10 for fine and 15 for coarse aerosol modes) instead of one bi-modal log-normal size dis-

tribution. The values used to model size distributions of fine and coarse modes (see Table 4.1) were taken from AERONET retrieval climatology corresponding to dominating modes of desert dust and biomass-burning aerosols (Dubovik et al., 2002a). Both distributions for fine and coarse modes were normalized to provide corresponding AOTs used in the study (see Table 4.1). To make the size distributions directly comparable with the actual AERONET observations the values of the generated bin radii were chosen corresponding to the ones of the standard AERONET retrieval.

The values of complex refractive indexes at $\lambda = 0.440$, 0.670,0.870 and $1.020\mu m$ for

Table 4.1: Parameters of log-normal size distributions used for size distribution modelling for application in GARRLiC sensitivity tests.

Mode	$r_{min}, \mu m$	$r_{max}, \mu m$	r_{mean}	r_{std}	$\tau(\tau_{total} = 1)$	$\tau(\tau_{total} = 0.05)$
Fine	0.05	0.576	0.148	0.4	0.8, 0.5, 0.2	0.04, 0.025, 0.01
Coarse	0.355	15.0	2.32	0.6	0.2, 0.5, 0.8	0.01, 0.025, 0.04

"urban pollution", "biomass burning" and "desert dust" aerosol models were adapted from actual long-time observation statistics over the GSFC, Banizombou and Solar Village AERONET sites correspondingly (Dubovik et al., 2002a).

The real part of the refractive index of dust shows good agreement with several models which suggest a value of 1.53 (Koepke et al., 1997; Shettle and Fenn, 1979). Moreover, in-situ values present deviations up to ± 0.05 which are attributed to differences in the dust composition and in the measurements techniques (Patterson and Gillette, 1977; Sokolik and Toon, 1999), therefore, a chosen value of 1.56 can be considered adequate. However, the imaginary part of the refractive index used is relatively lower than 0.008, suggested in some models (Shettle and Fenn, 1979). This issue is directly related to the discussion about desert dust absorption between in-situ models and remote sensing observations. The imaginary part dependence on λ is a distinctive feature of the desert dust; concretely, $\kappa(\lambda)$ is 3-4 times higher at 0.440 μm than at the longer wavelengths, while it remains constant for the others aerosol

types. This spectral dependence has been reported in many studies both about models (Sokolik and Toon, 1999)) and measurements (Kandler et al., 2007)).

The real part of the refractive index of urban aerosol is assumed to be constant, regardless of the wavelength, and equal to 1.36. This value is within the range 1.33 – 1.45 which is the estimation of TARFOX experiment. On the other hand, this experiment estimates the imaginary part to be between 0.001 and 0.008; so the value of 0.003, retrieved by AERONET (see Table 2.1), also agrees with the in-situ aircraft results.

The values of the refractive index of the biomass-burning aerosol do not depend on the aerosol optical depth and the high value of the imaginary part calls the attention. Due to the important absorption of this aerosol, the imaginary part (constant with wavelength and equal to 0.021) is one order of magnitude higher than in the other aerosol types. Finally, it can be observed that the value for the real part, 1.51 for all wavelengths, is a bit smaller than for desert dust (1.56) but much higher than the for the urban aerosols.

The values of complex refractive index for all aerosol types for spectral channels $\lambda = 0.355$, 0.532, and $1.064\mu m$ corresponding to lidar measurements were obtained by the linear extrapolation.

Two realistic scenarios with clear vertical separation of fine and coarse aerosol components were used. The fine mode was assumed to represent the background aerosol with specific vertical distribution, while coarse mode distribution had a thick layer approximately at 3 km. Both modes had significant amount of aerosol in the layers close to the ground to mimic the properties of the boundary layer. Both distributions had monotonous decrease over the altitude.

The values of the complex refractive indexes as well as vertical distribution profiles of the aerosol models could be found marked as "TRUE" at Figures 4.1 – 4.6, and 4.10 – 4.12.

Each aerosol mode was modelled as a mixture of spherical and spheroidal particles, as described in the previous chapter (see Eqs. 3.2, 3.3), with the same size distributions and with the percentage of spherical particles (C_{sph}) in the mixture of 10%.

To model realistic measurement conditions the random normally distributed noise was added to the generated measurements. The variance of noise in optical thickness measurement were set as 0.005, and the variance of noise in scattered irradiance were chosen as 3%, i.e. $\frac{\Delta I}{I} = 0.03$, the spectral and altitude dependent variances of lidar measurements were defined as:

$$\frac{\Delta L(\lambda, h)}{L(\lambda, h)} = \varepsilon(\lambda)\, n(h), \tag{4.1}$$

where for the $\varepsilon = 0.2$, 0.15 and 0.1 for $\lambda = 0.355$, 0.532 and 1.064 μm correspondingly, and vertical dependence were set as the following function:

$$n(h) = \begin{cases} 1, \log(h) < 1 \\ \log(h), \log(h) \geq 1. \end{cases} \tag{4.2}$$

It should be noted that such estimations of the lidar noise are higher than those that were used for the retrievals from the real measurements, such values were chosen to model the worst case scenario and to outline the retrieval error boundaries for a such unlikely situation.

Using above described microphysical model the synthetic AERONET and lidar measurements were simulated and then inverted. The results then were compared with the "assumed" properties.

4.2 Sensitivity test results

The discussion of the sensitivity study results will focus on the retrievals of the aerosol properties that were not a part of the standard AERONET inversion. Specif-

ically, we will pay particular attention on the retrieval of aerosol vertical profiles and differentiation between the properties of fine and coarse aerosol modes, including complex refractive indexes, size distributions and others. In addition, we would like to note that the accuracy of aerosol size distribution retrieval is not discussed here. The results of our sensitivity tests show generally very similar tendencies as observed in earlier studies by Dubovik et al. (2000).

The results of the sensitivity tests are presented in Figures 4.1 - 4.12. These results show that algorithm, in general, derives all aerosol parameters with good accuracy, and clearly distinguishes both aerosol modes. The addition of the realistic random noise did not dramatically affect the retrieval results, although once noise is added the retrieval results depart further from the "assumed" values.

Figures 4.1 - 4.12 depict the retrieval of the aerosol properties of the described aerosol models for noise free and noisy conditions, each for six different optical thickness of the corresponding aerosol component obtained for two types of aerosol mixtures ("Urban" + "Dust" and "Smoke" + "Dust").

Retrievals of the size distribution are shown in Figs. 4.1 – 4.3. The algorithm

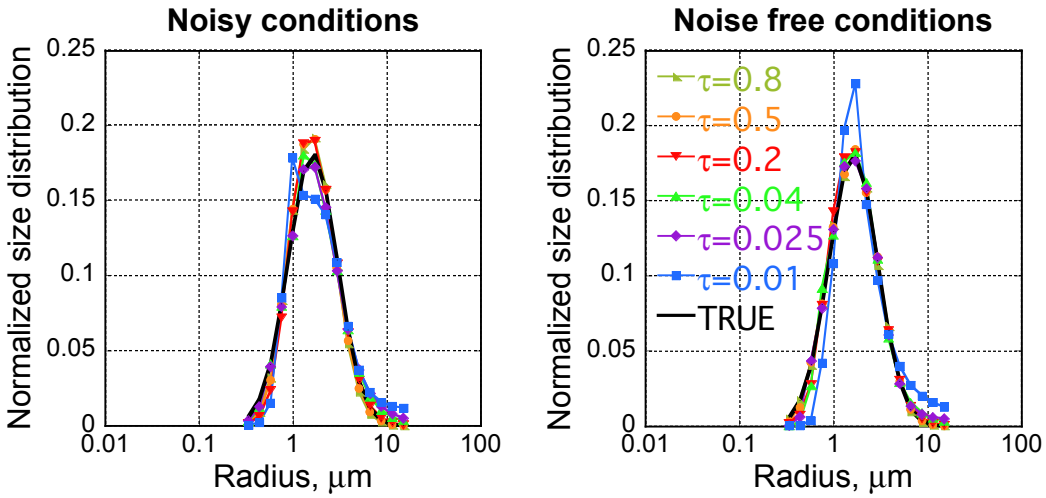

Figure 4.1: Retrievals of size distributions of "Dust" aerosol model under noisy and noise free conditions.

shows lower sensitivity to the size distributions of the aerosol models containing

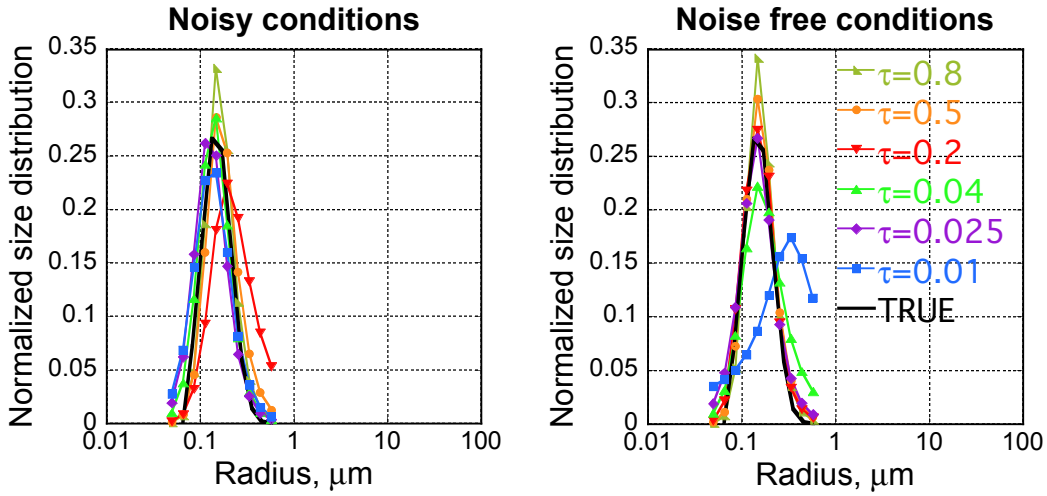

Figure 4.2: Retrievals of size distributions of "Smoke" aerosol model under noisy and noise free conditions.

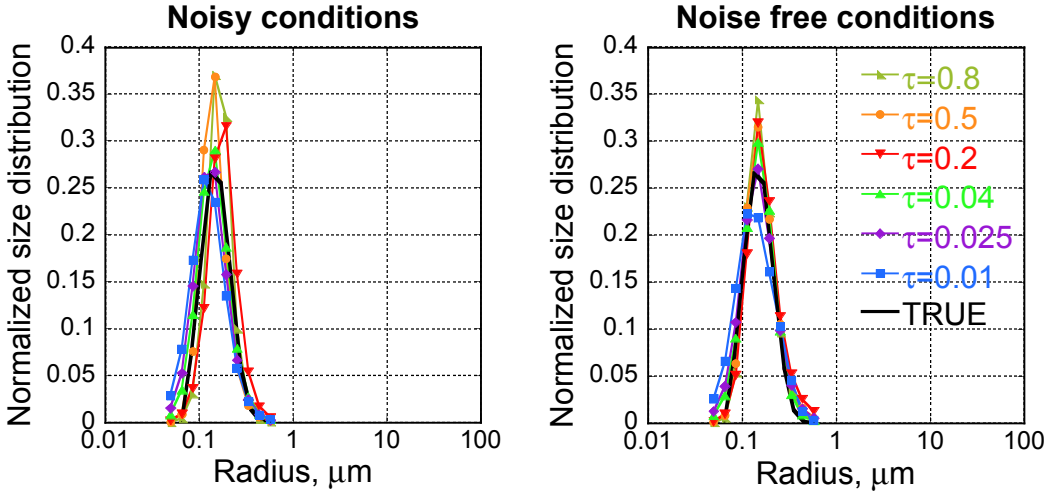

Figure 4.3: Retrievals of size distributions of "Urban" aerosol model under noisy and noise free conditions.

fine particles ("Smoke" and "Urban"), and uncertainties in the estimation of this parameter are higher than for the coarse mode ("Dust" model) even in noise free conditions. All retrievals show dependence of the retrieval accuracy on the aerosol optical thickness of the corresponding aerosol component. The presence of the random noise does not dramatically affect the retrievals, yet the dispersion is higher in the presence of noise, especially for cases when the studied mode does not dominate in the mixture and its optical thickness is low. The most dispersed points are

situated at the maximums and the boundaries of the distributions both for noise and noise free conditions. Such behaviour of the distributions on the particle size boundaries was also demonstrated by Dubovik et al. (2000). The difference of the size distribution values at the maximum point could be explained by uncertainty in the estimations of the concentration of the selected aerosol component.

Figures 4.4 – 4.6 show the retrievals of the aerosol complex refractive indices of each aerosol component under noisy and noise free conditions performed for 6 different AOTs and obtained for the two aerosol mixtures listed above. As it seen in Figures 4.4 – 4.6 method shows higher accuracy of the retrieval of this columnar property in the cases with higher aerosol loadings. Similar tendency is observed for the retrieval of vertical profiles.

The another observed trend is that the accuracy of the retrievals of complex refractive index for each aerosol mode strongly correlates with the contribution of this mode to the signal. Specifically, two following tendencies are observed. First, the higher the presence of the mode, the better retrieval accuracy of the refractive index for this mode. Second, the retrieval error of the refractive index increases from shorter wavelengths to longer ones for the fine mode, and for the coarse mode, the tendency is opposite. Also retrievals of the properties of the coarse mode have better accuracies, compared to the properties of the fine aerosol components in both noisy and noise free conditions, yet the presence of random noise sufficiently scatters the retrieval results, especially ones retrieved at low AOTs.

Figures 4.7 – 4.9 illustrate that similar tendencies are observed for the retrievals of the single-scattering albedo.

This trend is especially evident in the situations with low total AOTs and when one of the components dominates. As can be seen from Figs. 4.7 – 4.9, in such situation retrieval errors of the properties of minor aerosol mode become unacceptably high. This leads to incorrect separation of the total single-scattering

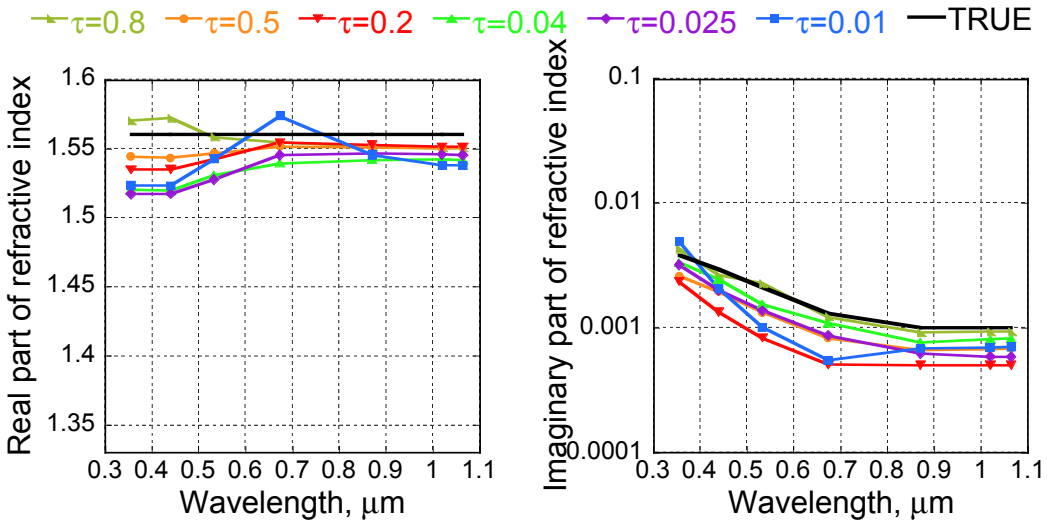

(a) noise free conditions.

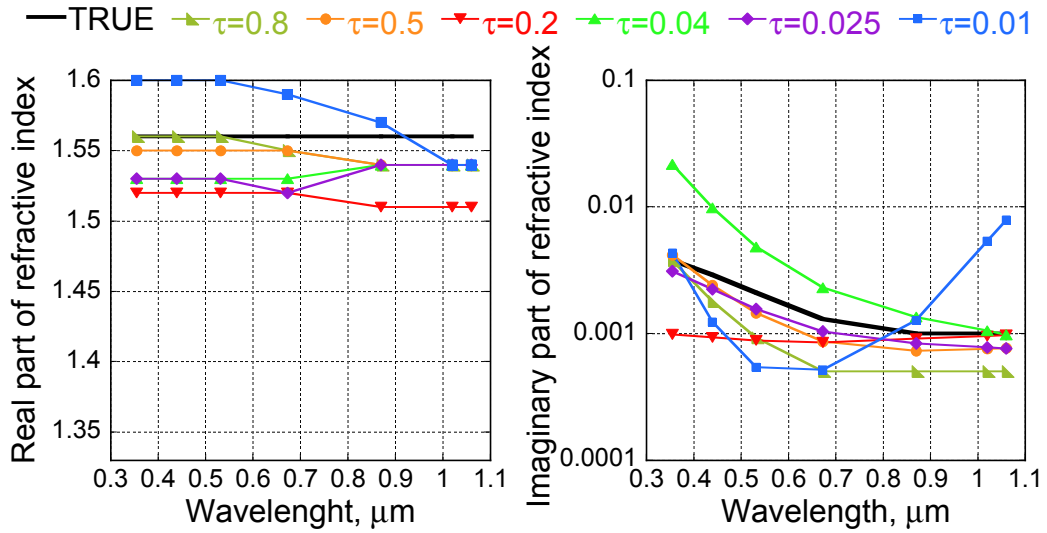

(b) noisy conditions.

Figure 4.4: Retrievals of complex refractive index of "Dust" aerosol model for different AOTs under (a) - noise free and (b) - noisy conditions.

albedo between these two aerosol components at shorter wavelengths. The retrievals of total single-scattering albedo depend on the total optical thickness similarly as observed by Dubovik et al. (2000). Thus, the scenario with high total AOT and equal partition between the modes is the most favourable for overall retrieval.

Figures 4.10 – 4.12 show the retrievals of the vertical distributions. As demonstrated by these figures the algorithm gives generally adequate vertical profiles for both modes. At the same time, it tends to slightly overestimate the amount of the fine

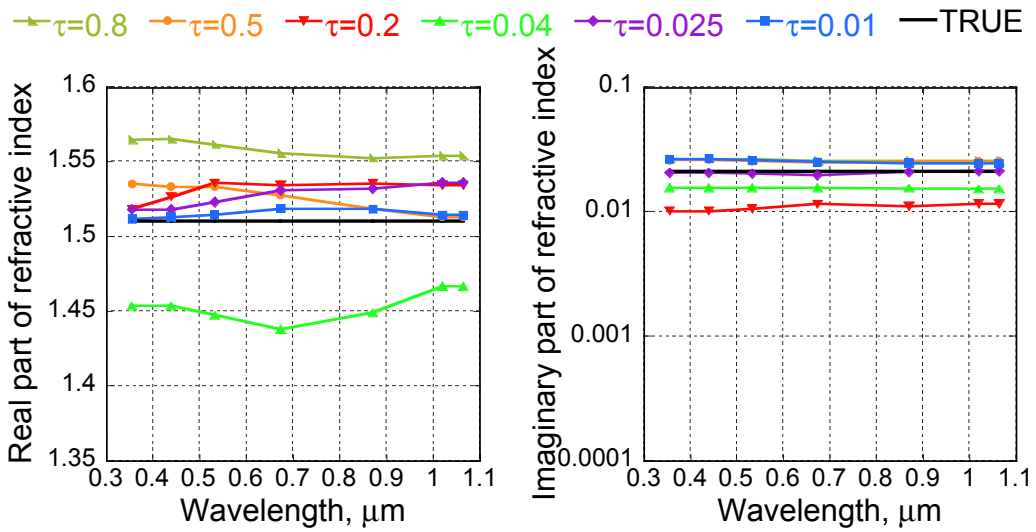

(a) noise free conditions.

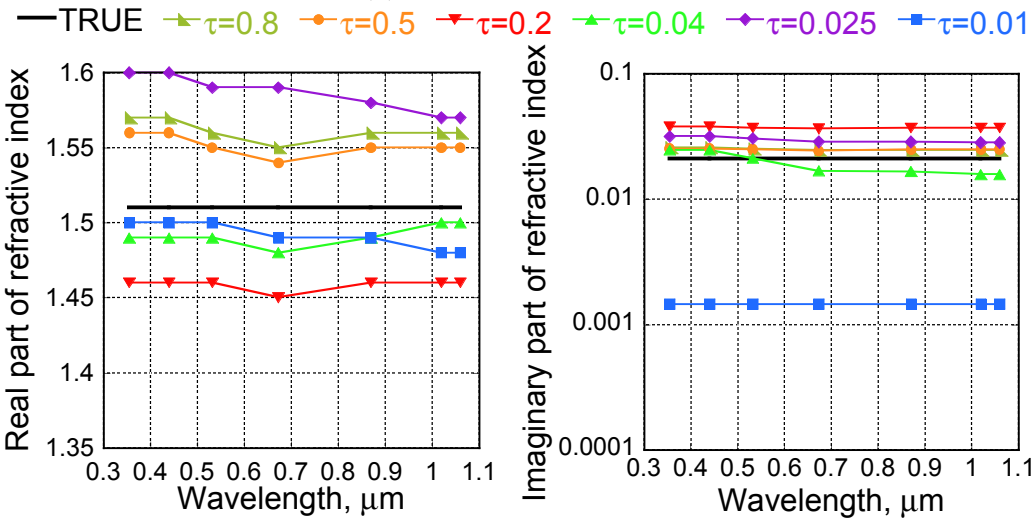

(b) noisy conditions.

Figure 4.5: Retrievals of complex refractive index of "Smoke" aerosol model for different AOTs under (a) - noise free and (b) - noisy conditions.

mode and to underestimate coarse mode content in the layers that contain the mixture of aerosols of both types. However, the algorithm always provides adequate total extinction estimations for the given layer.

This tendency remains even in noise free conditions. It probably can be explained by insufficient information content for perfect separation of fine and coarse mode contributions to the total backscatter signal in the mixed layers. The same as for the aerosol properties that were shown above (Figs. 4.1 – 4.12), the presence of

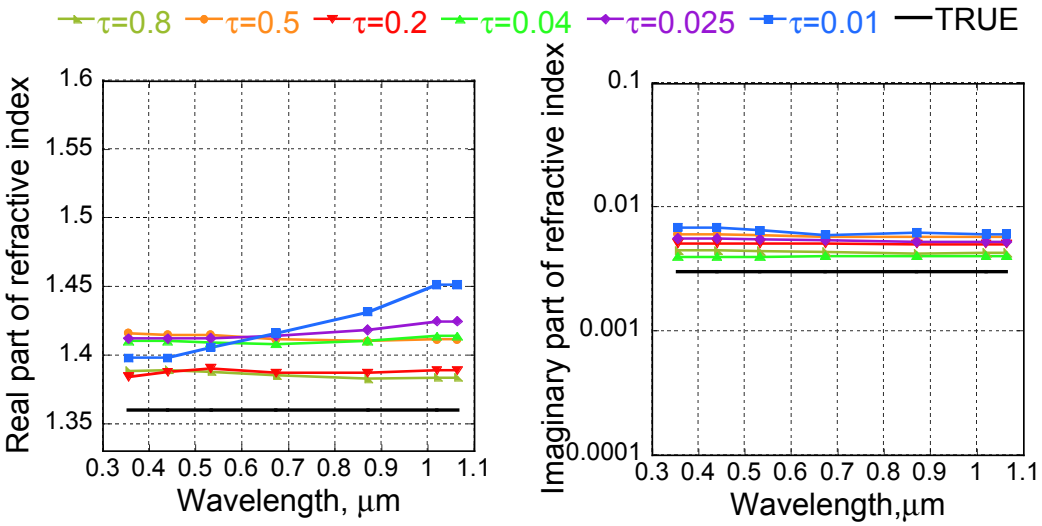

(a) noise free conditions.

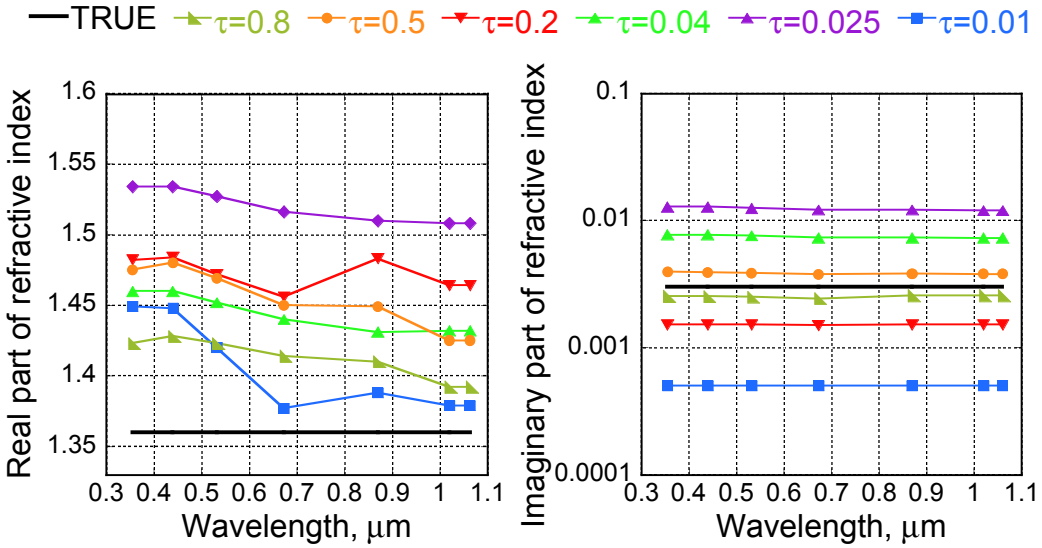

(b) noisy conditions.

Figure 4.6: Retrievals of complex refractive index of "Urban" aerosol model for different AOTs under (a) - noise free and (b) - noisy conditions.

the random noise amplifies the dispersion of the retrievals, especially those that were obtained at low AOTs. Another issue is the underestimation of the aerosol concentration at lower levels in the presence of noise. This could be directly addressed to overestimation of the total aerosol concentration that propagated from the size distribution retrievals. As different studies demonstrate that most of the aerosol content is situated close to the ground such particularity could be connected

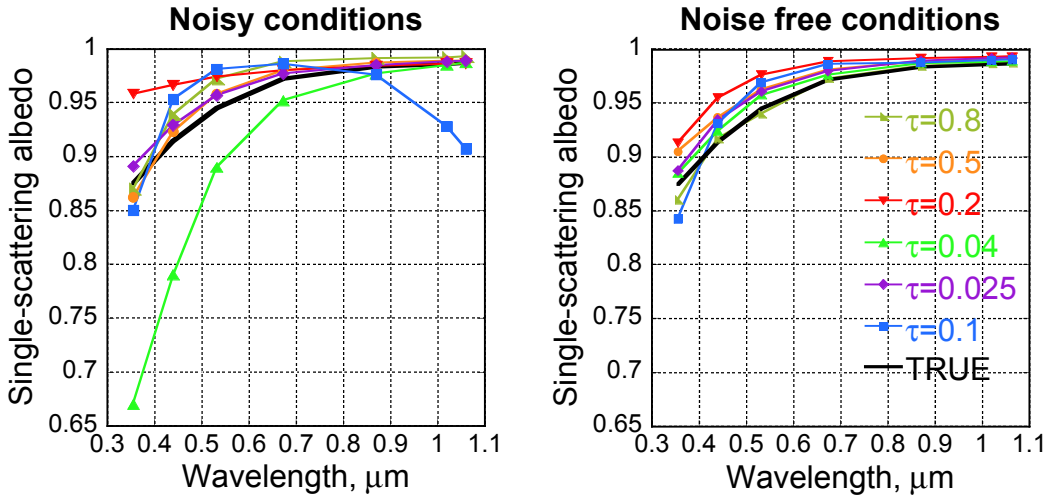

Figure 4.7: Retrievals of single-scattering albedo of "Dust" aerosol model under noisy and noise free conditions.

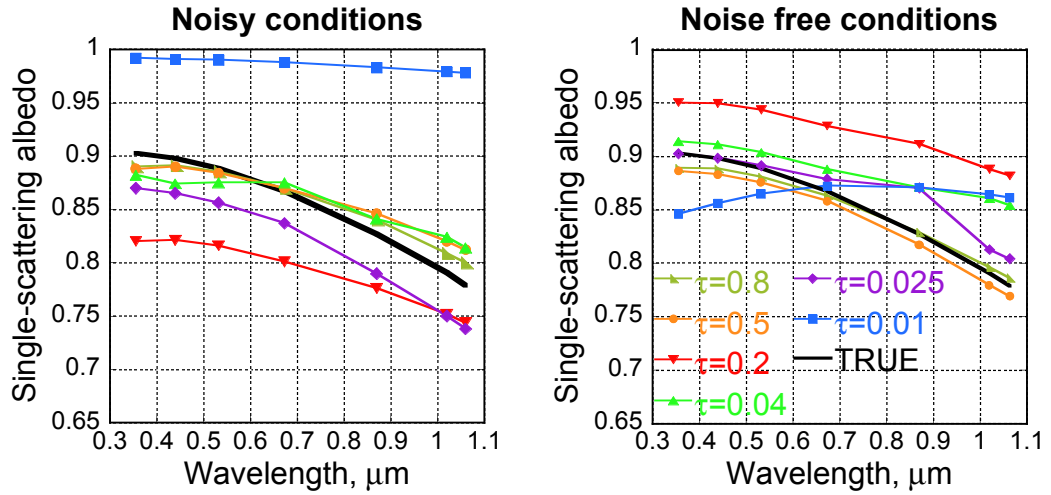

Figure 4.8: Retrievals of single-scattering albedo of "Smoke" aerosol model under noisy and noise free conditions.

with the errors in estimations of aerosol vertical distribution between the minimum sounding altitude of the LIDAR (h_{min}) and the altitude where the sun-photometer was installed. This issue will be addressed in the follow-on studies.

Another tendency observed in the sensitivity study is a lower sensitivity of the retrieval to the properties of the fine mode, especially to the complex refractive index. These high errors in derived complex indices of refraction propagate to the estimations of other optical properties of the fine mode. The trend remains even

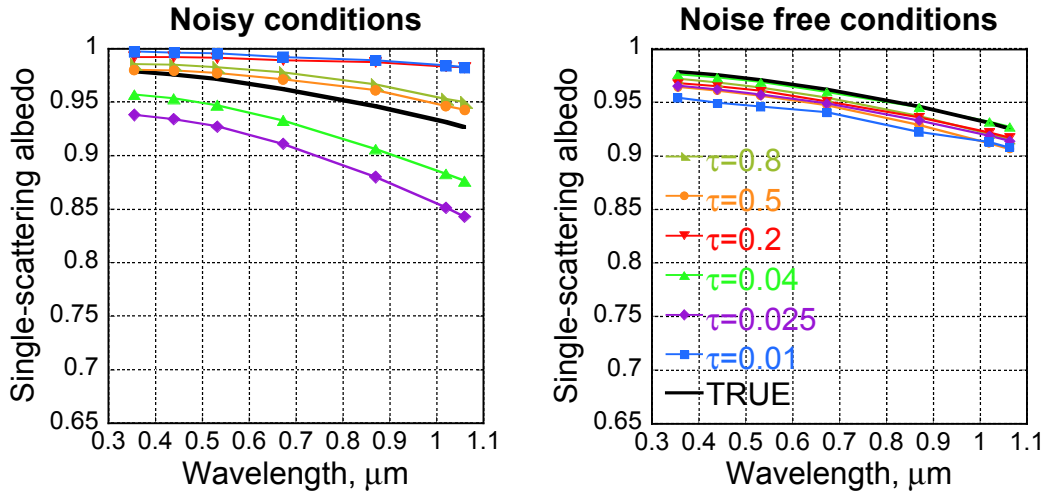

Figure 4.9: Retrievals of single-scattering albedo of "Urban" aerosol model under noisy and noise free conditions.

in situations with high aerosol loading and in noise free conditions. Figure 4.13 shows that fundamental reason for this feature is a selective sensitivity of the lidar measurement to the optical properties of the particles of different size and shape. Values of lidar ratios depicted in Fig. 4.13 were retrieved using size distributions mentioned in Table 4.1 with corresponding optical thickness of $\tau_f = \tau_c = 0.5$. To retrieve the lidar ratios of spherical and non-spherical particles parameter C_{sph} was set to 100% and 0% correspondingly. Both complex indices of refraction for fine and coarse mode were considered spectrally constant. Values of the fixed part of complex refractive index were set as $\kappa(\lambda) = 0.05$ for imaginary part and $n(\lambda) = 1.55$ for real part for the cases with changing real and imaginary parts correspondingly. Such values were chosen to make the studied dependencies more pronounced.

Specifically, Fig. 4.13 clearly indicates that lidar ratio of the aerosol fine mode is less affected by the changes in refractive index compared to the coarse mode. This could be explained by smaller sensitivity of light scattering to the particle shape of the fine mode that is well illustrated by Fig. 4.13, showing stronger dependence of the lidar ratio on complex refractive index for the spheroidal particles of coarse mode compared to spherical particles. Therefore, since lidar measurements are

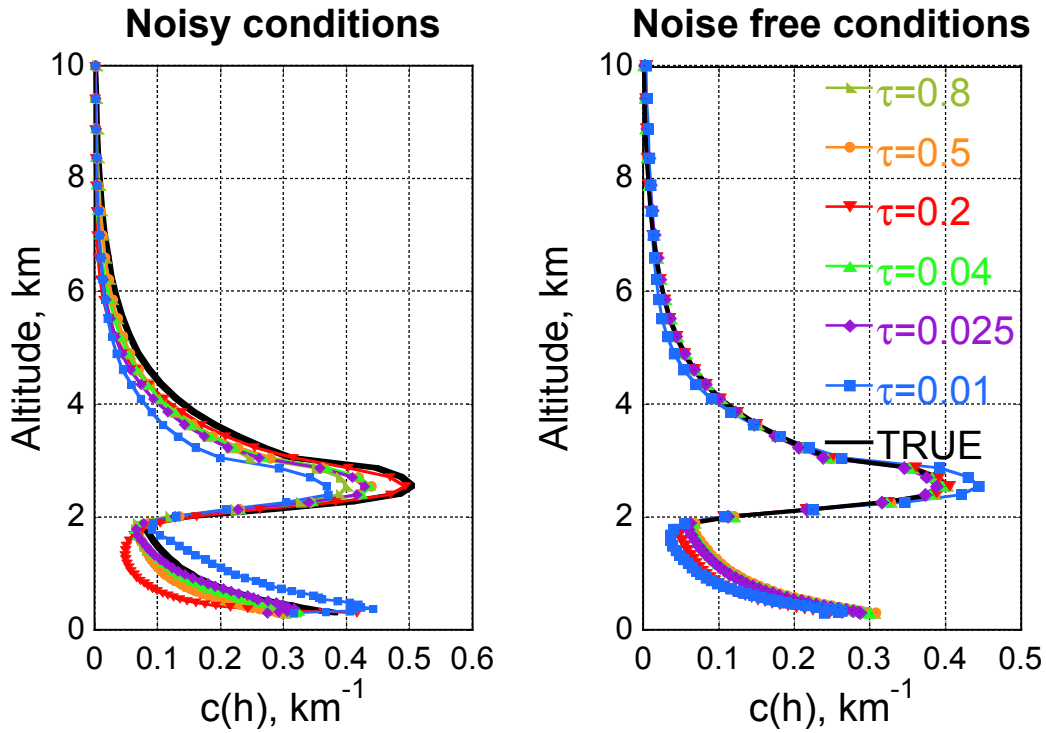

Figure 4.10: Retrievals of vertical distribution of "Dust" aerosol model under noisy and noise free conditions.

sensitive mainly to lidar ratio, lidar measurements do not provide significantly new information about refractive index of fine mode.

Also at shorter wavelengths the high molecular scattering reduces the aerosol contribution to the lidar signal. This also leads to decrease of the sensitivity to the fine mode aerosol properties since a significant part of information about fine fraction relies namely on shorter wavelengths.

It should be noted that a number of studies (Mishchenko et al., 2000, 2004; Dubovik et al., 2006) indicate high sensitivity of polarimetric passive measurements to the refractive index of the fine mode. Therefore, usage of photometers with polarimetric capabilities could potentially result in better retrieval of the aerosol parameters of the fine mode. The study on influence of the presence of polarimetric passive measurements on the retrieval accuracy of the fine mode parameters will be

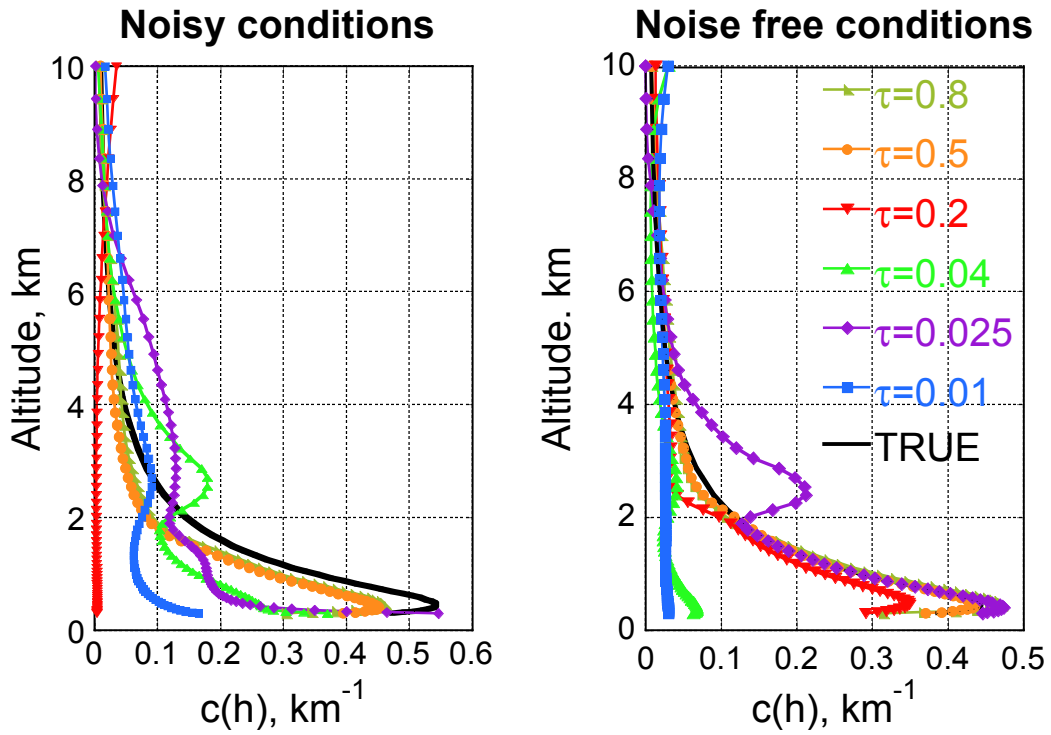

Figure 4.11: Retrievals of vertical distribution of "Smoke" aerosol model under noisy and noise free conditions.

given in the corresponding section 4.4.

4.3 Improvements introduced by joint inversion of lidar and AERONET

A synergetic handling of co-incident sun-photometer and lidar data is obviously beneficial for acquisition of improved vertical characterization of aerosol. The processing of lidar data always relies on assumptions about some aerosol properties. Obtaining this missing information from nearby photometer is evidently preferable to a simple assumption of these properties from climatologies. Therefore, the positive influence of the photometer data on the lidar retrieval was emphasized in a number of previous studies (Chaikovsky et al., 2002a,b, 2006b; Cuesta et al., 2008). However, all previ-

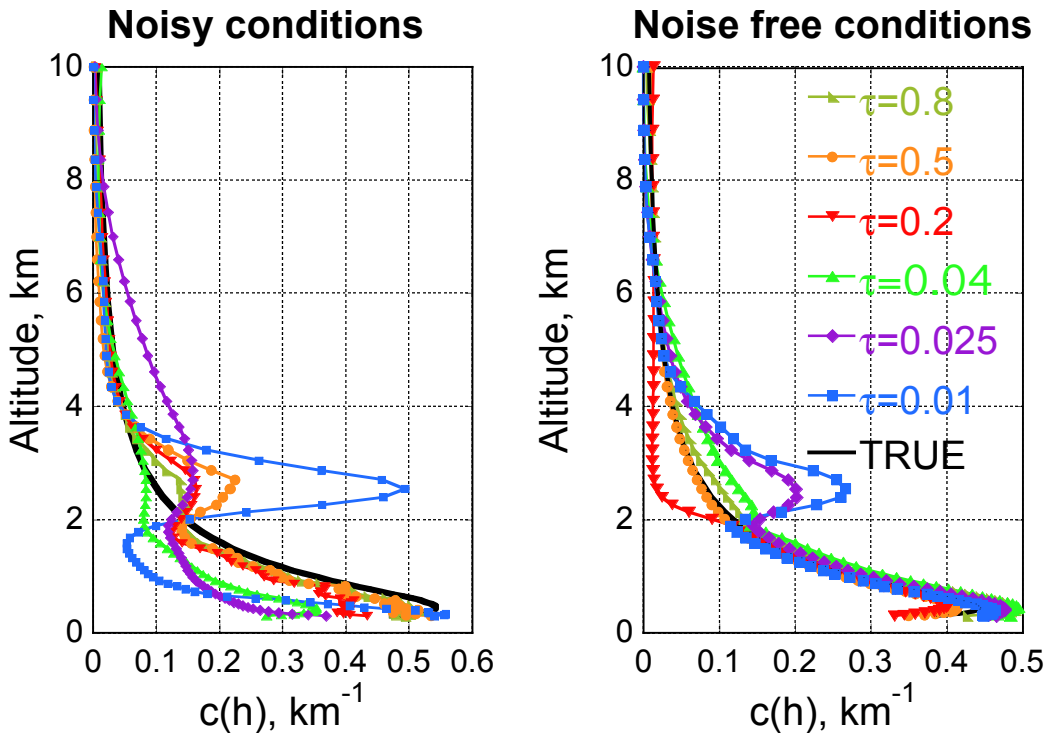

Figure 4.12: Retrievals of vertical distribution of "Urban" aerosol model under noisy and noise free conditions.

ous photometer-LIDAR synergy approaches used AERONET retrievals in the form of a priori assumptions for improving lidar retrievals. GARRLiC is the first development trying to explore possibility of improving AERONET retrieval by using extra information of co-located lidar observations. The possibility to distinguish indices of the refraction of fine and coarse particles is one of the most significant innovations proposed by GARRLiC, since it was not achievable using only AERONET data as shown in studies by Dubovik et al. (2000). The results of the sensitivity tests presented in previous section showed the achievable levels of retrieval accuracy of the complex refractive index using both lidar and photometer data. At the same time, it is clear that the lidar data provide additional information about aerosols properties because of high sensitivity of lidar data to aerosol lidar ratio. Therefore, in order to provide additional illustration of the positive effect from using lidar data on the aerosol columnar properties, we analyse the changes in accuracy of the retrieval of

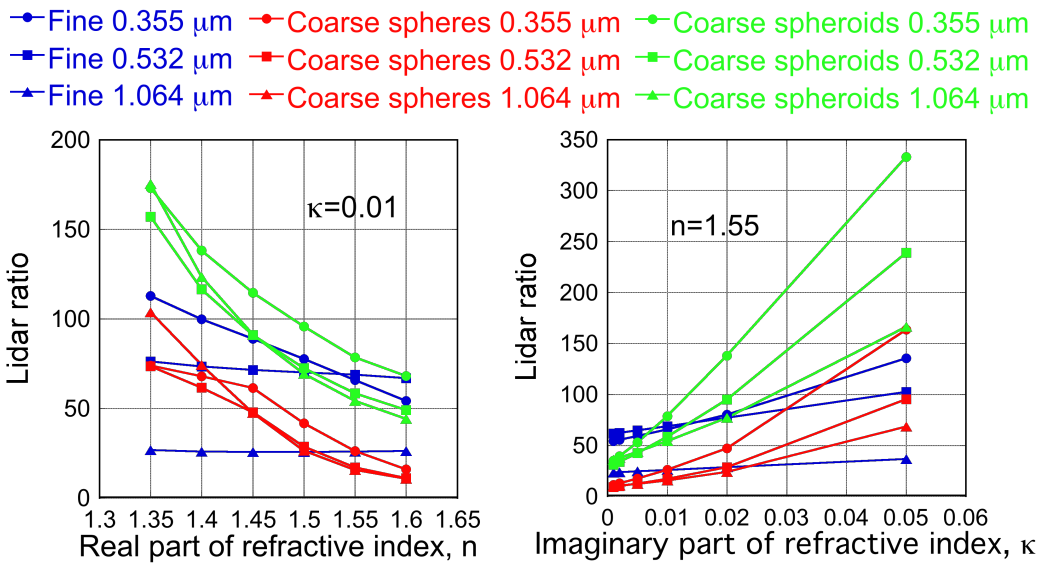

Figure 4.13: Dependencies of lidar ratios of fine and coarse modes on complex refractive index and shape.

lidar ratios by adding lidar data to the AERONET observations. Also any improvement in lidar ratio estimations brings straightforward enhancements in the retrieval of vertical profiles of aerosol concentrations.

With a purpose to access and illustrate possible improvements in the retrieval of

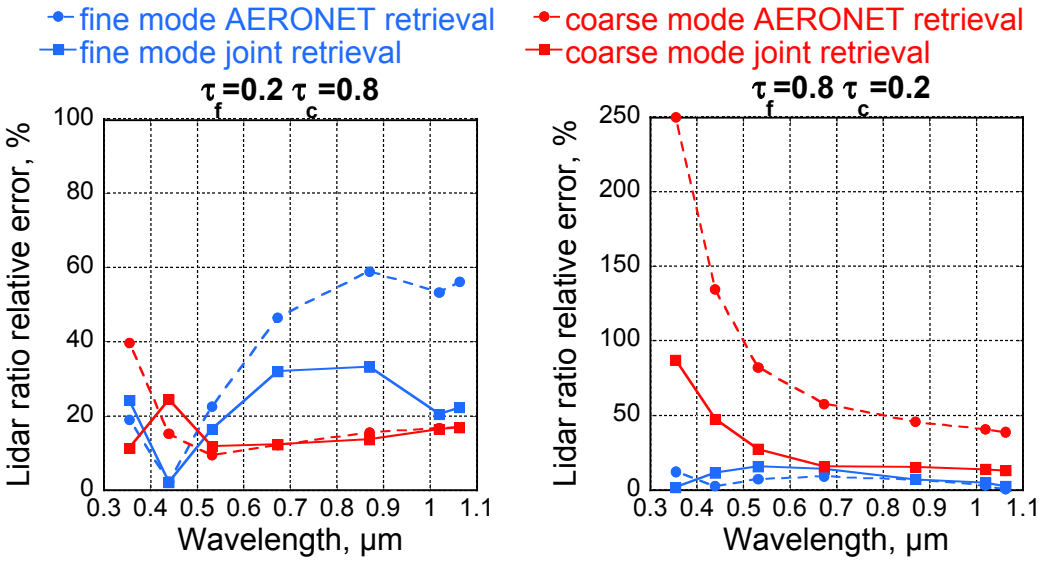

Figure 4.14: Retrieval errors of lidar ratios with and without accounting for lidar data.

aerosol columnar properties, additional scenario was added to the sensitivity study:

inversion, neglecting the measurements provided by lidar. Figure 4.14 shows the comparisons of lidar ratio retrievals conducted for AERONET data only and from a combination of AERONET and LIDAR. The results demonstrate that joint retrieval allows more accurate retrievals of the lidar ratio for both aerosol components in such challenging cases when one of the modes dominates in optical thickness. In such cases the retrieval without lidar measurements tends to estimate all properties of both modes close to those of the dominating one, leading to dramatic errors in the lidar ratio estimations. The errors of the retrieval of the dominating mode lidar ratio remain almost the same for both inversion strategies. These results lead to a conclusion that supplementing photometer data with lidar observations helps to improve the retrieval of aerosol properties of the minor mode in the aerosol mixture. Consequently, the retrieval of the vertical concentration profile of the minor mode is also should be more accurate compared to the retrievals by the approaches of Chaikovsky et al. (2012) and Cuesta et al. (2008) which assume lidar ratios from AERONET retrievals.

Figure 4.15 shows the comparison of the aerosol size distributions for the same cases depicted in Fig. 4.14. It is clearly seen from the Figure 4.15 that addition of lidar data hadn't seriously affected the retrievals. Following the results found in Fig. 4.13 and the fact that the AERONET retrieval uses only one refractive index for both aerosol components, the improvements of the lidar ratio retrievals (shown in Fig. 4.14) should be mostly provided by the noticeable difference in the refractive indices of the aerosol modes retrieved by the GARRLiC algorithm.

Also, based on the observations made from Fig. 4.13 that lidar ratio is very sensitive to the retrieval accuracy of the spherical particles fraction, we have evaluated the possible improvements in the retrieval of this parameter by using joint inversion of AERONET and lidar data.

Table 4.2 summarizes the relative errors of the retrieval of this parameter for three

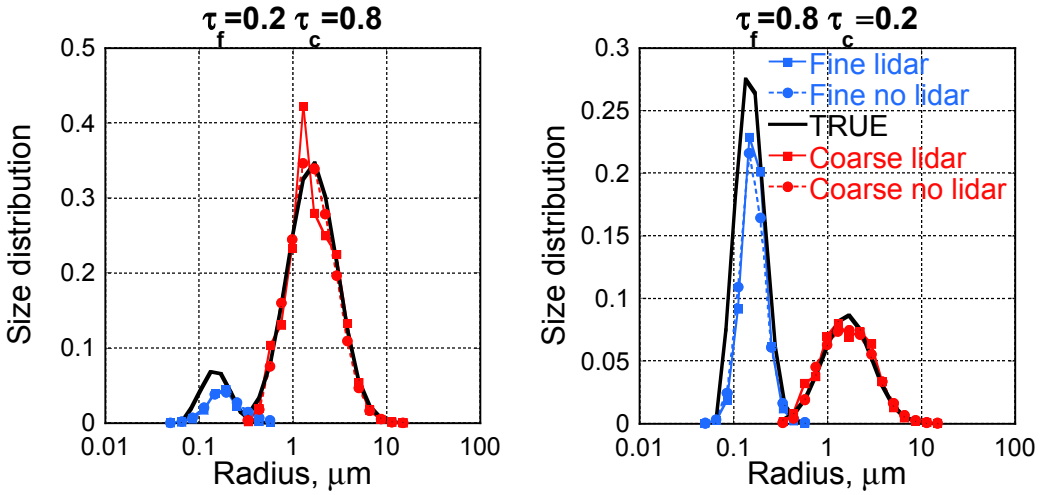

Figure 4.15: Retrieval of the aerosol size distribution with and without accounting of lidar data.

cases of aerosol with different partition of aerosol modes. The results were obtained for high aerosol load within three inversion scenarios: the joint inversion of photometer and lidar data without any noise added; the joint inversion with random noise added to the data and the inversion of photometer data only with random noise added to the observations. Although without the information about polarization the sensitivity to this parameter is quite low and depends on the aerosol optical thickness, the fact that backscatter depends on this parameter (illustrated by Fig. 4.13) allows decreasing retrieval errors in the situations when coarse mode dominates in the optical thickness. As it seen from the table, the absence of lidar data in the presence of the random noise makes accurate GARRLiC retrieval of this parameter impossible even in situation with significant amount of coarse mode, while in the presence of lidar data sensitivity to this parameter remains for the same case of aerosol load. Decrease of the retrieval error with growth of the coarse mode concentration is explained by the higher sensitivity of the measurements to the shape parameters of bigger particles.

The analysis of test results allows making a conclusion that being supplied with sufficient measurement information combined inversion could provide a deep synergy

Table 4.2: Relative errors of the retrieval of the spherical particles fraction.

$\frac{\tau_c}{\tau_f}$	τ_f	τ_c	AERONET +lidar no noise	AERONET noise added	AERONET +lidar noise added
0.25	0.8	0.2	0.99	1.00	0.98
1	0.5	0.5	0.28	0.99	0.99
4	0.2	0.8	0.02	0.89	0.03

of two different types of the aerosol remote sensing, resulting in more accurate and qualitative retrievals compared to the single instrument inversions.

4.4 Improvements introduced by inclusion of almucantar measurement of linear polarization degree

Both passive and active instruments are capable of performing polarization measurements. Instruments that observe the polarized radiance have several distinct advantages over the instruments that only measure total radiance. Multi-wavelength polarization measurements nearly double the input information of aerosol retrievals thus providing a unique opportunity for improving current aerosol inversion products. A number of studies suggest that accurate polarized observations provide additional information that can be used to distinguish aerosol optical properties (Mishchenko et al., 2002, 1997; Li et al., 2006, 2009).

In particular Li et al. (2009) studies the ground-based measurements and demonstrates that for the cases dominated by the fine mode aerosol inclusion to the inversion of polarization observations provides improved retrievals of the real part of the refractive index ($n(\lambda)$) and the volume of fine mode. In the cases of mixed aerosol when both coarse and fine mode aerosols are presented, additionally to

mentioned fine mode improvements, it provides significantly different estimations of the spherical particles fraction (C_{sph}) for the coarse mode.

Concerning space-borne instruments, polarization also makes it easier to differentiate the effects of aerosols from other components of the radiative transfer system as observed at the top of the atmosphere (Cairns et al., 2009). Compared to radiance only observations, polarized observations are more capable of distinguishing aerosols from reflecting surfaces underneath, such as the ocean, land or cloud layers. For this reason, polarized observations have the potential to retrieve aerosol properties more accurately than observations with radiance alone.

Passive ground-based systems usually supply information about degree of linear polarization (DoLP) in the principal plane (Holben, 1998; Torres, 2012) or almucantar (Li et al., 2006) measurement configurations. Active systems provide information about linear depolarization at different altitudes. Both systems are capable of performing multi-wavelength DoLP observations.

Despite of the prevalence of lidar depolarization measurements and measurements of linear polarization in the principal plane geometry, the latest trend in the passive measurements advancement is the spectral measurements of the linear polarization degree in the almucantar configuration (Li et al., 2006, 2009). This study will focus on such type of additional polarization measurement, because as it was shown by Torres (2012) principal plane configuration of the Cimel photometer that could be used for this study isn't faultless and accounting of vertical depolarization which is provided by lidar requires a more sophisticated 3-component aerosol model, as it was shown by Chaikovsky et al. (2012).

This study will enlighten the most illustrative situation with sufficient load of aerosol ($\tau_{total} = 1$) with domination of fine mode in particular ($\tau_f = 0.8$, $\tau_c = 0.2$). It also will focus on the retrievals of the aerosol columnar properties because additional polarization information is expected to affect them the most, since no altitude-resolved

polarization data from LIDAR were used. At the same time as vertical optical properties are highly dependent on columnar estimations the improvements should propagate directly to the profiles in the case if lidar measurements fits for both cases will have comparative accuracy.

This study was performed exactly as described earlier in the Section 4.1. The main difference was the inversion of almucantar measurements that contained not only intensity of the scattered radiation but also a degree of its linear polarization (see Table 4.1). DoLP measurements were simulated at the same wavelengths as intensity measurements (0.440, 0.675, 0.870 and 1.020 μm).

The retrievals for this study were also made in the presence of random noise. To make both intensity-only and combined intensity-polarization retrievals comparable the same noise models as described in section 4.1 both for lidar (Eqs. 4.1 – 4.2) and passive observations were used. Additionally polarization measurements were also distorted with the 1% random noise.

Figures 4.16 - 4.30 show the comparison of retrievals of the microphysical aerosol properties, single-scattering albedo and lidar ratios between inversions using intensity only (red) and combined intensity/polarized (blue) data with the aerosol properties that were used for measurements modelling.

The retrievals of the size distributions of fine mode still have lower accuracy than for the coarse mode, however, as it seen from Figures 4.17 and 4.18 inclusion of polarization measurements provides less biased estimations for the fine mode. Overall behaviour of the retrieved distributions of the fine mode on the size boundaries and on the maximum remains as described in the previous subsection, yet the magnitude of the variation is lower.

According to studies of Mishchenko et al. (2000, 2004) and Dubovik et al. (2006) the main benefit of inclusion of measurements of the linear polarization was expected in the accuracy increase in the fine mode refractive index retrievals. As it is depicted

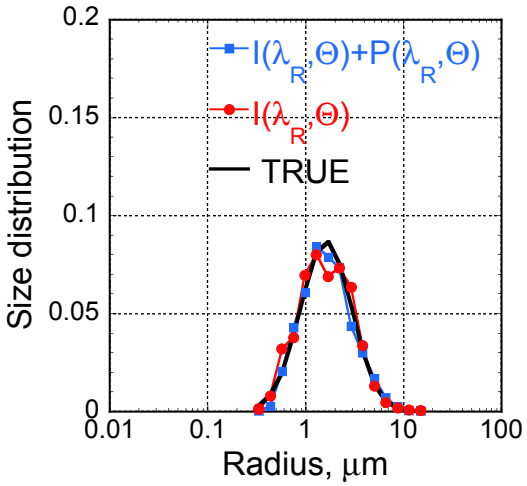

Figure 4.16: Retrievals of size distribution for "Dust" aerosol model using intensity only almucantars and combined intensity and linear polarization almucantars in combination with lidar data ($\tau = 0.2$).

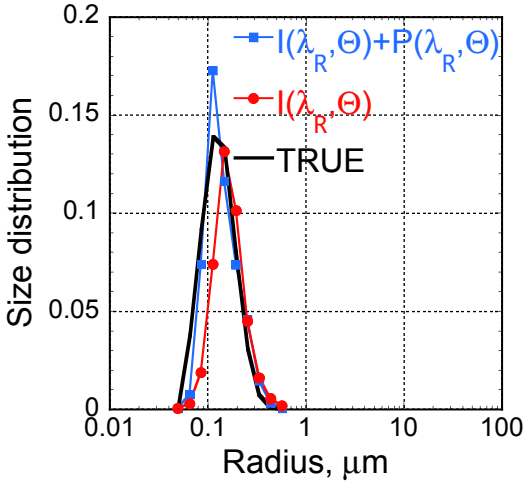

Figure 4.17: Retrievals of size distribution for "Smoke" aerosol model using intensity only almucantars and combined intensity and linear polarization almucantars in combination with lidar data ($\tau = 0.8$).

in Figures 4.19 – 4.21, inclusion of polarization measurements significantly improved the accuracy of the retrieval of this parameter. The effect of accounting for additional measurements on the non-dominating coarse mode could be considered insufficient, yet the retrieval is better on the longer wavelength. Such behaviour could be explained by more accurate discrimination of the optical properties of the aerosol modes, thus improving retrievals of the coarse mode microphysical parameters in the

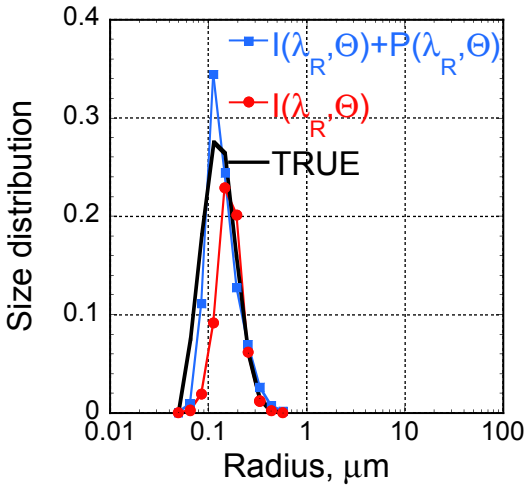

Figure 4.18: Retrievals of size distribution for "Urban" aerosol model using intensity only almucantars and combined intensity and linear polarization almucantars in combination with lidar data ($\tau = 0.8$).

spectral region that is affected the most by larger particles.

Figures 4.19 – 4.21 demonstrate the retrievals of imaginary part of refractive

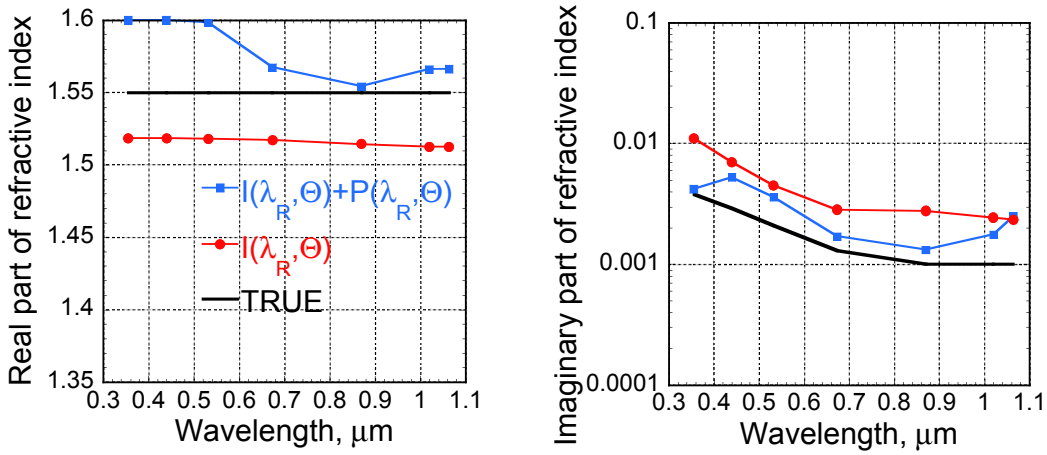

Figure 4.19: Retrievals of complex refractive index for "Dust" aerosol model using intensity only almucantars and combined intensity and linear polarization almucantars in combination with lidar data ($\tau = 0.2$).

indices for "Dust", "Smoke" and "Urban" aerosol models used in this study. Estimations of this parameter for the fine mode both retrieved with intensity only and combined intensity/polarized almucantars show good and comparable accuracies. At the same time some improvement could be observed in the case with inclusion of

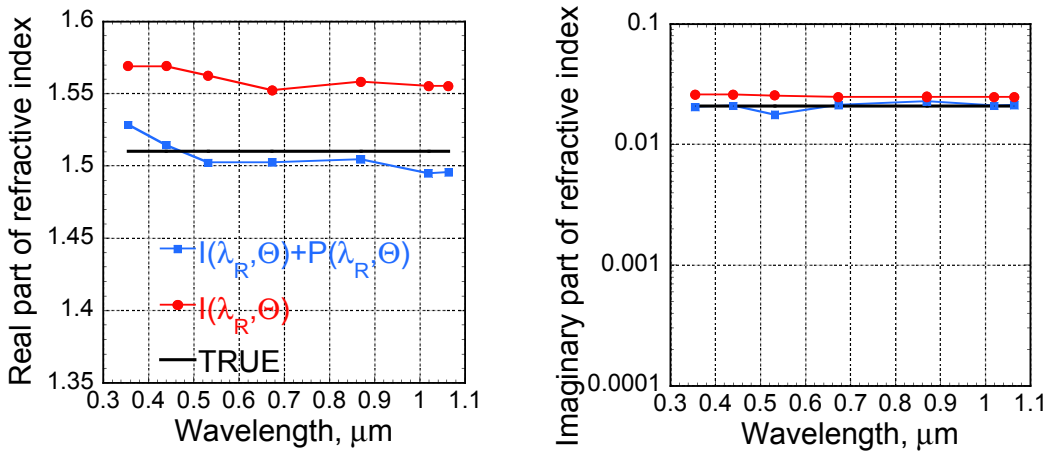

Figure 4.20: Retrievals of complex refractive index for "Smoke" aerosol model using intensity only almucantars and combined intensity and linear polarization almucantars in combination with lidar data ($\tau = 0.8$).

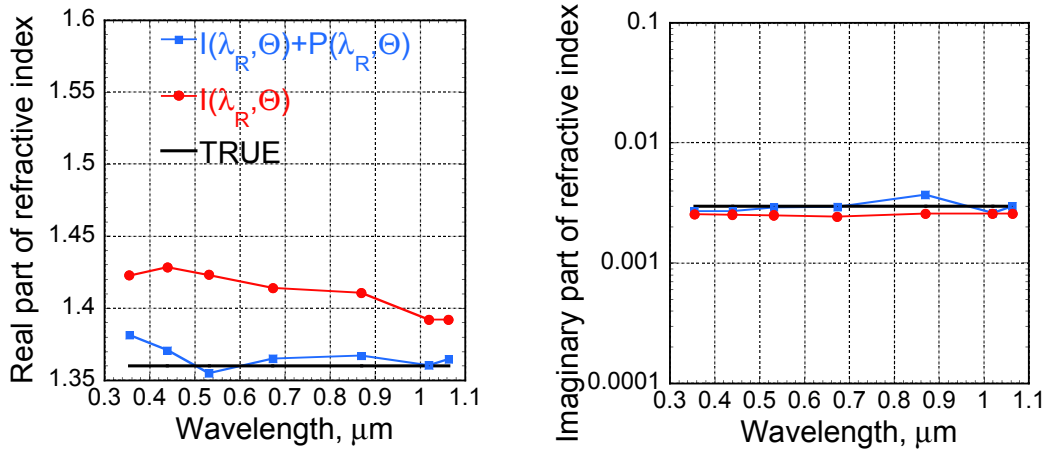

Figure 4.21: Retrievals of complex refractive index for "Urban" aerosol model using intensity only almucantars and combined intensity and linear polarization almucantars in combination with lidar data ($\tau = 0.8$).

polarization. The retrieval of the coarse mode is better in the case with polarization measurements. As seen from first plot in Fig. 4.19, more accurate reproduction of the spectral behaviour typical for the dust particles was achieved. More accurate estimation of the coarse mode absorption explained as the influence through better mode distinguishing due to a more accurate estimations of the dominating aerosol modes, the same as for real part of coarse mode refractive index.

Figures 4.22 – 4.24 show that more accurate differentiation of the aerosol com-

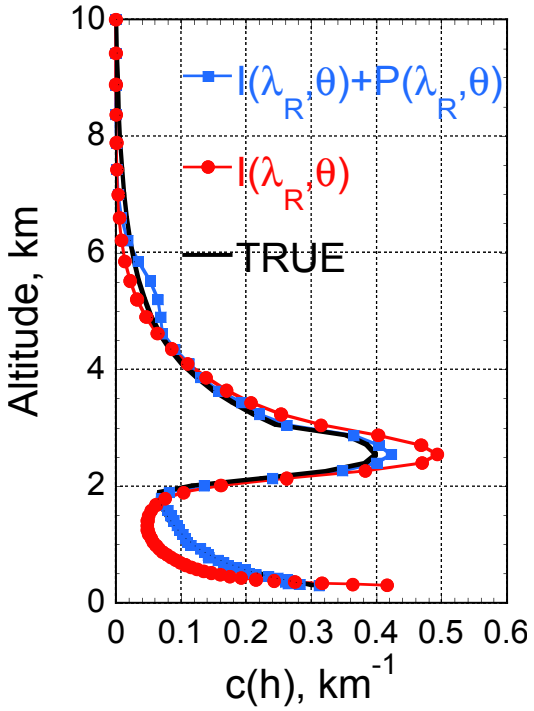

Figure 4.22: Retrievals of the vertical distribution for "Dust" aerosol model using intensity only almucantars and combined intensity and linear polarization almucantars in combination with lidar data ($\tau = 0.2$).

ponents in the layers containing mixture of both aerosol types could be achieved through introduction of linear polarization measurements into the combined lidar/photometer retrieval by GARRLiC. Such particularity deals directly with the higher quality of the fine mode refractive index estimation, which leads to a more accurate optical properties estimations of aerosol components in the mixture. This particularity affects both retrievals of fine and coarse modes vertical distributions, which are shown in Figures 4.22 – 4.24 for described aerosol models. Also, the issue of less accurate estimations of aerosol contents at lower altitudes addressed earlier is resolved for both fine and coarse components due to the polarimetric measurements. It should be noted that this improvement was achieved at the same levels of random noise added to the intensity measurements.

As it was shown by Figures 4.19 – 4.21 inclusion into inversion of almucantars containing measurements of degree of linear polarization positively affected the retrievals

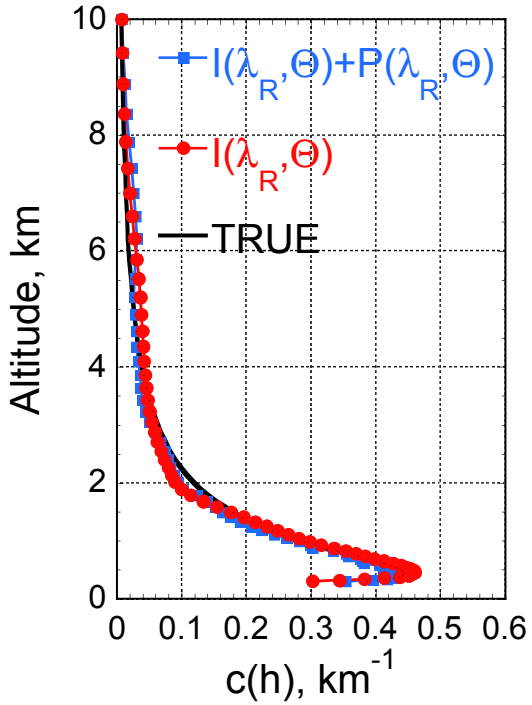

Figure 4.23: Retrievals of the vertical distribution for "Smoke" aerosol model using intensity only almucantars and combined intensity and linear polarization almucantars in combination with lidar data ($\tau = 0.8$).

of the fine mode refractive index. This should lead to a more accurate estimations of the single-scattering albedo of the smaller particles, which in by-turn should positively affect the retrieval of this parameter for the coarse mode which is well demonstrated in Figs. 4.25 – 4.27, showing retrievals of the spectral single-scattering albedo for the selected aerosol models.

It should be outlined that the total single-scattering albedo is retrieved with sufficient accuracy in the whole spectral range for both intensity and combined intensity/polarization retrievals.

The lidar ratio estimations for aerosol components should also be affected by the higher accuracy of refractive index retrievals, as it was shown in Figure 4.13. It is clearly seen in Figs. 4.28 – 4.30 that estimations of this parameter are more accurate for the inversion that includes polarization data. This by turn should improve the vertical profiles retrievals and lidar measurements fits, leading to an even deeper

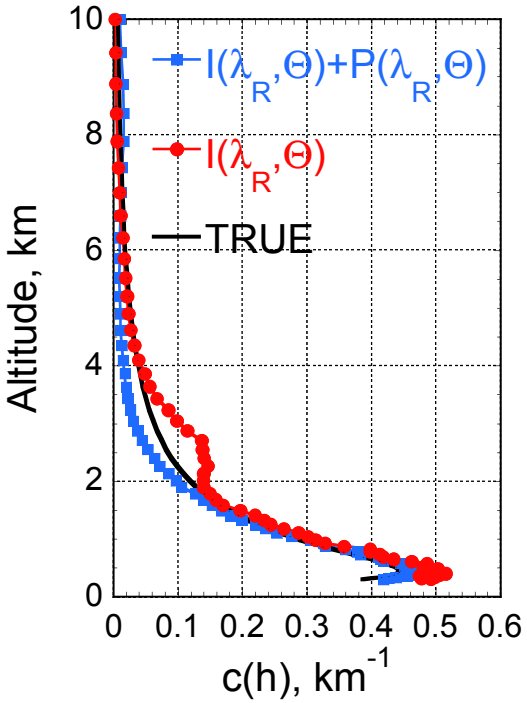

Figure 4.24: Retrievals of the vertical distribution for "Urban" aerosol model using intensity only almucantars and combined intensity and linear polarization almucantars in combination with lidar data ($\tau = 0.8$).

synergy between lidar and radiometric data.

Generally, addition of linear polarization measurements to almucantar measurements performed by sun-photometer positively affected all retrieved parameters, providing more accurate estimations both for fine and coarse modes, resolving most of the issues found in previous study addressed to intensity only inversions of combined lidar/sun-photometer measurements. As it was predicted, better refractive index estimations of the fine mode aerosol models were achieved due to the additional sensitivity of polarization measurements to this parameter. This improvement directly propagated to the estimations of fine mode optical properties, therefore, lowering the errors in estimations of other parameters of the fine mode, which, in by-turn, lowered the estimation errors of the coarse mode, due to a better mode distinguishing.

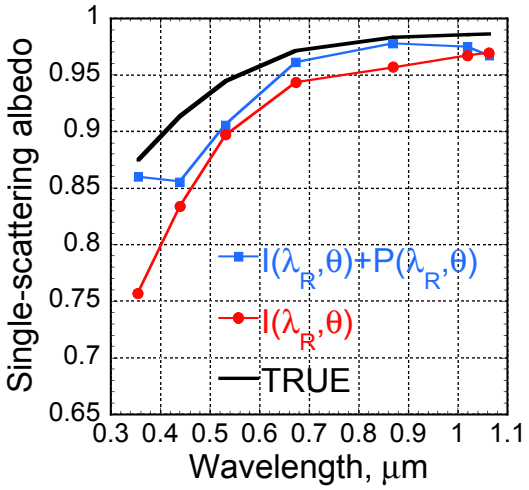

Figure 4.25: Retrieval of the single-scattering albedo for "Dust" aerosol model using intensity only almucantars and combined intensity and linear polarization almucantars in combination with lidar data ($\tau = 0.2$).

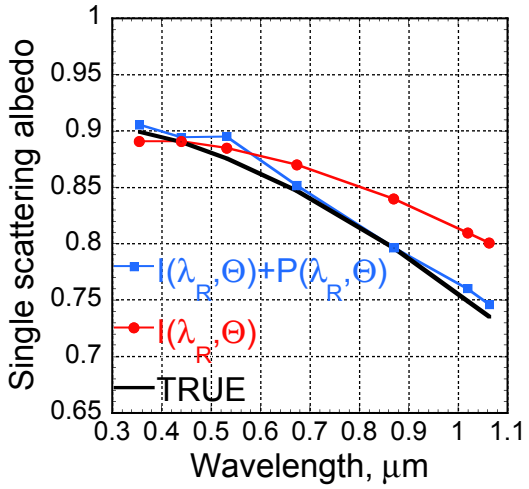

Figure 4.26: Retrieval of the single-scattering albedo for "Smoke" aerosol model using intensity only almucantars and combined intensity and linear polarization almucantars in combination with lidar data ($\tau = 0.8$).

Summarizing this Chapter, the new GARRLiC algorithm was tested on synthetic data in a variety of realistic cases. Both sensitivity to random noise, aerosol type and loading and data integrity were tested. Method showed ability to distinguish both microphysical and optical properties of fine and coarse aerosol components in the presence of random noise, providing microphysical estimations including vertical profiles of aerosol concentration suitable to model a full range of aerosol

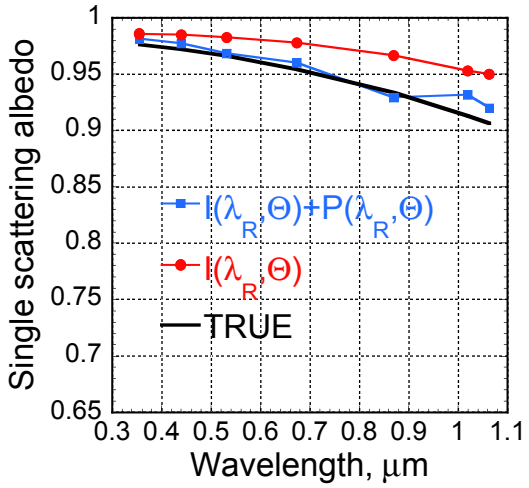

Figure 4.27: Retrieval of the single-scattering albedo for "Urban" aerosol model using intensity only almucantars and combined intensity and linear polarization almucantars in combination with lidar data ($\tau = 0.8$).

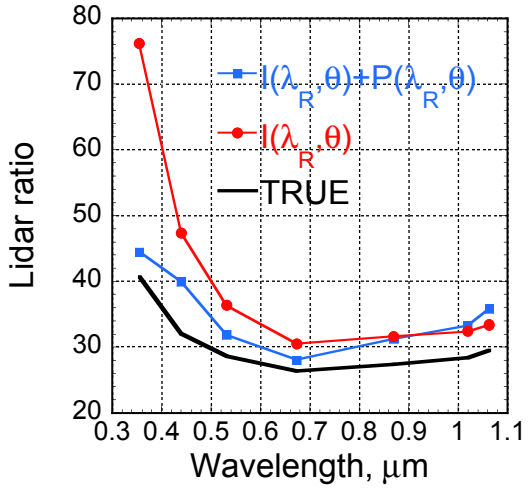

Figure 4.28: Retrieval of the lidar ratio for "Dust" aerosol model using intensity only almucantars and combined intensity and linear polarization almucantars in combination with lidar data ($\tau = 0.2$).

optical properties for each aerosol component. Dependence of the accuracy of aerosol parameter estimations on AOT and on the presence of random noise was demonstrated. The presence of random noise in the measurements affected more drastically the inversions performed at low optical thickness, causing higher errors in aerosol parameter estimations.

Lower sensitivity to the microphysical parameters of the fine particles unrelated

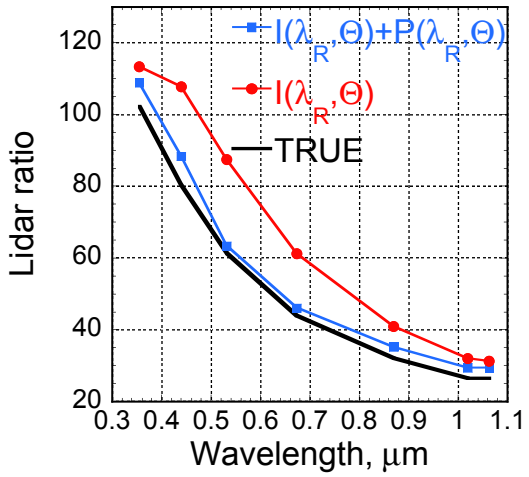

Figure 4.29: Retrieval of the lidar ratio for "Smoke" aerosol model using intensity only almucantars and combined intensity and linear polarization almucantars in combination with lidar data ($\tau = 0.8$).

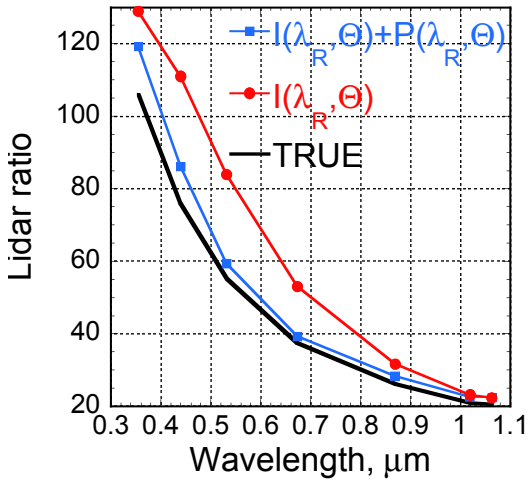

Figure 4.30: Retrieval of the lidar ratio for "Urban" aerosol model using intensity only almucantars and combined intensity and linear polarization almucantars in combination with lidar data ($\tau = 0.8$).

to the presence of random noise was found. This issue was most noticeable in the retrievals of the real part of the particle refractive index.

Improvements that are introduced into aerosol retrievals by inclusion of lidar measurements and passive polarimetric measurements were demonstrated. Inclusion of lidar measurements, despite of introducing vertical profiles of aerosol concentration, also positively affected the accuracy of the lidar ratio retrievals of non-dominating

modes. Accounting for polarization data most noticeably improved the retrievals of the real part of refractive index of the fine aerosol mode, thus positively affecting retrievals of other fine mode parameters and mode differentiation.

Therefore, the most perspective lidar/sun-photometer measurement combination appears to include both spectral intensity and polarimetric sun-photometer measurements, combined with spectral measurements of aerosol backscatter provided by lidar.

Chapter 5

GARRLiC applications to real lidar/sun-photometer observations

Real is what can be measured.

Max Planck

The algorithm has been applied to lidar/sun-photometer measurements collected at observation sites of the Laboratory of Scattering Media (LOSM) at Institute of Physics, Minsk, Belarus and the Laboratory of Atmospheric Optics (LOA) at Lille University, Lille, France. Both Minsk (53.920°N : 27.601°E, 200 msl) and Lille (50.612°N : 3.141°E, 60 msl) AERONET sites are situated in the similar conditions — inside a developed megapolis with approximate population of 2 million people. Both stations were equipped by standard AERONET sun-photometer and a multi-wavelength lidar that provided measurements of attenuated backscatter at 0.355, 0.532 and 1.064 μm. Parameters that describe noise (see Eq. 3.56) in this lidar system were estimated as shown in Table 5.1.

Three typical situations were chosen to illustrate the inversion results: (i) the observation of dust outburst from Sahara desert transported over Minsk on 2.06.08, (ii) observation of smoke plum transported from Russian forest fires over the East

Table 5.1: Estimations of lidar system noise parameters.

Parameter	v	g	q	u	α_1	α_2
Value	10^{-5}	10^{-4}	10^{-1}	1	10^{-1}	10^{-3}

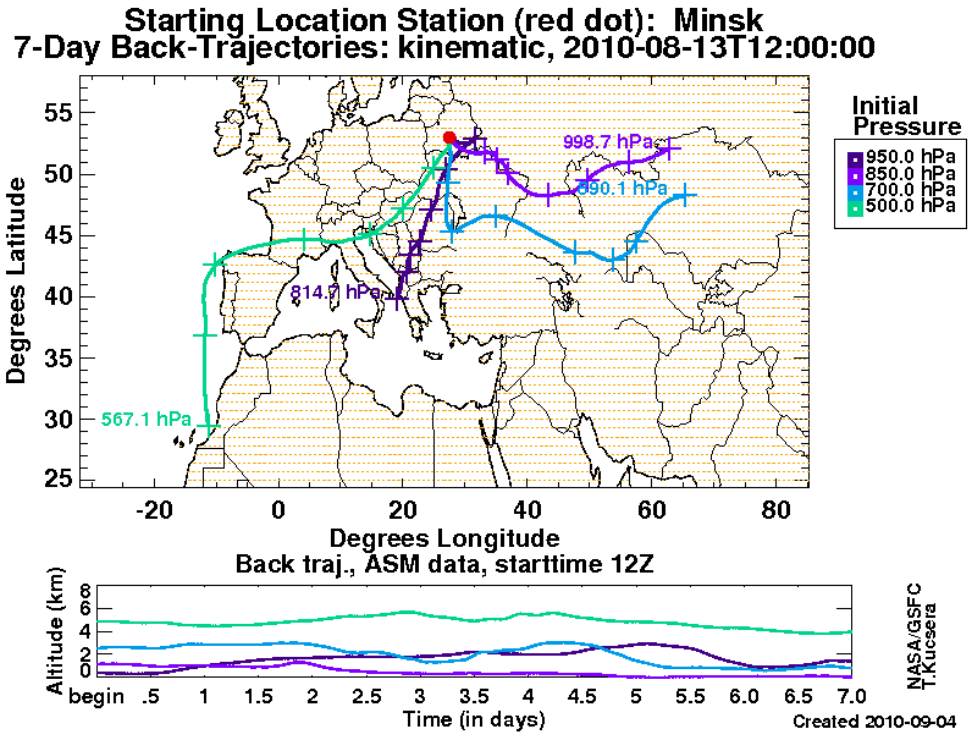

Figure 5.1: Air mass back trajectories for the Minsk measurement site on 13.08.2010.

Europe on 13.08.2010 and (iii) observation on 14.05.2010 made in Lille after an Eyjafjallajökull volcano eruption. The total optical thickness for these cases were $\tau_{440} = 0.36$, $\tau_{440} = 0.46$ and $\tau_{440} = 0.27$ correspondingly.

Figures 5.1 – 5.3 show the atmosphere back trajectories provided for Minsk and Lille AERONET sites, (`http://croc.gsfc.nasa.gov/aeronet/`; Schoeberl and Newman, 1995; Pickering et al., 2001) for these cases. The analysis of these back trajectories illustrates that air masses from the mentioned regions should be present over the observation sites during mentioned measurement periods. Particularly, Fig. 5.2 demonstrates the air masses enriched with dust particles that were transferred to the Eastern Europe from the Northern Africa and the Mediterranean, Fig. 5.1 indicates

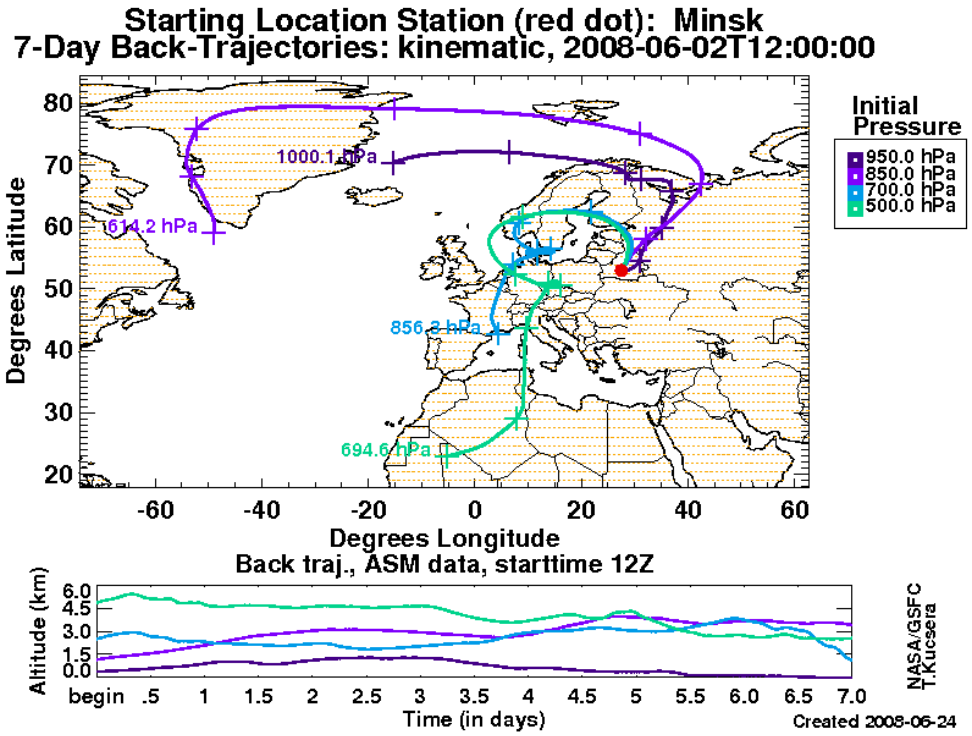

Figure 5.2: Air mass back trajectories for the Minsk measurement site on 02.06.2008.

that air mass from the central Russia that should contain smoke particles was present above Minsk and Fig. 5.3 shows that air masses above Lille came from Northern Atlantic, were the volcano eruption had taken place several weeks ago.

The retrieved results are grouped as follows: Figures 5.4 – 5.18 present the retrieved columnar aerosol parameters in comparison with standard AERONET retrievals for the mentioned sites. Figures 5.10 – 5.12 and 5.22 – 5.27 present the retrieved vertical profiles of microphysical and optical aerosol properties. Figures 5.28 – 5.30 and 5.31 – 5.33 are dedicated to the qualifications of the vertical retrievals. Figs. 5.28 – 5.30 are presenting the comparison of GARRLiC results with LiRIC retrievals made for the same measurements and Figs. 5.31 – 5.33 present achieved fits of the lidar measurements that were used for this study.

The retrieved size distributions (Figs. 5.4 – 5.6) are consistent with the expectations for the observed aerosol types: domination of fine mode for the smoke

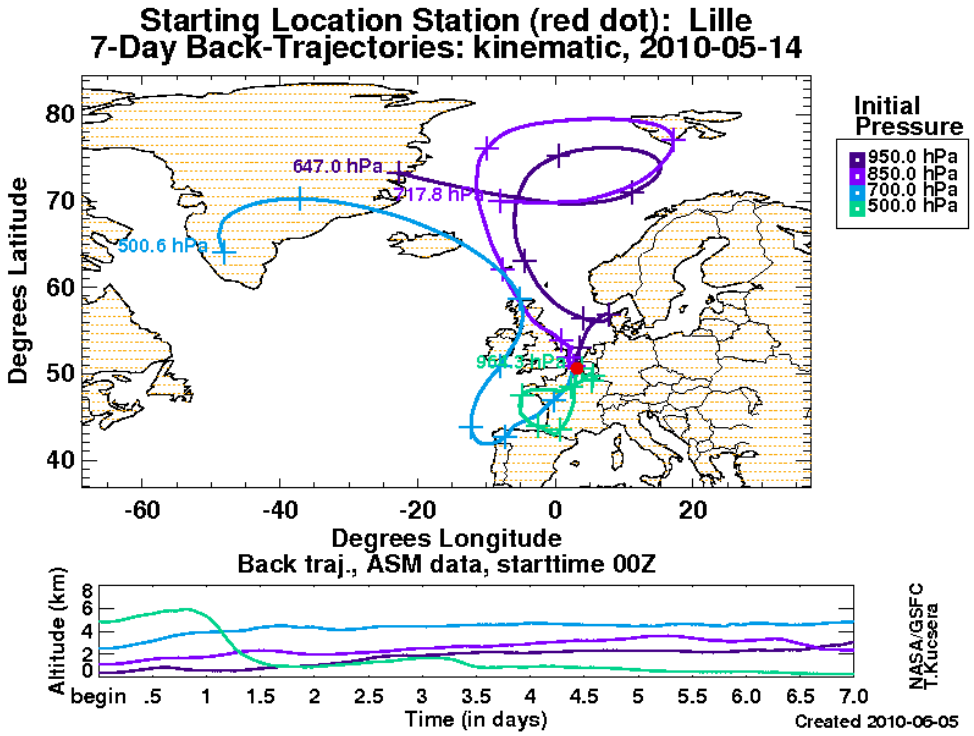

Figure 5.3: Air mass back trajectories for the Lille measurement site on 14.05.2010.

and of coarse mode for the desert dust and volcanic ash. All the size distributions show good agreement with AERONET retrievals performed for the same site and at the same time period. The difference in fine mode retrievals between two methods in the dust observation case (see Fig. 5.4) could probably be explained by lower sensitivity of the AERONET inversion to minor aerosol modes that was found out in the sensitivity study described earlier in the Chapter 4. Observed size shift in the favour of larger particles for the cases of dust and smoke outbursts (Figs. 5.4 and 5.5) could be explained by the influence of the lidar data on the retrieval.

The retrieved refractive indexes (Figs. 5.7 – 5.9) are clearly distinguished between modes and are coherent with the values expected for these aerosol types: highly absorbing fine mode for smoke (Fig. 5.8), the values of real part of the refractive index for coarse mode (Fig. 5.7) are close to the observations of this parameter for the dust (1.56) Dubovik et al. (2002a) and the values for the fine mode (Fig. 5.8)

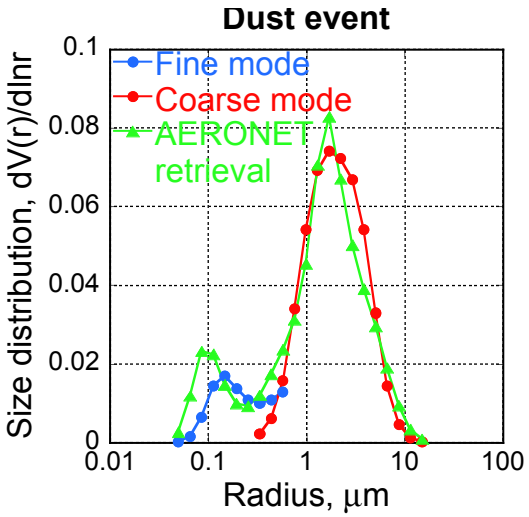

Figure 5.4: Retrieved aerosol size distribution during measurements at Minsk AERONET site on 02.06.2008 (dust event).

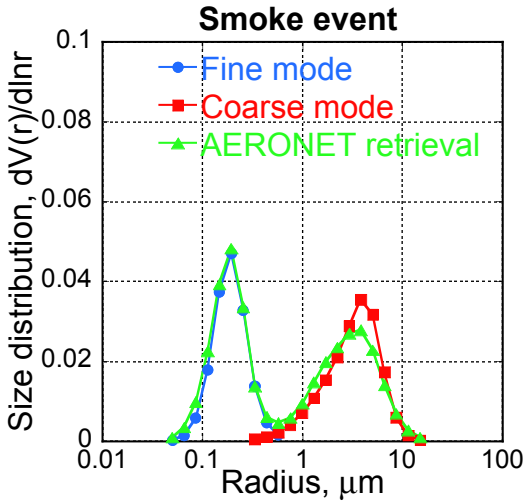

Figure 5.5: Retrieved aerosol size distribution during measurements at Minsk AERONET site on 13.08.2010 (smoke event).

are close to climatology estimations of this parameter for the smoke Dubovik et al. (2002a). Since, the AERONET retrieval does not discriminate the refractive index of the modes, the AERONET derived values can not be compared directly to the GARRLiC retrieval. Nonetheless, it is clear that there is logical agreement between two retrievals since AERONET derived indices are generally in the middle between values of fine and coarse modes obtained by GARRLiC.

The imaginary part of refractive index for the case dominated by smoke (Figure

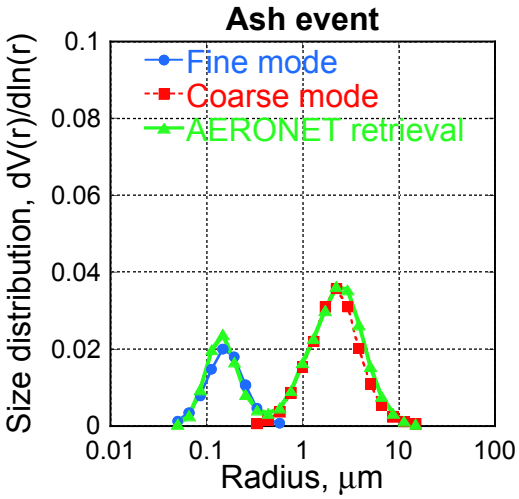

Figure 5.6: Retrieved aerosol size distribution during measurements at Lille AERONET site on 14.05.2010 (ash event).

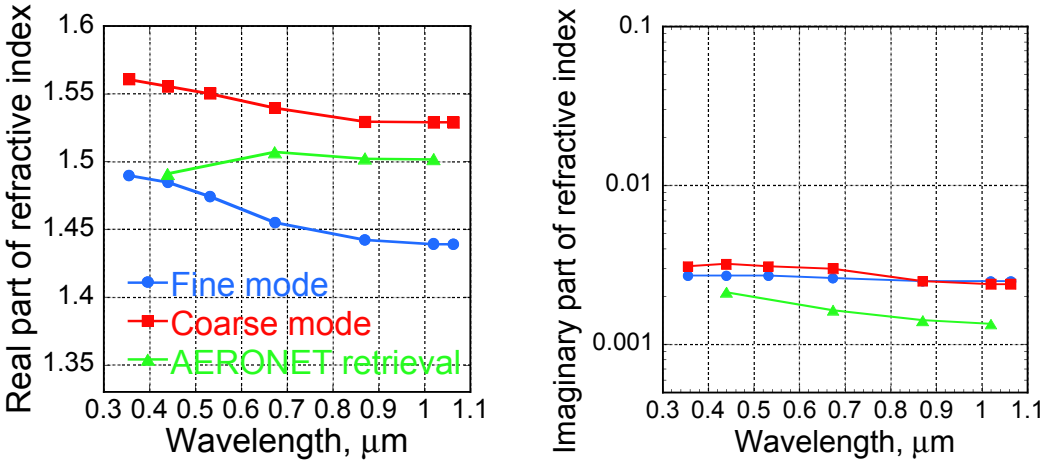

Figure 5.7: Retrieved aerosol complex refractive index during measurements at Minsk AERONET site on 02.06.2008 (dust event).

5.8) is in the range reported by observations of biomass burning (0.021 ± 0.004) (Dubovik et al., 2002a). Two trends observed in the retrievals of imaginary part of refractive indices should be outlined: high absorption of the fine particles in the dust and volcanic ash cases and very low absorption of the coarse particles for the smoke case (see right parts of Figs. 5.7 and 5.8). Such retrievals could be explained by very low optical thickness of the minor modes ($\tau_f = 0.19$ for the dust and ash cases and $\tau_c = 0.04$ for the smoke case correspondingly). As it was demonstrated by the sensitivity study described in the Chapter 4, such low contributions of the

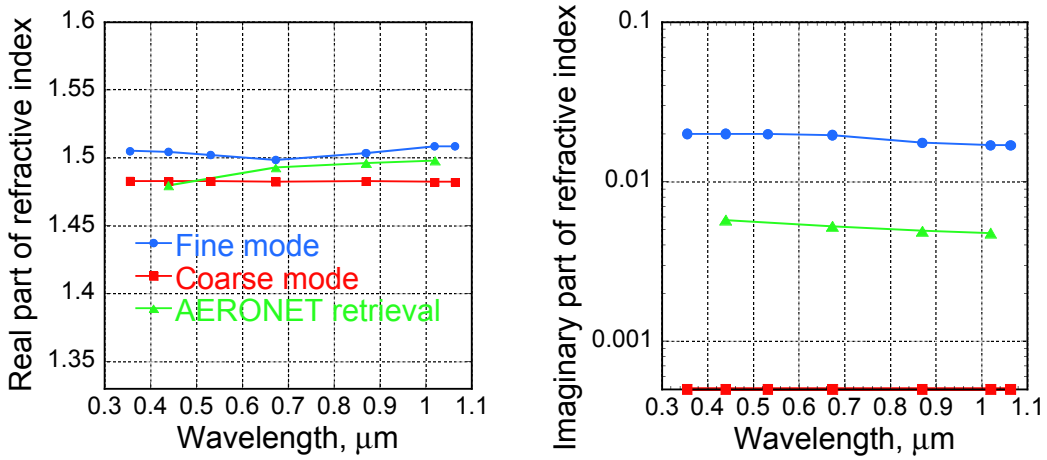

Figure 5.8: Retrieved aerosol complex refractive index during measurements at Minsk AERONET site on 13.08.2010 (smoke event).

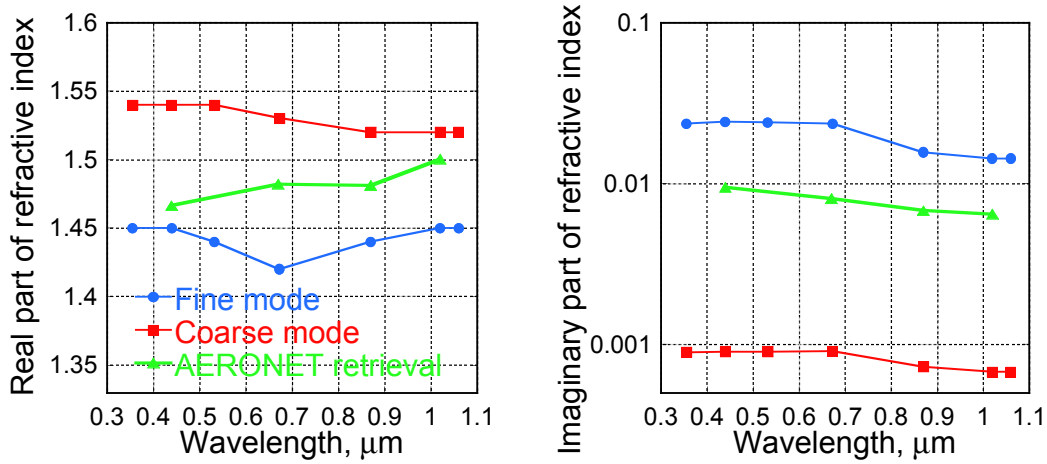

Figure 5.9: Retrieved aerosol complex refractive index during measurements at Lille AERONET site on 14.05.2010 (ash event).

minor modes could lead to high estimation errors in their complex refractive index. However, such behaviour is not the case for the measurements performed in Lille. The optical thickness of the fine mode for this case is $\tau_f = 0.16$ (with total optical thickness of 0.27) and high absorption could be explained by the presence of the background aerosols. As this site is situated within a big city it is logical to assume the presence of high absorbing industrial aerosols in the background. It also could be indicated by AERONET estimations, showing in overall high absorption of the observed aerosol in Lille (see right panel in Fig. 5.9).

The vertical distributions of fine and coarse modes (Figs. 5.10 – 5.12) clearly discriminate the vertical structure of the aerosols of different types. All the retrievals agree well with back-trajectory analysis: according to Fig. 5.1 the layer from the region of forest fires was expected at the altitude across 2 km, the layer from Sahara desert was expected around 4 km (figure 5.2) and the layer containing volcanic ash particles was expected at the altitudes around 3 km. All the profiles reflect the fine layer structure of the atmospheric aerosols, especially in the case with volcanic ash, showing a very thin and yet strong layer of coarse particles at 3 km.The retrieved profiles for smoke and volcanic ash cases indicate the presence of the background aerosols in the boundary layers (below 2 km). The vertical distribution profiles for the dust case also demonstrate sufficient amount of the coarse particle in this layer, however, despite of clear layer separation, it is impossible to guess if this is a background coarse aerosol or another layer of transported desert dust.

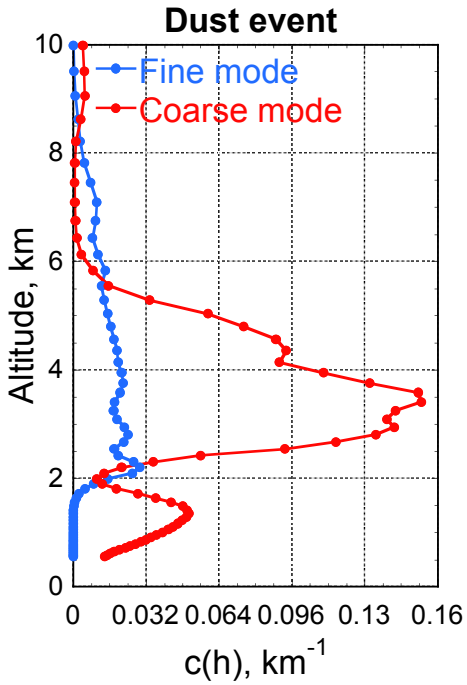

Figure 5.10: Retrieved aerosol vertical distribution during measurements at Minsk AERONET site on 02.06.2008 (dust event).

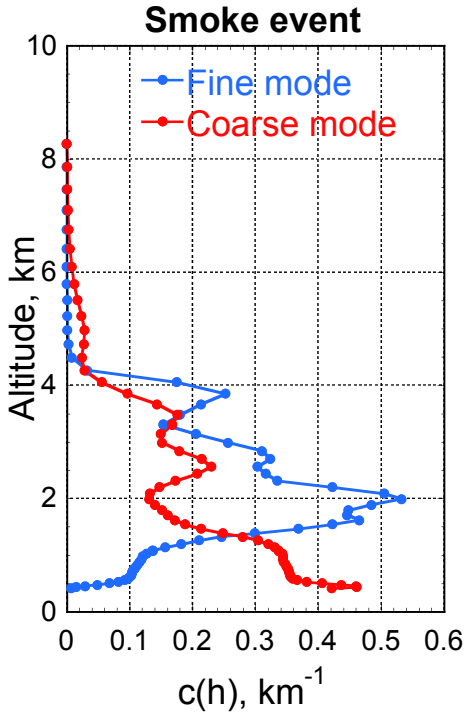

Figure 5.11: Retrieved aerosol vertical distribution during measurements at Minsk AERONET site on 13.08.2010 (smoke event).

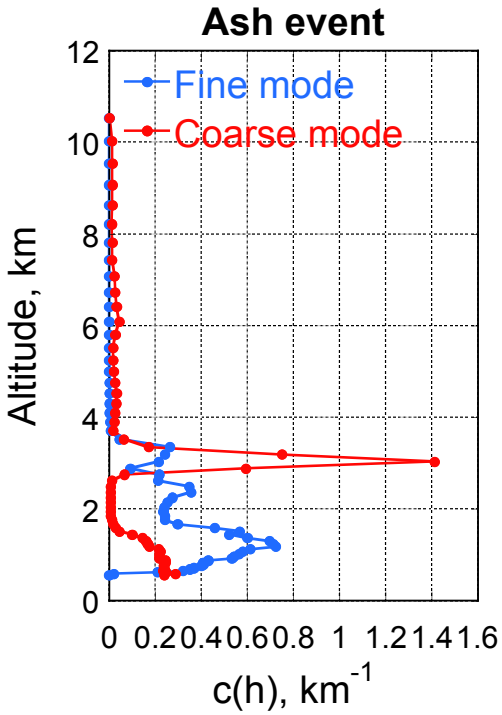

Figure 5.12: Retrieved aerosol vertical distribution during measurements at Lille AERONET site on 14.05.2010 (ash event).

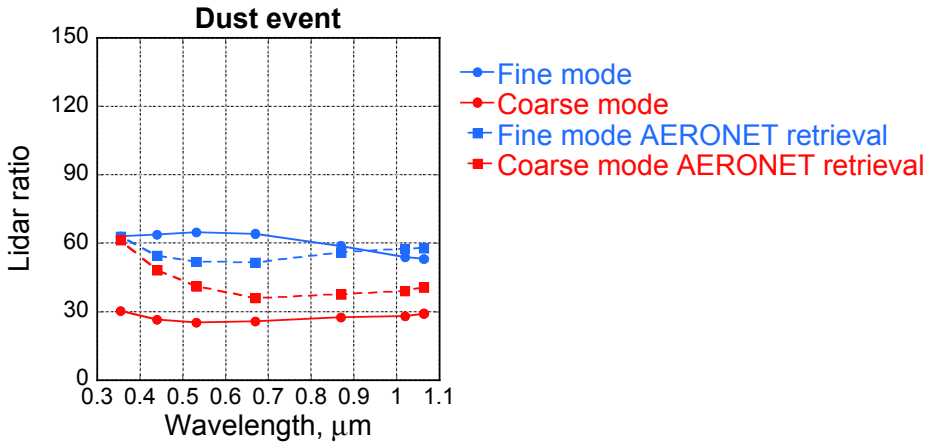

Figure 5.13: Retrieved aerosol lidar ratios during measurements at Minsk AERONET site on 02.06.2008 (dust event).

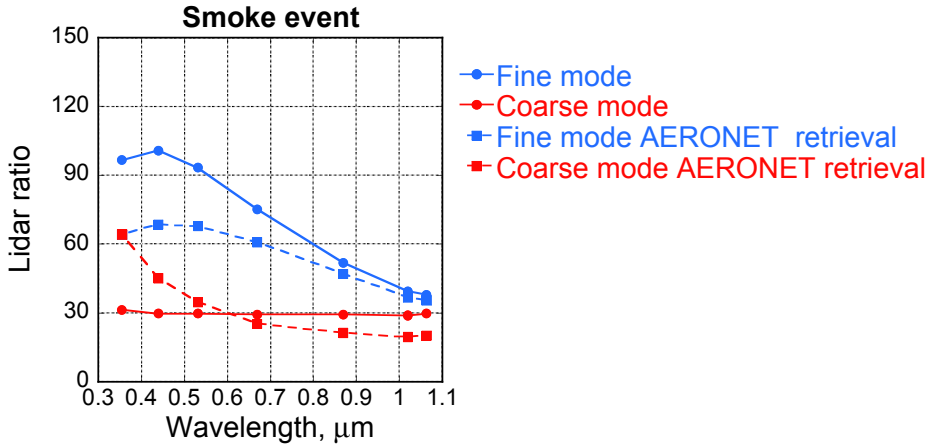

Figure 5.14: Retrieved aerosol lidar ratios during measurements at Minsk AERONET site on 13.08.2010 (smoke event).

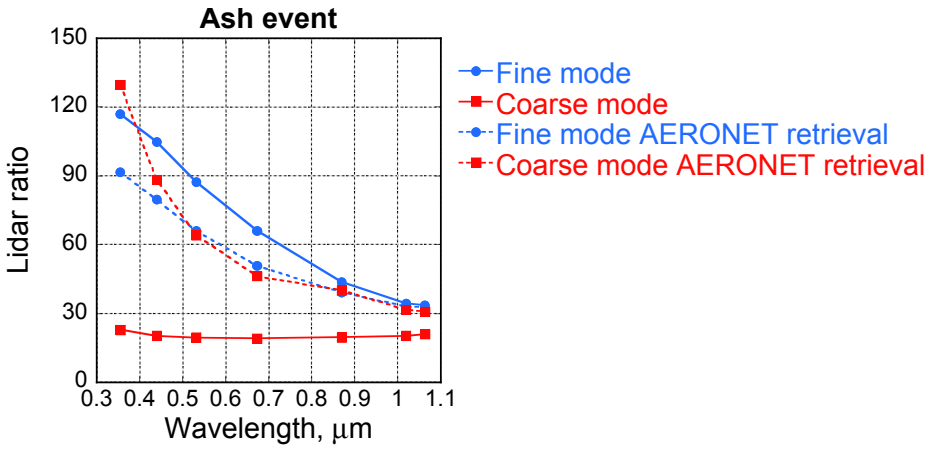

Figure 5.15: Retrieved aerosol lidar ratios during measurements at Lille AERONET site on 14.05.2010 (ash event).

Retrievals of the columnar lidar ratios are shown in Figures 5.13 – 5.15 and demonstrate notable differences between AERONET and GARRLiC values. The main differences are located at short wavelengths. These disagreements are probably caused by significant differences in sensitivities of both data sets, and by differences in assumptions. Specifically, AERONET photometer does not include observation in backscattering direction, and assumption of size independent refractive index may also result in an additional error in the lidar ratio estimation. The fraction of spherical particles retrieved for these two cases gave 40% of spherical particles for the smoke

event and 25% and 43% for the dust and volcanic ash, compared to the 99% and 2% and 43% from the corresponding AERONET retrievals. The difference for the dust and smoke cases can be explained by high sensitivity of the lidar measurements to the backscatter from non-spherical particles (Dubovik et al., 2006, see also Fig. 4.13). Another particularity of these retrievals are low values of the estimations of the lidar ratio for the coarse mode ($S_a \leq 30$) while such values are usually reported (Cattrall et al., 2005) only for maritime aerosols, whose presence could be justified only for the AERONET cite in Lille. Low values could be explained by the differences in the method of lidar ratio estimation. While lidar ratios of the aerosol types are estimated by other groups (see for e.g. Groß et al., 2011; Tesche et al., 2009, 2011; Toledano et al., 2011) including minor modes and background aerosols, GARRLiC provides this estimation only for the selected mode, disregarding the remaining part of the aerosol size distribution. In these regards vertical profiles of lidar ratio retrieved on the base of GARRLiC columnar estimations should provide more realistic values for the layers containing specified aerosol types (see Figs. 5.22 – 5.24).

Figures 5.16 – 5.18 illustrate the retrievals of columnar single-scattering albedo. Total (i.e. mixture of fine and coarse) SSA shows good agreement with AERONET retrievals. The total SSA is closer to the value of dominating aerosol mode for the retrievals of dust and smoke aerosols. This also could be explained by low contributions of the minor modes to the total optical thickness and higher absorption estimations of the dominating aerosol components.

The values of single-scattering albedo for fine mode in the smoke case and for the coarse mode in the dust case are within the ranges of estimations of this parameters (see Table 2.1, Figures 4.7 and 4.8) taken from climatological (Dubovik et al., 2002a) and observed (Toledano et al., 2011) data. Both specific spectral dependencies of smoke (lower values at longer wavelengths) and dust (bigger values at longer wavelengths) were reproduced by fine and coarse mode correspondingly in the mentioned

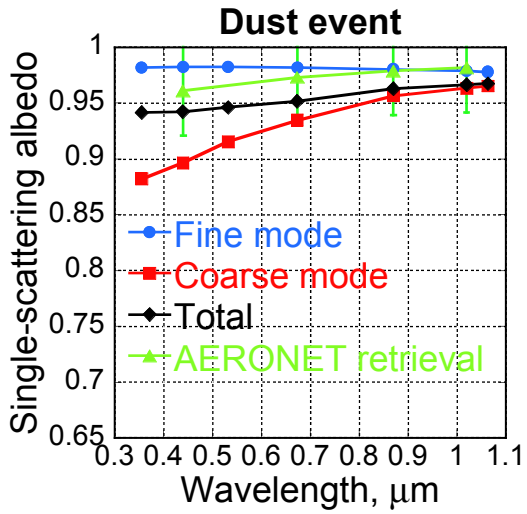

Figure 5.16: Retrieved aerosol single scattering albedo during measurements at Minsk AERONET site on 02.06.2008 (dust event).

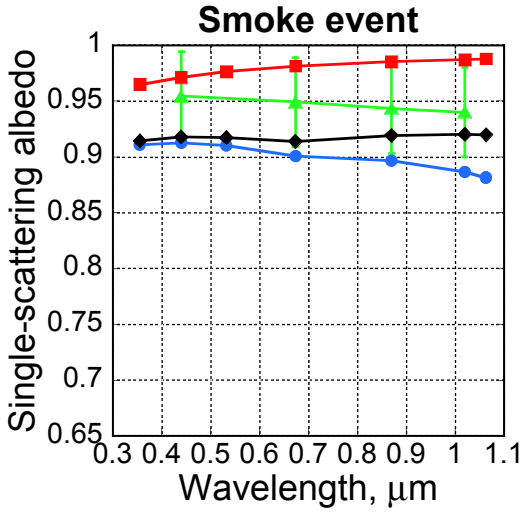

Figure 5.17: Retrieved aerosol single scattering albedo during measurements at Minsk AERONET site on 13.08.2010 (smoke event).

cases.

Figures 5.19 – 5.27 demonstrate the vertical distributions of single-scattering albedo, lidar ratios and extinction at the wavelengths of lidar measurements, calculated using retrieved parameters. All distributions have noticeable vertical structure that agrees with the retrieved vertical distributions of aerosol concentrations (Figs. 5.10 – 5.12). The values of single scattering albedo at all single layers are in the ranges of typical values for dust and smoke aerosols (e.g. Toledano et al., 2011) and close to the esti-

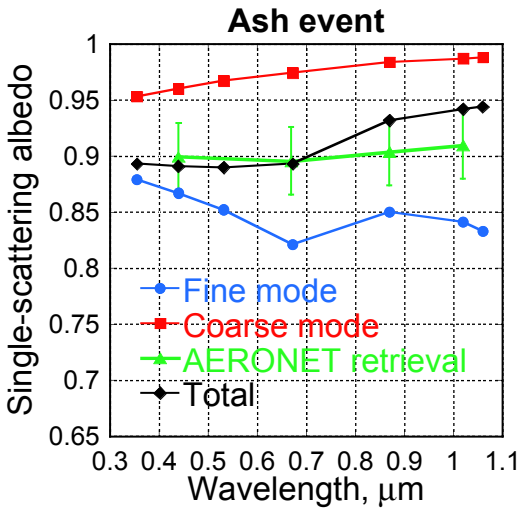

Figure 5.18: Retrieved aerosol single scattering albedo during measurements at Lille AERONET site on 14.05.2010 (ash event).

mations of this parameter for volcanic ash (e.g. Wagner et al., 2013). However, such comparison is hard to make for the case of volcanic ash outburst, because the properties of volcanic aerosols are less studied due to the irregularities in their observation (e.g. Ivanov et al., 1997, 2000).

The vertical profile of single-scattering albedo for the ash event demonstrates the opposite spectral behaviour between layers close to 3 km, and ones situated around 2 km. This has taken an effect due to the domination of different aerosol types at these altitudes (see Fig. 5.12). Lower altitudes are dominated by the fine mode which spectral behaviour of SSA mimics the one of smoke, and the upper layers are dominated by volcanic ash which shows spectral behaviour of single-scattering albedo similar to dust.

The retrieved lidar ratios are in the ranges of values for dust and smoke aerosols given by Dubovik et al. (2002a) and Cattrall et al. (2005) for the layers that are expected to contain corresponding aerosol type. This values, however, are lower than the assumptions for dust particles given by Schuster et al. (2012), Groß et al. (2011) or by Tesche et al. (2009, 2011). The lower lidar ratios in this case could have been caused by the contamination of the pure dust layers during the long range aerosol

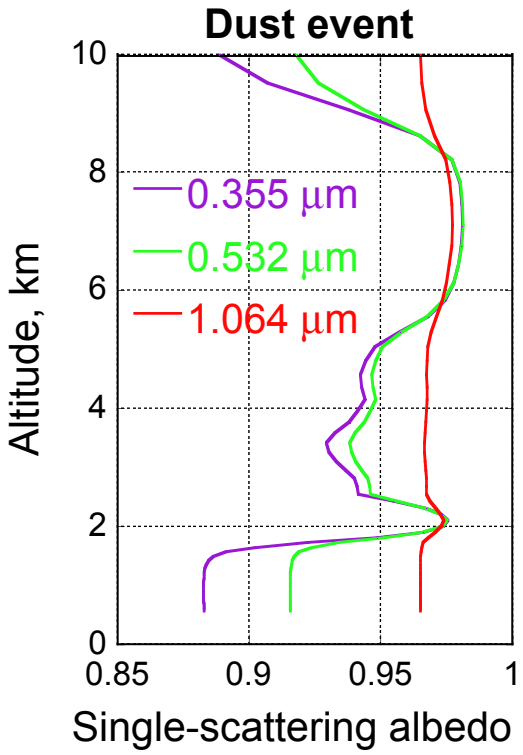

Figure 5.19: Retrieved vertical profile of aerosol single-scattering albedo during measurements at Minsk AERONET site on 02.06.2008 (dust event).

transport depicted in Figures 5.1 – 5.3. Strong spectral dependence of the smoke lidar ratio observed in Fig. 5.23 illustrates the fact that infrared light has less pronounced scattering on the smoke particles than light at the shorter wavelengths.

It should be noted, that the particular behaviour of profiles in Figs. 5.19 – 5.24 at higher altitudes could be explained by a very small amount of the aerosol present in the upper atmosphere layers and very weak signal returned from this altitude range.

Figures 5.25 – 5.27 show the retrieved vertical profiles of total extinction at 0.532 μm together with the profiles of fine and coarse mode. Figure 5.26 clearly indicates the domination of the fine mode in the total extinction at all altitudes, while according to the Fig. 5.27 coarse mode (volcanic ash) dominates only in the layer where it is disposed. Meanwhile, Fig. 5.25 demonstrates a more sophisticated distribution of contributions of fine and coarse mode to the total aerosol extinction. However, all these figures are in logical agreement with the values of columnar extinction of

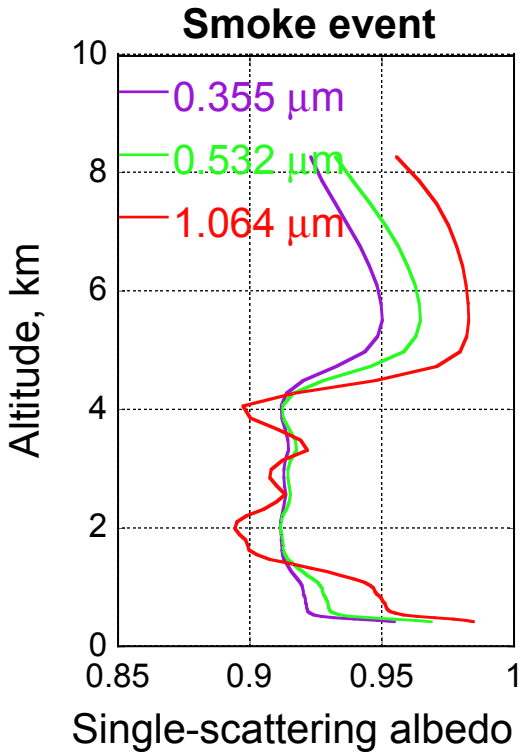

Figure 5.20: Retrieved vertical profile of aerosol single-scattering albedo during measurements at Minsk AERONET site on 13.08.2010 (smoke event).

aerosol components and vertical distribution of their concentration.

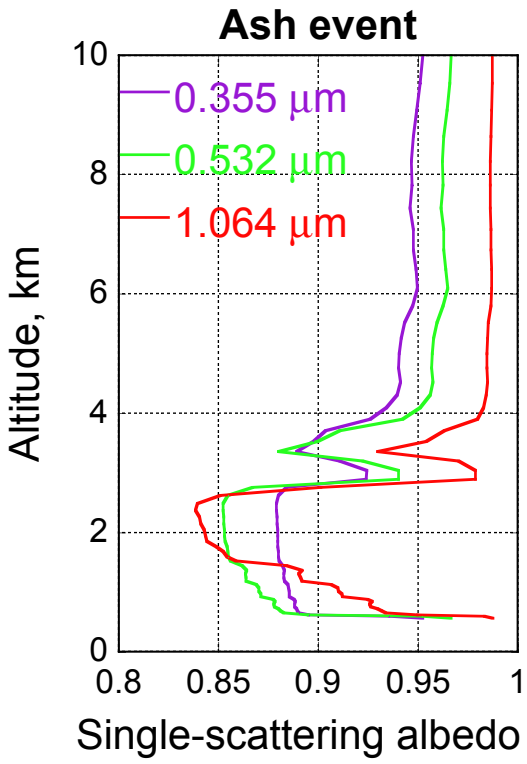

Figure 5.21: Retrieved vertical profiles of aerosol single scattering albedo during measurements at Lille AERONET site on 14.05.2010 (ash event).

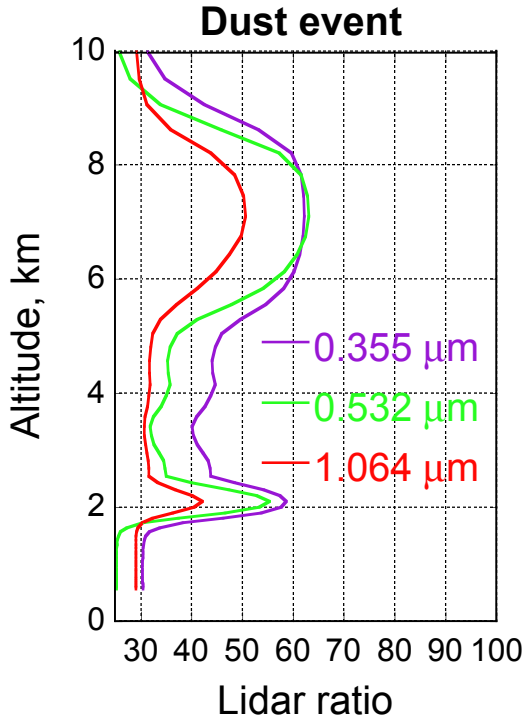

Figure 5.22: Retrieved vertical profile of aerosol lidar ratio during measurements at Minsk AERONET site on 02.06.2008 (dust event).

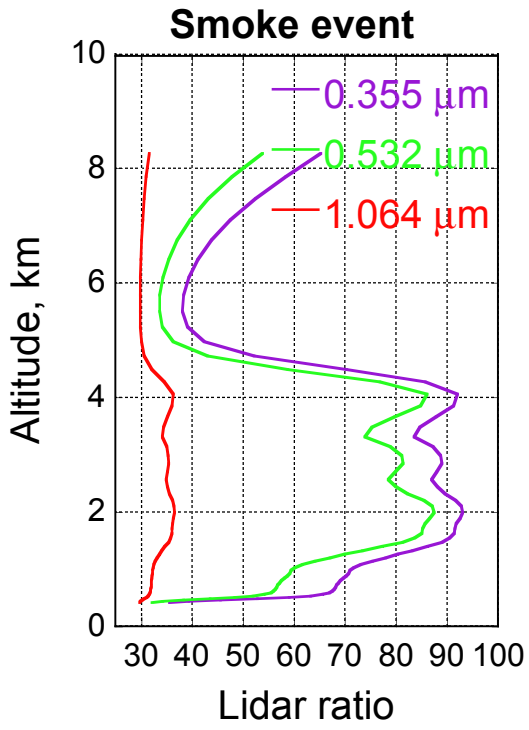

Figure 5.23: Retrieved vertical profile of aerosol lidar ratio during measurements at Minsk AERONET site on 13.08.2010 (smoke event).

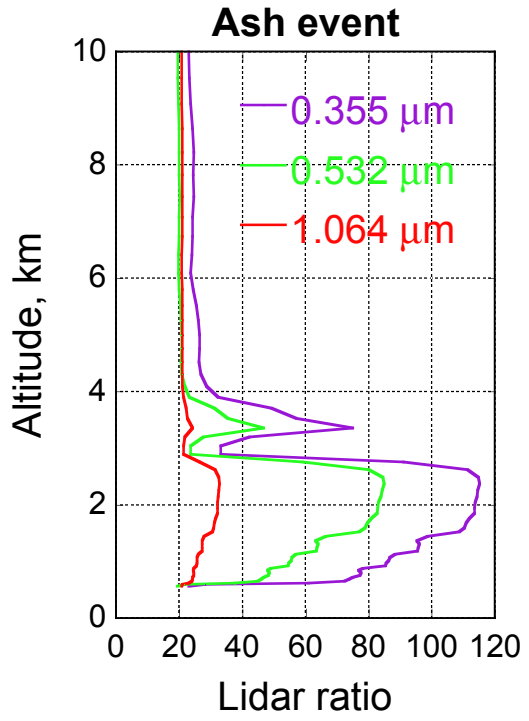

Figure 5.24: Retrieved vertical profile of aerosol lidar ratio during measurements at Lille AERONET site on 14.05.2010 (ash event).

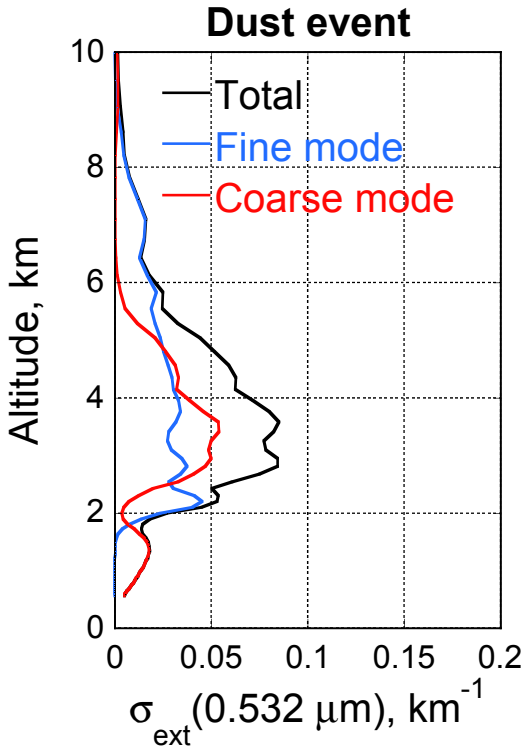

Figure 5.25: Retrieved vertical profiles of aerosol extinction during measurements at Minsk AERONET site 02.06.2008 (dust event).

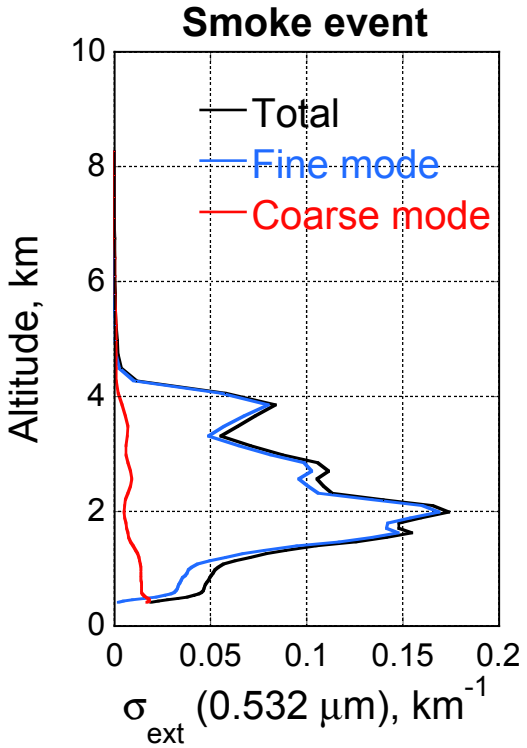

Figure 5.26: Retrieved vertical profiles of aerosol extinction during measurements at Minsk AERONET site on 13.08.2010 (smoke event).

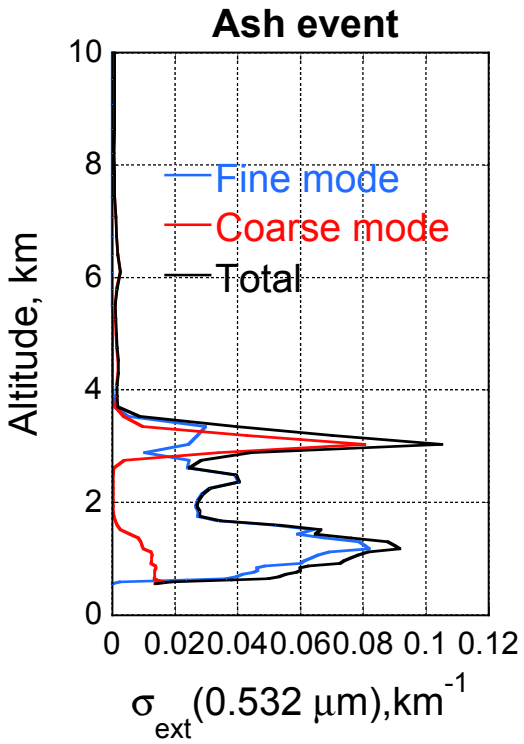

Figure 5.27: Retrieved vertical profiles of aerosol extinction during measurements at Lille AERONET site on 14.05.2010 (ash event).

Figures 5.28 – 5.30 are aimed to demonstrate the consistency between the LiRIC and GARRLiC retrievals in different cases, including cases where no differences are expected. Both algorithms provide two distinct vertical concentration profiles for different aerosol components and the comparison of profiles retrieved by GARRLiC and LiRIC was made. The main difference is that GARRLiC modifies the retrieved columnar properties of aerosol. In addition, GARRLiC uses bi-component aerosol model that may have different complex refractive indices. This assumption affects the estimations of lidar ratios for each mode and therefore the retrieved vertical profiles. Therefore, the demonstration of LiRIC and GARRLiC codes consistency has been performed using the case with small difference in complex refractive indices of fine and coarse aerosol modes (smoke event, see Fig. 5.8), for the case with small difference in columnar lidar ratio estimations (dust event, see Fig. 5.13) and for the case with sufficient difference in columnar aerosol parameters of fine and coarse modes (ash event, see Figs. 5.9 and 5.15).

Figures 5.28 – 5.30 show vertical distributions retrieved by the GARRLiC compared with the results of LiRIC inversion (Chaikovsky et al., 2012) all normalized and made for the same measurements set. Both retrieved profiles show good agreement for the dust and smoke cases. The minor differences could be explained by smaller amount of altitude layers in the GARRLiC retrieval and small disagreements in lidar ratios estimations for both modes. Therefore, for the situations when the usage of the same values of complex refractive index for both aerosol modes could be justified, these two methods should provide similar results, demonstrating the succession of the newer method. On the contrary, in less favourable situation AERONET estimates of lidar ratio can show more significant deviations (Fig. 5.15), affecting the retrievals of vertical concentration profiles more drastically (see. Fig. 5.30).

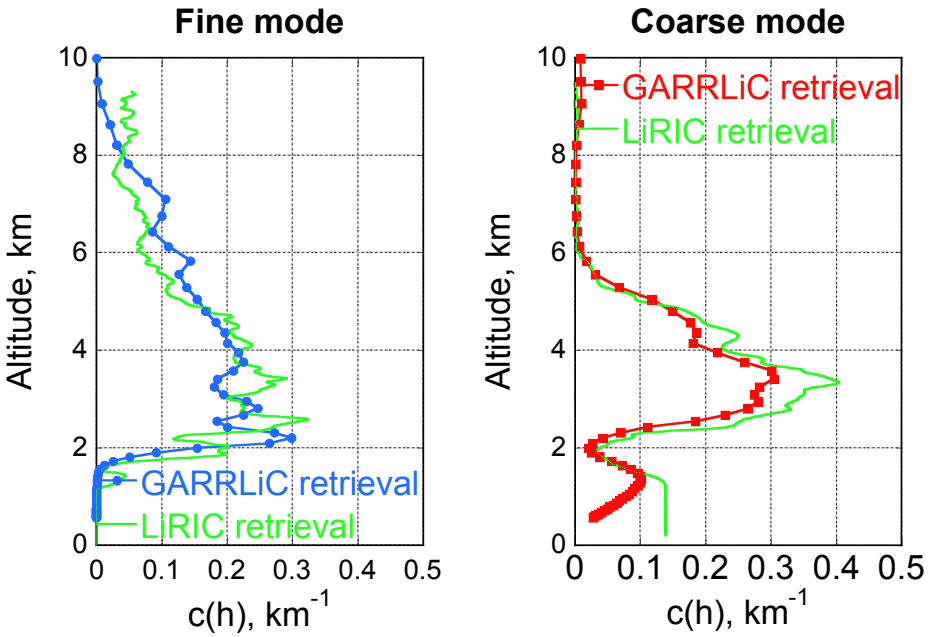

Figure 5.28: Comparison of vertical profiles retrieved by GARRLiC and LiRIC inversions for the measurements performed at Minsk AERONET site on 02.06.2008 (dust event).

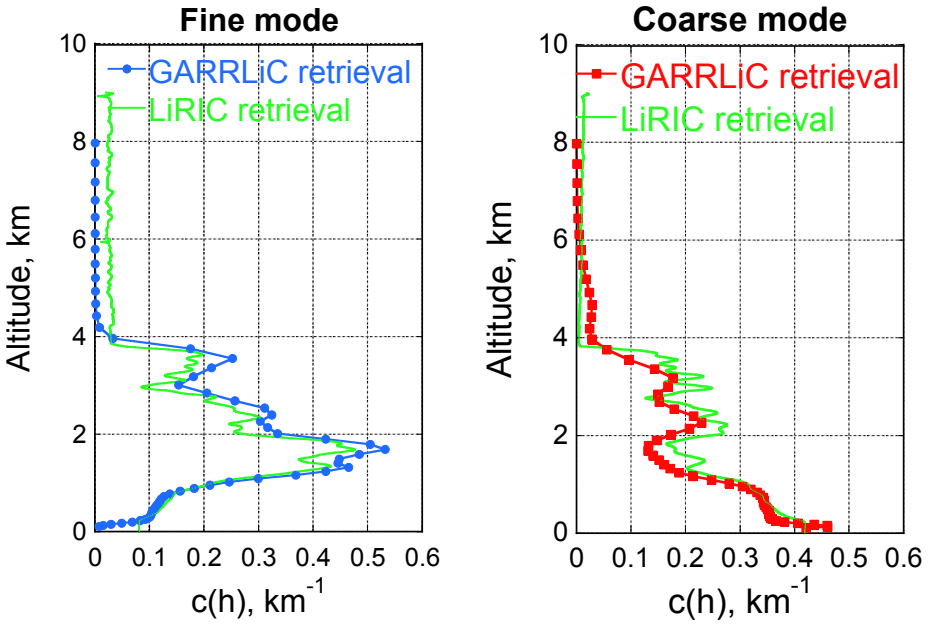

Figure 5.29: Comparison of vertical profiles retrieved by GARRLiC and LiRIC inversions for the measurements performed at Minsk AERONET site on 13.08.2010 (smoke event).

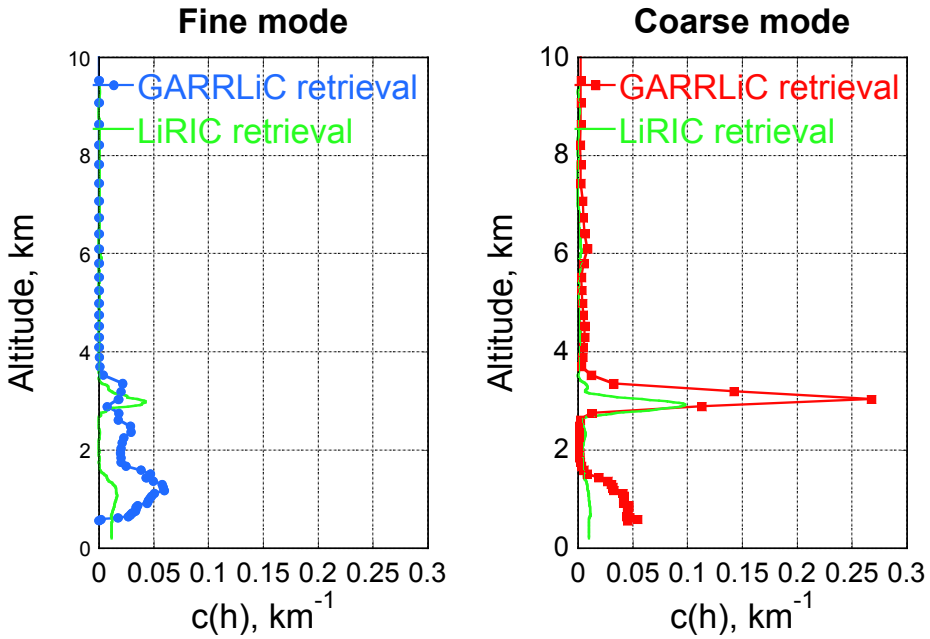

Figure 5.30: Comparison of vertical profiles retrieved by GARRLiC and LiRIC inversions for the measurements performed at Lille AERONET site on 14.05.2010 (ash event).

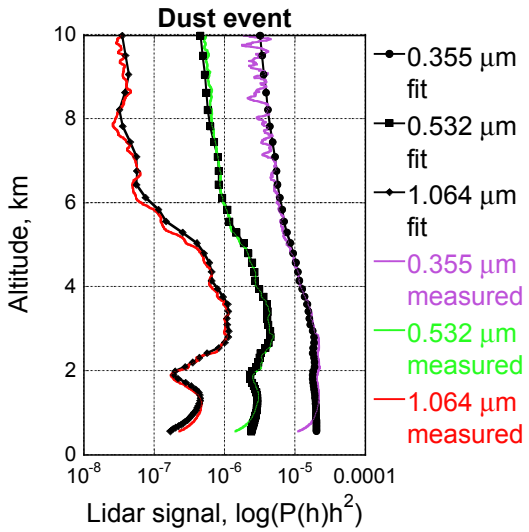

Figure 5.31: Achieved lidar measurements fits for the observations performed at Minsk AERONET site on 02.06.2008 (dust event).

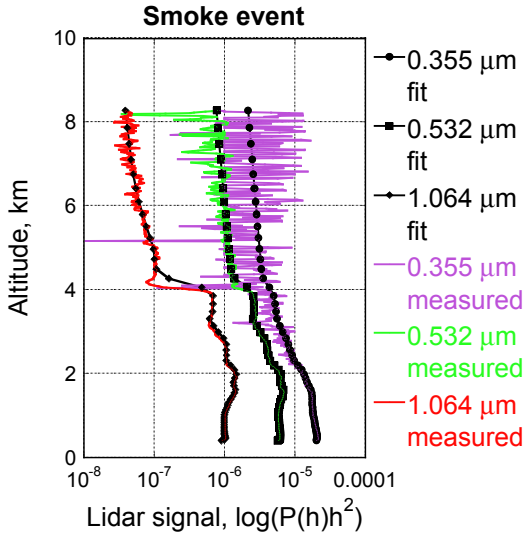

Figure 5.32: Achieved lidar measurements fits for the observations performed at Minsk AERONET site on 13.08.2010 (smoke event).

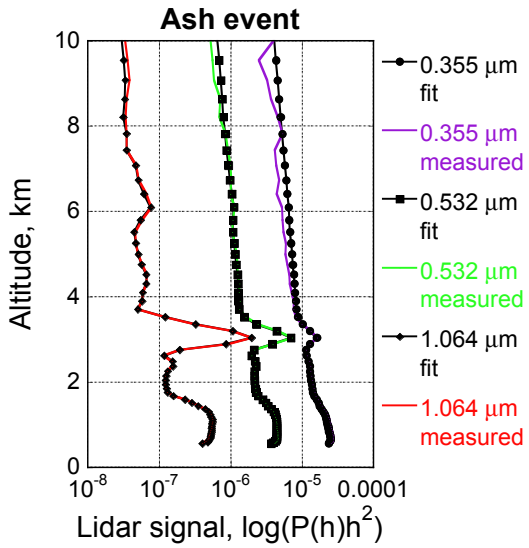

Figure 5.33: Achieved lidar measurements fits for the observations performed at Lille AERONET site on 14.05.2010 (ash event).

In Figures 5.31 – 5.33 lidar measurements fits achieved during GARRLiC inversions are presented. Since both measurements were made with different duration, the noise at higher altitudes is much stronger in the case with smoke observations due to the smaller accumulation of the lidar signal (see Fig. 5.32). The use of lidar measurements down-sampling and applying of additional smoothness constrains allowed us to diminish the influence of high noise and stabilize the retrievals in the presence of random noise. The misfits at shorter wavelengths that could be observed at lower altitudes in the part of Figure 5.31 referring to the dust observation are caused by the overlap of the receiver and emitter of the lidar system.

Thus, the results of GARRLiC application to the real data and their comparisons with AERONET and LiRIC retrieval results showed an encouraging agreement for both columnar and vertical properties of aerosol. At the same time, the GARRLiC retrieval differentiates between columnar optical properties of fine and coarse modes of aerosol, relying on additional information contained in lidar observations.

Chapter 6

Conclusion

> The future always looks differently
> than we can imagine it.
>
> Stanislaw Lem

This thesis has discussed in detail a concept of enhanced remote sensing of atmospheric aerosol by joint inversion of active and passive remote sensing observations. The approach proposed in this work takes advantage from all sensitivities in lidar and radiometric data to both vertical and columnar aerosol properties. The retrieval is designed as simultaneous fitting of both lidar and radiometer data by a single set of aerosol parameters describing both vertical and columnar properties of aerosol. The new concept of the algorithm is aimed to achieve higher accuracy of the retrieval, since in such an approach the solution usually relying only on passive measurement of the radiometer is benefiting from information contained in coincident active observations by lidar and method uses a smaller number of assumptions about aerosol.

The chapter 3 provides detailed description of the full set of formulations necessary for realizing a new GARRLiC algorithm developed for deriving detailed properties of two atmospheric aerosol components from coincident lidar and photometric measurements.

A unified aerosol model suitable for description of both columnar and vertical vari-

ability of aerosol optical properties was developed. This model utilizes the positive heritage of the aerosol modelling achieved in the previous studies. It is simple (in terms of quantity of parameters used to describe the model and ease of their interpretation) and applicable for use with large variety of available remote sensing instruments.

The GARRLiC algorithm was developed using the heritage of the AERONET, PARASOL and LiRIC algorithms. It is designed to invert the co-incident observations of CIMEL sun/sky photometer that registers direct and scattered atmospheric radiation at four wavelengths in up to 35 directions and multi-wavelength elastic lidar that registers backscattered radiation at three wavelength in up to 1000 altitude layers. In a contrast to the majority of existing aerosol retrieval algorithms, the one used in this work is one of the first attempts to develop an aerosol retrieval using statistically optimized multi-variable fitting of multi-instrumental data. The inversion is designed as a search for the best fit of the multi-source measurements and a priori constraints on aerosol characteristics through the continuous space of all possible solutions under statistically formulated criteria and allows harmonious utilization not only of a priori estimate term, but also a priori terms limiting derivatives of the solution. The algorithm derives an extended set of parameters for both columnar and vertical aerosol properties, including aerosol sizes, shape, spectral complex refractive index for both fine and coarse aerosol modes, as well as vertical profiles of mode's concentrations.

The generality of the approach to modelling of aerosol columnar and vertically resolved properties, combined with modular organization of the retrieval algorithm provides comprehensible and accessible instrumentation for the development of advanced multi-instrumental aerosol retrievals. This approach is not only limited to the ground-based instruments and could be used for retrievals from all possible combinations of existing remote sensing instruments including space-borne and airborne instruments, radiometric and polarimetric multi-spectral and multi-angular observa-

tions, both passive and active.

In the Chapter 4 the performance of the developed algorithm has been demonstrated by application to synthetically generated coincident sun photometer and lidar observations. First, a series of sensitivity tests were conducted by applying the algorithm to the synthetic sun photometer and lidar observations for the cases of aerosol mixtures containing desert dust with urban pollution and biomass-burning aerosols. The simulations were designed to mimic observations of real aerosol. With this purpose, the aerosol models derived from AERONET observations in Solar Village (Saudi Arabia), Mongu (Zambia) and GSFC (Greenbelt, USA) were used to generate synthetic proxy measurements, both photometric and lidar. The data were perturbed by random noise before applying the retrieval algorithm. The results of the tests showed that the complete set of aerosol parameters for each aerosol component can be robustly derived with acceptable accuracy in all considered situations. Dependence of the accuracy of aerosol parameter estimations on AOT and on the presence of the random noise were demonstrated. The presence of random noise in the measurements has more drastic effect on inversions performed at low optical thicknesses, causing higher errors in aerosol parameter estimations. Lower sensitivity to the microphysical parameters of the fine particles unrelated to the presence of random noise was found. It was most noticeable in the retrievals of the real part of refractive index.

Improvements that are introduced into aerosol retrievals by inclusion of lidar measurements and passive polarimetric measurements in almucantar configuration were demonstrated. Inclusion of lidar measurements despite of introducing vertical profiles of aerosol concentration also positively affected accuracy of the lidar ratio retrievals of the non-dominating modes. Accounting for polarization data most noticeably improved the retrievals of complex refractive index of the fine aerosol mode, thus positively affecting the retrievals of other fine mode parameters and providing more distinct differentiation of the properties of aerosol components.

Chapter 5 describes the GARRLiC algorithm application to coincident lidar and sun-photometer observations performed at Minsk (Belarus) and Lille (France) AERONET sites. The comparison of the derived aerosol properties with available observations by AERONET ground-based sun/sky-radiometers indicated encouraging consistency of microphysical parameters of aerosol components derived from joint inversion with those obtained by AERONET retrieval. Analysis of the retrieval of vertical aerosol properties by GARRLiC and LiRIC algorithm has shown good accordance for the situations when both aerosol components, fine and coarse, have close optical properties (complex refractive index and lidar ratio in particular). For the cases with significant difference in the optical properties of aerosol components GARRLiC provides more accurate retrievals, extracting from the same set of the measurements additional information on refractive indices of aerosol modes.

More comprehensive studies for testing and tuning the developed algorithm including accounting for polarization effects of sun photometer and lidar observations are planned in future efforts. Such important aspects of algorithm implementation as co-incident measurements requirements are to be addressed in the follow-on studies.

Outline

- Performing additional sensitivity study on lidar ratio retrievals.
- Application of the GARRLiC to more cases of real coincident lidar/sun-photometer aerosol observations over different sites.
- Implementation of the retrieval procedure to the EARLINET observations.
- Expand the list of possible measurements used in the GARRLiC retrieval with depolarization measurements by elastic lidars and inelastic measurements performed by Raman lidars.

- Apply algorithm concept to a space-borne remote sensing systems like PARASOL and CALIPSO.

Bibliography

Standard Atmosphere, ISO 2533:1975, International Organization for Standardization, 1975.

U.S. Standard Atmosphere, 1976, U.S. Government Printing Office, Washington, D.C., 1976.

Manual of the ICAO Standard Atmosphere (extended to 80 kilometres (262 500 feet)), vol. Doc 7488-CD, International Civil Aviation Organization, third edn., 1993.

CALIOP Algorithm Theoretical Basis Document, Calibration and Level 1 Data Products, PC-SCI-201, release 1.0 edn., 2006.

Ackerman, A. S., Toon, O. B., Stevens, D. E., Heymsfield, A. J., Ramanathan, V., and Welton, E. J.: Reduction of tropical cloudiness by soot, Science, 288, 1042, 2000.

Adams, P., Seinfeld, J., and Koch, D.: Global concentrations of tropospheric sulphate, nitrate and ammonium aerosol simulated in a general circulation model, Journal of Geophysical Research, 104, 13 791–13 823, 1999.

Albrecht, B. A.: Aerosols, Cloud Microphysics, and Fractional Cloudiness, Science, 245, 1227, 1989.

Althausen, D., Engelmann, R., Baars, H., Heese, B., Ansmann, A., and Müller, D.: Portable Raman Lidar PollyXT for Automated Profiling of Aerosol Backscatter, Extinction, and Depolarization, Journal of Atmospheric and Oceanic Technology, 26, 2366–2378, 2009.

Andreae, M. O., Rosenfeld, D., Artaxo, P., Costa, A. A., Frank, G. P., Longo, K. M., and Silvas-Dias, M. A. F.: Smoking rain clouds over the amazon, Science, 303, 1337–1342, 2004.

Ansmann, A., Riebersell, M., Wandinger, U., Weitkamp, C., Lahmann, E. V. W., and Michaelis, W.: Combined raman-elastic lidar for vertical profiling of moisture, aerosols extinction, backscatter and lidar ratio, Applied Optics, 18, 1992.

Ansmann, A., Wandinger, U., Wiedensohler, A., and Leiterer, U.: Lindenberg Aerosol Characterization Experiment 1998 (LACE 98): Overview, Journal of Geophysical

Research: Atmospheres, 107, LAC 11–1–LAC 11–12, doi:10.1029/2000JD000233, URL http://dx.doi.org/10.1029/2000JD000233, 2002.

Ansmann, A., Tesche, M., Groß, S., Freudenthaler, V., Seifert, P., Hiebsch, A., Schmidt, J., Wandinger, U., Mattis, I., Müller, D., and Wiegner, M.: The 16 April 2010 major volcanic ash plume over central Europe: EARLINET lidar and AERONET photometer observations at Leipzig and Munich, Germany, Geophysical Research Letters, 37, 2010.

Ansmann, A., Tesche, M., Seifert, P., Groß, S., Freudenthaler, V., Apituley, A., Wilson, K. M., Serikov, I., Linné, H., Heinold, B., Hiebsch, A., Schnell, F., Schmidt, J., Mattis, I., Wandinger, U., and Wiegner, M.: Ash and fine mode particle mass profiles from EARLINET/AERONET observations over central Europe after the eruptions of the Eyjafjallajökull volcano in 2010, Journal of Geophysical Research, 116, 2011.

Antuña, J., Andrade, M., Landulfo, E., Clemesha, B., Quel, E., and Bastidas, A.: Building a Lidar Network in Latin America: Progress and Difficulties, in 23rd International Laser Radar Conference, Nara, Japan, July 24-28, 2006.

Baars, H., Althausen, D., Engelmann, R., Ansmann, A., Müller, D., Artaxo, P., Pauliquevis, T., Souza, R., and Martin, S. T.: Automated Raman lidar measurements in the Amazon rain forest during the wet and dry season 2008, in: Proceedings of the 8th International Symposium on Tropospheric Profiling, edited by Apituley, A., Russchenberg, H., and Monna, W., vol. S04, pp. 1–4, 2009.

Bates, T., Huebert, B., Gras, J., Griffiths, F., and Durkee, P.: The International Global Atmospheric Chemistry (IGAC) Project's First Aerosol Characterization Experiment (ACE-1)–Overview, Journal of Geophysical Research, 103, 16 297–16 318, 1998.

Bates, T., Quinn, P., Coffman, D., Johnson, J., Miller, T., Covert, D., Wiedensohler, A., Leinert, S., Nowak, A., and Neusüb, C.: Regional physical and chemical properties of the marine boundary layer aerosol across the Atlantic during Aerosols99: An overview, Journal of Geophysical Research, 106, 20 767–20 782, 2001.

Bevington, P. R.: Data Reduction and Error Analysis for the Physical Sciences, McGraw-Hill, 1969.

Böckmann, C., Wandinger, U., Ansmann, A., Bösenberg, J., Amiridis, V., Boselli, A., Delaval, A., De Tomasi, F., Frioud, M., Grigorov, I., Hågård, A., Horvat, M., Iarlori, M., Komguem, L., Kreipl, S., Larchevèque, G., Matthias, V., Papayannis, A., Pappalardo, G., Rocadenbosch, F., Rodrigues, J., Schneider, J., Shcherbakov, V. N., and Wiegner, M.: Aerosol Lidar Intercomparison in the Framework of the EARLINET Project. 2. Aerosol Backscatter Algorithms, Applied Optics, 43, 977–989, 2004.

Bohren, C. and Huffman, D.: Absorption and Scattering of Light by Small Particles, Wiley-VCH Verlag GmbH and Co. KGaA, 1983.

Bösenberg, J.: EARLINET-A European Aerosol Research Lidar Network, Advances in Laser Remote sensing, in: Selected papers 20th Int. Laser Radar Conference (ILRC), Vichi, France, 10-14 July 2000, pp. 155–158, 2000.

Bösenberg, J. and et al.: EARLINET-A European Aerosol Research Lidar Network, in: Advances in Laser Remote sensing, Selected papers 20th Int. Laser Radar Conference (ILRC), pp. 155–158, Vichi, France, 2000.

Bösenberg, J. and Hoff, R.: Plan for the implementation of the GAW Aerosol Lidar Observation Network GALION, WMO/TD-No. 1443 178, GAW, 2007.

Boucher, O.: Air traffic may increase cirrus cloudiness, Nature, 397, 30–31, 1999.

Bréon, F.-M.: How Do Aerosols Affects Cloudiness and Climate?, Science, 313, 623–624, doi:10.1126/science.1131668, 2006.

Bréon, F.-M., Buriez, J. C., Couvert, P., Deschamps, P. Y., Deuzé, J.-L., Herman, M., Goloub, P., Leroy, M., Lifermann, A., Moulin, C., Parol, F., Seze, G., Tanré, D., Vanbauce, C., and Vesperini, M.: Scientific results from the POLarization and Directionality of the Earth's Reflectances (POLDER), Advances in Space Research, 30, 2383–2386, 2002.

Burton, S. P., Ferrare, R. A., Hostetler, C. A., Hair, J. W., Rogers, R. R., Obland, M. D., Butler, C. F., Cook, A. L., Harper, D. B., and Froyd, K. D.: Aerosol classification using airborne High Spectral Resolution Lidar measurements – methodology and examples, Atmospheric Measurement Techniques, 5, 73–98, doi:10.5194/amt-5-73-2012, URL http://www.atmos-meas-tech.net/5/73/2012/, 2012.

Cairns, B., Waquet, F., Knobelspiesse, K., Chowdhary, J., and Deuzé, J.-L.: Satellite Aerosol Remote Sensing over Land, chap. Polarimetric remote sensing of aerosols over land surfaces, pp. 295–325, Springer-Praxis Books in Environmental Sciences, 2009.

Cattrall, C., Reagan, J., Thome, K., and Dubovik, O.: Variability of aerosol and spectral lidar and ectinction raios of key aerosol types derived from selected Aerosol Robotic network locations, Journal of Geophysical Research, 110, 2005.

Chaikovsky, A., Dubovik, O., Holben, B. N., and Bril, A. I.: Methodology to retrieve atmospheric aerosol parameters by combining ground-based measurements of multi-wavelength lidar and sun sky-scanning radiometer, in: Proceeding of Eight International Symposium on Atmospheric and Ocean and Ocean Optics: Atmospheric Physics, edited by Zherebtsov, G. A., Matvienko, G. G., Banakh, V. A., and Koshelev, V. V., vol. 4678, SPIE, 2002a.

Chaikovsky, A., Dubovik, O., Holben, D., Bril, A., and Barun, V.: Retriving atmospheric aerosol parameters on the base of multiwavelength lidar and sun sky-scanning radiometer data, in: Reviewed and revised papers at the twenty-first International Laser radar Conference (ILRC21) Quebec, Canada, 8-12 July 2002, pp. 593–594, 2002b.

Chaikovsky, A., Bril, A., Dubovik, O., Holben, B., Thompson, A., Goloub, P., O'Neill, N., Sobolewski, P., Bösenberg, J., Ansmann, A., Wandinger, U., and Mattis, I.: CIMEL and multiwavelength lidar measurements for troposphere aerosol altitude distributions investigation, long-range transfer monitoring and regional ecological problems solution: field validation of retrieval techniques, Óptica Pura y Aplicada, 37, 3241–3246, 2004.

Chaikovsky, A., Bril, A., Denisov, S., and Balashevich, N.: Algorithms and software for lidar data processing in CIS-LiNet, in: Reviewed and Revised Papers Presented at the 23rd International Laser radar Conference, 24 - 28 July 2006, Nara, Japan, edited by Chikao Nagasava, N. S., pp. 667–670, 2006a.

Chaikovsky, A., Ivanov, A., Korol, M., Slesar, A., S., D., Osipenko, F., Hutko, I., Dubovik, O., Holben, B., and Goloub, P.: Atmospheric participate matter variability in an industrial center from multi-wavelength lidar and Sun-sky radiometer measurements, Proceedings of SPIE, 6160, 2006b.

Chaikovsky, A., Dubovik, O., Goloub, P., Tanré, D., Chaikovskaya, L., Denisov, S., Grudo, Y., Lopatsin, A., Karol, Y., Lapyonok, T., Korol, M., Osipenko, F., Savitski, D., and Slesar, A.: Combined lidar and radiometric sounding of atmospheric aerosol: algorithm of data processing, software, dessimination, in: Proceedings of XVIII International symposium "Atmospheric and ocean optics. Atmosphere physics ", Irkutsk, Russian Federation, 2—6 July, pp. C1–C4, 2012.

Charlson, R. J., Schwartz, S. E., Hales, J. M., Cess, R. D., Coakley, J. A., Hansen, J. E., and Hofmann, D. J.: Aerosols and global warming response, Science, 256, 598–599, 1992.

Chin, M.: Atmospheric Aerosol Properties and Climate Impacts, Tech. rep., U.S. Climate Change Science Program Synthesis and Assessment Product 2.3, 2009.

Comeron, A., Rocadenbosch, F., Lopez, M. A., Rodrguez, A., Munoz, C., Garcia-Vizcano, D., and Sicard, M.: Effects of noise on lidar data inversion with the backward algorithm, Applied Optics, 43, 2572–2577, 2004.

Costa, M., Levizzani, V., and Silva, A. M.: Part II: Aerosol characterization and direct radiative forcing assessment over the ocean: Application to test cases and validation, Journal of Applied Meteorology, 43, 1818–1833, 2004.

Cuesta, J., Flamant, H. P., and Flamant, C.: Synergetic technique combining elastic backscatter lidar data and sunphotometer AERONET inversion for retrieval by

layer of aerosol optical and microphysical properties, Applied Optics, 47, 4598–4611, 2008.

D'Almeida, G. A., Koepke, P., and Shettle, E. P.: Atmospheric Aerosols: Global Climatology and Radiative Characteristics, p. 561, A Deepak Pub, 1991.

Deering, D. and Leone, P.: A sphere-scanning radiometer for rapid directional mesurements of sky and ground reflectance, Remote Sensing of Environment, 19, 1–24, 1986.

Denisov, S., Chaikovsky, A., Bril, A., and Balashevich, N.: Integrated software for lidar data processing, in: Proceedings Of International Workshop ISTC "Baikal 2006", Monitoring of large-scale atmosphere changes in CIS regions: co-operation of the international measuring networks AERONET, EARLINET, AD-Net, NDSC, as well as scientific groups in CIS, August, 15 –19, 2006, Irkutsk, Russia, pp. 41–43, 2006.

Derimian, Y., Leon, J.-F., Dubovik, O., Chiapello, I., Tanré, D., Sinyuk, A., Auriol, F., Podvin, T., Brogniez, G., and Holben, B. N.: Radiative properties of aerosol mixture observed during the dry season 2006 over M'Bour, Senegal (African Monsoon Multidisciplinary Analysis campaign), Journal of Geophysical Research, 113, doi:10.1029/2008JD009904, 2008.

Deuzé, J.-L., Bréon, F.-M., Devaux, C., Goloub, P., Herman, M., Lafrance, B., Maignan, F., Marchand, A., Perry, G., and Tanré, D.: Remote Sensing of aerosols over land surfaces from POLDER/ADEOS-1 polarized measurements, Journal of Geophysical Research, 106, 4913–4926, 2001.

Dockery, D. W., Speizer, F. E., Stram, D. O., Ware, J. H., Spengler, J. D., and Ferris, B. G.: Effects of Inhalable Particles on Respiratory Health of Children, American Review of Respiratory Disease, 139, 587–594, 1989.

Dockery, D. W., Pope, C. A., Xu, X. P., Spengler, J. D., Ware, J. H., Fay, M. E., Ferris, B. G., and Speizer, F. E.: An Association between Air-Pollution and Mortality in 6 United States Cities, New England Journal of Medicine, 329, 1753–1759, 1993.

Doicu, A.: Numerical Regularization for Atmospheric Inverse Problems, Springer, Berlin, 2010.

Draine, B. T. and Flatau, P. J.: Discrete-dipole approximation for scattering calculations, Journal of the Optical Society of America, 11, 1491–1499, doi:10.1364/JOSAA.11.001491, URL `http://josaa.osa.org/abstract.cfm?URI=josaa-11-4-1491`, 1994.

Dubovik, O.: Optimization of Numerical Inversion in Photopolarimetric Remote Sensing, in: Photopolarimetry in Remote Sensing, edited by Videen, G. nad Yatskiv, Y. and Mishchenko, M., pp. 65–106, Kluwer Academic Publishers, Dordrecht, The Netherlands, 2004.

Dubovik, O. and King, M.: A flexible inversion algorithm for retrieval of aerosol optical propierties from Sun and sky radiance measurements, Journal of Geophysical Research, 105, 20 673–20 696, 2000.

Dubovik, O., Lapyonok, T., and Oshchepkov, S.: Improved technique for data inversion: optical sizing of multicomponent aerosols, Applied Optics, 34, 8422–8436, 1995.

Dubovik, O., Yokota, T., and Sasano, Y.: Improved technique for data inversion and its application to the retrieval algorithm for adeos/ilas., Advances in Space Research, 21, 397–403, 1998.

Dubovik, O., Smirnov, A., Holben, B. N., King, M., Kaufman, Y. J., Eck, T. F., and Slutsker, I.: Accuracy assesmenbts of aerosol optical properties retrieved from Aerosol Robotik Network (AERONET) sun and sky radiance measurements, Journal of Geophysical Research, 105, 9791–9806, 2000.

Dubovik, O., Holben, B., Eck, T., Smirnov, A., Kaufman, Y., King, M., Tanré, D., and Slutsker, I.: Variability of absorption and optical properties of key aersol types observed in worldwide locations, Journal of the Atmospheric Sciences, 59, 590–608, 2002a.

Dubovik, O., Holben, B. N., Lapyonok, T., Sinyuk, A., Mishchenko, M. I., Yang, P., and Slutsker, I.: Non-spherical aerosol retrieval method employing light scattering by spheroids, Geophysical Research Letters, 29, doi:10.1029/2001GL014506, 2002b.

Dubovik, O., Sinyuk, A., Lapyonok, T., Holben, B. N., Mishchenko, M., Yang, P., Eck, T. F., Volten, H., Munoz, O., Veihelmann, B., van der Zande, W. J., Leon, J.-F., Sorokin, M., and Slutsker, I.: Application of spheroid models to account for aerosol particle nonsphericity in remote sensing of desert dust, Journal of Geophysical Research, 111, doi:10.1029/2005JD006619, 2006.

Dubovik, O., Lapyonok, T., Kaufman, Y. J., Chin, M., Ginoux, P., Kahn, R. A., and Sinyuk, A.: Retrieving global aerosol sources from satellites using inverse modeling, Atmospheric Chemistry and Physics, pp. 209–250, doi:10.5194/acp-8-209-2008, 2008.

Dubovik, O., Herman, M., Holdak, A., Lapyonok, T., Tanré, D., Deuzé, J.-L., Ducos, F., Sinyuk, A., and Lopatin, A.: Statistically optimized inversion algorithm for enhanced retrieval of aerosol properties from spectral multi-angle polarimetric satellite observations, Atmospheric Measurement Techniques, pp. 975–1018, 2011.

Eck, T. F., Holben, B. N., Dubovik, O., Smirnov, A., Goloub, P., Chen, H. B., Chatenet, B., Gomes, L., Zhang, X.-Y., Tsay, S.-C., Ji, Q., Giles, D., and Slutsker, I.: Columnar aerosol optical properties at AERONET sites in Central-eastern Asia and aerosol transport to the tropical mid Pacific, Journal of Geophysical Research, 110, 975–1018, doi:10.1029/2004JD005274, 2005.

Fehsenfeld, F. C., Ancellet, G., Bates, T. S., Goldstein, A. H., Hardesty, R. M., Honrath, R., Law, K. S., Lewis, A. C., Leaitch, R., McKeen, S., Meagher, J., Parrish, D. D., Pszenny, A. A. P., Russell, P. B., Schlager, H., Seinfeld, J., Talbot, R., and Zbinden, R.: International Consortium for Atmospheric Research on Transport and Transformation (ICARTT): North America to Europe—Overview of the 2004 summer field study, Journal of Geophysical Research: Atmospheres, 111, doi: 10.1029/2006JD007829, URL http://dx.doi.org/10.1029/2006JD007829, 2006.

Feingold, G., Eberhard, W., Veron, D., and Previdi, M.: First measurements of the Twomey indirect effect using ground-based remote sensors, Geophysical Research Letters, 30, 1287, 2003.

Ferrare, R., Feingold, G., Ghan, S., Ogren, J., Schmid, B., Schwartz, S. E., and Sheridan, P.: Preface to special section: Atmospheric Radiation Measurement Program May 2003 Intensive Operations Period examining aerosol properties and radiative influences, Journal of Geophysical Research: Atmospheres, 111, doi: 10.1029/2005JD006908, URL http://dx.doi.org/10.1029/2005JD006908, 2006.

Ferrare, R. A., Melfi, S. H., Whiteman, D. N., Evans, K. D., Leifer, R., and Kaufman, Y. J.: Raman lidar measurements of aerosol extinction and backscattering 1. Methods and comparisons, Journal of Geophysical Research, 103, 19 663–19 672, 1998a.

Ferrare, R. A., Melfi, S. H., Whiteman, D. N.and Evans, K. D., Poellot, M., and Kaufman, Y. J.: Raman lidar measurements of aerosol extinction and back- scattering 2. Derivation of aerosol real refractive index, single-scattering albedo, and humidification factor using Raman lidar and aircraft size distribution measurements, Journal of Geophysical Research, 103, 19 673–19 690, 1998b.

Fishman, J., Hoell, J., Bendura, R., McNeal, R., and Kirchhoff, V.: NASA GTE TRACE A experiment (Septemner-October 2002): Overview, Journal of Geophysical Research, 101, 23 865–23 880, 1996.

Forster, P., Ramaswany, V., Artaxo, P., Bernsten, T., Betts, R., Fahey, D. W., Haywood, J., Lean, J., Lowe, D., Myhre, G., Nganga, J., Prinn, R., Raga, G., Schulz, M., and Dorland, R. V.: Changes in atmospheric constituents and in radiative forcing. Climate change 2007: the physical science basis. Contribution of working group I to the fourth assessment report of Intergovernmental Panel on Climate change, IPCC report, 2007.

Freudenthaler, V.: Rayleigh scattering coefficients and linear depolarization ratios at several EARLINET lidar wavelengths, EARLINET, version 1.4d edn., 2010.

Garcia, O. E., Diaz, A. M., Exposito, F. J., Diaz, J. P., Dubovik, O., Dubuisson, P., Roger, J.-C., Eck, T. F., Sinyuk, A., Derimian, Y., Dutton, E. G., Schafer, J. S., Holben, B. N., and Garc a, C. A.: Validation of AERONET estimates of atmospheric solar fluxes and aerosol radiative forcing by ground-based broadband

measurements, Journal of Geophysical Research, 113, doi:10.1029/2008JD010211, 2008.

Gobbi, G. P., Barnaba, F., van Dingenen, R., Putaud, J. P., Mircea, M., and Facchini, M. C.: Lidar and in situ observations of continental and Saharan aerosol: Closure analysis of particles optical and physical properties, Atmospheric Chemistry and Physics Discussions, pp. 445–477, 2003.

Gong, S., Barrie, L., Blanchet, J.-P., and Spacek, L.: Modeling size-distributed sea salt aerosols in the atmosphere: An application using Canadian climate models, in: Air Pollution Modeling and Its Applications XII, edited by Gryning, S.-E. and Chaumerliac, N., Plenum Press, New York, USA, 1998.

Govaerts, Y. M., Wagner, S., Lattanzio, A., and Watts, P.: Joint retrieval of surface reflectance and aerosol optical depth from MSG/SEVIRI observations with an optimal estimation approach: 1. Theory, Journal of Geophysical Research, 111, doi:10.1029/2009JD011779, 2010.

Groß, S., Tesche, M., Freudenthaler, V., Toledano, C., Wiegner, M., Ansmann, A., Althausen, D., and Seefeldner, M.: Characterization of Saharan dust, marine aerosols and mixtures of biomass-burning aerosols and dust by means of multi-wavelength depolarization and Raman lidar measurements during SAMUM 2, Tellus B, 63B, doi:10.1111/j.1600-0889.2011.00556.x, 2011.

Groß, S., Esselborn, M., Abicht, F., Wirth, M., Fix, A., and Minikin, A.: Airborne high spectral resolution lidar observation of pollution aerosol during EUCAARI-LONGREX, Atmospheric Chemistry and Physics, 13, 2435–2444, doi:10.5194/acp-13-2435-2013, URL `http://www.atmos-chem-phys.net/13/2435/2013/`, 2013.

Gutkowicz-Krusin, D.: Multiangle lidar performance in the presence of horizontal inhomogeneities in atmospheric extinction and scattering, Applied Optics, pp. 3266–3272, 1993.

Hair, J., Hostetler, C., Cook, A., Harper, D., Ferrare, R., Mack, T., Welch, W., Izquierdo, L., and Hovis, F. E.: Airborne High Spectral Resolution Lidar for Profiling Aerosol Optical Properties, Applied Optics, doi:10.1364/AO.47.006734, 2008.

Hansen, J., Sato, M., Kharecha, P., and von Schuckmann, K.: Earth's energy imbalance and implications, Atmospheric Chemistry and Physics, 11, 13 421–13 449, 2011.

Haywood, J. and Boucher, O.: Estimates of the direct and indirect radiative forcing due to tropospheric aerosols: A review, Reviews of Geophysics, 38, doi:10.1029/1999RG000078, 2000.

Haywood, J. M. and Shine, K. P.: The effect of anthropogenic sulfate and soot aerosol on the clear sky planetary radiation budget, Geophysical Research Letters, 22, 603–606, 1995.

Haywood, J. M., Pelon, J., Formenti, P., Bharmal, N., Brooks, M., Capes, G., Chazette, P., Chou, C., Christopher, S., Coe, H., Cuesta, J., Derimian, Y., Desboeufs, K., Greed, G., Harrison, M., Heese, B., Highwood, E. J., Johnson, B., Mallet, M., Marticorena, B., Marsham, J., Milton, S., Myhre, G., Osborne, S. R., Parker, D. J., Rajot, J.-L., Schulz, M., Slingo, A., Tanré, D., and Tulet, P.: Overview of the Dust and Biomass-burning Experiment and African Monsoon Multidisciplinary Analysis Special Observing Period-0, Journal of Geophysical Research: Atmospheres, 113, doi:10.1029/2008JD010077, URL http://dx.doi.org/10.1029/2008JD010077, 2008.

Heintzenberg, J.: The SAMUM-1 experiment over Southern Morocco: overview and introduction, Tellus B, 61, 2–11, doi:10.1111/j.1600-0889.2008.00403.x, URL http://dx.doi.org/10.1111/j.1600-0889.2008.00403.x, 2009.

Herman, M., Deuzé, J.-L., Marchant, A., Roger, B., and Lallart, P.: Aerosol remote sensing from POLDER/ADEOS over the ocean: Improved retrieval using a nonspherical particle model, Journal of geophysical research, 110, 2005.

Hinds, W. C.: Aerosol Technology: Properties, Behavior, and Measurement of Airborne Particles, Second Edition., Wiley-Interscience, New York, USA, second edn., 1999.

Hobbs, P. V.: Aerosol-cloud interactions, in Aerosol-Cloud-Climate Interactions, pp. 33–69, Academic, San Diego, California, 1993.

Hoell, J., Davis, D., Liu, S.C. abd Newell, R., Shipham, M., Akimoto, H., McNeal, R., Bemdura, R., and Drewry, J.: Paci c Exploratory Mission-West A (PEM-WEST A): Sep- tember-October, 1991, Journal of Geophysical Research, 101, 1641–1653, 1996.

Hoell, J., Davis, D., Liu, S., Newell, R., Shipham, M., Akimoto, H., McNeal, R., Bemdura, R., and Drewry, J.: The Paci c Exploratory Mission-West Phase B: February-March, 1994, Journal of Geophysical Research, 102, 28 223–28 239, 1997.

Hoffmann, T., Odum, J. R., Bowman, F., Collins, D., Klowckow, D., Flagan, R. C., and Seinfeld, J. H.: Formation of Organic Aerosols from the Oxidation of Biogenic Hydrocarbons, Journal of Atmospheric Chemistry, 26, 189–222, 1997.

Holben, B.: AERONET — A federated instrument network and data archive for aerosol characterization, Remote Sensing of Environment, 66, 1–16, 1998.

Holben, B., Eck, T., Schafer, J., Giles, D., and Sorokin, M.: Distributed Regional Aerosol Gridded Observation Networks (DRAGON), White Paper, 2011.

Holben, B. N., Tanré, D., Smirnov, A., Eck, T. F., Slutsker, I., Abuhassan, N., Newcomb, W. W., Schafer, J. S., Chatenet, B., Lavenu, F., Kaufman, Y. J., Castle, J. V., Setzer, A., Markham, B., Clark, D., Frouin, R., Halthore, R., Karneli, A., O'Neill, N. T., Pietras, C., Pinker, R. T., Voss, K., and Zibordi, G.: An emerging

ground-based aerosol climatology: Aerosol optical depth from AERONET, Journal of Geophysical Research, 106, 12 067–12 097, 2001.

Holben, B. N., Eck, T. F., Slutsker, I., Smirnov, A., Sinyuk, A., Schafer, J., Giles, D., and Dubovik, O.: AERONET's Version 2.0 quality assurance criteria, in: Remote Sensing of the Atmosphere and Clouds, edited by Tsay, S.-C., Nakajima, T., Singh, R., and Sridharan, R., vol. 6408 of *Proceedings of the Society of Photo-optical Instrumentation Engineers (SPIE)*, p. Q4080, 2006.

Huebert, B. J., Bates, T., Russell, P. B., Shi, G., Kim, Y. J., Kawamura, K., Carmichael, G., and Nakajima, T.: An overview of ACE-Asia: Strategies for quantifying the relationships between Asian aerosols and their climatic impacts, Journal of Geophysical Research: Atmospheres, 108, doi:10.1029/2003JD003550, URL `http://dx.doi.org/10.1029/2003JD003550`, 2003.

Hughes, H. G., Ferguson, J. A., and Stephens, D. H.: Sensitivity of a lidar inversion algorithm to parameters relating atmospheric backscatter and extinction, Applied Optics, 24, 1609–1913, 1985.

IPCC: Climate Change 2001: The Scientific Basis, Cambridge Universtiy Press, Cambridge, 2001.

Ivanov, A., Osipenko, F., Chaikovskii, A., Shcherbakov, V. N., and Tauroginskaya, S.: Dynamics of Optical Parameters of the Stratospheric Aerosol Layer Following the Eruption of Mt. Pinatubo from Lidar Data, Izvestia of Atmospheric and Oceanic Physics, 33, 184–189, 1997.

Ivanov, A., Chaikovskii, A., Osipenko, F., Shcherbakov, V. N., Pukhalskii, S., and Sobolevskii, P.: Dynamics of the Optical Parameters of the Pinatubo Aerosol Layer from Spectral Polarization Lidar Measurements, Izvestia of Atmospheric and Oceanic Physics, 36, 95–101, 2000.

Jacob, D. J., Crawford, J. H., Kleb, M. M., Connors, V. S., Bendura, R. J., Raper, J. L., Sachse, G. W., Gille, J. C., Emmons, L., and Heald, C. L.: Transport and Chemical Evolution over the Pacific (TRACE-P) aircraft mission: Design, execution, and first results, Journal of Geophysical Research: Atmospheres, 108, doi: 10.1029/2002JD003276, URL `http://dx.doi.org/10.1029/2002JD003276`, 2003.

Jiang, H., Feingold, G., Jonsson, H. H., Lu, M.-L., Chuang, P. Y., Flagan, R. C., and Seinfeld, J. H.: Statistical comparison of properties of simulated and observed cumulus clouds in the vicinity of Houston during the Gulf of Mexico Atmospheric Composition and Climate Study (GoMACCS), Journal of Geophysical Research: Atmospheres, 113, doi:10.1029/2007JD009304, URL `http://dx.doi.org/10.1029/2007JD009304`, 2008.

Kalman, R. E.: A New approach to linear filtering and prediction problems, Journal of Basic Engineering, 82, 35–40, 1960.

Kamens, R. M. and Jaoui, M.: Modeling Aerosol Formaiton from α-Pinene + NOx in the Presence of Natural Sunlight Using Gas-Phase Kinetics and Gas-Particle Partitioning Theory, Environmental Science and Technology, 35, 1394–1405, 2001.

Kandler, K., Benker, N., Bundke, U., Cuevas, E., Ebert, M., Knippertz, P., Rodriguez, S., Schuetz, L., and Weinbruch, S.: Chemical composition and complex refractive index of Saharan Mineral Dust at Izana, Tenerife (Spain) derived by electron microscopy., Atmospheric Environment, 41, 8058–8074, 2007.

Kasten, F. and Young, A.: Revised optical airmass tables and approximation formula., Applied Optics, 28, 4735–4738, 1989.

Kaufman, Y., Setzer, A., Ward, D., Tanré, D., Holben, B. N., Menzel, P., Pereira, M. C., and Rasmussen, R.: Biomass Burning Airborne and Spaceborne Experiment in the Amazonas (BASE-A), Journal of Geophysical Research, 97, 14 581–14 599, 1992.

Kaufman, Y., Hobbs, P. V., Kirchhoff, V. W. J. H., Artaxo, P., Remer, L. A., Holben, B. N., King, M. D., Ward, D. E., Prins, E. M., Longo, K. M., Mattos, L. F., Nobre, C. A., Spinhirne, J. D., Ji, Q., Thompson, A. M., Gleason, J. F., and Christopher, S. A.: Smoke, clouds, and radiation—Brazil (SCAR-B) experiment, Journal of Geophysical Research, 103, 31 783–31 808, 1998.

King, M., Kaufman, Y., Tanré, D., and Nakajima, T.: Remote sensing of Tropospheric aerosols from Space: Past, Present, and Future, Bulletin of the American Meteorological Society, 80, 2229–2259, 1999.

King, M. D., Byrne, D. M., Herman, B. M., and Reagan, J. A.: Aerosol size distributions obtained by inversion of spectral optical depth measurements, Journal of Atmospheric Scienses, 21, 2153–2167, 1978.

King, M. D., Platnick, S., Moeller, C. C., Revercomb, H. E., and Chu, D. A.: Remote sensing of smoke, land, and clouds from the NASA ER-2 during SAFARI 2000, Journal of Geophysical Research: Atmospheres, 108, doi:10.1029/2002JD003207, URL `http://dx.doi.org/10.1029/2002JD003207`, 2003.

Kinne, S., Lohmann, U., Feichter, J., Schulz, M., Timmreck, C., Ghan, S., Easter, R., Chin, M., Ginoux, P., Takemura, T., Tegen, I., Koch, D., Herzog, M., Penner, J., Pitari, G., Holben, B., Eck, T., Smirnov, A., Dubovik, O., Slutsker, I., Tanré, D., Torres, O., Mishchenko, M., Geogdzhayev, I., Chu, D. A., and Kaufman, Y. J.: Monthly averages of aerosol properties: A global comparison among models, satellite data and AERONET ground data, Journal of Geophysical Research, 108, doi:10.1029/2001JD001253, 2003.

Kinne, S., Schulz, M., Textor, C., Guibert, S., Balkanski, Y., Bauer, S. E., Berntsen, T., Berglen, T. F., Boucher, O., Chin, M., Collins, W., Dentener, F., Diehl, T., Easter, R., Feichter, J., Fillmore, D., Ghan, S., Ginoux, P., Gong, S., Grini, A., Hendricks, J., Herzog, M., Horowitz, L., Isaksen, I., Iversen, T., Kirkavag, A.,

Kloster, S., Koch, D., Kristjansson, J. E., Krol, M., Lauer, A., Lamarque, J. F., Lesins, G., Liu, X., Lohmann, U., Montanaro, V., Myhre, G., Penner, J. E., Pitari, G., Reddy, S., Seland, O., Stier, P., Takemura, T., and Tie, X.: An AeroCom initial assessment - optical properties in aerosol component modules of global models, Atmospheric Chemistry and Physics, 6, 1815–1834, 2006.

Klett, D.: Stable analytical inversion solution for processing lidar returns, Applied Optics, 20, 211–220, 1981.

Klett, D.: Lidar inversion with variable backscatter/extinction ratios, Applied Optics, 31, 1638–1643, 1985.

Koch, D. and Del Genio, A.: Black carbon absorption effects on cloud cover, review and synthesis, Atmospheric Chemistry and Physics, pp. 7685–7696, 2010.

Koch, D., Schulz, M., Kinne, S., McNaughton, C., Spackman, J. R., Balkanski, Y., Bauer, S., Berntsen, T., Bond, T. C., Boucher, O., Chin, M., Clarke, A., De Luca, N., Dentener, F., Diehl, T., Dubovik, O., Easter, R., Fahey, D. W., Feichter, J., Fillmore, D., Freitag, S., Ghan, S., Ginoux, P., Gong, S., Horowitz, L., Kirkevåg, T. I. A., Klimont, Z., Kondo, Y., Krol, M., Liu, X., Miller, R., Montanaro, V., Moteki, N., Myhre, G., Penner, J. E., Perlwitz, J.and Pitari, G., Reddy, S., Sahu, L., Sakamoto, H., Schuster, G., Schwarz, J. P., Seland, Ø., Stier, P., Takegawa, N., Takemura, T., Textor, C., van Aardenne, J. A., and Zhao, Y.: Evaluation of black carbon estimations in global aerosol models, Atmospheric Chemistry and Physics, pp. 9001–9026, 2009.

Koepke, P., Hess, M., Schult, I., and Shettle, E.: Global aerosol data set, Tech. Rep. 243, MPI Meteorologie Hamburg, 1997.

Kokhanovsky, A., Bréon, F. M., Cacciari, A., and et. al.: Aerosol remote sensing over land: A comparison of satellite retrievals using different algorithms and instruments, Atmospheric Research, 85, 372–394, 2007.

Kotelnikov, V. A.: On the carrying capacity of the ether and wire in telecommunications, in: Material for the First All-Union Conference on Questions of Communication, Izd. Red. Upr. Svyazi RKKA, Moscow, 1933.

Kovalev, V. A.: Sensitivity of the lidar solution to errors of the aerosol backscatter-to-extinction ratio: Influence of a monotonic change in the aerosol extinction coefficient, Applied Optics, 34, 3457–3462, 1995.

Kovalev, V. A. and Oller, H. M.: Distortion of particulate extinction profiles measured with lidar in a two-component atmosphere, Applied Optics, 33, 6499–6570, 1994.

Kulmala, M., Vehkamaki, H., Petajda, T., Dal Maso, M., Lauri, A., Kerminen, V. M., Birmili, W., and McMurry, P. H.: Formation and Growth Rates of Ultrafine Atmospheric Particles: A Review of Observations., Journal of Aerosol Science, 35, 143–176, 2004.

Lelieveld, J., Berresheim, H., Borrmann, S., Crutzen, P. J., Dentener, F. J., Fischer, H., Feichter, J., Flatau, P. J., Heland, J., Holzinger, R., Korrmann, R., Lawrence, M. G., Levin, Z., Markowicz, K. M., Mihalopoulos, N., Minikin, A., Ramanathan, V., de Reus, M., Roelofs, G. J., Scheeren, H. A., Sciare, J., Schlager, H., Schultz, M., Siegmund, P., Steil, B., Stephanou, E. G., Stier, P., Traub, M., Warneke, C., Williams, J., and Ziereis, H.: Global air pollution crossroads over the Mediterranean, Science, 298, 794–799, doi:10.1126/science.1075457, 2002.

Lenoble, J., Herman, M., Deuzé, J.-L., Lafrance, B., Santer, R., and Tanré, D.: A successive order of scattering code for solv- ing the vector equation of transfer in the earth's atmosphere with aerosols, Journal of Quantitative Spectroscopy and Radiative Transfer, 107, 479–507, 2007.

Levy, R. C., Remer, L., and Dubovik, O.: Global aerosol optical models and application to MODIS aerosol retrieval over land, Journal of Geophysical Research, 112, doi:10.1029/2006JD007815, 2007a.

Levy, R. C., Remer, L. R., Mattoo, S., Vermote, E. F., and Kaufman, Y. J.: Second-generation operational algorithm: Retrieval of aerosol properties over land from inversion of Moderate Resolution Imaging Spectroradiometer spectral reflectance, Journal of Geophysical Research, 112, doi:10.1029/2006JD007811, 2007b.

Li, Z., Goloub, P., Devaux, C., Gu, X., Deuzé, J.-L., Qiao, Y., and Zhao, F.: Retrieval of aerosol optical and physical properties from ground-based spectral, multi-angular, and polarized sun-photometer measurements, Remote Sensing of Environment, 101, 519–533, doi:http://dx.doi.org/10.1016/j.rse.2006.01.012, URL `http://www.sciencedirect.com/science/article/pii/S003442570600037X`, 2006.

Li, Z., Chen, H., Cribb, M., Dickerson, R., Holben, B., Li, C., Lu, D., Luo, Y., Maring, H., Shi, G., Tsay, S.-C., Wang, P., Wang, Y., Xia, X., Zheng, Y., Yuan, T., and Zhao, F.: Preface to special section on East Asian Studies of Tropospheric Aerosols: An International Regional Experiment (EAST-AIRE), Journal of Geophysical Research: Atmospheres, 112, doi:10.1029/2007JD008853, URL `http://dx.doi.org/10.1029/2007JD008853`, 2007.

Li, Z., Goloub, P., Dubovik, O., Blarel, L., Zhang, W., Podvin, T., Sinyuk, A., Sorokin, M., Chen, H., Holben, B. N., Tanré, D., Canini, M., and Buis, J.-P.: Improvements for ground-based remote sensing of atmospheric aerosol properties by additional polarimetric measurements, Journal of Quantitative Spectroscopy and Radiative Transfer, 110, 1954–1961, 2009.

Lindesay, J. A., Andreae, M., Goldammer, J., Harris, G., Annegarn, H., Garstang, M., Scholes, R., and van Wilgen, B.: International Geosphere Biosphere Programme/International Global Atmospheric Chemistry SAFARI-92 field experiment: Background and overview, Journal of Geophysical Research, 101, 23 521–23 530, 1996.

Liu, Z., Sugimoto, N., and Murayama, T.: Extinction-to- backscatter ratio of Asian dust observed with high-spectral- resolution lidar and Raman lidar, Applied Optics, 41, 2760–2767, 2002.

Lohmann, U. and Feichter, J.: Global indirect aerosol effects: a review, Atmospheric Chemistry and Physics, 5, 715–737, 2005.

Lohmann, U. and Hoose, C.: Sensitivity studies of different aerosol indirect effects in mixed- phase clouds, Atmospheric Chemistry and Physics, pp. 8917–8934, 2009.

Lohmann, U., Karcher, B., and Timmreck, C.: Impact of the Mount Pinatubo eruption on cirrus clouds formed by homogeneous freezing in the ECHAM4 GCM, Journal of Geophysical Research, 108, 4568, 2003.

Lopatin, A., Dubovik, O., Chaikovsky, A., Goloub, P., Lapyonok, T., Tanré, D., and Litvinov, P.: Enhancement of aerosol characterization using synergy of lidar and sun-photometer coincident observations: the GARRLiC algorithm, Atmospheric Measurement Techniques, 6, 2065–2088, doi:10.5194/amt-6-2065-2013, URL `http://www.atmos-meas-tech.net/6/2065/2013/`, 2013.

Lu, M.-L., Feingold, G., Jonsson, H. H., Chuang, P. Y., Gates, H., Flagan, R. C., and Seinfeld, J. H.: Aerosol-cloud relationships in continental shallow cumulus, Journal of Geophysical Research: Atmospheres, 113, doi:10.1029/2007JD009354, URL `http://dx.doi.org/10.1029/2007JD009354`, 2008.

Matsumoto, M. and Takeuchi, N.: Effects of misestimated far-end boundary values on two common lidar inversion solutions, Applied Optics, 33, 6451–6456, 1994.

McCormick, M. P., Wang, P.-H., and Poole, L. R.: Stratospheric aerosols and clouds, in Aerosol-Cloud-Climate Interactions, pp. 205–222, Academic Press, San Diego., California, 1993.

McKendry, I., Strawbridge, K. B., O'Neill, N. T., Macdonald, A. M., Liu, P. S. K., Leaitch, W. R., Anlauf, K. G., Jaegle, L., Fairlie, T. D., and Westphal, D. L.: Trans-Pacific transport of Saharan dust to western North America: A case study, Journal of Geophysical Research, 112, doi:10.1029/2006JD007129, 2007.

Menon, S., Hansen, J., Nazarenko, L., and Luo, Y.: Climate effects of black carbon aerosols in China and India, Science, 297, 2250, 2002.

Mishchenko, M., Travis, L., and Mackowski, D.: T-Matrix Computations of Light Scattering by Nonspherical Particles: a Review, Journal of Quantitative Spectroscopy and Radiative Transfer, 55, 1996.

Mishchenko, M., Travis, L., and Lacis, A.: Scattering, Absorption, and Emission of Light by Small Particles, Cambridge University Press, 2002.

Mishchenko, M. I. and Travis, L. D.: Capabilities and limitations of a current FORTRAN implementation of the T-matrix method for randomly oriented, rotationally symmetric scatterers-Computational Methods, Journal of Quantitative Spectroscopy and Radiative Transfer, 60, 309–324, 1998.

Mishchenko, M. I., Travis, L. D., Kahn, R. A., and West, R. A.: Modeling phase functions for dustlike tropospheric aerosols using a shape mixture of randomly oriented polydisperse spheroids, Journal of Geophysical Research: Atmospheres, 102, 16 831–16 847, doi:10.1029/96JD02110, URL http://dx.doi.org/10.1029/96JD02110, 1997.

Mishchenko, M. I., Hovenier, J. W., and Travis, L. D.: Light scattering by nonspherical particles, Elsevier, New York, 2000.

Mishchenko, M. I., Cairns, B., Ha, Travis, L. D., Burg, R., Ka, Martins, J. V., and Shettle, E. P.: Monitoring of aerosol forcing of climate from space: Analysis of measurement requirements, Journal of Quantitative Spectroscopy and Radiative Transfer, 79/80, 149–161, 2004.

Mishchenko, M. I., Cairns, B., Kopp, G., Schueler, C. F., Fafaul, B. A., Hansen, J. E., Hooker, R. J., Itchkawich, T., Maring, H. B., and Travis, L. D.: Accurate monitoring of terrestrial aerosol and total solar irradiance: introducing the Glory, Mission, Bulletin of the American Meteorological Society, 88, 677–691, 2007.

Molina, L. T., Madronich, S., Gaffney, J., and Singh, H.: Overview of MILAGRO/INTEX-B Campaign. IGAC activities, Newsletter of International Global Atmospheric Chemistry Project, 38, 2–15, 2008.

Müller, D., Wandinger, U., and Ansmann, A.: Microphysical particle parameters from extinction and backscatter lidar data by inversion with regularization: Theory, Applied Optics, 38, 2346–2357, 1999.

Müller, D., Mattis, I., Wandinger, U., Ansmann, A., Althausen, D., Dubovik, O., Eckhardt, S., and Stohl, A.: Saharan dust over a Central European EARLINET-AERONET site: Combined observations with Raman lidar and Sun photometer, Journal of Geophysical Research, p. 4345, doi:10.1029/2002JD002918, 2003.

Müller, D., Mattis, I., Ansmann, A., Wehner, B., Althausen, D., Wandinger, U., and Dubovik, O.: Closure study on optical and microphysical properties of a mixed urban and Arctic haze air mass observed with Raman lidar and Sun photometer, Journal of Geophysical Research, 109, doi:10.1029/2003JD004200, 2004.

Müller, D., Mattis, I., Wandinger, U., Ansmann, A., Althausen, D., and Stohl, A.: Raman lidar observations of aged Siberian and Canadian forest fire smoke in the free troposphere over Germany in 2003: Microphysical particle characterization, Journal of Geophysical Research, 110, doi:doi:10.1029/2004JD005756, 2005.

Müller, D., Ansmann, A., Mattis, I., Tesche, M., Wandinger, U., Althausen, D., , and Pisani, G.: Aerosol-type-dependent lidar ratios observed with Raman lidar, Journal of Geophysical Research, 112, doi:10.1029/2006JD008292, 2007.

Müller, D., Lee, K.-H., Gasteiger, J., Tesche, M., Weinzierl, B., Kandler, K., Müller, T., Toledano, C., Otto, S., Althausen, D., and Ansmann, A.: Comparison of optical and microphysical properties of pure Saharan mineral dust observed with AERONET Sun photometer, Raman lidar, and in situ instruments during SAMUM 2006, Journal of Geophysical Research, 117, doi:10.1029/2011JD016825, 2012.

Murayama, T. and et al.: Lidar Network Observation of Asian Dust / Advances in Laser Remote sensing /, in: Selected papers 20th Int. Laser Radar Conference (ILRC), Vichi, France, 10-14 July 2000, pp. 169–177, 2000.

Nakajima, T., Tanaka, M., and Yamauchi, T.: Retrieval of the optical properties of aerosols from aureole and extinction data, Applied Optics, 22, 2951–2959, 1983.

Nakajima, T., Tonna, G., Rao, R., Kaufman, Y. J., and Holben, B. N.: Use of sky brightness measurements from ground for remote sensing of particulate polydispersions, Applied Optics, 35, 2672–2686, 1996.

Nakajima, T., Yoon, S. C., Ramanathan, V., Shi, G.-Y., Takemura, T., Higurashi, A., Takamura, T., Aoki, K., Sohn, B.-J., Kim, S.-W., Tsuruta, H., Sugimoto, N., Shimizu, A., Tanimoto, H., Sawa, Y., Lin, N.-H., Lee, C.-T., Goto, D., and Schutgens, N.: Overview of the Atmospheric Brown Cloud East Asian Regional Experiment 2005 and a study of the aerosol direct radiative forcing in east Asia, Journal of Geophysical Research, 112, doi:10.1029/2007JD009009, 2007.

Nyquist, H.: Certain topics in telegraph transmission theory, Transactions of the American Institute of Electrical Engineers, 47, 617–644, 1928.

O'Dowd, C. D., Jimenez, J. L., Bahreini, R., Flagan, R. C., Seinfeld, J. H., Hameri, K., Pirjola, L., Kulmala, M., Jennings, S. G., and Hoffmann, T.: Marine Aerosol Formation from Biogenic Iodine Emissions, Nature, 417, 632–636, 2002.

Omar, A. H., Won, J. G., Winker, D. M., Yoon, S. C., Dubovik, O., and McCormick, M. P.: Development of global aerosol models using cluster analysis of AERONET measurements, Journal of Geophysical Research, 110, doi:10.1029/2004JD004874, 2005.

on Climate Control (IPCC), I. P.: Climate Change 2001, the Third Assessment Report of the IPCC, Cambridge Univ. Press, New York, 2001.

Oshchepkov, S., Sasano, Y., and Yokota, T.: New method for simultaneous gas and aerosol retrievals from space limb-scanning spectral observation of the atmosphere, Applied Optics, 41, 4234–4244, 2002.

Pahlow, M., Kovalev, V. A., and Parlange, M. B.: Calibration method for multiangle lidar measurements, Applied Optics, 43, 2948–2956, 2004.

Papayannis, A., Balis, D., Amiridis, V., Chourdakis, G., Tsaknakis, G., Zerefos, C., Castanho, A. D. A., Nickovic, S., Kazadzis, S., and Grabowski, J.: Measurements of Saharan dust aerosols over the Eastern Mediterranean using elastic backscatter-Raman lidar, spectrophotometric and satellite observations in the frame of the EARLINET project, Atmospheric Chemistry and Physics, pp. 2065–2079, 2005.

Patterson, E. and Gillette, D.: Commonalities in measured size distributions for aerosols having a soil-derived component., Journal of Geophysical Research: Oceans and Atmospheres, 82, 2074–2082, 1977.

Pelon, J., Tanré, D., Garnier, A., and Lifermann, A.: L'apport des nouvelles missions spatiales à sondeurs actifs : Résultats récents de CALIPSO, CloudSat et l'A-Train, La Météorologie, 75, 15–22, 2011.

Phillips, D. L.: A technique for numerical solution of certain integral equation of first kind, Journal of the Association for Computing Machinery, pp. 84–97, 1962.

Pickering, K. E., Thompson, A. M., Kim, H., DeCaria, A. J., Pfister, L., Kucsera, T. L., Witte, J. C., Avery, M. A., Blake, D. R., Crawford, J. H., Heikes, B. G., Sachse, G. W., Sandholm, S. T., and Talbot, R. W.: Trace gas transport and scavenging in PEM-Tropics B South Pacific Convergence Zone convection, Journal of Geophysical Research, 106, 32 591–32 602, 2001.

Pilinis, C., Pandis, S. N., and Seinfeld, J. H.: Sensitivity of direct climate forcing by atmospheric aerosols to aerosol size and composition, Journal of Geophysical Research, 100, 18 739–18 754, 1995.

Pincus, R. and Baker, M.: Effect of precipitation on the albedo susceptibility of clouds in the marine boundary layer, Nature, 1994.

Pope, C. A. and Dockery, D. W.: Acute Health-Effects of PM10 Pollution on Symptomatic and Asymptomatic Children., American Review of Respiratory Disease, 145, 1123–1128, 1992.

Pope, C. A., Dockery, D. W., Spengler, J. D., and Raizenne, M. E.: Respiratory Health and PM10 Pollution - a Daily Time-Series Analysis, American Review of Respiratory Disease, 144, 668–674, 1991.

Pope, C. A., Thun, M. J., Namboodiri, M. M., Dockery, D. W., Evans, J. S., Speizer, F. E., and Heath, C. W.: Particulate Air Pollution as a Predictor of Mortality in a Prospective Study of U.S. Adults, American Journal of Respiratory and Critical Care Medicine, 151, 669–674, 1995.

Pope, C. A., Burnett, R. T., Thun, M. J., Calle, E. E., Krewski, D., Ito, K., and Thurston, G. D.: Lung Cancer, Cardiopulmonary Mortality, and Long-Term Exposure to Fine Particulate Air Pollution, Journal of the American Medical Association, 287, 1132–1141, 2002.

Press, W. H., Teukolsky, S. A., Vetterling, W. T., and Flannery, B. P.: Numerical Recipes in FORTRAN. The art of Scientific Computing, Cambridge University Press, 1992.

Quinn, P. and Bates, T.: North American, Asian, and In- dian haze: Similar regional impacts on climate?, Geophysical Research Letters, 30, 1555, doi: 10.1029/2003GL016934, 2003.

Quinn, P., Coffman, D., Kapustin, V., Bates, T., and Covert, D.: Aerosol optical properties in the marine boundary layer during ACE 1 and the underlying chemical and physical aerosol properties, Journal of Geophysical Research, 103, 16 547–16 563, 1998.

Raes, F., Bates, T., McGovern, F., and van Liedekerke, M.: The 2nd Aerosol Characterization Experiment (ACE-2): General overview and main results., Tellus B, 52B, 111–125, 2000.

Ramanathan, V. and Crutzen, P.: Atmospheric Brown "Clouds", Atmospheric Environment, 37, 4033–4035, 2003.

Ramanathan, V., Crutzen, P., Lelieveld, J., Mitra, A., Althausen, D., Anderson, J., Andreae, M., Cantrell, C., Cass, G., Chung, C., Clarke, A., Coakley, J., Collins, W., Conant, W., Dulac, F., Heintzenberg, J., Heymsfield, A., Holben, B., Howell, S., Hudson, J., Jayaraman, A., Kiehl, J., Krishnamurti, T., Lubin, D., McFarquhar, G., Novakov, T., Ogren, J., Podgorny, I., Prather, K., Priestley, K., Prospero, J., Quinn, P., Rajeev, K., Rasch, P., Rupert, S., Sadourny, R., Satheesh, S., Shaw, G., Sheridan, P., and Valero, F.: The Indian Ocean Experiment: An integrated assessment of the climate forcing and effects of the great Indo-Asian haze, Journal of Geophysical Research, 106, 28 371–28 393, 2001.

Reid, J. S., Halflidi, H., Maring, H. B., Smirnov, A., Savoie, D. L., Cliff, S. S., Reid, E. A., Livingston, J. M., Meier, M. M., Dubovik, O., and Tsay, S.-C.: Comparison of Size and Morphological Measurements of Coarse Mode Dust Particles from Africa, Journal of Geophysical Research, 108, 8593, doi:10.1029/2002JD002485, 2003.

Reid, J. S., Piketh, S. J., Walker, A. L., Burger, R. P., Ross, K. E., Westphal, D. L., Bruintjes, R. T., Holben, B. N., Hsu, C., Jensen, T. L., Kahn, R. A., Kuciauskas, A. P., Al Mandoos, A., Al Mangoosh, A., Miller, S. D., Porter, J. N., Reid, E. A., and Tsay, S.-C.: An overview of UAE2 flight operations: Observations of summertime atmospheric thermodynamic and aerosol profiles of the southern Arabian Gulf, Journal of Geophysical Research: Atmospheres, 113, doi:10.1029/2007JD009435, URL http://dx.doi.org/10.1029/2007JD009435, 2008.

Remer, L., Gassó, S., Hegg, D., Kaufman, Y., and Holben, B.: Urban/industrial aerosol: ground based sun/sky radiometer and airborne in situ measurements., Journal of Geophysical Research, 102, 16 849–16 859, 1997.

Rocadenbosch, F., Nadzri Md. Reba, M., Sicard, M., and Comerón, A.: Practical analytical backscatter error bars for elastic one-component lidar inversion algorithm, Applied Optics, 49, 2010.

Rodgers, C. D.: Retrieval of atmospheric temperature from remote measurements of thermal radiation, Reviews of Geophysics, 14, 609–624, 1976.

Rodgers, C. D.: Inverse methods for atmospheric sounding: theory and practice, World Scientific, Singapore, 2000.

Roujeau, J.-L., Tanré, D., Bréon, F.-M., and Deuzé, J.-L.: Retrieval of land surface parameters from airborne POLDER bidirectional reflectance distribution function during HAPEX-Sahel, Journal of Geophysical Research, 102, 11 201–112 018, 1997.

Russell, P., Livingston, J., Hignett, P., Kinne, S., Wong, J., Chien, A., Bergstrom, R., Durkee, P., and Hobbs, P.: Aerosol-induced radiativeflux changes off the United States mid-Atlantic coast: comparison of values calculated from sun photometer and in situ data with those measured by airborne pyranometer, Journal of Geophysical Research, 104, 2289–2307, 1999.

Russell, P. B., Swissler, T. J., and McCormick, M. P.: Methodology for error analysis and simulation of lidar aerosol measurements, Applied Optics, 18, 3783–3797, 1979.

Sasano, Y., Browell, E. V., and Ismail, S.: Error caused by using a constant extinction backscattering ratio in the lidar solution, Applied Optics, 24, 3929–3932, 1985.

Schoeberl, M. R. and Newman, P. A.: A multiple-level trajectory analysis of vortex filaments, Journal of Geophysical Research, 100, 25 801–25 816, 1995.

Schuster, G. L., Vaughan, M., MacDonnell, D., Su, W., Winker, D., Dubovik, O., Lapyonok, T., and Trepte, C.: Comparison of CALIPSO aerosol optical depth retrievals to AERONET measurements, and a climatology for the lidar ratio of dust, Atmospheric Chemistry and Physics, 12, 7431–7452, doi:10.5194/acp-12-7431-2012, 2012.

Schwartz, J., Dockery, D. W., and Neas, L. M.: Is Daily Mortality Associated Specifically with Fine Particles?, Journal of Air and Waste Management Association, 46, 927–939, 1996.

Seinfeld, J. H. and Pandis, S. N.: Atmospheric Chemistry and Physics: From Air Pollution to Climate Change, Chichester, John Wiley & Sons, New York, USA, 1998.

Seinfeld, J. H., Carmichael, G. R., Arimoto, R., Conant, W. C., Brechtel, F. J., Bates, T. S., Cahill, T. A., Clarke, A. D., Doherty, S. J., Flatau, P. J., Huebert, B. J., Kim, J., Markowicz, K. M., Quinn, P. K., Russell, L. M., Russell, P. B., Shimizu, A., Shinozuka, Y., Song, C. H., Tang, Y., Uno, I., Vogelmann, A. M., Weber, R. J., Woo, J.-H., and Zhang, X. Y.: ACE-ASIA: Regional Climatic

and Atmospheric Chemical Effects of Asian Dust and Pollution, Bulletin of the American Meteorological Society, 85, 367–380, doi:10.1175/BAMS-85-3-367, URL http://dx.doi.org/10.1175/BAMS-85-3-367, 2004.

Shaw, G. E.: Sun photometry., Bulletin of the American Meteorological Society, 64, 4–10, 1983.

Shcherbakov, V. N.: Regularized algorithm for Raman lidar data processing, Applied Optics, 46, 4879–4889, 2007.

Shettle, E. and Fenn, R.: Models of aerosols of lower troposphere and the effect of humidity variations on their optical propoerties, Tech. Rep. 79 0241, AFCRL, 1979.

Shipley, S. T., Tracy, D. H., Eloranta, E. W., Trauger, J. T., Sroga, J. T., Roesler, F. L., and Weinman, J. A.: High spectral resolution lidar to measure optical scattering properties of atmospheric aerosols, Applied Optics, 23, 3716–3724, 1983.

Sicard, M., Chazette, P., Pelon, J., Gwang-Won, J., and Yoon, S.-C.: Variational method for the retrieval of the optical thickness and the backscatter coefficient from multiangle lidar profiles, Applied Optics, 41, 493–502, 2002.

Singh, H. B., Brune, W. H., Crawford, J. H., Flocke, F., and Jacob, D. J.: Chemistry and transport of pollution over the Gulf of Mexico and the Pacific: spring 2006 INTEX-B campaign overview and first results, Atmospheric Chemistry and Physics, 9, 2301–2318, doi:10.5194/acp-9-2301-2009, URL http://www.atmos-chem-phys.net/9/2301/2009/, 2009.

Sinyuk, A., Dubovik, O., Holben, B., Schafer, J., Giles, D., Eck, T., Slutsker, I., Sorokine, M., Smirnov, A., Bréon, F., and Khan, R.: Multi-sensor aerosol retrievals using joint inversion of AERONET and satellite observations: concept and applications., Eos Transactions AGU, Fall Meeting Supplements, 53, 2008.

Smirnov, A., Holben, B., Eck, T., Dubovik, O., and Slutsker, I.: Cloud-screening and quality control algorithms for the AERONET database., Remote Sensing of Environment, 73, 337–349, 2000.

Smith, W. L., Charlock, T. P., Kahn, R., Martins, J. V., Remer, L. A., Hobbs, P. V., Redemann, J., and Rutledge, C. K.: EOS terra aerosol and radiative flux validation: an overview of the chesapeake lighthouse and aircraft measurements for satellites (clams) experiment., Journal of Atmospheric Scienses, 62, 903–918, doi:10.1175/JAS3398.1, 2005.

Sokolik, I. and Toon, O.: Incorporation of mineralogical composition into models of the radiative properties of mineral aerosol from UV to IR wavelengths., Journal of Geophysical Research: Atmospheres, 104, 9423–9444, 1999.

Stephens, G., Vane, D., Boain, R., Mace, G., Sassen, K., Wang, Z., Illingworth, A., O'Conner, E., Rossow, W., Durden, S., Miller, S., Austin, R., Benedetti, A., and

Mitrescu, C.: The CloudSat mission and the A-Train, Bulletin of the American Meteorological Society, 83, 1771–1790, 2002.

Takamura, T., Sasano, Y., and Hayasaka, T.: Tropospheric aerosol optical properties derived from lidar, sun photometer, and optical particle counter measurements, Applied Optics, 33, 7132–7140, 1994.

Tanré, D., Haywood, J., Pelon, J., Léon, J. F., Chatenet, B., Formenti, P., Francis, P., Goloub, P., Highwood, E. J., and Myhre, G.: Measurement and modeling of the Saharan dust radiative impact: Overview of the Saharan Dust Experiment (SHADE), Journal of Geophysical Research: Atmospheres, 108, doi:10.1029/2002JD003273, URL http://dx.doi.org/10.1029/2002JD003273, 2003.

Tanré, D., Bréon, F.-M., Deuzé, J.-L., Dubovik, O., Ducos, F., Francois, P., Goloub, P., Herman, M., Lifermann, A., and Waquet, F.: Remote sensing of aerosols by using polarized, directional and spectral measurements within the A-Train: the PARASOL mission, Atmospheric Measurement Technique Discussions, pp. 2037–2069, doi:10.5194/amtd-4-2037-2011, 2011.

Tarantola, A.: Inverse Problem Theory: Methods for Data Fitting and Model Parameter Estimation, Elsevier, Amsterdam, 1987.

Targino, A. C.: Regional studies of the optical, chemical and microphysical properties of atmospheric aerosols: Radiative impacts and cloud formation, Ph.D. thesis, Department of Meteorology, Stockholm University, SE-106, 91, Stockholm, Sweden, 2005.

Tesche, M., Ansmann, A., Müller, D., Althausen, D., Mattis, I., Heese, B., Freudenthaler, V., Wiegner, M., Esselborn, M., Pisani, G., and Knippertz, P.: Vertical profiling of Saharan dust with Raman lidars and airborne HSRL in southern Morocco during SAMUM, Tellus B, 61B, 144–164, 2009.

Tesche, M., Gross, S., Ansmann, A., Müller, D., Althausen, D., Freudenthaler, V., and Esselborn, M.: Profiling of Saharan dust and biomass-burning smoke with multiwavelength polarization Raman lidar at Cape Verde, Tellus B, 63B, 649–676, 2011.

Textor, C., Schulz, M., Guibert, S., Kinne, S., Balkanski, Y., Bauer, S., Berntsen, T., Berglen, T., Boucher, O., Chin, M., Dentener, F., Diehl, T., Easter, R., Feichter, H., Fillmore, D., Ghan, S., Ginoux, P., Gong, S., Kristjansson, J. E., Krol, M., Lauer, A., Lamarque, J. F., Liu, X., Montanaro, V., Myhre, G., Penner, J., Pitari, G., Reddy, S., Seland, O., Stier, P., Takemura, T., and Tie, X.: Analysis and quantification of the diversities of aerosol life cycles within AeroCom, Atmospheric Chemistry and Physics, 6, 1777–1813, 2006.

Tikhonov, A. N.: On the solution of incorrectly stated problems and a method of regularization, Doklady Akademii Nauk SSSR, 151, 501–504, 1963.

Tikhonov, A. N. and Arsenin, V. Y.: Solution of Ill-Posed Problems, Wiley, New York, 1977.

Toledano, C., Wiegner, M., Groß, S., Freudenthaler, V., Gasteiger, J., Müller, D., Müller, T., Schladitz, A., Weinzierl, B., Torres, B., and O'neill, N. T.: Optical properties of aerosol mixtures derived from sun-sky radiometry during SAMUM-2, Tellus B, 63B, 635–648, doi:10.1111/j.1600-0889.2011.00573.x, 2011.

Tomasi, C., Vitake, V., and Santis, L.: Relative optical mass functions for air, water vapour, ozone and nitrogen dioxide in atmospheric models presenting different latitudinal and seasonal conditions, Meteorology and Atmospheric Physics, 65, 11–30, doi:10.1007/BF01030266, URL `http://dx.doi.org/10.1007/BF01030266`, 1998.

Torres, B.: Study on the influence of different error sources on sky radiance measurements and inversion-derived aerosol products in the frame of AERONET, Ph.D. thesis, University of Valladolid, 2012.

Turner, D. D., Ferrare, R. A., Heilman-Brasseur, L. A., Feltz, W. F., and Tooman, T. P.: Automated retrievals of water vapor and aerosol profiles from an operational Raman lidar, Journal of Atmospheric and Oceanic Technology, 19, 37–50, 2002.

Twomey, S.: On the numerical solution of Fredholm integral equations of the first kind by the inversion of the linear system produced by quadrature, Journal of the Association for Computing Machinery, pp. 97–101, 1963.

Twomey, S.: Pollution and the planetary albedo, Atmospheric Environment, 8, 1251–1256, 1974.

Twomey, S.: Introduction to the Mathematics of Inversion in Remote Sensing and Indirect Measurements, Elsevier, New York, 1977a.

Twomey, S.: The influence of pollution on the shortwave albedo of clouds, Journal of the Atmospheric Sciences, 34, 1149–1152, 1977b.

van de Hulst, H. C.: Light scattering by small particles, John Wiley, 1957.

Veselovskii, I., Kolgotin, A., Griaznov, V., Mu ller, D., Franke, K., and Whiteman, D. N.: Inversion of multiwavelength Raman lidar data for retrieval of bimodal aerosol size distribution, Applied Optics, 43, 1180–1195, 2004.

Veselovskii, I., Dubovik, O., Kolgotin, A., Lapyonok, T., Di Girolamo, P., Summa, D., Whiteman, D. N., Mishchenko, M., and Tanré, D.: Application of randomly oriented spheroids for retrieval of dust particle parameters from multi- wavelength lidar measurements, Journal of Geophysical Research, 115, doi:10.1029/2010JD014139, 2010.

Volten, H., Munoz, O., Rol, E., de Haan, J. F., Vassen, W., Hovenier, J. W., Muinonen, K., and Nousiainen, T.: Scattering matrices of mineral aerosol particles at 441.6 nm and 632.8 nm, Journal of Geophysical Research, 106, 17 375–17 401, 2001.

Wagner, J., Ansmann, A., Wandinger, U., Seifert, P., Schwarz, A., Tesche, M., Chaikovsky, A., and Dubovik, O.: Evaluation of the Lidar/Radiometer Inversion Code (LIRIC) to determine microphysical properties of volcanic and desert dust, Atmospheric Measurement Techniques, 6, 1707–1724, doi:10.5194/amt-6-1707-2013, URL http://www.atmos-meas-tech.net/6/1707/2013/, 2013.

Wagner, S. C., Govaerts, Y. M., and Lattanzio, A.: Joint retrieval of surface reflectance and aerosol optical depth from MSG/SEVIRI observations with an optimal estimation approach: 2. Implementation and evaluation, Journal of Geophysical Research, 115, doi:10.1029/2009JD011780, 2010.

Wandinger, U.: Lidar — range-resolved optical remote sensing of the atmosphere, edited by C. Weitkamp, chap. Introduction to lidar, Springer, New York, 2005a.

Wandinger, U.: Lidar — range-resolved optical remote sensing of the atmosphere, edited by C. Weitkamp, chap. Raman lidar, Springer, New York, 2005b.

Wandinger, U. and Ansmann, A.: Experimental determination of the lidar overlap profile with Raman Lidar, Applied Optics, 41, 511–514, 2002.

Wandinger, U., Mattis, I., Tesche, M., Ansmann, A., Bösenberg, J., Chaikovsky, A., Freudenthaler, V., Komguem, L., Linné, H., Matthias, V., Pelon, J., Sauvage, L., Sobolewski, P., Vaughan, G., and Wiegner, M.: Air-mass modification over Europe: EARLINET aerosol observations from Wales to Belarus, Journal of Geophysical Research, 109, 2004.

Wanner, W., Strahler, A., Hu, B., Lemis, P., Muller, J.-P., Li, X., barker Schaat, C., and Barnsley, M.: Global retrieval of bidirectional reflectance and albedo over land from EOS MODIS and MISR data: theory and algorithm, Journal of Geophysical Research, 102, 17 143–171 162, 1997.

Waquet, F., Léon, J.-F., Goloub, P., Pelon, J., Tanré, D., and Deuzé, J.-L.: Maritime and dust aerosol retrieval from polarized and multispectral active and passive sensors, Journal of Geophysical Research, 110, doi:10.1029/2004JD004839, 2005.

Welton, E. and et al.: The Micro-pulse Lidar Network (MPL-Net) / Lidar Remote Sensing in Atmospheric and Earth Sciences, in: Reviewed and revised papers at the twenty-first International Laser Radar Conference (ILRC21), pp. 285–288, Quebec, Canada,, 2002.

Welton, E. J., Voss, K. J., Gordon, H. R., Maring, H., Smirnov, A., Holben, B., Schmid, B., Livingston, J. M., Russell, P. B., Durkee, P. A., Formenti, P., and Andreae, M. O.: Ground-based lidar measurements of aerosols during ACE-2: instrument description, results, and comparisons with other ground-based and airborne measurements, Tellus B, 52, 636–651, doi:10.1034/j.1600-0889.2000.00025.x, URL http://dx.doi.org/10.1034/j.1600-0889.2000.00025.x, 2000.

Winker, D., Pelon, J., Coakley, J. J. A., Ackerman, S., Charlson, R., Colarco, P., Flamant, P., Fu, Q., Hoff, R., Kittaka, C., and et. al.: The CALIPSO mission: A global 3D view of aerosols and clouds, Bulletin of the American Meteorological Society, 91, 1211–1229, 2010.

Winker, D. M., Hunt, W. H., and McGill, M. J.: Initial perfomance assessment of CALIOP, Geophysical Research Letters, L19803, doi:10.1029/2007GL030135, 2007.

Yang, P., Liou, K. N., Mishchenko, M. I., and Gao, B.-C.: Efficient Finite-Difference Time-Domain Scheme for Light Scattering by Dielectric Particles: Application to Aerosols, Applied Optics, 39, 3727–3737, doi:10.1364/AO.39.003727, URL `http://ao.osa.org/abstract.cfm?URI=ao-39-21-3727`, 2000.

Appendix A

Article published in AMT

The following pages contain an article that describes the milestones of this Thesis and was published in Journal "Atmospheric Measurements Techniques" on 20 August 2013.

Atmos. Meas. Tech., 6, 2065–2088, 2013
www.atmos-meas-tech.net/6/2065/2013/
doi:10.5194/amt-6-2065-2013

Atmospheric Measurement Techniques
Open Access

Enhancement of aerosol characterization using synergy of lidar and sun-photometer coincident observations: the GARRLiC algorithm

A. Lopatin[1,2], O. Dubovik[2], A. Chaikovsky[1], P. Goloub[2], T. Lapyonok[2], D. Tanré[2], and P. Litvinov[2]

[1]Laboratory of scattering media, NASB – B. I. Stepanov Institute of Physics, Minsk, Belarus
[2]Laboratoire d'Optique Atmosphérique, CNRS – UMR8518, Université de Lille 1, Villeneuve d'Ascq, France

Correspondence to: A. Lopatin (anton.lapatsin@ed.univ-lille1.fr, lopatsin@scat.bas-net.by)

Received: 29 January 2013 – Published in Atmos. Meas. Tech. Discuss.: 1 March 2013
Revised: 5 June 2013 – Accepted: 10 July 2013 – Published: 20 August 2013

Abstract. This paper presents the GARRLiC algorithm (Generalized Aerosol Retrieval from Radiometer and Lidar Combined data) that simultaneously inverts coincident lidar and radiometer observations and derives a united set of aerosol parameters. Such synergetic retrieval results in additional enhancements in derived aerosol properties because the back-scattering observations by lidar improve sensitivity to the columnar properties of aerosol, while radiometric observations provide sufficient constraints on aerosol amount and type that are generally missing in lidar signals.

GARRLiC is based on the AERONET algorithm, improved to invert combined observations by radiometer and multi-wavelength elastic lidar observations. The algorithm is set to derive not only the vertical profile of total aerosol concentration but it also differentiates between the contributions of fine and coarse modes of aerosol. The detailed microphysical properties are assumed height independent and different for each mode and derived as a part of the retrieval. The GARRLiC inversion retrieves vertical distribution of both fine and coarse aerosol concentrations as well as the size distribution and complex refractive index for each mode.

The potential and limitations of the method are demonstrated by the series of sensitivity tests. The effects of presence of lidar data and random noise on aerosol retrievals are studied. Limited sensitivity to the properties of the fine mode as well as dependence of retrieval accuracy on the aerosol optical thickness were found. The practical outcome of the approach is illustrated by applications of the algorithm to the real lidar and radiometer observations obtained over Minsk AERONET site.

1 Introduction

Atmospheric aerosols are known to be important part of the complex physical–chemical processes that impact Earth's climate. Such impacts take their effects both on global and regional scales (e.g. D'Almeida et al., 1991; Charlson et al., 1992; Hobbs, 1993; Pilinis et al., 1995; Ramanathan et al., 2001; Forster et al., 2007; Hansen et al., 2011). Also, aerosol pollution affects a population's health (e.g. Jones, 1999; Harrison and Yin, 2000) and ecological equilibrium (e.g. Barker and Tingey, 1992).

In order to estimate these impacts, a large variety of methods for monitoring atmospheric aerosols were developed. Among others, remote sensing methods, both active and passive, proved to be fruitful and convenient. A number of developed and launched space instruments (e.g. Bréon et al., 2002; Winker et al., 2007) provide global monitoring of aerosol properties (e.g. King et al., 1999; Kokhanovsky et al., 2007). Observations by ground-based instruments generally provide more detailed and accurate information about aerosol properties (e.g. Nakajima et al., 1996; Dubovik and King, 2000) but cover only the local area near the observation site. In order to obtain such data at extended geographical scales, the ground-based observations are often collected within observational networks employing identical instrumentation and standardized data processing procedures. At present, there is a number of global and regional networks conducting both passive and active ground-based observations. For example, the global AERONET (Holben, 1998) and East Asian SKYNET (Nakajima et al., 2007) networks of sun photometers, as well as, a variety of lidar networks including regional EARLINET (Bösenberg, 2000), ADNET (Murayama et al.,

Published by Copernicus Publications on behalf of the European Geosciences Union.

2001), MPL-Net (Welton et al., 2002), ALiNe (Antuña et al., 2006), Cis-LiNet (Chaikovsky et al., 2006b) and a recent global lidar network GALION (Bösenberg and Hoff, 2007) have been established during the last two decades. Aerosol data collected by these networks provide valuable aerosol information that is widely used for validating satellite observations (e.g. Remer et al., 2002, 2005; Schuster et al., 2012; Hasekamp et al., 2011; Yoon et al., 2011; Kahn et al., 2010; Ahmad et al., 2010) and constraining aerosol properties in climate simulation efforts (e.g. Kinne et al., 2003, 2006; Textor et al., 2006; Koch et al., 2009).

Despite of the achieved progress in aerosol remote sensing the limited accuracy in the knowledge of aerosol properties remains one of the main uncertainties in climate assessments (Forster et al., 2007; Hansen et al., 2011). The expected improvements in the ground-based aerosol monitoring are associated with two kinds of efforts: (i) enhancement of the observation completeness by employing a variety of complimentary observational techniques and (ii) improvement of the accuracy of derived aerosol information. For example, the number of extensive multi-instrumental aerosol campaigns have been organized (e.g. Russell et al., 1999; Raes et al., 2000; Ramanathan et al., 2001; Müller et al., 2003; Papayannis et al., 2005; McKendry et al., 2007; Huebert et al., 2003; Ansmann et al., 2011a; Holben et al., 2011). In addition, the number of permanent monitoring sites equipped with several instruments is continuously increasing (e.g. Takamura et al., 1994; Waquet et al., 2005; Müller et al., 2004; Ansmann et al., 2010). In these regards, the columnar properties of aerosol derived by the photometers and aerosol vertical profiles provided by the lidars are clearly complimentary pieces of information about aerosol, both important for climatic studies. Specifically, the columnar properties are important for direct aerosol forcing estimations both on global and regional scales (Pilinis et al., 1995; Costa et al., 2004). On the other hand, the vertical structure of the aerosol is needed for accounting of the indirect effects like influence on cloud formation (McCormick et al., 1993; Bréon, 2006). The importance of obtaining simultaneous information about both columnar and vertical aerosol properties is rather evident for the scientific community, and, a substantial number of sites within ground-based networks conducting coincident lidar and photometric measurements have been established.

In addition, the accumulation of a variety of complementary data is not the only positive effect. It also helps to improve the accuracy of the obtained data and derive qualitatively new aerosol characteristics. Indeed, processing of both passive and active remote measurements relies on a set of several assumptions. For example, retrievals of aerosol columnar properties from passive methods use an assumption of the vertical distribution of aerosol. The uncertainties in this assumption may have a notable effect on the retrieval result, especially in the case of polarimetric observations. Retrievals from active sounding, on the other hand, deal with relatively limited information from the altitude profiles of the spectral backscattering and usually rely on assumptions about aerosol columnar properties. For example, information about aerosol type is usually used for constraining the lidar ratio that defines relation between aerosol backscatter and extinction. Combined with known boundary conditions, this provides missing information and allows quantitative interpretation of lidar signals and retrieval of vertical profiles of aerosol backscatter and extinction (Klett, 1981, 1985). Commonly, the lidar ratio is chosen using a priori climatological data sets. For example, processing of lidar observations from the CALIPSO spaceborne platform relies on the climatological models of lidar ratio derived by cluster analysis of the entire database of AERONET retrievals obtained for ~ 10 yr of observations (Omar et al., 2005). However, inconsistencies in the chosen lidar ratio directly propagate into derived results and may strongly affect the lidar retrievals (Sasano et al., 1985; Kovalev, 1995). The most reliable and therefore preferable approach is to define lidar ratio using coincident measurement by developing enhanced lidar capabilities or by obtaining missing information from other instruments (Ferrare et al., 1998a; Gobbi et al., 2003). For example, enhancement of lidar observation can be achieved by employing lidar systems registering combined elastic-Raman signals (Ansmann et al., 1992; Ferrare et al., 1998a,b; Turner et al., 2002; Müller et al., 2007) or by conducting high spectral resolution lidar observations (Shipley et al., 1983; Liu et al., 2002; Hair et al., 2008; Burton et al., 2012; Groß et al., 2013). Usage of approaches with non-elastic observations result in significant enhancement of the information contents in backscattering observations, which allows derivation of aerosol extinction profiles and even estimations of aerosol microphysical properties without a priori constraints on aerosol type or loading (Müller et al., 1999, 2005; Veselovskii et al., 2004). Despite of the achieved progress in non-elastic lidar technology (Baars et al., 2009; Althausen et al., 2009) the bulk of monitoring of vertical aerosol variability is conducted by the conventional lidars and the constraining of aerosol type is done using coincident airborne measurements by nephelometers (Hoff et al., 1996; Adam et al., 2004), spectrophotometers (Marenco et al., 1997) or using ground-based measurements by sun photometers (Waquet et al., 2005).

The straightforward constraining of the lidar retrievals using values of total aerosol optical thickness is a common way of utilizing coincident sun-photometer measurements for the improvement of lidar observations processing (Fernald et al., 1972; Fernald, 1984). In addition, several more sophisticated approaches of combining two types of measurements were proposed recently for exploring additional sensitivities in both lidar and photometric observations. Such methods are usually aimed not only at improving accuracy of the retrieved aerosol characteristics, but rather at retrieving qualitatively new aerosol information. For example, the most common lidar products include vertical profiles of extinction or/and concentration of aerosols that are derived using a lidar ratio fixed under some assumptions about aerosol type,

and coincident data from sun photometers could provide the required information about aerosol type. However, aerosol type may change vertically, for example, when background aerosol is mixed with layers of transported aerosols as those from desert dust or biomass burning aerosols. Ground-based radiometric data have practically no sensitivity to vertical variability of aerosol; they can only provide some indication of possible aerosol mixtures. On the other hand, spectral (sensitive to variations of aerosol sizes) and polarimetric (sensitive to particle shape) lidar measurements can trace a rather clear qualitative picture of vertical variability of aerosol properties. Utilization of such lidar data in a combination with coincident radiometric data allows some quantitative description of vertical distribution of aerosol mixtures.

Generally, information about sizes and composition of aerosol particles obtained from radiometers is used for defining a number of different aerosol components and their detailed properties (size distributions, complex refractive index and particle shape). Then lidar data are fitted using optical properties of these assumed aerosol components by searching for their vertical mixture that provides the best match of lidar data. For example, studies by Chaikovsky et al. (2002, 2004, 2006a, 2012) and Cuesta et al. (2008) used the measured spectral dependence of backscatter and extinction to derive vertical distribution of two optically distinct aerosol modes assuming that only concentrations of the each aerosol mode can change vertically. The size distributions and complex refractive indices of each aerosol component were fixed using the aerosol retrievals from AERONET radiometers. In the LiRIC (Lidar/Radiometer Inversion Code) algorithm Chaikovsky et al. (2012) assumed two mono-modal fine and coarse aerosol components with the size distributions obtained by dividing AERONET derived distribution into two using the minimum in the range of sizes from 0.194 to 0.576 µm as a separation point. The complex refractive index for both modes was assumed the same and equal to the one retrieved by the AERONET. Cuesta et al. (2008) used more complex procedure. First, the AERONET size distribution was decomposed into log-normal mono-modal distributions. Then both bi-modal size distributions of each mode and complex refractive indices were defined using available ancillary data. Ansmann et al. (2011b) used measured depolarization profiles in order to derive vertical distribution of spherical and non-spherical aerosol components with size distributions and complex refractive indices fixed from modelling. Also Sinyuk et al. (2008) have proposed retrieval of both columnar and vertical aerosol properties by inverting a combined data from coincident observations by CALIPSO satellite lidar and AERONET radiometers.

The GARRLiC (Generalized Aerosol Retrieval from Radiometer and Lidar Combined data) approach proposed in this paper pursues even deeper synergy of lidar and radiometer data in the retrievals. Indeed, the methods described above are aimed at enhanced processing of lidar data and do not include any feedback on aerosol columnar properties. At the same time, some additional sensitivity to columnar properties of aerosol compared to radiometric data is provided from lidar measurements. For example, the radiometric observations from ground do not include observation in back scattering direction. In addition, the radiation field observed by the radiometers, in particular its polarimetric properties, has some sensitivity to aerosol vertical distribution but usage of this sensitivity is practically impossible without relying on independent information about vertical variability of aerosol. Therefore, the approach proposed here is aimed to take the advantage from all sensitivities in lidar and radiometric data to both vertical and columnar aerosol properties and to combine the benefits of the most powerful approaches to combined lidar/radiometer data treatment.

2 The GARRLiC algorithm concept

Both LiRIC and GARRLiC algorithms use positive heritage of the AERONET retrieval. For example, several key elements of the statistically optimized inversion approach designed for AERONET by Dubovik and King (2000) were adapted in LiRIC. In addition, LiRIC uses the identical to AERONET model of aerosol microphysics. At the same time, LiRIC takes its roots from earlier lidar retrievals adopting some elements of the AERONET retrieval. In this regard, GARRLiC was created by direct modification of AERONET and PARASOL algorithms adapting them for inclusion of lidar data. The comparison of the mentioned algorithm inputs is given in Fig. 1. The approach for treating lidar data strongly relies on LiRIC heritage. Therefore, below we will review the key aspects of all these algorithms that are used in the GARRLiC design.

The AERONET operational retrieval is implemented successfully for more than a decade by the algorithm described by Dubovik and King (2000). It had been tested (Dubovik et al., 2000), improved and upgraded over time. For example, the following new modelling aspects have been included: (i) accounting for particle non-sphericity in aerosol scattering (Dubovik et al., 2002b, 2006), (ii) simulation of bi-directional land and ocean surface properties (Sinyuk et al., 2007), and (iii) both modelling of linear polarization and using the polarimetric measurements in the retrieval (Dubovik et al., 2006; Li et al., 2009). Years of the algorithm's exploitation has shown the possibility to provide new valuable details of aerosol properties (e.g. Dubovik et al., 2002a; Eck et al., 2005, 2012, etc.). The algorithm by Dubovik and King (2000) has been developed with the idea to achieve high flexibility in using the various observations and deriving the extended set of aerosol parameters. Specifically, the algorithm is based (see Dubovik and King, 2000; Dubovik, 2004) on multi-term LSM (least square method) that allows flexible and rigorous inversion of the various combinations of the independent multi-source measurements. As a result, the modifications of the algorithm have been used for inverting the

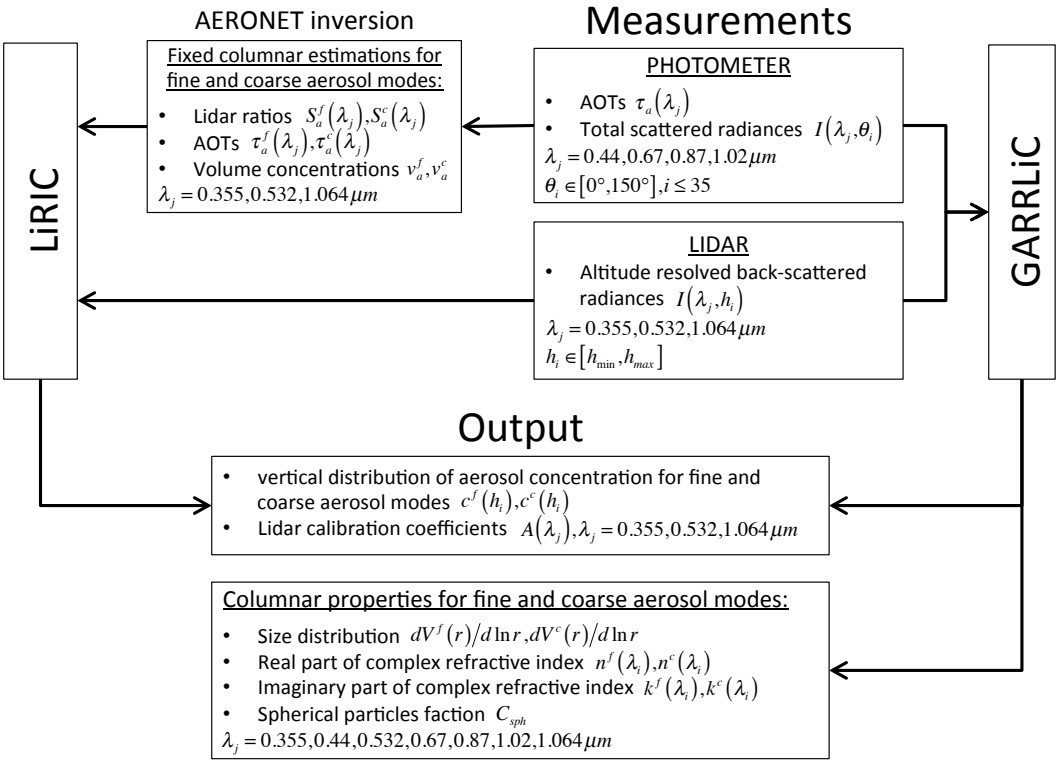

Fig. 1. Comparison of LiRIC and GARRLiC algorithms.

various combined data. For example, Sinyuk et al. (2007) used a modified algorithm for deriving both aerosol and surface properties from coincident ground-based radiometer and satellite observations. Gatebe et al. (2010) have implemented a modification for inverting the combination of the ground-based AERONET observations with the airborne observations by the photometer and up- and down-looking radiometer and derived the detailed properties of aerosol both over and under the airplane together with properties of surface reflectance. The latest modification of the algorithm has been developed by Dubovik et al. (2011) for retrieving both properties of aerosol and surface from observations of PARASOL/POLDER. This version of the algorithm generalizes and includes most of precedent modifications. Moreover, the main part of the computer routine realizing the algorithm has been significantly rewritten with the objective of the enhancing algorithm flexibility in order that it could be used in multiple applications with no or only minor modifications of the main body of the algorithm routine. The algorithm has the nearly independent modules "forward model" and "numerical inversion" (see Fig. 2) in the respect that these modules can be modified independently. Correspondingly, if a possibility of simulating a new measured atmospheric characteristic is included in the "forward model" this characteristic can be inverted with no modifications of the "numerical inversion" module in the source code. Only input parameters of the inversion program need to be changed. As a result, the algorithm by Dubovik et al. (2011) can be used with no modifications in multiple applications. For example, the same program can be used for aerosol retrieval from satellite (e.g. POLDER/PARASOL), ground-based (e.g. AERONET) or aircraft observations. In the present development we used this last version of the algorithm and modified it by adding a possibility to invert lidar observations together with passive radiometric data. With that purpose modelling of lidar observations was included in the "forward model" and the "numerical inversion" module was adapted for inverting the combined radiometer and lidar observations. The details of these modifications are described in two following sections.

3 Modifications employed in the "forward model"

The previous versions of the retrieval code (Dubovik and King, 2000; Dubovik et al., 2011) and its modifications (Sinyuk et al., 2007; Gatebe et al., 2010) were developed for inverting only passive observations by ground-based, satellite and airborne radiometers. Therefore, for the needs of the current study a possibility of modelling lidar observations was included into the "forward model" module. The diagram in Fig. 3 illustrates the concept of accounting for the aerosol vertical variability in the "forward model" module of the present algorithm. Although the concept has significant similarities with LiRIC, it has several new aspects.

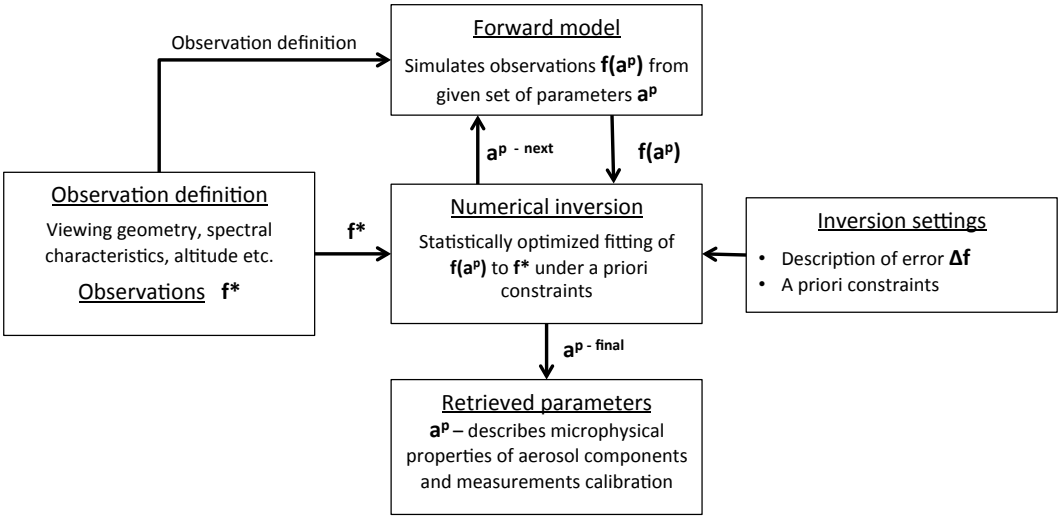

Fig. 2. General structure of the inversion algorithm.

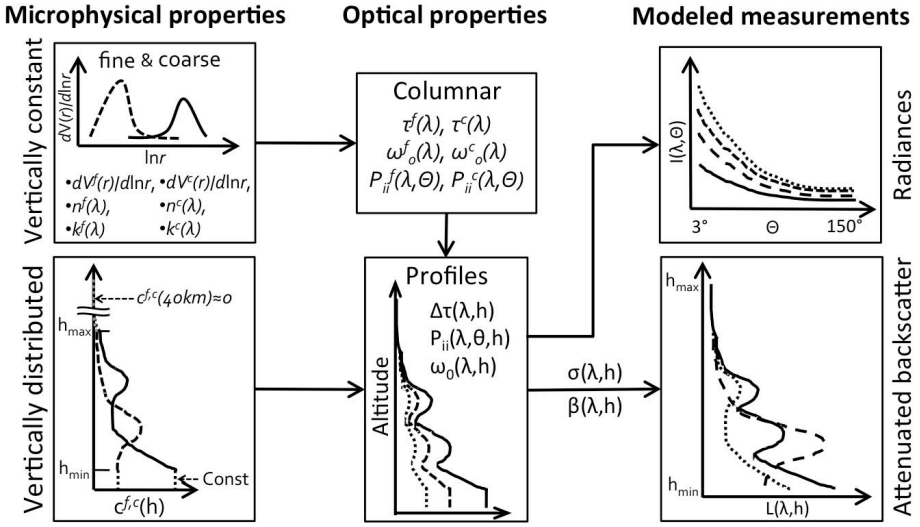

Fig. 3. General scheme of the measurements modelling using a two-component vertically distributed aerosol model.

Similarly to LiRIC, GARRLiC is designed to provide two independent vertical profiles of the concentrations of fine and coarse modes that are among the retrieved characteristics. Aerosol is described as a bi-component mixture of fine and coarse aerosol modes. The microphysical properties of each mode (particle sizes, complex index of refraction and shape) are height independent, while vertical profiles of concentrations vary with altitude. Such approach minimizes the amount of a priori estimations used in the retrieval, and it is expected to provide more detailed and accurate information about both vertical and columnar aerosol properties. In a contrast to LiRIC, in the GARRLiC model the size intervals of the modes may overlap and the size independent complex refractive index may be different for each aerosol component.

3.1 Attenuated backscatter

The attenuated backscatter $L(\lambda, h)$ measured by lidar was modelled in single-scattering approximation using the lidar equation:

$$L(\lambda, h) = A(\lambda)\,\beta(\lambda, h)\,\exp\left(-2\int_0^h \sigma(\lambda, h')\,\mathrm{d}h'\right), \qquad (1)$$

where $A(\lambda)$ is the lidar calibration parameter, $\sigma(\lambda, h)$ is the vertical profile of atmospheric extinction, and $\beta(\lambda, h)$ is the vertical profile of the atmospheric backscattering that is modelled using profiles of atmosphere single-scattering albedo $\omega_0(\lambda, h)$ and the phase function $P_{11}(\Theta, \lambda, h)$ at scattering angle $\Theta = 180°$ as follows:

$$\beta(\lambda, h) = \frac{1}{4\pi}\sigma(\lambda, h)\,\omega_0(\lambda, h)\,P_{11}\left(180^\circ\lambda, h\right). \quad (2)$$

The extinction and backscattering of the atmosphere are affected by gaseous absorption, molecular scattering and aerosol scattering and absorption:

$$\sigma(\lambda, h) = \sigma^{\text{abs}}_{\text{gas}}(\lambda, h) + \sigma^{\text{scat}}_{\text{mol}}(\lambda, h) + \sigma^{\text{ext}}_{\text{aer}}(\lambda, h), \quad (3)$$

$$\beta(\lambda, h) = \beta_{\text{mol}}(\lambda, h) + \beta_{\text{aer}}(\lambda, h). \quad (4)$$

The lidar measurements are made in window channels (0.355, 0.532 and 1.064 µm) with very minor gaseous absorption that is accounted using known climatological data. The effects of molecular scattering are also accounted by usage of climatological data. Specifically, the phase function $P^{\text{mol}}_{11}(180^\circ\lambda, h)$ of molecular scattering is constant and well known. The variability of a molecular scattering profile $\sigma^{\text{scat}}_{\text{mol}}(\lambda, h)$ over an observation site can be simulated with acceptable accuracy based on the information about site's geographical coordinates and elevation (Fleming et al., 1988, http://ccmc.gsfc.nasa.gov/modelweb/atmos/cospar1.html). However, the aerosol properties $\sigma^{\text{ext}}_{\text{aer}}(\lambda, h)$ and $\beta_{\text{aer}}(\lambda, h)$ are highly variable and cannot be modelled using climatologies. Therefore, in the "forward model" these properties are driven by the parameters included in the vector of unknowns that are retrieved during inversion. The radiometric observations both from ground and space are mostly sensitive to columnar properties of aerosol; therefore the "forward model" in the previous version of the algorithm was driven by the parameters describing these columnar properties. The aerosol was assumed as a mixture of the several aerosol components. Each aerosol component was represented by a sum of spherical and non-spherical fractions. The spherical fraction was modelled as a polydisperse mixture of the spheres. The non-spherical fraction was modelled as mixture of randomly oriented polydisperse spheroids. The distributions of particle volumes and the complex refractive indices were assumed the same in both spherical and non-spherical aerosol fractions. The extinction, absorption and scattering properties of the aerosol in the total atmospheric column were modelled as

$$\tau_{\text{ext/abs}}(\lambda) = \sum_{k=1,\ldots,N_k}\left[\sum_{i=1,\ldots,N_i}\left(c_{\text{sph}}\,\mathbf{K}^{\text{sph}}_{\text{ext/abs}}(\ldots, r_i) + \left(1 - c_{\text{sph}}\right)\mathbf{K}^{\text{ns}}_{\text{ext/abs}}(\ldots, r_i)\right)\frac{\mathrm{d}V_k(r_i)}{\mathrm{d}\ln r}\right], \quad (5)$$

$$\omega_0(\lambda)\,P_{ii'}(\Theta, \lambda) = \sum_{k=1,\ldots,N_k}\left[\sum_{i=1,\ldots,N_i}\left(c_{\text{sph}}\,\mathbf{K}^{\text{sph}}_{ii'}(\ldots, r_i) + \left(1 - c_{\text{sph}}\right)\mathbf{K}^{\text{ns}}_{ii'}(\ldots, r_i)\right)\frac{\mathrm{d}V_k(r_i)}{\mathrm{d}\ln r}\right], \quad (6)$$

where $\mathbf{K}^{\text{sph}}_{\text{ext/abs}}(\ldots, r_i)$ and $\mathbf{K}^{\text{ns}}_{ii'}(\ldots, r_i)$ are the kernels of extinction, absorption and scattering properties of spherical and non-spherical aerosol fractions (Dubovik et al., 2011). For reducing calculation time in the numerical integration of spheroid optical properties over size and shape, these kernels were arranged as the look-up tables simulated for quadrature coefficients employed as discussed in details by Dubovik et al. (2006). The calculations of kernels for non-spherical fraction were done assuming non-spherical aerosol as a mixture of randomly oriented polydisperse spheroids with the distribution of the aspect ratios fixed to the one providing the best fit to the laboratory measurements of mineral dust (feldspar sample) phase matrices by Volten et al. (2001). Such strategy of accounting for non-spherical shape of desert dust aerosol is successfully used in the operational AERONET retrieval.

It is noteworthy that the spheroid model developed by Dubovik et al. (2002b, 2006) appeared to be rather useful for other aerosol remote sensing applications. It was shown that the spheroid model allows qualitative reproduction of the main features of lidar observations of non-spherical desert dust (Cattrall et al., 2005; Schuster et al., 2012). Furthermore, Veselovskii et al. (2010), Di Girolamo et al. (2012) and Müller et al. (2013) have incorporated the spheroid model into the algorithm retrieving aerosol properties from lidar observations, which were, probably, one of the first attempts to interpret quantitatively the sensitivity of the lidar observations to particle non-sphericity. It should be noted that the studies by Müller et al. (2010, 2012) outlined some potential issues in the ability of the spheroidal model to reproduce accurately some specific features of the obtained backscattering observations. More recent comparisons of detailed Raman observations with LiRIC retrievals (based on spheroid model) by Wagner et al. (2013) and with AERONET retrieved columnar aerosol properties by Müller et al. (2013) provided notably more positive conclusions regarding the potential of using spheroids for modelling aerosol backscattering properties. Though uncertainties in interpretation of the lidar observations using spheroids exist, all above studies are in consensus that using spheroids as models of aerosol particles instead of spheres provides significant improvements in interpretation of desert dust observations. Moreover, at present, a polydisperse mixture of spheroids is the only physical model used rigorously in operational aerosol retrievals and, based on accumulated results and experience, there are numerous efforts dedicated to improving the spheroid model or identifying a more accurate alternative model.

It should be noted that Eqs. (5) and (6) are written for aerosol composed by $N_k (k = 1, \ldots, N_k)$ components, where each component has different values of complex refractive index n_k, k_k and size distribution $\frac{\mathrm{d}V_k(r_i)}{\mathrm{d}\ln r}$. Such possibility of modelling multi-component aerosol is included in the previous version of the algorithm for both inverting ground based (Dubovik and King, 2000) and satellite (Dubovik et al., 2011) observations. In principle, such assumption allows for accurate modelling of scattering by mixtures of aerosols of different types with distinctly different

indices of the refraction. Such situations often appear in reality, for example, when smoke is mixed with a transported layer of desert dust. The differentiation and retrieval of both the size distributions and the complex refractive indices for each fraction of mixed aerosol from remote sensing is highly demanded and recommended (Mishchenko et al., 2007). However, due to the limited information content of radiometric observation, realizing such retrieval is a very challenging task. For example, sensitivity studies by Dubovik et al. (2000) demonstrated and studied such retrieval in a series of numerical tests with synthetic AERONET data and found that the retrieval of bi-component ($N_k = 2$) aerosol was non-unique. Specifically, using different initial guesses the retrieval algorithm was finding several different bi-component aerosol mixtures providing an equally good fit of the observations. As a result of this feature, the operational AERONET algorithm uses the assumption of mono-component aerosol with size independent complex refractive index. Nonetheless, in the present study we use a bi-component aerosol model, where aerosol is composed by fine ($k = 1$) and coarse ($k = 2$) aerosol components with different size distributions and complex refractive indices. It is expected that a combination of the observations by ground-based radiometer with the spectral lidar observations provide sufficient information for satisfactory retrieval of bi-component aerosol mixture properties. Indeed, the spectral observations of lidar have sensitivity to mixture of aerosol layers at different altitudes. This sensitivity should help to differentiate the properties of a bi-component mixture.

The vertical variability of the atmosphere is modelled using vertical profiles of the volume concentrations $c_k(h)$ of the aerosol components under an assumption that such characteristics as size distribution, complex refractive index and particle shape of each aerosol component are vertically independent. Therefore, aerosol backscattering $\beta_{\text{aer}}(\lambda, h)$ and extinction properties $\sigma_{\text{aer}}(\lambda, h)$ can be modelled as

$$\beta_{\text{aer}}(\lambda, h) = \frac{1}{4\pi} \sum_{k=1,2} \sigma^k_{\text{aer}}(\lambda, h)\, \omega^k_0(\lambda)\, P^k_{11}\left(180^\circ, \lambda\right) \quad (7)$$

and

$$\sigma^k_{\text{aer}}(\lambda, h) = \tau_k(\lambda)\, c_k(h), \quad (8)$$

where the vertical profiles of the volume concentrations $c_k(h)$ of aerosol components are normalized to unity: $\int_0^{h_{\text{TOA}}} c_k(h)\, \mathrm{d}h = 1$.

Thus, this approach is convenient for both modelling columnar aerosol properties by Eqs. (5) and (6) and vertical lidar observations by Eq. (1).

In addition, vertical variability of aerosol may have some effect on the outgoing atmospheric radiances measured from space (Dubovik et al., 2011). This variability is accounted by solving full radiative transfer equations in the plane parallel approximation using vertically dependent optical characteristics of the atmosphere:

$$\Delta\tau_i = \Delta\tau_i^{\text{gas}} + \Delta\tau_i^{\text{mol}} + \sum_{k=1,2} \Delta\tau_i^{\text{aer},k}, \quad (9)$$

$$\omega_0(\lambda) = \frac{\Delta\tau_i^{\text{mol}} + \sum\limits_{k=1,2} \Delta\tau_i^{\text{aer},k}\, \omega_0(\lambda)}{\Delta\tau_i^{\text{gas}} + \Delta\tau_i^{\text{mol}} + \sum\limits_{k=1,2} \Delta\tau_i^{\text{aer},k}}, \quad (10)$$

$$P^i_{ii'}(\Theta, \lambda) = \frac{\Delta\tau_k^{\text{mol}}\, P_{ii'}(\Theta, \lambda) + \sum\limits_{k=1,2} \Delta\tau_i^{\text{aer},k}\, \omega_0^k(\lambda)\, P_{ii'}^{\text{aer},k}(\Theta, \lambda)}{\Delta\tau_i^{\text{mol}} + \sum\limits_{k=1,2} \Delta\tau_i^{\text{aer},k}\, \omega_0(\lambda)}, \quad (11)$$

where $\Delta\tau_i$, $\omega_0^i(\lambda)$ and $P^i_{ii'}(\Theta, \lambda)$ represent optical properties of i-th homogeneous layer of the atmosphere. It should be noted that in the AERONET retrieval algorithm (Dubovik and King, 2000) the accountancy for aerosol vertical variability is also possible. However, the sensitivity studies by Dubovik et al. (2000) show practically no sensitivity to aerosol vertical profile and, as a result, the operational AERONET retrievals are conducted under the assumption of vertically homogeneous atmosphere. The PARASOL aerosol retrieval by Dubovik et al. (2011) accounts for vertical variability of aerosol (similarly as shown in Eq. (8), and is designed to retrieve some information about aerosol vertical distribution. However, the passive radiometric and polarimetric observations from space have very moderate sensitivity to aerosol vertical variability. Therefore, vertical profiles of aerosol concentrations $c_k(h)$ in the PARASOL algorithm are approximated by the Gaussian distribution and only the median height of aerosol layer h_a is retrieved. In contrast, the profiles $c_k(h)$ in the present study are not approximated by any specific function and could have practically arbitrary shapes. Such approach is necessary for adequate modelling of lidar observations. In principle, such accurate accounting for aerosol vertical variability in radiative transfer calculations is not necessary for processing of passive observations, however, this may have some positive effects once radiometric data are combined with lidar observations, as it was done in this study.

3.2 Adjustments of the "forward model" to model lidar observations

Theoretically, the profiles $c_k(h)$ should describe the variability of aerosol at all altitudes from ground to space. However, the height range of lidar measurements has limitations. Usually ground-based lidar measurements do not cover all atmosphere altitudes and are conducted between the upper $h_{\max}$ and the lower $h_{\min}$ limits. Therefore, the vertical profiles $c_k(h)$ can be derived only between these limits and some assumptions about $c_k(h)$ for $h > h_{\max}$ and $h < h_{\min}$ should be made in order to describe the vertical distribution of aerosol in the whole atmosphere column which is required for radiative transfer calculations. Here, the aerosol over $h_{\max}$ was

Table 1. Parameters retrieved by the algorithm.

Aerosol characteristics	
$\frac{dV^k(r_i)}{d\ln r}$	($i = 1, \ldots, N_i^k$; $k = 1,2$) values of volume size distribution in size bins of k-th aerosol component
$c^k(h_i)$	($k = 1, 2$) vertical distribution of aerosol concentration of k-th aerosol component, normalized to 1
C_{sph}	Faction of spherical particles of coarse aerosol component
$n^k(\lambda_i)$	($i = 1, \ldots, N_\lambda = 7$; $k = 1, 2$) the real part of the refractive index for k-th aerosol component at every λ_i of combined lidar/photometric measurement
$k^k(\lambda_i)$	($i = 1, \ldots, N_\lambda = 7$; $k = 1, 2$) the imaginary part of the refractive index for k-th aerosol component at every λ_i of combined lidar/photometric measurement
Lidar calibration parameters	
$A(\lambda_i)$	($i = 1, \ldots, 3$) Lidar calibration coefficient at each λ_i of the lidar measurement

assumed exponentially, decreasing from $c_k(h_{\max})$ to a value close to zero (10^{-30}) on the top of the atmosphere h_{TOA}, and under $h_{\min}$ it was assumed constant and equal to the lowest estimated point $c_k(h_{\min})$ as the following:

$$c(h) = c(h_{\min}),\ h \le h_{\min}$$
$$c(h) = c(h_{\max}) \exp(-\alpha h),\ h > h_{\max}, \quad (12)$$

where α is chosen from the condition that $c_k(h_{\text{TOA}}) \to 0$.

The actual lidar observations used in the present study had an altitude range from 0.5 up to 10 km, with the altitude resolution Δh of 15 m, which provides information about aerosol backscatter properties in $N_h \simeq 600$ altitude points h_i. In order to avoid an excessively high number of the retrieved parameters in the algorithm N_h was limited to a smaller number (60). Since air density decreases exponentially and a similar scale is expected for the variability of aerosol profiles, the logarithmically equidistant ($\Delta \ln h = \text{Const}$) h_i have been chosen for describing profiles $c_k(h)$ in the algorithm.

The lidar measurements $L(\lambda, h)$ were also scaled down from $N_h \simeq 600$ to a smaller number. This decreases calculation time, and in addition, helps to decrease the effect of high frequency noise. Since the power of the laser pulse returned to a receiver decreases as square of the distance during beam propagation in the atmosphere the level of noise strongly increases with the altitude. Therefore, the decimation of lidar signals in logarithmic scale over altitude provides practically useful noise suppression. Since lidar signal is measured with constant vertical resolution ($\Delta h = \text{Const}$), the decimation in logarithmic scale results in a decrease of sampling rate with the increase of altitude. According to the Kotelnikov–Nyquist theorem (Nyquist, 1928; Kotelnikov, 1933) the lower sampling rate at high altitudes decreases the amplitudes of high frequency oscillations, which usually are attributed to noise. The described decimation method could be considered as an expanding sliding window low pass filter, allowing efficient noise suppression without loss of significant information about aerosol vertical structure.

3.3 The calibration of lidar signal

Commonly, retrievals use the attenuated backscatter (Eq. 1) normalized by attenuated backscatter at the reference altitude h_{ref}. This reference altitude is chosen from the altitudes higher than $h_{\max}$, assuming that amount of the aerosol over that altitude is negligible, i.e.

$$L(\lambda, h_{\text{ref}}) = \beta_{\text{mol}}(\lambda, h_{\text{ref}}) \times \exp\left(-2\left(\tau^{\text{aer}}(\lambda) + \int_{h_0}^{h_{\text{ref}}} \left(\sigma_{\text{gas}}(\lambda, h') + \sigma_{\text{mol}}(\lambda, h')\right) \mathrm{d}h'\right)\right). \quad (13)$$

Correspondingly if $\tau^{\text{aer}}(\lambda)$ is known the above attenuated backscattering at the reference altitude h_{ref} can be easily calculated. However, due to the high presence of noise at high altitudes the selection of the reference point remains a manual procedure that influences lidar retrievals (Kovalev and Oller, 1994; Matsumoto and Takeuchi, 1994). To address this problem Chaikovsky et al. (2004) have introduced the "calibration coefficient" $A(\lambda)$ in Eq. (1) and included this value into the set of the retrieved parameters. If the error is small $A(\lambda) \to 1$. Here we follow the same concept and derive $A(\lambda)$ together with the other unknowns (see the list of the retrieved parameters in Table 1).

4 "Numerical inversion" organization

The retrieval is organized as a multi-term LSM fitting similarly to the previous developments (Dubovik and King, 2000; Dubovik, 2004; Dubovik et al., 2011). This approach has shown to be convenient for designing efficient inversions of combined complex data sets (Sinyuk et al., 2007; Gatebe et al., 2010). This approach considers an inversion as a statistically optimized simultaneous solution of a system of several independent equations:

$$f_k^* = f_k(a) + \Delta_k\ (k = 1,\ 2,\ \ldots,\ N_k), \quad (14)$$

where f_k^* are the data from different sources; i.e. f_k^* are the estimations of the characteristics $f_k(a)$. Since these estimations are originated from different sources their errors Δ_k are independent. Correspondingly, under the assumption of the Gaussian distribution of errors Δ_k the optimum solution is provided by multi-term LSM corresponding to a minimum of the quadratic form $\Psi(a)$ defined as

$$2\,\Psi(a) = \sum_{k=1}^{N_k} \left(f_k^* - f_k(a)\right)^T \mathbf{C}_k^{-1} \left(f_k^* - f_k(a)\right) \to \min, \quad (15)$$

where $\mathbf{C}_k$ are covariance matrices of the errors Δ_k. According to the suggestion of earlier studies (Dubovik and King, 2000, etc.) the above condition can be conveniently reformulated using weighting matrices $\mathbf{W}_k = \frac{1}{\varepsilon_k^2}\mathbf{C}_k$ (ε_k^2 is the first diagonal element of $\mathbf{C}_k$):

$$2\,\Psi(a) = \sum_{k=1}^{N_k} \frac{\varepsilon_0^2}{\varepsilon_k^2} \left(f_k^* - f_k(a)\right)^T \mathbf{W}_k^{-1} \left(f_k^* - f_k(a)\right) \to \min, \quad (16)$$

where ε_0^2 is first diagonal element of $\mathbf{C}_{k=1}$ – covariance matrix of the data set corresponding to $k = 1$. Correspondingly, the contribution of each term in Eq. (16) is scaled by the ratios of error variances $\frac{\varepsilon_0^2}{\varepsilon_k^2}$. As outlined by Dubovik and King (2000) this coefficient can be considered as the Lagrange multiplier used in the constrained inversion techniques. In addition, in a case when noise properties are assumed correctly, the achieved minimum can be used for estimating ε_0^2 as

$$\left(\Psi(a)\,\varepsilon_0^2\right)_{\min} \to \varepsilon_0^2. \quad (17)$$

Additionally, in previous studies (Dubovik and King, 2000; Dubovik, 2004; Dubovik et al., 2011) the data both obtained from actual observations and from a priori knowledge are considered equally in equation system (Eq. 14). Such consideration allows convenient interpretation of a priori constraints and development of flexible retrieval formalism with use of multiple constraints. Specifically, for the convenience of interpretation of the present algorithm, the quadratic form (Eq. 16) can be represented by two terms:

$$2\left(\Psi(a)\,\varepsilon_0^2\right) = \sum_{k=1}^{N_{\text{meas}}} \frac{\varepsilon_0^2}{\varepsilon_k^2} \left(f_k^* - f_k(a)\right)^T \mathbf{W}_k^{-1} \left(f_k^* - f_k(a)\right) + \sum_{p=1}^{N_{\text{prior}}} \frac{\varepsilon_0^2}{\varepsilon_p^2} \left(s_p^* - s_p(a)\right)^T \mathbf{W}_p^{-1} \left(s_p^* - s_p(a)\right). \quad (18)$$

Here, the first group unites N_{meas} sets of independent measurements (with different level of accuracies) and the second represents a priori constraints. It unites N_{prior} sets of known a priori data sets (s_p^*) used as a priori values of characteristics $s_p(a)$. The measurements group has $N_{\text{meas}} = 5$ and includes ($k = 1$) AERONET spectral and angular measurements of atmospheric sky-radiances, ($k = 2$) AERONET spectral measurements of aerosol optical thickness and ($k = 3, \ldots, 5$) lidar spectral measurements of attenuated backscatter. Thus, compared to the AERONET retrieval (Dubovik and King, 2000) the measurement group in Eq. (18) includes additional terms corresponding to the measurements of attenuated backscatter at different wavelengths.

It should be noted that in many practical situations the observations are uncorrelated and provide equally accurate data, i.e. weighting matrices are equal to unity matrices $\mathbf{W}_k = \mathbf{I}$. Such weight matrix structure directly applicable to the passive measurements both for sky radiances and aerosol optical thickness performed at different wavelengths. However such estimations that were implied in the AERONET and POLDER retrievals are not applicable to lidar measurements, as their variances depend both on the altitude and on the wavelength. Thus the weight matrix of lidar measurement will have a form of diagonal matrix that describes relative altitude dependence of the variance for the given spectral channel:

$$\mathbf{W}_{\lambda_{...}} = \frac{1}{\varepsilon_{\lambda_{...}}^2} \begin{pmatrix} C_{\lambda_{...}}(h_{\min}) & 0 & 0 \\ 0 & \ddots & 0 \\ 0 & 0 & C_{\lambda_{...}}(h_{\max}) \end{pmatrix}, \quad (19)$$

where $\varepsilon_{\lambda_{...}}^2$ is the minimum diagonal element of covariance matrix $\mathbf{C}_{\lambda_{...}}$ whose elements are defined similar with the approach proposed for LiRIC (Chaikovsky et al., 2006a; Denisov et al., 2006; Chaikovsky et al., 2012):

$$C_{\lambda_j}(h_i) = v^2 + \frac{g^2 + q^2\,P^*\left(h_i, \lambda_j\right)}{A\,M\left(P^* - B^*\left(\lambda_j\right)\right)^2} + \frac{u^2}{\left(P^* - B^*\left(\lambda_j\right)\right)^2} + 4\alpha_1^2 + 4\alpha_2^2, \quad (20)$$

where $P^*(\lambda_j, h_i)$ is recorded during lidar measurements, $B^*(\lambda_j)$ is the background noise estimation, A is the number of lidar profiles used for the time averaging, M is the number of the lidar signal counts in the altitude-averaging interval, g is the total deviation of the dark current and noise in receiving channel, q is the index that characterizes fluctuation noise of the photo receiver and could be estimated on dark measurements of the photo-receiving module, u is the coefficient that characterizes the amplitude of synchronous noise in receiving channel, v is the non-linearity parameter; α_1 and α_2 are the relative errors of molecular optical thickness and backscatter coefficient estimations. Parameters g, q, u, and v are system dependent and estimated from testing of the lidar registration system, and parameters α_1 and α_2 are known for the used model of molecular atmosphere (Fleming et al., 1988, http://ccmc.gsfc.nasa.gov/modelweb/atmos/cospar1.html). The second group in Eq. (18) unites N_{prior} sets of known a priori derivatives of the aerosol characteristics. Specifically, we used the derivatives of retrieved size distributions $\mathrm{d}V_{f,c}(r)/\mathrm{dln}\,r$, the complex refractive indices spectral dependencies $n_{f,c}(\lambda)$ and $k_{f,c}(\lambda)$, and the vertical variability of profiles $c_{f,c}(h)$. In order to avoid

unrealistic oscillations of retrieved aerosol parameters, we assume that a priori values of s_p are zeros, i.e. $s_p^* = 0$ and Eq. (18) can be written as

$$2\left(\Psi(a)\,\varepsilon_0^2\right) = \sum_{k=1}^{N_{\text{meas}}} \frac{\varepsilon_0^2}{\varepsilon_k^2}\left(f_k^* - f_k(a)\right)^T \mathbf{W}_k^{-1}\left(f_k^* - f_k(a)\right) + \sum_{p=1}^{N_{\text{prior}}} \frac{\varepsilon_0^2}{\varepsilon_k^2}\, a\, \mathbf{S}_p^T\, \mathbf{S}_p\, a^T, \quad (21)$$

here matrix $\mathbf{S}_p$ represents coefficients for calculating finite differences used to estimate the derivatives. The explicit form of these matrices is given in Dubovik (2004) and Dubovik et al. (2011). Thus, compared to the AERONET algorithm the a priori constraint group uses limitations on the derivatives of vertical profiles of aerosol concentrations. Additionally, in the present algorithm we use the limitation on the derivatives separately for $\mathrm{d}V_{f,c}(r)/\mathrm{dln}\,r$, $n_{f,c}(\lambda)$ and $k_{f,c}(\lambda)$ for both fine and coarse modes. As a result, the algorithm used $N_{\text{prior}} = 8$ complementary a priori constraints.

It should be noted that limitations of the derivatives of the vertical profiles appears to be a rather useful and very logical approach to avoid unrealistic spiky vertical variations in profiling that is also used in the LiRIC algorithm by Chaikovsky et al. (2002). Surprisingly, such apparently natural constraining is rarely used in profiling techniques (with few exceptions: Dubovik et al., 1998; Oshchepkov et al., 2002). For example, even the cornerstone methodological studies of atmosphere profiling (e.g. Rodgers, 1976) propose limiting directly the values of profile using a priori estimations. Such approach is generally rather restrictive and can lead to the notable biases in the retrieval in the case when a priori assumed profiles are significantly different from the real ones. For example, in the aerosol microphysical applications where aerosol size distributions are retrieved from the measurements of spectral and angular scattering such approach appears to be unfruitful. Indeed, the shape and magnitudes of aerosol size distribution may strongly vary and direct restriction of its magnitude by a priori values is too restrictive. As a result, although the use of a priori estimates as a constrain in the retrieval of size distribution was proposed and tried by Twomey (1963) much earlier than in atmospheric profiling (e.g. Rodgers, 1976) it was never widely used. Instead, most of established aerosol retrieval algorithms (e.g. King et al., 1978; Nakajima et al., 1983, 1996; Dubovik et al., 1995; Dubovik and King, 2000, etc.) use the limitations of derivatives of aerosol size distribution. Such limitations are obviously more universal and do not have apparent dependence on aerosol type, loading, etc. The same property of derivatives constraining seems to be very advantageous for constraining vertical profile retrievals (as it was done in the present work).

The actual minimization of Eq. (21) in the present algorithm is performed in exactly the same way as described by Dubovik et al. (2011) for "single-pixel" retrieval scenario.

5 GARRLiC algorithm functionality and sensitivity tests

Series of sensitivity tests have been performed to verify the performance of the developed algorithm and to provide the illustration of capabilities and limitations of the algorithm to derive a set of aerosol parameters (see Table 1) from coincident lidar and sun-photometer observations.

The sensitivity tests had been designed to conform with realistic conditions of each of the measurements. The tests were carried out for two cases representing situations when desert dust is mixed with urban pollution and biomass burning aerosols. Six different scenarios were considered for the each mixture. Among them 3 scenarios were performed for high aerosol loading with total AOT of $\tau_a^{0.532} = 1$ and 3 with very low AOT of $\tau_a^{0.532} = 0.05$ at $\lambda = 0.532$ µm. These two situations where chosen from the following considerations. At the high aerosol loading we expect that synergetic retrieval would maximally benefit from information from radiometric observations, while at very low AOT, the lidar data should provide maximum benefits. Indeed, the accuracy of AERONET retrievals is generally higher at high aerosol loading and significantly falls at very low AOT (Dubovik et al., 2000). In contrast, the lidar data remain reliable even at low aerosol loadings. For both high and low aerosol loading cases, three different cases of fine/coarse mode partition were modelled: $\tau_f/\tau_c = 4$, $\tau_f/\tau_c = 1$ and $\tau_f/\tau_c = 0.25$. Thus, resulting in six mixture scenarios: $\tau_f = 0.8$, $\tau_c = 0.2$, $\tau_f = \tau_c = 0.5$, $\tau_f = 0.2$, $\tau_c = 0.8$ and $\tau_f = 0.04$, $\tau_c = 0.01$, $\tau_f = \tau_c = 0.025$, $\tau_f = 0.01$, $\tau_c = 0.04$ correspondingly.

For each of the six scenarios, two series of the tests were made: (i) tests to estimate the sensitivity to random noise were made without any noise added and with random noise added to the simulated measurements, and (ii) tests to illustrate the possible improvements introduced by using both radiometric and lidar measurements in comparison with the standard AERONET inversion.

5.1 Description of aerosol and noise models used for sensitivity study

Two log-normal size distributions were used to generate 25 size bins (10 for fine and 15 for coarse aerosol modes). To make the size distributions directly comparable with actual AERONET observations the values of the generated bin radii were chosen corresponding to the ones of the standard AERONET retrieval. The values used to model size distributions of fine and coarse modes (see Table 2) were taken from the AERONET retrieval climatology corresponding to desert dust and biomass-burning aerosols (Dubovik et al., 2002a).

The values of complex refractive indices at $\lambda = 0.44$, 0.67, 0.87 and 1.02 µm for "urban pollution", "biomass burning" and "desert dust" aerosol models were adapted from actual long-time observation statistics over the GSFC

Table 2. Parameters of log-normal distributions used for aerosol size distribution modelling.

Aerosol mode	r_{min}, µm	r_{max}, µm	r_{mean}, µm	r_{std}	τ, $(\tau_{total} = 1)$	τ, $(\tau_{total} = 0.05)$
Fine	0.05	0.576	0.148	0.4	0.8, 0.5, 0.2	0.04, 0.025, 0.01
Coarse	0.355	15.0	2.32	0.6	0.2, 0.5, 0.8	0.01, 0.025, 0.04

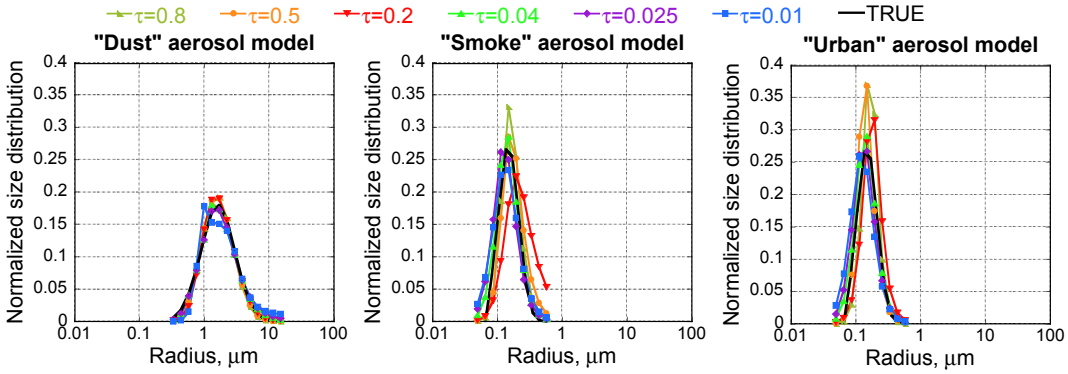

Fig. 4. Retrievals of size distributions of "Dust", "Smoke" and "Urban" aerosol models under different AOT.

(Goddard Space Flight Center), Banizombou and Solar Village AERONET sites correspondingly, where the listed types of the aerosols usually dominate in aerosol load (Dubovik et al., 2002a). The values for spectral channels $\lambda = 0.355$, 0.532 and 1.064 µm corresponding to lidar measurements were obtained by the extrapolation.

Each of the aerosol components was modelled as a mixture of polydisperse spheres and spheroids following Eqs. (5) and (6) with faction of spherical particles (C_{sph}) of 10 %, the faction of non-spherical particles was 90 % correspondingly. The same C_{sph} for coarse and fine aerosol modes was chosen due to the limited sensitivity of the measurements to the shape of smaller particles.

Two scenarios with clear vertical separation of fine and coarse aerosol components were used. The fine mode was assumed to represent the background aerosol with specific vertical distribution, while coarse mode distribution had a thick layer approximately at 3 km. Both modes had a significant amount of aerosol in the layers close to the ground and monotonous decrease over the altitude. Such distributions were chosen to mimic the particularities of aerosol vertical distribution usually found in the real lidar observations.

The values of the complex refractive indices, size distributions as well as vertical distribution profiles of the aerosol models could be found marked as "TRUE" in Figs. 4–9.

To model realistic measurement conditions the random normally distributed noise was added to the generated measurements. The variance of noise in optical thickness measurement was set as 0.005, and the variance of noise in scattered irradiance was chosen as 3 %, i.e. $\frac{\Delta I}{I} = 0.03$; spectral and altitude dependent variances of lidar measurements were defined as

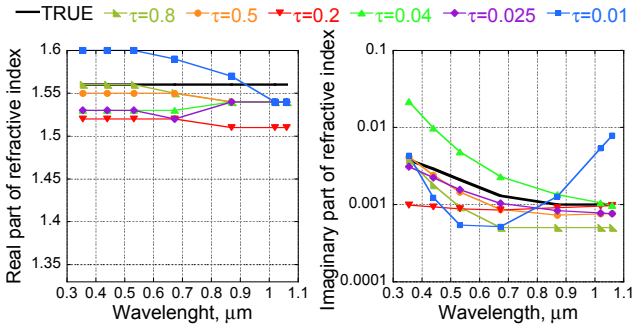

Fig. 5. Retrievals of complex refractive index of the "Dust" aerosol model under different AOT.

$$\frac{\Delta L(\lambda, h)}{L(\lambda, h)} = \varepsilon(\lambda) n(h), \tag{22}$$

where $\varepsilon(\lambda) = 0.2$, 0.15 and 0.1 for $\lambda = 0.355$, 0.532 and 1.064 µm, correspondingly, and vertical dependence was set as the following function:

$$n(h) = 1, \ \log(h) < 1,$$
$$n(h) = \log(h), \ \log(h) \geq 1. \tag{23}$$

Using the above described microphysical model the synthetic AERONET and lidar measurements were simulated and then inverted. The results were compared with the "assumed" properties.

5.2 Sensitivity test results

The discussion of the sensitivity study results will focus on the retrievals of the aerosol properties that were not part of

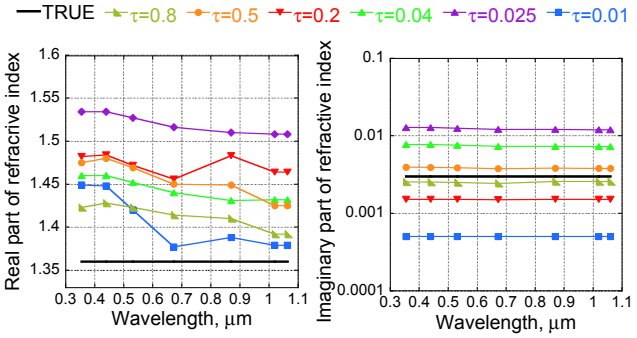

Fig. 6. Retrievals of complex refractive index of the "Urban" aerosol model under different AOT.

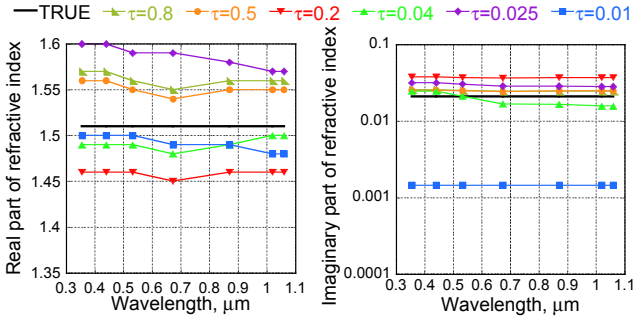

Fig. 7. Retrievals of complex refractive index of the "Smoke" aerosol model under different AOT.

the standard AERONET inversion. Specifically, we will pay particular attention to the retrieval of aerosol vertical profiles and differentiation between the properties of fine and coarse aerosol mode parameters including complex refractive indices, size distributions, etc. The results of the sensitivity tests are presented in Figs. 4–9. These results show that the algorithm derives all aerosol parameters with good accuracy, and clearly distinguishes both aerosol modes. The addition of the realistic random noise did not dramatically affect the retrieval results, although once noise is added the retrieval results depart further from the "assumed" values. In addition, we would like to note that the accuracy of aerosol size distribution retrieval is not discussed here. The results of our sensitivity tests show generally very similar tendencies as observed in earlier studies by Dubovik et al. (2000). However, Fig. 4 shows the retrievals of size distributions of aerosol components under different aerosol loads in the presence of random noise for a more descriptive presentation of the sensitivity study.

Figures 5–7 show the retrievals of aerosol complex refractive indices of each aerosol component under noisy conditions performed for six different AOTs and obtained for two aerosol mixtures listed above. As it is seen in Figs. 5–7, the method shows higher accuracy of columnar property retrieval in the cases with higher aerosol loadings. A similar tendency is observed for the retrieval of vertical profiles.

Another observed trend is that the accuracy of the retrievals of complex refractive index for each aerosol mode strongly correlates with the contribution of this mode to the signal. Specifically, the two following tendencies are observed. First, the higher relative contribution of the aerosol mode into the total optical thickness the better is the accuracy in the retrieval of the optical properties of this aerosol mode. Second, the retrieval error of the refractive index increases from shorter wavelengths to longer ones for the fine mode. The tendency for the coarse mode is opposite. Such behaviour could be explained by the fact that the efficiency of scattering by small particles reaches the maximum values when the size parameter is comparable with the wavelength, thus scattering of small particles is more pronounced at the short wavelengths, and scattering of the big particles is more pronounced at long ones.

Figure 8 illustrates that a similar tendency is observed for the retrievals of single-scattering albedo. This trend is especially evident in the situations with low total AOT and when of one of the components dominates. As can be seen in Fig. 8, in such situation retrieval errors of the properties of minor aerosol mode become unacceptably high. This leads to incorrect separation of the total single-scattering albedo between these two aerosol components at shorter wavelengths. The retrievals of total single-scattering albedo depend on the total optical thickness similarly as observed by Dubovik et al. (2000). The scenario with high total AOT and equal partition between the modes is the most favourable for overall retrieval.

Figure 9 shows the retrievals of vertical distributions. As can be seen from these plots the algorithm gives generally adequate vertical profiles for both modes. At the same time, it tends to slightly overestimate the amount of the fine mode and to underestimate coarse mode content in the layers that contain the mixture of aerosols of both types. However, the algorithm always provides adequate total extinction estimations for the given layer.

This tendency remains even in noise free conditions, yet having less drastic scales. It probably can be explained by insufficient information content for the perfect separation of fine and coarse mode contributions to the total lidar signal in the mixed layers.

Another tendency observed in the sensitivity study is lower sensitivity of the retrieval to the properties of the fine mode, especially to the complex refractive index. These high errors in derived complex indices of refraction propagate to the estimations of other optical properties of fine mode. The trend is less pronounced in situations with high aerosol loading in noise free conditions. Figure 10 showing the dependence of lidar ratios of fine and coarse modes on the complex refractive index for particles of different shape indicates that the fundamental reason for this feature is a selective sensitivity of the lidar measurement to the optical properties of the particles of different size and shape. Values of lidar ratios

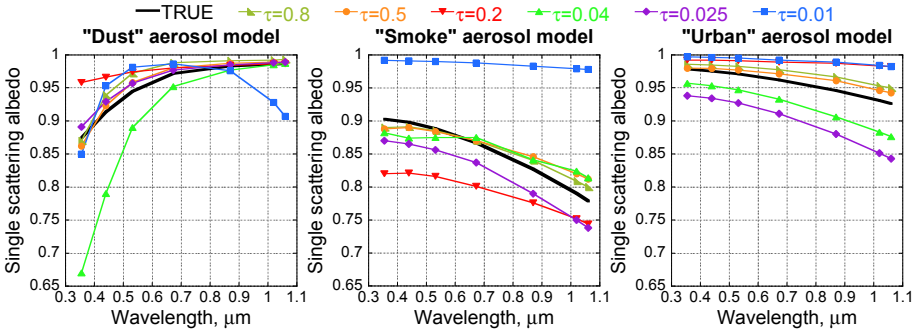

Fig. 8. Retrievals of the single-scattering albedo of aerosol components under different AOT.

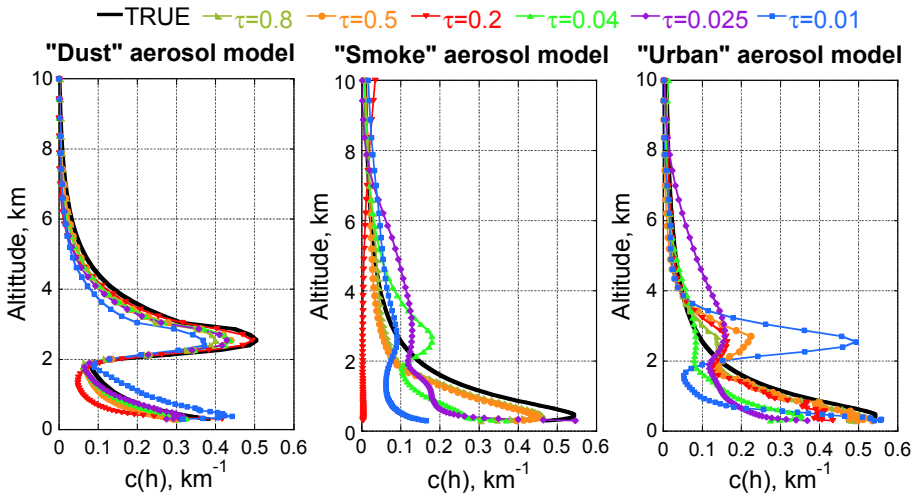

Fig. 9. Retrievals of the vertical distributions of aerosol components under different AOT.

depicted in Fig. 10 were retrieved using size distributions mentioned in Table 2 with corresponding optical thickness of $\tau_f = \tau_c = 0.5$. To retrieve the lidar ratios of spherical and non-spherical particles parameter C_{sph} was set to 100 and 0 % correspondingly. Values of the fixed parts of the complex refractive index were set as 0.05 for the imaginary part and 1.55 for the real part, for the cases with changing real and imaginary parts correspondingly. Specifically, Fig. 10 indicates that lidar ratio of the fine mode is less affected by the changes in refractive index compared to the coarse mode. This could be explained by smaller sensitivity of light scattering to the particle shape of the fine mode that is well illustrated in Fig. 10, showing stronger dependence of the lidar ratio on complex refractive index for the spherical particles of coarse mode. Therefore, since lidar measurements are sensitive mainly to the lidar ratio, lidar measurements do not provide significantly new information about the refractive index of fine mode.

Also, at shorter wavelengths the high molecular scattering reduces the aerosol contribution to the lidar signal. This also leads to a decrease of the sensitivity to the fine mode aerosol properties, as it was seen in Figs. 5–8, since a significant part of the information about fine fraction relies namely on shorter wavelengths.

It should be noted that a number of studies (Mishchenko et al., 2000, 2004; Dubovik et al., 2006) indicate high sensitivity of polarimetric passive measurements to the refractive index of the fine mode. Therefore, usage of radiometers with polarimetric capabilities could potentially result in better retrievals of the aerosol parameters of the fine mode.

5.3 Improvements introduced by joint inversion of lidar and AERONET

A synergetic handling of coincident radiometer and lidar data is obviously beneficial for the acquisition of improved vertical characterization of aerosol. The processing of lidar data always relies on assumptions about some aerosol properties. Obtaining this missing information from a nearby radiometer is evidently preferable to a simple assumption of these properties from climatologies. Therefore, the positive influence of the radiometer data on the lidar retrievals was emphasized in a number of previous studies (Chaikovsky et al., 2006c; Cuesta et al., 2008). However, all previous radiometer/lidar

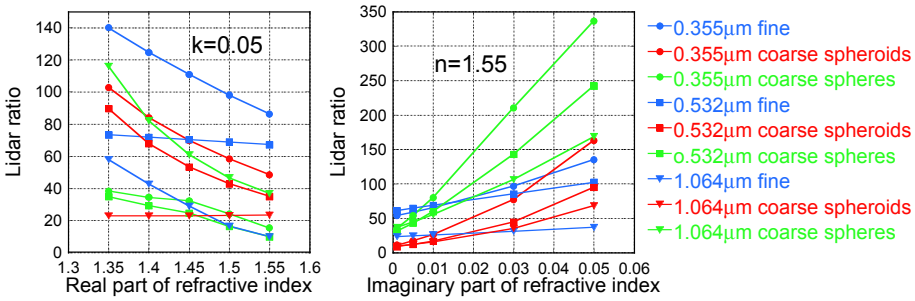

Fig. 10. Dependence of lidar ratio of fine and coarse modes on complex refractive index and particle shape.

synergy approaches used AERONET retrievals in the form of a priori assumptions for improving lidar retrievals. GARRLiC is the first development trying to explore the possibility of improving AERONET retrieval by using extra information of co-located lidar observations. The possibility to distinguish indices of the refraction of fine and coarse particles is one of the most significant innovations proposed by GARRLiC, since it was not achievable using only AERONET data as shown in studies by Dubovik et al. (2000). The results of sensitivity tests presented in a previous section showed the achievable levels of retrieval accuracy of the complex refractive index using both lidar and radiometer data. At the same time, it is clear that the lidar data provide additional information about aerosol properties because of high sensitivity of lidar data to aerosol lidar ratio. Therefore, in order to provide additional illustration of the positive effect from using lidar data on aerosol columnar properties, we analyse the changes in accuracy of the retrieval of lidar ratios by adding lidar data to AERONET observations. Also, any improvement in lidar ratio estimations brings straightforward enhancements in the retrieval of vertical profiles of aerosol concentrations.

With a purpose to access and illustrate the possible improvements in the retrieval of aerosol columnar properties, an additional scenario was added to the sensitivity study: inversion neglecting the measurements provided by lidar. Figure 11 shows the comparisons of errors of lidar ratio retrievals conducted for the AERONET data only and for a combination of AERONET and lidar. The lidar ratios were derived from size distributions that could be found in Fig. 4 for the "Urban" + "Dust" aerosol mixture with corresponding optical thickness of 0.8/0.2 and 0.2/0.8. The results demonstrate that joint retrieval allows more accurate retrievals of lidar ratio for both aerosol components in such challenging cases when one mode dominates in optical thickness. In such cases retrieval without lidar measurements tends to estimate all properties of both modes close to those of dominating one, leading to dramatic errors in lidar ratio estimations. The errors of the retrieval of the dominating mode lidar ratio remain almost the same for both inversion strategies. These results lead us to conclude that supplementing radiometer data by lidar observations helps to improve the retrieval of aerosol properties of minor mode in the aerosol

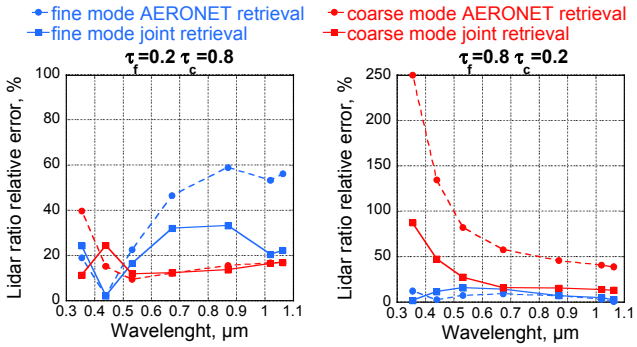

Fig. 11. Retrieval errors of lidar ratio with and without accountancy for lidar data.

mixture. Consequently, the retrieval of the vertical profile of the minor mode concentration also should be more accurate compared to the retrievals by the approaches of Chaikovsky et al. (2006c) and Cuesta et al. (2008) which assume lidar ratios from the AERONET retrievals.

Also, based on the observations made in Fig. 10, i.e. that lidar ratio is very sensitive to the retrieval accuracy of spherical particles faction, we have evaluated the possible improvements in the retrieval of this parameter by using joint inversion of AERONET and lidar data.

Table 3 summarizes the relative errors in retrieval of this parameter for three cases of aerosol with different partition of aerosol modes. The results were obtained for high aerosol load within three inversion scenarios: the joint inversion of radiometer and lidar data without any noise added; the joint inversion with random noise added to the data and the inversion of radiometer data only with random noise added to the observations. Although without information about polarization the sensitivity to this parameter is quite low and depends on aerosol optical thickness, the fact that backscatter depends on this parameter (see Fig. 10) allows decreasing retrieval errors in the situations when coarse mode dominates in optical thickness. As it is seen in Table 3, the absence of lidar data in the presence of the random noise makes accurate GARRLiC retrieval of this parameter impossible even in a situation with significant amount of coarse mode, while in the presence of

Table 3. Relative errors of spherical particle faction retrieval.

$\frac{\tau_c}{\tau_f}$	τ_f	τ_c	AERONET + lidar no noise	AERONET noise added	AERONET + lidar noise added
0.25	0.8	0.2	0.99	1.00	0.98
1	0.5	0.5	0.28	0.99	0.99
4	0.2	0.8	0.02	0.89	0.03

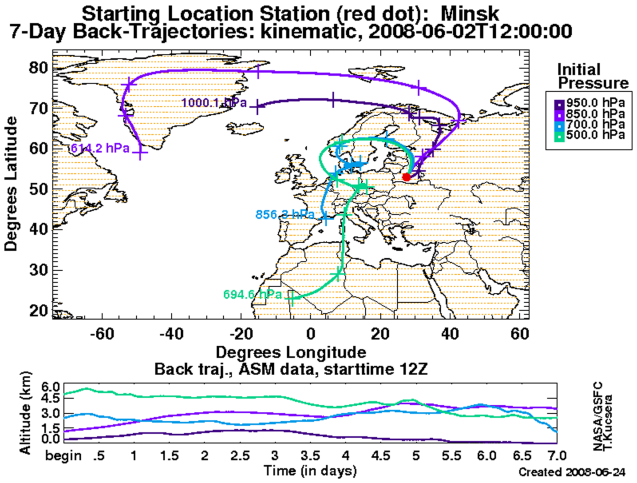

Fig. 12. Air mass back trajectories for the Minsk measurement site on 2 June 2008.

lidar data, sensitivity to this parameter remains for the same case of aerosol load.

The decrease of the retrieval error with growth of the coarse mode concentration is explained by higher sensitivity of the measurements to the shape parameters of bigger particles.

The analysis of test results allows us to conclude that, being supplied with sufficient measurement information, the combined inversion could provide deep synergy of two different types of aerosol remote sensing, resulting in more accurate and qualitative retrievals compared to the single instrument inversions.

6 GARRLiC applications to real lidar/sun-photometer observations

The algorithm has been applied to lidar/sun-photometer measurements collected at the observation site of the Laboratory of Scattering Media at the Institute of Physics, Minsk, Belarus. The station is equipped with the standard AERONET sun photometer and several multi-wavelength lidars that provided measurements of attenuated backscatter at 0.355, 0.532 and 1.064 µm.

Parameters that characterize noise (Eq. 20) in these lidar systems were estimated as shown in Table 4.

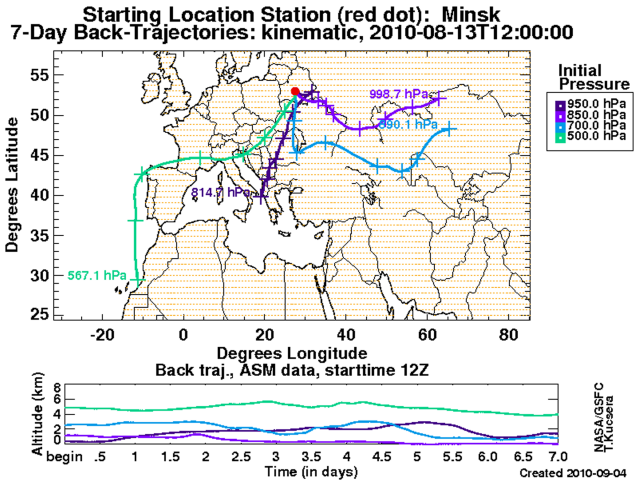

Fig. 13. Air mass back trajectories for the Minsk measurement site on 13 August 2010.

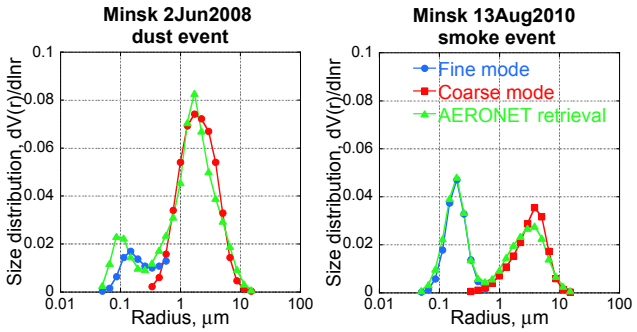

Fig. 14. Retrieved aerosol size distributions.

Two typical situations were chosen to illustrate the inversion results: (i) the observation of dust outburst from the Sahara transported over Minsk on 2 June 2008 and (ii) observation on 13 August 2010 of smoke plum transported from Russian forest fires over eastern Europe. The total optical thicknesses for these cases were $\tau_{440} = 0.36$ and $\tau_{440} = 0.46$ correspondingly. Figures 12 and 13 show the atmosphere back trajectories provided for Minsk AERONET site (http://croc.gsfc.nasa.gov/aeronet/, Schoeberl and Newman, 1995; Pickering et al., 2001) for these cases. The analysis of these back trajectories illustrates that air masses from mentioned regions should be present over Minsk during measurement periods.

Figures 14 and 15 present the retrieved aerosol columnar microphysical properties and Figs. 17 and 18 show the retrieved columnar optical parameters all in comparison with standard AERONET retrievals for this site. Figures 16 and 19–21 present the retrieved vertical profiles of microphysical and optical aerosol properties. Figure 22 is dedicated to qualifications of the vertical retrievals, presenting

Table 4. Parameters of noise estimations for the lidar system.

Parameter	v	g	q	u	α_1	α_2
Value	10^{-5}	10^{-4}	10^{-1}	1	10^{-1}	10^{-3}

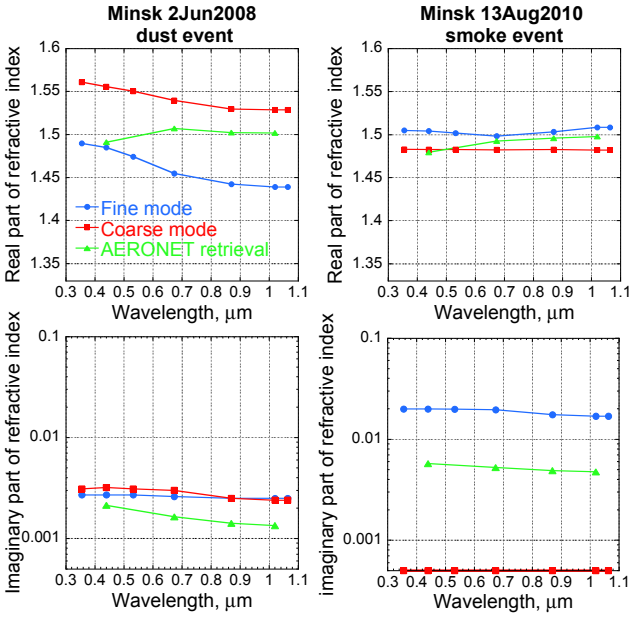

Fig. 15. Retrieved aerosol complex refractive indices.

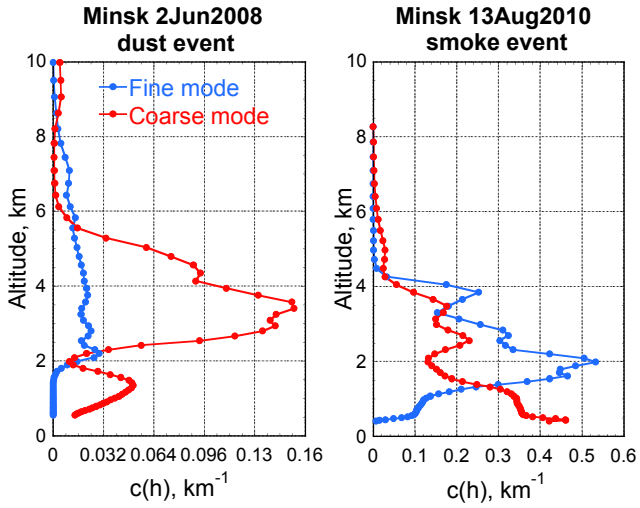

Fig. 16. Retrieved vertical concentration profiles.

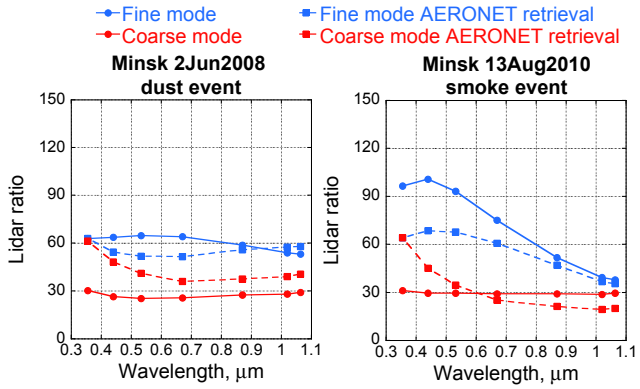

Fig. 17. Retrieved aerosol lidar ratios.

the comparison of GARRLiC results with LiRIC retrievals made for the same measurements.

The retrieved size distributions (Fig. 14) are consistent with the expectations for observed aerosol types: domination of fine mode for smoke and of coarse mode for desert dust. Both retrievals show good agreement with AERONET retrievals. The difference in the fine mode retrievals between the two methods in the dust observation case could probably be explained by lower sensitivity of the AERONET inversion to minor aerosol modes. Observed size shift in the favour of larger particles for both cases could be explained by influence of the lidar data on the retrieval.

The retrieved refractive indices (Fig. 15) are clearly distinguished between modes and are coherent with the values expected for these aerosol types: highly absorbing fine mode for smoke, and the real part of the refractive index for coarse mode close to the observations of this parameter for dust (Dubovik et al., 2002a). Since, the AERONET retrieval does not discriminate the refractive index of the modes, the AERONET derived values cannot be compared directly to the GARRLiC retrieval. Nonetheless, it is clear that there is logical agreement between two retrievals since the AERONET derived refractive indices are generally in the middle between values of fine and coarse modes obtained by GARRLiC. Two trends observed in the retrievals of the imaginary part of refractive indexes should be outlined: high absorption of the fine particles in the dust case and very low absorption of the coarse particles for the smoke case (see bottom panels in Fig. 15). Such retrievals could be explained by very low optical thickness of the minor modes ($\tau_f = 0.19$ for the dust case and $\tau_c = 0.04$ for the smoke case). As it was demonstrated by the sensitivity study, such low contributions of the minor modes could lead to high estimation errors in their complex refractive index.

The vertical distributions of fine and coarse modes (Fig. 16) clearly discriminate the vertical structure of the aerosols of different types. Both retrievals agree well with back-trajectory analysis: according to Figs. 12 and 13, the atmospheric layer from the region of forest fires was expected at the altitude of about 2 km, and the layer from the Sahara was expected at around 4 km.

Retrievals of lidar ratios shown in Fig. 17 demonstrate notable differences between the AERONET and GARRLiC values. The main difference is located at shorter wavelengths. These differences are probably caused by the significant differences in the sensitivities of both data sets, and by the

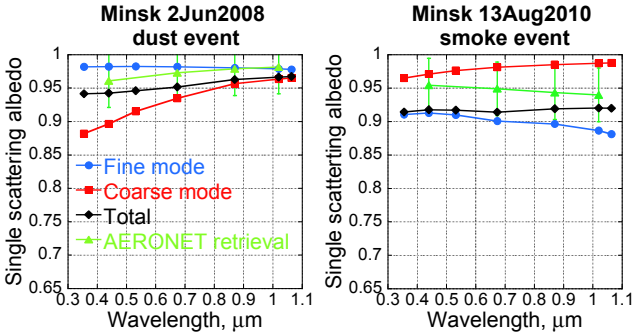

Fig. 18. Retrieved aerosol single-scattering albedo.

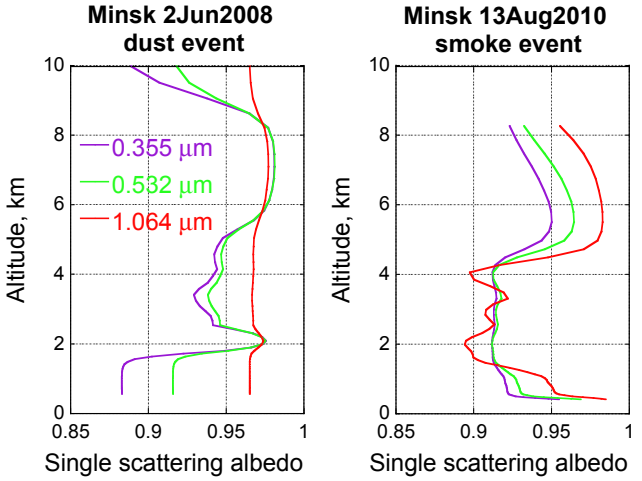

Fig. 19. Retrieved vertical profiles of aerosol single-scattering albedo.

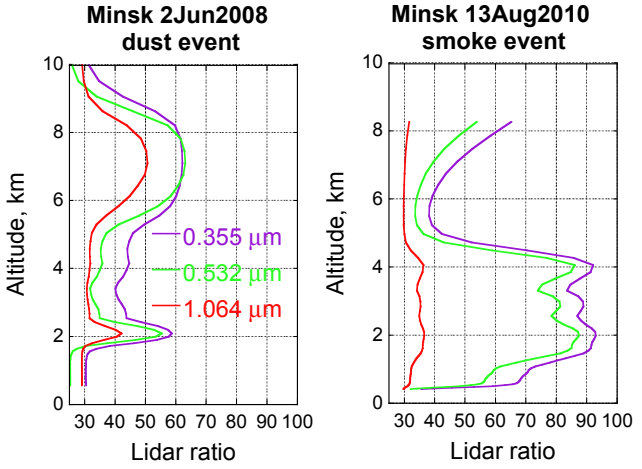

Fig. 20. Retrieved vertical profiles of aerosol lidar ratio.

differences in assumptions. Specifically, the AERONET radiometer does not include observations in backscattering direction, and assumption of size independent refractive index may also result in an additional error in the lidar ratio estimation.

The spherical particles faction retrieved for these two cases gave 40 % of spherical particles for the smoke event and 25 % for the dust event, compared to the 99 and 2 % from the AERONET retrievals. This difference can be explained by high sensitivity of the lidar measurements to backscatter from non-spherical particles (see Dubovik et al., 2006 and Fig. 10).

Figure 18 illustrates the retrievals of columnar single-scattering albedo (SSA). The total (i.e. mixture of fine and coarse) SSA shows good agreement with AERONET retrievals, climatological (Dubovik et al., 2002a) and observed (Toledano et al., 2011) values. Both spectral dependencies of smoke and dust single-scattering albedos were retrieved. The total single-scattering albedo is closer to the value of the dominating aerosol mode for both retrievals. This also could be explained by low contributions of the minor modes to the total optical thickness and higher absorption estimations of the dominating aerosol components.

Figures 19–21 demonstrate the vertical distributions of single-scattering albedos, lidar ratios and extinction calculated using retrieved parameters at the wavelengths of lidar measurements. All distributions have a noticeable vertical structure that agrees with the retrieved vertical distributions of aerosol concentrations. The values of single-scattering albedo (see Fig. 19) at all single layers are in the ranges of typical values for dust and smoke aerosols (e.g. Toledano et al., 2011). The retrieved lidar ratios (Fig. 20) are in the ranges of values for dust and smoke aerosols given by Dubovik et al. (2002a) and Cattrall et al. (2005). These values, however, are lower than the assumptions for dust particles given by Schuster et al. (2012), Groß et al. (2011) or by Tesche et al. (2009, 2011). The lower lidar ratios in this case could have been caused by contamination of the pure dust layers during the long-range aerosol transport depicted in Fig. 12. Strong spectral dependence of the smoke lidar ratio observed in Fig. 20 illustrates the fact that IR (infrared) light has less pronounced scattering on the smoke particles than light at the shorter wavelengths.

It should be noted, that the particular behaviour of profiles in Figs. 19 and 20 at higher altitudes could be explained by a very small amount of the aerosol present in the upper atmosphere layers and very weak signal returned from this altitude range.

Figure 22 is aimed to demonstrate the consistency between the LiRIC and GARRLiC retrievals in a case where no differences are expected. Both algorithms provide two distinct vertical concentration profiles for different aerosol components and the comparison of profiles retrieved by GARRLiC and LiRIC was made. The main difference is that GARRLiC modifies the retrieved columnar properties of aerosol. In addition, GARRLiC uses a bi-component aerosol model that may have different complex refractive indexes. This assumption affects estimations of lidar ratios for each mode and

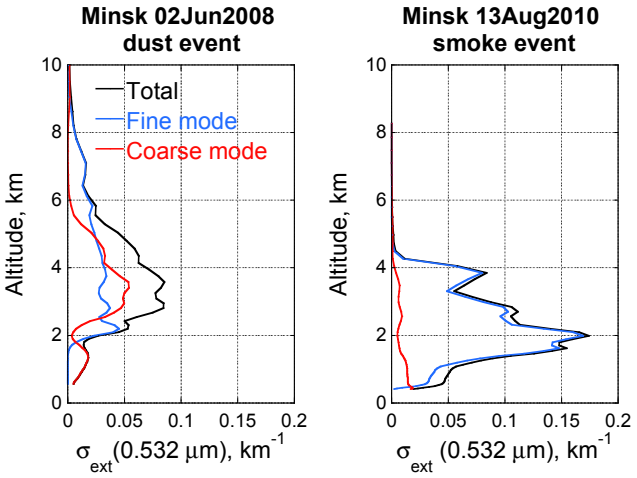

Fig. 21. Retrieved vertical profiles of aerosol extinction.

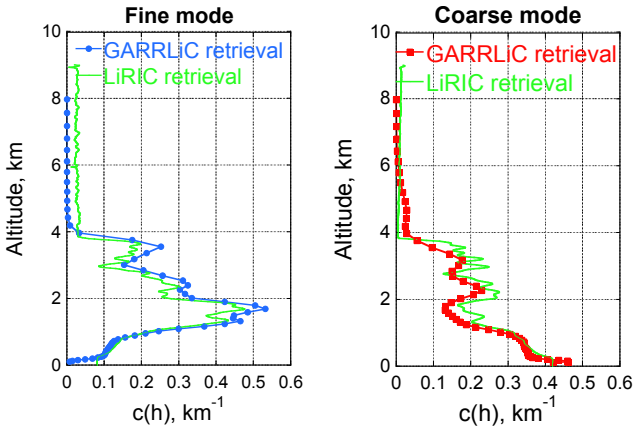

Fig. 22. Comparison of the retrieved vertical profiles with LiRIC inversion for observations on 13 August 2010.

therefore affects the retrieved vertical profiles. Therefore, the demonstration of LiRIC and GARRLiC codes consistency has been performed using the case with small difference in complex refractive indices of fine and coarse aerosol modes (see Fig. 15).

Figure 22 shows vertical distributions retrieved by GARRLiC compared with the results of the LiRIC inversion (Chaikovsky et al., 2012) made for the same measurement set during a smoke event. Both retrieved profiles are in good agreement. The minor differences could be explained by the smaller amount of altitude layers in the GARRLiC retrieval and differences in lidar ratio estimations for both modes. Therefore, in situations when the usage of the same values of complex refractive indices for both aerosol modes could be justified, these two methods should provide similar results, demonstrating the succession of the newer method. We have observed that in less favourable situations the AERONET estimates of the lidar ratio for aerosol components can show more significant deviations compared with the ones retrieved by GARRLiC, thus affecting the retrievals of vertical concentration profiles more drastically.

Thus, the results of GARRLiC application to the real data and their comparisons to the AERONET and LiRIC retrieval results showed an encouraging agreement for both columnar and vertical properties of aerosol. At the same time, the GARRLiC retrieval differentiates between columnar optical properties of fine and coarse modes of aerosol relying on additional information contained in lidar observations.

7 Conclusions

This paper has discussed in detail a concept for a new GARRLiC algorithm developed for deriving detailed properties of two atmospheric aerosol components from coincident lidar and photometric measurements. The algorithm is developed using the heritage of the AERONET, PARASOL and LiRIC algorithms. The algorithm is designed to invert the coincident observations of the CIMEL sun/sky photometer that registers direct and scattered atmospheric radiation at four wavelengths in up to 35 directions and multi-wavelength elastic lidar that registers backscattered radiation at three wavelengths in up to 1000 altitude layers. The algorithm derives an extended set of parameters for both columnar and vertical aerosol properties, including aerosol sizes, shape, spectral complex refractive index for both fine and coarse aerosol modes, as well as vertical profiles of mode concentrations.

The concept of the algorithm is aimed to achieve a higher accuracy in the retrieval, since in such an approach the solution usually relying only on passive measurement of the radiometer is benefiting from information contained in coincident active observations by lidar, and this method uses a smaller number of assumptions about aerosol. This paper provides a detailed description of the full set of formulations necessary for realizing this concept.

The performance of the developed algorithm has been demonstrated by application to both synthetically generated and real coincident sun-photometer and lidar observations. First, a series of sensitivity tests were conducted by applying the algorithm to the synthetic sun-photometer and lidar observations for the cases of aerosol mixtures containing desert dust with urban pollution and biomass burning aerosols. The simulations were designed to mimic the observations of real aerosol. With this purpose, aerosol models derived from the AERONET observations at Solar Village (Saudi Arabia), African savanna (Zambia) and the GSFC (Greenbelt, MD) were used to generate synthetic proxy measurements, both photometric and both photometric and lidar. The data were perturbed by random noise before applying the retrieval algorithm. The results of the tests showed that the complete set of aerosol parameters for each aerosol component can be robustly derived with acceptable accuracy in all considered situations. Lower estimation errors for lidar ratios of the aerosol components compared to the AERONET

retrievals were achieved. The better accuracy was observed for the higher aerosol load.

In addition, the GARRLiC algorithm was applied to coincident lidar and sun-photometer observations performed at Minsk (Belarus) AERONET site. The comparison of the derived aerosol properties with available observations by AERONET ground-based sun/sky-radiometers indicated encouraging consistency of microphysical parameters of aerosol components derived from joint inversion with those obtained by the AERONET retrieval. More comprehensive studies for testing and tuning the developed algorithm including accountancy for polarization effects both for sun-photometer and lidar observations are planned in future efforts. Such important aspects of algorithm implementation as coincident measurements requirements are to be addressed in follow-up studies.

The described GARRLiC algorithm is not only limited to ground observations or to the used instrument types. The presented concept could be adapted to a variety of aerosol remote sensing instruments available, including ground-based polarimetric measurements of both sun photometers and lidars, Raman scattering lidars and spaceborne systems like PARASOL and CALIPSO, providing wider opportunities in global comprehensive aerosol characterization.

Acknowledgements. The authors are very thankful to AERONET for establishing and maintaining the sites used in this work. This research has been supported by the University of Lille, and Region Nord-Pas-de-Calais. A. Lopatin was supported by a CROUS/CNOUS fellowship of the French Government. The research leading to these results has received funding from the European Union Seventh Framework Program (FP7/2007-2013) under grant agreement No. 262254. The publication of this article is financed by CNRS-INSU.

Edited by: T. Wagner

The publication of this article
is financed by CNRS-INSU.

References

Adam, M., Pahlow, M., Kovalev, V. A., Ondov, J. M., Parlange, M. B., and Nair, N.: Aerosol optical characterization by nephelometer and lidar: The Baltimore Supersite experiment during the Canadian forest fire smoke intrusion, J. Geophys. Res., 109, D16S02, doi:10.1029/2003JD004047, 2004.

Ahmad, Z., Franz, B. A., McClain, C. R., Kwiatkowska, E. J., Werdell, J., Shettle, E. P., and Holben, B. N.: New aerosol models for the retrieval of aerosol optical thickness and normalized water-leaving radiances from the SeaWiFS and MODIS sensors over coastal regions and open oceans, Appl. Optics, 49, 5545–5560, 2010.

Althausen, D., Engelmann, R., Baars, H., Heese, B., Ansmann, A., and Müller, D.: Portable Raman Lidar PollyXT for Automated Profiling of Aerosol Backscatter, Extinction, and Depolarization, J. Atmos. Ocean. Tech., 26, 2366–2378, 2009.

Ansmann, A., Riebersell, M., Wandinger, U., Weitkamp, C., Voss, E., Lahmann, W., and Michaelis, W.: Combined raman-elastic lidar for vertical profiling of moisture, aerosols extinction, backscatter and lidar ratio, Appl. Phys., 55, 18–28, 1992.

Ansmann, A., Tesche, M., Groß, S., Freudenthaler, V., Seifert, P., Hiebsch, A., Schmidt, J., Wandinger, U., Mattis, I., Müller, D., and Wiegner, M.: The 16 April 2010 major volcanic ash plume over central Europe: EARLINET lidar and AERONET photometer observations at Leipzig and Munich, Germany, Geophys. Res. Lett., 37, L13810, doi:10.1029/2010GL043809, 2010.

Ansmann, A., Petzold, A., Kandler, K., Tegen, I., Wendisch, M., Müller, D., Weinzierl, B., Müller, T., and Heintzenberg, J.: Saharan Mineral Dust Experiments SAMUM-1 and SAMUM-2: what have we learned?, Tellus B, 63, 403–429, doi:10.1111/j.1600-0889.2011.00555.x, 2011a.

Ansmann, A., Tesche, M., Seifert, P., Groß, S., Freudenthaler, V., Apituley, A., Wilson, K. M., Serikov, I., Linné, H., Heinold, B., Hiebsch, A., Schnell, F., Schmidt, J., Mattis, I., Wandinger, U., and Wiegner, M.: Ash and fine mode particle mass profiles from EARLINET/AERONET observations over central Europe after the eruptions of the Eyjafjallajökull volcano in 2010, J. Geophys. Res., 116, D16S02, doi:10.1029/2003JD004047, 2011b.

Antuña, J., Andrade, M., Landulfo, E., Clemesha, B., Quel, E., and Bastidas, A., Clemesha, B., Quel, E., and Bastidas, A.: Building a Lidar Network in Latin America: Progress and Difficulties, in: 23rd International Laser Radar Conference, 24–28 July 2006, Nara, Japan, 2006.

Baars, H., Althausen, D., Engelmann, R., Ansmann, A., Müller, D., Artaxo, P., Pauliquevis, T., Souza, R., and Martin, S. T.: Automated Raman lidar measurements in the Amazon rain forest during the wet and dry season 2008, in: Proceedings of the 8th International Symposium on Tropospheric Profiling, 19–23 October 2009, vol. S04, edited by: Apituley, A., Russchenberg, H., and Monna, W., Delft, the Netherlands, 1–4, 2009.

Barker, J. and Tingey, D. T.: Air Pollution Effects on Biodiversity, Springer, New York, 1992.

Bösenberg, J.: EARLINET-A European Aerosol Research Lidar Network, Advances in Laser Remote sensing, in: Selected papers 20th Int. Laser Radar Conference (ILRC), 10–14 July 2000, Vichi, France, 155–158, 2000.

Bösenberg, J. and Hoff, R. M.: Plan for the implementation of the GAW Aerosol Lidar Observation Network GALION, WMO/TD-No. 1443 178, GAW, Hamburg, Germany, 2007.

Bréon, F.-M.: How Do Aerosols Affects Cloudiness and Climate?, Science, 313, 623–624, doi:10.1126/science.1131668, 2006.

Bréon, F. M., Buriez, J. C., Couvert, P., Deschamps, P. Y., Deuzé, J. L., Herman, M., Goloub, P., Leroy, M., Lifermann, A., Moulin, C., Parol, F., Seze, G., Tanré, D., Vanbauce, C., and Vesperini, M.: Scientific results from the POLarization and Directionality of the Earth's Reflectances (POLDER), Adv. Space Res., 30, 2383–2386, 2002.

Burton, S. P., Ferrare, R. A., Hostetler, C. A., Hair, J. W., Rogers, R. R., Obland, M. D., Butler, C. F., Cook, A. L., Harper, D. B., and Froyd, K. D.: Aerosol classification using airborne High Spectral Resolution Lidar measurements – methodology and examples, Atmos. Meas. Tech., 5, 73–98, doi:10.5194/amt-5-73-2012, 2012.

Cattrall, C., Reagan, J., Thome, K., and Dubovik, O.: Variability of aerosol and spectral lidar and backscatter and extinction ratios of key aerosol types derived from selected Aerosol Robotic network locations, J. Geophys. Res., 110, D10S11, doi:10.1029/2004JD005124, 2005.

Chaikovsky, A., Dubovik, O., Holben, B. N., and Bril, A. I.: Methodology to retrieve atmospheric aerosol parameters by combining ground-based measurements of multiwavelength lidar and sun sky-scanning radiometer, in: Proceeding of Eight International Symposium on Atmospheric and Ocean and Ocean Optics: Atmospheric Physics, edited by: Zherebtsov, G. A., Matvienko, G. G., Banakh, V. A., and Koshelev, V. V., Proc. SPIE, 4678, 257–268, doi:10.1117/12.458450, 2002.

Chaikovsky, A., Bril, A., Dubovik, O., Holben, B., Thompson, A., Goloub, P., O'Neill, N., Sobolewski, P., Bösenberg, J., Ansmann, A., Wandinger, U., and Mattis, I.: CIMEL and multiwavelength lidar measurements for troposphere aerosol altitude distributions investigation, long-range transfer monitoring and regional ecological problems solution: field validation of retrieval techniques, Óptica Pura y Aplicada, 37, 3241–3246, 2004.

Chaikovsky, A., Bril, A., Denisov, S., and Balashevich, N.: Algorithms and software for lidar data processing in CIS-LiNet, in: Reviewed and Revised Papers Presented at the 23rd International Laser radar Conference, 24–28 July 2006, edited by: Chikao Nagasava, N. S., Nara, Japan, 667–670, 2006a.

Chaikovsky, A., Ivanov, A., Balin, Y., Elnikov, A., Tulinov, G., Plusnin, I., Bukin, O., and Chen, B.: Lidar network CIS- LiNet for monitoring aerosol and ozone in CIS regions, in: Proc. Twelfth Joint International Symposium on Atmospheric and Ocean Optics/Atmospheric Physics, edited by: Zherebtsov, G. G. M., Proc. SPIE, 6160, 616035–616039, doi:10.1117/12.675920, 2006b.

Chaikovsky, A., Ivanov, A., Korol, M., Slesar, A. S. D., Osipenko, F., Hutko, I., Dubovik, O., Holben, B., and Goloub, P.: Atmospheric participate matter variability in an industrial center from multi-wavelength lidar and Sun-sky radiometer measurements, in: Proc. Twelfth Joint International Symposium on Atmospheric and Ocean Optics/Atmospheric Physics, edited by: Zherebtsov, G. G. M., Proc. SPIE, 6160, 61601Y–61601Y-12, doi:10.1117/12.675466, 2006c.

Chaikovsky, A., Dubovik, O., Goloub, P., Tanré, D., Chaikovskaya, L., Denisov, S., Grudo, Y., Lopatsin, A., Karol, Y., Lapyonok, T., Korol, M., Osipenko, F., Savitski, D., and Slesar, A.: Combined lidar and radiometric sounding of atmospheric aerosol: algorithm of data processing, software, dessimination, in: Proceedings of XVIII International symposium "Atmospheric and ocean optics. Atmosphere physics", 2–6 July 2012, Irkutsk, Russian Federation, C1–C4, 2012.

Charlson, R. J., Schwartz, S. E., Hales, J. M., Cess, R. D., Coakley, J. A., Hansen, J. E., and Hofmann, D. J.: Aerosols and global warming response, Science, 256, 598–599, 1992.

Costa, M., Levizzani, V., and Silva, A. M.: Part II: Aerosol characterization and direct radiative forcing assessment over the ocean: Application to test cases and validation, J. Appl. Meteorol., 43, 1818–1833, 2004.

Cuesta, J., Flamant, H. P., and Flamant, C.: Synergetic technique combining elastic backscatter lidar data and sunphotometer AERONET inversion for retrieval by layer of aerosol optical and microphysical properties, Appl. Optics, 47, 4598–4611, 2008.

D'Almeida, G. A., Koepke, P., and Shettle, E. P.: Atmospheric Aerosols: Global Climatology and Radiative Characteristics, A. Deepak Pub., p. 561, 1991.

Denisov, S., Chaikovsky, A., Bril, A., and Balashevich, N.: Integrated software for lidar data processing, in: Proceedings Of International Workshop ISTC "Baikal 2006", Monitoring of large-scale atmosphere changes in CIS regions: co-operation of the international measuring networks AERONET, EARLINET, ADNet, NDSC, as well as scientific groups in CIS, 15–19 August 2006, Irkutsk, Russia, 41–43, 2006.

Di Girolamo, P., Summa, D., Bhawar, R., Di Lorio, T., Cacciani, M., Veselovskii, I., Dubovik, O., and Kolgotin, A.: Raman lidar observations of a Saharan dust outbreak event: Characterization of the dust optical properties and determination of particle size and microphysical parameters, J. Atmos. Environ., 50, 66–78, doi:10.1016/j.atmosenv.2011.12.061, 2012.

Dubovik, O.: Optimization of Numerical Inversion in Photopolarimetric Remote Sensing, in: Photopolarimetry in Remote Sensing, edited by: Videen, G., Yatskiv, Y., and Mishchenko, M., Kluwer Academic Publishers, Dordrecht, the Netherlands, 65–106, 2004.

Dubovik, O. and King, M.: A flexible inversion algorithm for retrieval of aerosol optical properties from Sun and sky radiance measurements, J. Geophys. Res., 105, 20673–20696, doi:10.1029/2000JD900282, 2000.

Dubovik, O., Lapyonok, T., and Oshchepkov, S.: Improved technique for data inversion: optical sizing of multicomponent aerosols, Appl. Optics, 34, 8422–8436, 1995.

Dubovik, O., Yokota, T., and Sasano, Y.: Improved technique for data inversion and its application to the retrieval algorithm for adeos/ilas, Adv. Space Res., 21, 397–403, 1998.

Dubovik, O., Smirnov, A., Holben, B. N., King, M., Kaufman, Y. J., Eck, T. F., and Slutsker, I.: Accuracy assessments of aerosol optical properties retrieved from Aerosol Robotic Network (AERONET) sun and sky radiance measurements, J. Geophys. Res., 105, 9791–9806, 2000.

Dubovik, O., Holben, B., Eck, T., Smirnov, A., Kaufman, Y., King, M., Tanré, D., and Slutsker, I.: Variability of absorption and optical properties of key aerosol types observed in worldwide locations, J. Atmos. Sci., 59, 590–608, 2002a.

Dubovik, O., Holben, B. N., Lapyonok, T., Sinyuk, A., Mishchenko, M. I., Yang, P., and Slutsker, I.: Non-spherical aerosol retrieval method employing light scattering by spheroids, Geophys. Res. Lett., 29, 54-1–54-4, doi:10.1029/2001GL014506, 2002b.

Dubovik, O., Sinyuk, A., Lapyonok, T., Holben, B. N., Mishchenko, M., Yang, P., Eck, T. F., Volten, H., Munoz, O., Veihelmann, B., van der Zande, W. J., Leon, J.-F., Sorokin, M., and Slutsker, I.: Application of spheroid models to account for aerosol particle nonsphericity in remote sensing of desert dust, J. Geophys. Res., 111, D11208, doi:10.1029/2005JD006619, 2006.

Dubovik, O., Herman, M., Holdak, A., Lapyonok, T., Tanré, D., Deuzé, J. L., Ducos, F., Sinyuk, A., and Lopatin, A.: Statistically optimized inversion algorithm for enhanced retrieval of aerosol properties from spectral multi-angle olarimetric satellite observations, Atmos. Meas. Tech., 4, 975–1018, doi:10.5194/amt-4-975-2011, 2011.

Eck, T. F., Holben, B. N., Dubovik, O., Smirnov, A., Goloub, P., Chen, H. B., Chatenet, B., Gomes, L., Zhang, X.-Y., Tsay, S.-C., Ji, Q., Giles, D., and Slutsker, I.: Columnar aerosol optical properties at AERONET sites in Central-eastern Asia and aerosol transport to the tropical mid Pacific, J. Geophys. Res., 110, 975–1018, doi:10.1029/2004JD005274, 2005.

Eck, T. F., Holben, B. N., Reid, J. S., Giles, D. M., Rivas, M. A., Singh, R. P., Tripathi, S. N., Bruegge, C. J., Platnick, S., Arnold, G. T., Krotkov, N. A., Carn, S. A., Sinyuk, A., Dubovik, O., Arola, A., Schafer, J. S., Artaxo, P., Smirnov, A., Chen, H., and Goloub, P.: Fog- and cloud-induced aerosol modification observed by the Aerosol Robotic Network (AERONET), J. Geophys. Res., 117, D07206, doi:10.1029/2011JD016839, 2012.

Fernald, F. G.: Analysis of atmospheric lidar observations – Some comments, Appl. Optics, 23, 652–653, 1984.

Fernald, F. G., Herman, B. M., and Reagan, J. A.: Determination of aerosol height distributions by lidar, J. Appl. Meteorol., 11, 482–489, 1972.

Ferrare, R. A., Melfi, S. H., Whiteman, D. N., Evans, K. D., Leifer, R., and Kaufman, Y. J.: Raman lidar measurements of aerosol extinction and backscattering 1. Methods and comparisons, J. Geophys. Res., 103, 19663–19672, 1998a.

Ferrare, R. A., Melfi, S. H., Whiteman, D. N., Evans, K. D., Poellot, M., and Kaufman, Y. J.: Raman lidar measurements of aerosol extinction and back-scattering 2. Derivation of aerosol real refractive index, single-scattering albedo, and humidification factor using Raman lidar and aircraft size distribution measurements, J. Geophys. Res., 103, 19673–19690, 1998b.

Fleming, E., Chandra, S., Shoeberl, M., and Barnett, J.: Mean Global Climatology of Temperature, Wind, Geopotential Height, and Pressure for 0–120 km, NASA Technical Memorandum 100697, NASA, Washington, D.C., 1988.

Forster, P., Ramaswany, V., Artaxo, P., Bernsten, T., Betts, R., Fahey, D. W., Haywood, J., Lean, J., Lowe, D., Myhre, G., Nganga, J., Prinn, R., Raga, G., Schulz, M., and Dorland, R. V.: Changes in atmospheric constituents and in radiative forcing, Climate change 2007: the physical science basis. Contribution of working group I to the fourth assessment report of Intergovernmental Panel on Climate change, IPCC report, IPCC, Cambridge University Press, Cambridge, UK and New York, NY, USA, 2007.

Gatebe, C. K., Dubovik, O., King, M. D., and Sinyuk, A.: Simultaneous retrieval of aerosol and surface optical properties from combined airborne- and ground-based direct and diffuse radiometric measurements, Atmos. Chem. Phys., 10, 2777–2794, doi:10.5194/acp-10-2777-2010, 2010.

Gobbi, G. P., Barnaba, F., Van Dingenen, R., Putaud, J. P., Mircea, M., and Facchini, M. C.: Lidar and in situ observations of continental and Saharan aerosol: closure analysis of particles optical and physical properties, Atmos. Chem. Phys., 3, 2161–2172, doi:10.5194/acp-3-2161-2003, 2003.

Groß, S., Tesche, M., Freudenthaler, V., Toledano, C., Wiegner, M., Ansmann, A., Althausen, D., and Seefeldner, M.: Characterization of Saharan dust, marine aerosols and mixtures of biomass-burning aerosols and dust by means of multi-wavelength depolarization and Raman lidar measurements during SAMUM 2, Tellus B, 63, 706–724, doi:10.1111/j.1600-0889.2011.00556.x, 2011.

Groß, S., Esselborn, M., Abicht, F., Wirth, M., Fix, A., and Minikin, A.: Airborne high spectral resolution lidar observation of pollution aerosol during EUCAARI-LONGREX, Atmos. Chem. Phys., 13, 2435–2444, doi:10.5194/acp-13-2435-2013, 2013.

Hair, J., Hostetler, C., Cook, A., Harper, D., Ferrare, R., Mack, T., Welch, W., Izquierdo, L., and Hovis, F. E.: Airborne High Spectral Resolution Lidar for Profiling Aerosol Optical Properties, Appl. Optics, 47, 6734–6752, doi:10.1364/AO.47.006734, 2008.

Hansen, J., Sato, M., Kharecha, P., and von Schuckmann, K.: Earth's energy imbalance and implications, Atmos. Chem. Phys., 11, 13421–13449, doi:10.5194/acp-11-13421-2011, 2011.

Harrison, R. M. and Yin, J.: Particulate matter in the atmosphere: Which particle properties are important for its effects on health, Sci. Total Environ., 249, 85–101, 2000.

Hasekamp, O. P., Litvinov, P., and Butz, A.: Aerosol properties over the ocean from PARASOL multiangle photopolarimetric measurements, J. Geophys. Res.-Atmos., 116, D14204, doi:10.1029/2010JD015469, 2011.

Hobbs, P. V.: Aerosol-cloud interactions, in Aerosol-Cloud-Climate Interactions, Academic, San Diego, California, 33–69, 1993.

Hoff, R. M., Wiebe, H. A., and Guise-Bagley, L.: Lidar, nephelometer, and in situ aerosol experiments in southern Ontario, J. Geophys. Res., 101, 19199–19209, 1996.

Holben, B.: AERONET-A federated instrument network and data archive for aerosol characterization, Remote Sens. Environ., 66, 1–16, 1998.

Holben, B., Eck, T., Schafer, J., Giles, D., and Sorokin, M.: Distributed Regional Aerosol Gridded Observation Networks (DRAGON), White Paper, http://aeronet.gsfc.nasa.gov/new_web/Documents/DRAGON_White_Paper_A_system_of_experiment.pdf (last access: August 2013), 2011.

Huebert, B. J., Bates, T., Russell, P. B., Shi, G., Kim, Y. J., Kawamura, K., Carmichael, G., and Nakajima, T.: An overview of ACE-Asia: Strategies for quantifying the relationships between Asian aerosols and their climatic impacts, J. Geophys. Res., 8, 8633, doi:10.1029/2003JD003550, 2003.

Jones, A. P.: Indoor air quality and health, Atoms. Environ, 33, 4535–4564, 1999.

Kahn, R. A., Gaitley, B. J., Garay, M. J., Diner, D. J., Eck, T. F., Smirnov, A., and Holben, B. N.: Multiangle Imaging SpectroRadiometer global aerosol product assessment by comparison with the Aerosol Robotic Network, J. Geophys. Res.-Atmos., 115, D23209, doi:10.1029/2010JD014601, 2010.

King, M. D., Byrne, D. M., Herman, B. M., and Reagan, J. A.: Aerosol size distributions obtained by inversion of spectral optical depth measurements, J. Atmos. Sci., 21, 2153–2167, 1978.

King, M. D., Kaufman, Y., Tanré, D., and Nakajima, T.: Remote sensing of Tropospheric aerosols from Space: Past, Present, and Future, B. Am. Meteorol. Soc., 80, 2229–2259, 1999.

Kinne, S., Lohmann, U., Feichter, J., Schulz, M., Timmreck, C., Ghan, S., Easter, R., Chin, M., Ginoux, P., Takemura, T., Tegen, I., Koch, D., Herzog, M., Penner, J., Pitari, G., Holben, B., Eck, T., Smirnov, A., Dubovik, O., Slutsker, I., Tanré, D., Torres, O., Mishchenko, M., Geogdzhayev, I., Chu, D. A., and Kaufman, Y. J.: Monthly averages of aerosol properties: A global comparison among models, satellite data and AERONET ground data, J. Geophys. Res., 108, 4634, doi:10.1029/2001JD001253, 2003.

Kinne, S., Schulz, M., Textor, C., Guibert, S., Balkanski, Y., Bauer, S. E., Berntsen, T., Berglen, T. F., Boucher, O., Chin, M., Collins, W., Dentener, F., Diehl, T., Easter, R., Feichter, J., Fillmore, D., Ghan, S., Ginoux, P., Gong, S., Grini, A., Hendricks, J., Herzog, M., Horowitz, L., Isaksen, I., Iversen, T., Kirkevåg, A., Kloster, S., Koch, D., Kristjansson, J. E., Krol, M., Lauer, A., Lamarque, J. F., Lesins, G., Liu, X., Lohmann, U., Montanaro, V., Myhre, G., Penner, J., Pitari, G., Reddy, S., Seland, O., Stier, P., Takemura, T., and Tie, X.: An AeroCom initial assessment – optical properties in aerosol component modules of global models, Atmos. Chem. Phys., 6, 1815–1834, doi:10.5194/acp-6-1815-2006, 2006.

Klett, D.: Stable analytical inversion solution for processing lidar returns, Appl. Opics, 20, 211–220, 1981.

Klett, D.: Lidar inversion with variable backscatter/extinction ratios, Appl. Optics, 31, 1638–1643, 1985.

Koch, D., Schulz, M., Kinne, S., McNaughton, C., Spackman, J. R., Balkanski, Y., Bauer, S., Berntsen, T., Bond, T. C., Boucher, O., Chin, M., Clarke, A., De Luca, N., Dentener, F., Diehl, T., Dubovik, O., Easter, R., Fahey, D. W., Feichter, J., Fillmore, D., Freitag, S., Ghan, S., Ginoux, P., Gong, S., Horowitz, L., Iversen, T., Kirkevåg, A., Klimont, Z., Kondo, Y., Krol, M., Liu, X., Miller, R., Montanaro, V., Moteki, N., Myhre, G., Penner, J. E., Perlwitz, J., Pitari, G., Reddy, S., Sahu, L., Sakamoto, H., Schuster, G., Schwarz, J. P., Seland, Ø., Stier, P., Takegawa, N., Takemura, T., Textor, C., van Aardenne, J. A., and Zhao, Y.: Evaluation of black carbon estimations in global aerosol models, Atmos. Chem. Phys., 9, 9001–9026, doi:10.5194/acp-9-9001-2009, 2009.

Kokhanovsky, A., Bréon, F. M., Cacciari, A., Carboni, E., Diner, D., Di Nicolantonio, W., Grainger, R., Grey, W., Höller, R., Lee, K.-H., Li, Z., North, P., Sayer, A., Thomas, G., and von Hoyningen-Huene, W.: Aerosol remote sensing over land: A comparison of satellite retrievals using different algorithms and instruments, Atmos. Res., 85, 372–394, 2007.

Kotelnikov, V. A.: On the carrying capacity of the ether and wire in telecommunications, in: Material for the First All-Union Conference on Questions of Communication, Izd. Red. Upr. Svyazi RKKA, Moscow, 1933.

Kovalev, V. A.: Sensitivity of the lidar solution to errors of the aerosol backscatter-to-extinction ratio: Influence of a monotonic change in the aerosol extinction coefficient, Appl. Optics, 34, 3457–3462, 1995.

Kovalev, V. A. and Oller, H. M.: Distortion of particulate extinction profiles measured with lidar in a two-component atmosphere, Appl. Optics, 33, 6499—6570, 1994.

Li, Z., Goloub, P., Dubovik, O., Blarel, L., Zhang, W., Podvin, T., Sinyuk, A., Sorokin, M., Chen, H., Holben, B. N., Tanré, D., Canini, M., and Buis, J.-P.: Improvements for ground-based remote sensing of atmospheric aerosol properties by additional polarimetric measurements, J. Quant. Spectrosc. Ra., 110, 1954–1961, 2009.

Liu, Z., Sugimoto, N., and Murayama, T.: Extinction-to- backscatter ratio of Asian dust observed with high-spectral-resolution lidar and Raman lidar, Appl. Optics, 41, 2760–2767, 2002.

Marenco, F., Santacesaria, V., Bais, A. F., Balis, D., di Sarra, A., Papayannis, A., and Zerefos, C.: Optical properties of tropospheric aerosols determined by lidar and spectrophotometric measurements (Photochemical Activity and Solar Ultraviolet Radiation Campaign), Appl. Optics, 36, 6875–6886, 1997.

Matsumoto, M. and Takeuchi, N.: Effects of misestimated far-end boundary values on two common lidar inversion solutions, Appl. Optics, 33, 6451–6456, 1994.

McCormick, M. P., Wang, P.-H., and Poole, L. R.: Stratospheric aerosols and clouds, in Aerosol-Cloud-Climate Interactions, Academic Press, San Diego, California, 205–222, 1993.

McKendry, I., Strawbridge, K. B., O'Neill, N. T., Macdonald, A. M., Liu, P. S. K., Leaitch, W. R., Anlauf, K. G., Jaegle, L., Fairlie, T. D., and Westphal, D. L.: Trans-Pacific transport of Saharan dust to western North America: A case study, J. Geophys. Res., 112, D01103, doi:10.1029/2006JD007129, 2007.

Mishchenko, M. I., Hovenier, J. W., and Travis, L. D.: Light scattering by nonspherical particles, Elsevier, New York, 2000.

Mishchenko, M. I., Cairns, B., Ha, Travis, L. D., Burg, R., Kaufman, Y. J., Martins, J. V., and Shettle, E. P.: Monitoring of aerosol forcing of climate from space: Analysis of measurement requirements, J. Quant. Spectrosc. Ra., 79/80, 149–161, 2004.

Mishchenko, M. I., Cairns, B., Kopp, G., Schueler, C. F., Fafaul, B. A., Hansen, J. E., Hooker, R. J., Itchkawich, T., Maring, H. B., and Travis, L. D.: Accurate monitoring of terrestrial aerosol and total solar irradiance: introducing the Glory, Mission, B. Am. Meteorol. Soc., 88, 677–691, 2007.

Müller, D., Wandinger, U., and Ansmann, A.: Microphysical particle parameters from extinction and backscatter lidar data by inversion with regularization: Theory, Appl. Optics, 38, 1999.

Müller, D., Mattis, I., Wandinger, U., Ansmann, A., Althausen, D., Dubovik, O., Eckhardt, S., and Stohl, A.: Saharan dust over a Central European EARLINET-AERONET site: Combined observations with Raman lidar and Sun photometer, J. Geophys. Res., 108, 4345, doi:10.1029/2002JD002918, 2003.

Müller, D., Mattis, I., Ansmann, A., Wehner, B., Althausen, D., Wandinger, U., and Dubovik, O.: Closure study on optical and microphysical properties of a mixed urban and Arctic haze air mass observed with Raman lidar and Sun photometer, J. Geophys. Res., 109, D13206, doi:10.1029/2003JD004200, 2004.

Müller, D., Mattis, I., Wandinger, U., Ansmann, A., Althausen, D., and Stohl, A.: Raman lidar observations of aged Siberian and Canadian forest fire smoke in the free troposphere over Germany in 2003: Microphysical particle characterization, J. Geophys. Res., 110, D17201, doi:10.1029/2004JD005756, 2005.

Müller, D., Ansmann, A., Mattis, I., Tesche, M., Wandinger, U., Althausen, D., and Pisani, G.: Aerosol-type-dependent lidar ratios observed with Raman lidar, J. Geophys. Res., 112, D16202, doi:10.1029/2006JD008292, 2007.

Müller, D., Weinzierl, B., Petzold, A., Kandler, K., Ansmann, A., Müller, T., Tesche, M., Freudenthaler, V., Esselborn, M., Heese, B., Althausen, D., Schladitz, A., Otto, S., and Knippertz, P.: Mineral dust observed with AERONET Sun photometer, Raman lidar, and in situ instruments during SAMUM 2006: Shape-independent particle properties, J. Geophys. Res., 115, D07202, doi:10.1029/2009JD012520, 2010.

Müller, D., Lee, K.-H., Gasteiger, J., Tesche, M., Weinzierl, B., Kandler, K., Müller, T., Toledano, C., Otto, S., Althausen, D., and Ansmann, A.: Comparison of optical and microphysical properties of pure Saharan mineral dust observed with AERONET Sun photometer, Raman lidar, and in situ instruments during SAMUM 2006, J. Geophys. Res., 117, D07211, doi:10.1029/2011JD016825, 2012.

Müller, D., Veselovskii, I., Kolgotin, A., Tesche, M., Ansmann, A., and Dubovik, O.: Vertical profiles of pure dust and mixed smoke–dust plumes inferred from inversion of multiwavelength Raman/polarization lidar data and comparison to AERONET retrievals and in situ observations, Appl. Optics, 52, 3178–3202, doi:10.1364/AO.52.003178, 2013.

Murayama, T., Sugimoto, N., Matsui, I., Liu, Z., Sakai, T., Shibata, T., Iwsasaka, Y., Won, J.-G., Yoon, S.-C., Li, T., Zhou, J., and Hu, H.: Lidar Network Observation of Asian Dust, in: Advances in Laser Remote sensing, Selected papers 20th Int. Laser Radar Conference (ILRC), Vichy, France, 10–14 July 2000, edited by: Dabas, A., Loth, C., and Pelon, J., Vichy, France, 169–177, 2001.

Nakajima, T., Tanaka, M., and Yamauchi, T.: Retrieval of the optical properties of aerosols from aureole and extinction data, Appl. Optics, 22, 2951–2959, 1983.

Nakajima, T., Tonna, G., Rao, R., Kaufman, Y. J., and Holben, B. N.: Use of sky brightness measurements from ground for remote sensing of particulate polydispersions, Appl. Optics, 35, 2672–2686, 1996.

Nakajima, T., Yoon, S. C., Ramanathan, V., Shi, G.-Y., Takemura, T., Higurashi, A., Takamura, T., Aoki, K., Sohn, B.-J., Kim, S.-W., Tsuruta, H., Sugimoto, N., Shimizu, A., Tanimoto, H., Sawa, Y., Lin, N.-H., Lee, C.-T., Goto, D., and Schutgens, N.: Overview of the Atmospheric Brown Cloud East Asian Regional Experiment 2005 and a study of the aerosol direct radiative forcing in east Asia, J. Geophys. Res., 112, D24S91, doi:10.1029/2007JD009009, 2007.

Nyquist, H.: Certain topics in telegraph transmission theory, Trans. AIEE, 47, 617–644, 1928.

Omar, A. H., Won, J. G., Winker, D. M., Yoon, S. C., Dubovik, O., and McCormick, M. P.: Development of global aerosol models using cluster analysis of AERONET measurements, J. Geophys. Res., 110, D10S14, doi:10.1029/2004JD004874, 2005.

Oshchepkov, S., Sasano, Y., and Yokota, T.: New method for simultaneous gas and aerosol retrievals from space limb-scanning spectral observation of the atmosphere, Appl. Optics, 41, 4234–4244, 2002.

Papayannis, A., Balis, D., Amiridis, V., Chourdakis, G., Tsaknakis, G., Zerefos, C., Castanho, A. D. A., Nickovic, S., Kazadzis, S., and Grabowski, J.: Measurements of Saharan dust aerosols over the Eastern Mediterranean using elastic backscatter-Raman lidar, spectrophotometric and satellite observations in the frame of the EARLINET project, Atmos. Chem. Phys., 5, 2065–2079, doi:10.5194/acp-5-2065-2005, 2005.

Pickering, K. E., Thompson, A. M., Kim, H., DeCaria, A. J., Pfister, L., Kucsera, T. L., Witte, J. C., Avery, M. A., Blake, D. R., Crawford, J. H., Heikes, B. G., Sachse, G. W., Sandholm, S. T., and Talbot, R. W.: Trace gas transport and scavenging in PEM-Tropics B South Pacific Convergence Zone convection, J. Geophys. Res., 106, 32591–32602, 2001.

Pilinis, C., Pandis, S. N., and Seinfeld, J. H.: Sensitivity of direct climate forcing by atmospheric aerosols to aerosol size and composition, J. Geophys. Res., 100, 18739–18754, 1995.

Raes, F., Bates, T., McGovern, F., and Liedekerke, M. V.: The 2nd Aerosol Characterization Experiment (ACE-2): general overview and main results, Tellus B, 52, 111–125, 2000.

Ramanathan, V., Crutzen, P. J., Lelieveld, J., Mitra, A. P., Althausen, D., Anderson, J., Andreae, M. O., Cantrell, W., Cass, G. R., Chung, C. E., Clarke, A. D., Coakley, J. A., Collins, W. D., Conant, W. C., Dulac, F., Heintzenberg, J., Heymsfield, A. J., Holben, B., Howell, S., Hudson, J., Jayaraman, A., Kiehl, J. T., Krishnamurti, T. N., Lubin, D., McFarquhar, G., Novakov, T., Ogren, J. A., Podgorny, I. A., Prather, K., Priestley, K., Prospero, J. M., Quinn, P. K., Rajeev, K., Rasch, P., Rupert, S., Sadourny, R., Satheesh, S. K., Shaw, G. E., Sheridan, P., and Valero, F. P. J.: Indian Ocean Experiment: An integrated analysis of the climate forcing and effects of the great Indo-Asian haze, J. Geophys. Res., 106, 28371–28398, doi:10.1029/2001JD900133, 2001.

Remer, L. A., Tanré, D., Kaufman, Y. J., Ichoku, C., Mattoo, S., Levy, R., Chu, D. A., Holben, B., Dubovik, O., Smirnov, A., Martins, J. V., Li, R. R., and Ahmad, Z.: Validation of MODIS aerosol retrieval over ocean, Geophys. Res. Lett., 29, 1618, doi:10.1029/2001GL013204, 2002.

Remer, L. A., Kaufman, Y. J., Tanré, D., Mattoo, S., Chu, D. A., Martins, J. V., Li, R. R., Ichoku, C., Levy, R. C., Kleidman, R. G., Eck, T. F., Vermote, E., and Holben, B. N.: The MODIS aerosol algorithm, products, and validation, J. Atmos. Sci., 62, 947–973, doi:10.1175/JAS3385.1, 2005.

Rodgers, C. D.: Retrieval of atmospheric temperature from remote measurements of thermal radiation, Rev. Geophys., 14, 609–624, 1976.

Russell, P. B., Hobbs, P. V., and Stowe, L. L.: Aerosol properties and radiative effects in the United States East Coast haze plume. An overview of the Tropospheric Aerosol Radiative Forcing Observational Experiment (TARFOX), J. Geophys. Res., 104, 2213–2222, 1999.

Sasano, Y., Browell, E. V., and Ismail, S.: Error caused by using a constant extinction backscattering ratio in the lidar solution, Appl. Optics, 24, 3929–3932, 1985.

Schoeberl, M. R. and Newman, P. A.: A multiple-level trajectory analysis of vortex filaments, J. Geophys. Res., 100, 25801–25816, 1995.

Schuster, G. L., Vaughan, M., MacDonnell, D., Su, W., Winker, D., Dubovik, O., Lapyonok, T., and Trepte, C.: Comparison of CALIPSO aerosol optical depth retrievals to AERONET measurements, and a climatology for the lidar ratio of dust, Atmos. Chem. Phys., 12, 7431–7452, doi:10.5194/acp-12-7431-2012, 2012

Shipley, S. T., Tracy, D. H., Eloranta, E. W., Trauger, J. T., Sroga, J. T., Roesler, F. L., and Weinman, J. A.: High spectral resolution lidar to measure optical scattering properties of atmospheric aerosols, Appl. Optics, 23, 3716–3724, 1983.

Sinyuk, A., Dubovik, O., Holben, B., Eck, T. F., Bréon, F.-M., Martonchik, J., Kahn, R., Diner, D. J., Vermote, E. F., Roger, J.-C., Lapyonok, T., and Slutsker, I.: Simultaneous retrieval of aerosol and surface properties from a combination of AERONET and satellite data, Remote Sens. Environ., 107, 90–108, doi:10.1016/j.rse.2006.07.022, 2007.

Sinyuk, A., Dubovik, O., Holben, B., Schafer, J., Giles, D., Eck, T., Slutsker, I., Sorokine, M., Smirnov, A., Bréon, F., and Khan, R.: Multi-sensor aerosol retrievals using joint inversion of AERONET and satellite observations: concept and applications, Eos Trans. AGU, Fall Meet. Suppl., 53, B287, 2008.

Takamura, T., Sasano, Y., and Hayasaka, T.: Tropospheric aerosol optical properties derived from lidar, sun photometer, and optical particle counter measurements, Appl. Optics, 33, 7132–7140, 1994.

Tesche, M., Ansmann, A., Müller, D., Althausen, D., Mattis, I., Heese, B., Freudenthaler, V., Wiegner, M., Esselborn, M., Pisani, G., and Knippertz, P.: Vertical profiling of Saharan dust with Raman lidars and airborne HSRL in southern Morocco during SAMUM, Tellus B, 61, 144–164, 2009.

Tesche, M., Groß, S., Ansmann, A., Müller, D., Althausen, D., Freudenthaler, V., and Esselborn, M.: Profiling of Saharan dust and biomass-burning smoke with multiwavelength polarization Raman lidar at Cape Verde, Tellus B, 63, 649–676, 2011.

Textor, C., Schulz, M., Guibert, S., Kinne, S., Balkanski, Y., Bauer, S., Berntsen, T., Berglen, T., Boucher, O., Chin, M., Dentener, F., Diehl, T., Easter, R., Feichter, H., Fillmore, D., Ghan, S., Ginoux, P., Gong, S., Grini, A., Hendricks, J., Horowitz, L., Huang, P., Isaksen, I., Iversen, I., Kloster, S., Koch, D., Kirkevåg, A., Kristjansson, J. E., Krol, M., Lauer, A., Lamarque, J. F., Liu, X., Montanaro, V., Myhre, G., Penner, J., Pitari, G., Reddy, S., Seland, Ø., Stier, P., Takemura, T., and Tie, X.: Analysis and quantification of the diversities of aerosol life cycles within AeroCom, Atmos. Chem. Phys., 6, 1777–1813, doi:10.5194/acp-6-1777-2006, 2006.

Toledano, C., Wiegner, M., Groß, S., Freudenthaler, V., Gasteiger, J., Müller, D., Müller, T., Schladitz, A., Weinzierl, B., Torres, B., and O'neill, N. T.: Optical properties of aerosol mixtures derived from sun-sky radiometry during SAMUM-2, Tellus B, 63, 635–648, doi:10.1111/j.1600-0889.2011.00573.x, 2011.

Turner, D. D., Ferrare, R. A., Heilman-Brasseur, L. A., Feltz, W. F., and Tooman, T. P.: Automated retrievals of water vapor and aerosol profiles from an operational Raman lidar, J. Atmos. Ocean. Tech., 19, 37–50, 2002.

Twomey, S.: On the numerical solution of Fredholm integral equations of the first kind by the inversion of the linear system produced by quadrature, J. Assoc. Comp. Mach., 10, 97–101, 1963.

Veselovskii, I., Kolgotin, A., Griaznov, V., Müller, D., Franke, K., and Whiteman, D. N.: Inversion of multiwavelength Raman lidar data for retrieval of bimodal aerosol size distribution, Appl. Optics, 43, 1180–1195, 2004.

Veselovskii, I., Dubovik, O., Kolgotin, A., Lapyonok, T., Di Girolamo, P., Summa, D., Whiteman, D. N., Mishchenko, M., and Tanré, D.: Application of randomly oriented spheroids for retrieval of dust particle parameters from multi-wavelength lidar measurements, J. Geophys. Res., 115, D21203, doi:10.1029/2010JD014139, 2010.

Volten, H., Munoz, O., Rol, E., de Haan, J. F., Vassen, W., Hovenier, J. W., Muinonen, K., and Nousiainen, T.: Scattering matrices of mineral aerosol particles at 441.6 nm and 632.8 nm, J. Geophys. Res., 106, 17375–17401, 2001.

Wagner, J., Ansmann, A., Wandinger, U., Seifert, P., Schwarz, A., Tesche, M., Chaikovsky, A., and Dubovik, O.: Evaluation of the Lidar/Radiometer Inversion Code (LIRIC) to determine microphysical properties of volcanic and desert dust, Atmos. Meas. Tech. Discuss., 6, 911–948, doi:10.5194/amtd-6-911-2013, 2013.

Waquet, F., Léon, J.-F., Goloub, P., Pelon, J., Tanré, D., and Deuzé, J.-L.: Maritime and dust aerosol retrieval from polarized and multispectral active and passive sensors, J. Geophys. Res., 110, D10S10, doi:10.1029/2004JD004839, 2005.

Welton, E. J., Campbell, J. R., Berkoff, T. A., Spinhirne, J. D., Tsay, S.-C., Holben, B., and Shiobara, M.: The Micro-pulse Lidar Network (MPL-Net), in: Lidar Remote Sensing in Atmospheric and Earth Sciences, Reviewed and revised papers at the twenty-first International Laser Radar Conference (ILRC21), 8–12 July, edited by: Bisonnette, L. R., Roy, G., and Vallee, G., Defence R&D Canada – Vacartier, Quebec, Canada, 285–288, 2002.

Winker, D. M., Hunt, W. H., and McGill, M. J.: Initial perfomance assessment of CALIOP, Geophys. Res. Lett., 34, L19803, doi:10.1029/2007GL030135, 2007.

Yoon, J., von Hoyningen-Huene, W., Vountas, M., and Burrows, J. P.: Analysis of linear long-term trend of aerosol optical thickness derived from SeaWiFS using BAER over Europe and South China, Atmos. Chem. Phys., 11, 12149–12167, doi:10.5194/acp-11-12149-2011, 2011.